The unexpected softening of the undrained shear strength of organic and silty clays in Rhine delta: a conceptual study

Determining the Undrained Shear Strength of soft Dutch soils using conventional laboratory equipment

by

Antoine Gori

in partial fulfilment of the requirements for the degree of

Master of Science
in Applied Earth Sciences

Thesis committee:

Prof.dr.ir. C. Jommi	TU Delft
Ir. A. Wiggers	Royal Haskoning DHV
Dr.ir. A.A.M. Dieudonné	TU Delft
Dr. F. Pisanò	TU Delft

Preface

This Master thesis forms the penultimate requirement in obtaining the Master of Science degree of Geoengineering at Delft University of Technology. During this journey I was involved on the topic of the stability of dikes for a project in the South of the Netherlands. This experience was by far the most challenging and educational step in my education. I would therefore like to address the following words to those who contributed to this project.

I would first of all like to thank Royal Haskoning DHV for giving me the opportunity to graduate on this topic. I particularly want to thank my daily supervisor, Albert Wiggers, for giving me the trust, support and yet the flexibility for me to perform my research in the best possible conditions. It has been a very pleasant experience to work together and an eye opening experience to witness the process from design to execution, to witness how the development of understanding in the academic world translates back into the industry and the repercussions on societal issues.

Next, I would like to express my gratitude to the chair of the assessment committee Professor Cristina Jommi for her support and guidance. It was an extremely rich and pleasant experience to work together. This experience considerably enhanced my understanding and critical thinking towards norms, laboratory tests and 'school book' theory versus what is seen in the field and also about the challenges ahead in this particular field.

I would like to thank the other members of the assessment committee Anne-Catherine Dieudonné and Federico Pisanò for their support, advice and constructive criticism regarding the completion of my work.

Next to the members of the assessment committee I also closely worked Stefano Muraro who I would like to thank for his precious comments and advice. I particularly appreciated his eagerness to share the results of his ongoing research on similar issues for me to understand even more about the challenges ahead in this field.

During my thesis I was often closely working with co-workers of the GraafReinald alliance. I would in particular like to thank Rens Servais (Heijmans) for his valuable guidance and advice throughout this project, as well as Jaap Wierenga (Heijmans) for his enthusiasm in shearing his experience from the field.

Finally, I would like to thank my parents, brothers, girlfriend, friends and classmates for their support over the last years. This has been a great journey full of challenges and I look forward to the future.

Antoine Gori
Delft, January 2020

Abstract

The current Dutch norms for the macro-stability of flood protection embankments and more specifically the determination of SHANSEP parameters has been subject of debate since its implementation in 2017. The main concerns arise from the apparent over-conservative nature of the guidelines and the apparent underestimation of shear strength of organic and silty clays. In this Master thesis, an assessment of the normalised normally consolidated undrained shear strength is performed for a dike stability reinforcement project between Gorinchem and Waardenburg in the South west of the Netherlands on a problematic clay layer called the 'Gorinchem Clay' throughout this thesis. The main goal is the confirmation of the current norms or towards a more optimised and less conservative assessment of the strength parameters and in doing so, discusses one of the most recurrent questions in geotechnical engineering: do some of the measurements from laboratory tests reveal true material behaviour or do the limitations of such laboratory tests produce this particular behaviour? This analysis was performed on Triaxial Compression, Direct Simple Shear and Triaxial Extension tests from which the SHANSEP parameters are derived as input for the available shear strength along a slip surface according to the methodology developed by Ladd (1991) and following the Critical State Soil Mechanics.
The structure of this thesis is as follows: first, a literature study is performed on the strength parameters assessment in chapter 1, the principles of the Critical State Soil Mechanics and the difficulties encountered in the determination of the strength parameters from laboratory tests in chapter 2. The laboratory results are then exploited in chapters 4 to 5 according to the current guidelines and more extended methods in which the limitations of the Classical Critical State Soil Mechanics are shown. The next chapters focus on a more fundamental understanding of the considered material consisting of modelling the material behaviour in chapter 6 using a simplified academic constitutive model featuring non-associative elasto-plasticity with mixed volumetric and deviatoric hardening allowing for hardening or softening.
The outcomes of this thesis show Critical State conditions as traditionally understood could not be reached reliably for undrained conditions in Triaxial Compression, Triaxial Extension and Direct Simple Shear. The tests showed to be particularly unreliable beyond 10% axial strain in Triaxial Compression and Extension, and beyond 15% shear strain in Direct Simple Shear. The difficulties encountered in determining the Critical State friction angle and undrained shear strength were shown to be minimised by performing drained and undrained Triaxial compression tests on slightly over-consolidated soil samples. Additionally, the limitations of the Classical Critical State theory were highlighted and a more advanced constitutive model including a non-associative flow rule and deviatoric hardening was successfully used to predict the behaviour in Triaxial Compression for undrained conditions. The predictions for drained conditions and particularly undrained Triaxial Extension were however limited.

Contents

1 Dike Design in the Netherlands **14**
- 1.1 Overview general design and macro-stability . . . 14
- 1.2 The 'traditional' macro-stability strength assessment and limitations . . . 16
- 1.3 Current Dutch macro-stability assessment: Undrained Critical State strengths . . . 17
  - 1.3.1 Principles of critical state soil mechanics and SHANSEP method . . . 17
  - 1.3.2 Parameter selection according to the new Dutch guidelines . . . 18

2 Classical Critical state soil mechanics and experimental practices **20**
- 2.1 Critical State fundamentals . . . 20
- 2.2 Determining Critical State in practice . . . 23
  - 2.2.1 Determining the Critical State for soft soil using the Triaxial test . . . 23
  - 2.2.2 Determining the Critical State for soft soil using the Direct simple shear (DSS) test . . . 26
  - 2.2.3 Determining the Critical State for soft soil using the Triaxial Extension test 27
- 2.3 Strategy to find the Critical State . . . 28

3 Data overview and testing procedures **33**
- 3.1 Material properties . . . 35
- 3.2 Triaxial Compression tests . . . 37
- 3.3 Direct Simple Shear (DSS) tests . . . 39
- 3.4 Triaxial Extension tests . . . 40
- 3.5 Constant Rate of Strain (CRS) and Oedometer tests . . . 40

4 Preliminary results **42**
- 4.1 Preliminary results of the Triaxial Compression tests . . . 42
  - 4.1.1 Unexpected behaviour of the soil . . . 42
  - 4.1.2 Strain based correlations . . . 44
  - 4.1.3 Stress Path trends of the results in soil parameters and classification . . . 48
- 4.2 Preliminary results of the Direct Simple Shear tests . . . 56
- 4.3 Preliminary results of the Triaxial Extension tests . . . 56
- 4.4 Combined preliminary results in Triaxial Compression, Direct Simple Shear and Triaxial Extension . . . 57
- 4.5 Preliminary results of the Constant Rate of Strain test (CRS) and Oedometer test 60

5 Extended Results **62**
- 5.1 Matching samples of equal properties . . . 62
- 5.2 Outlier removal . . . 63
- 5.3 Limitations of the Classical Critical State theory in explaining the test results . . . 65
- 5.4 Normally consolidated undrained stress path in DSS and Triaxial Compression for matching samples . . . 69

6 Modelling the behaviour of the soil in Triaxial tests **71**
6.1 On the behaviour of soils . . . 71
6.1.1 Elastic models . . . 71
6.1.2 The elastic-perfectly plastic model, an introduction to yield criterion and plastic potential . . . 72
6.1.3 Elasto-plastic models . . . 73
6.1.4 The modified Cam-Clay model . . . 74
6.1.5 Advanced Modified Cam-Clay based constitutive models with strain softening prediction capabilities . . . 75
6.2 Use of an non-associative elasto-plastic Constitutive model with volumetric and deviatoric hardening or softening contributions in understanding the experimental results . . . 78
6.2.1 Constitutive model background . . . 78
6.2.2 Work flow in determining the model parameters . . . 79
6.3 Modelling Triaxial compression test results for matching Plasticity Index . . . 81
6.3.1 Results of the Modified Cam-Clay, non-associative and non-associative with deviatoric hardening model in Triaxial Compression . . . 81
6.3.2 Sensitivity of the shape of the plastic potential . . . 86
6.4 Modelling of a Triaxial Extension test . . . 88

7 Conclusions and Discussions **90**

8 Recommendations **93**

Bibliography **94**

Appendix:

A Soil Classification **97**

B Results Triaxial Compression tests and Direct Simple Shear tests **100**

C Results CRS tests **108**

D Correlations parameters a and b from CRS tests **111**

E Constitutive model basic parametric analysis **116**
E.1 Modified Cam-Clay . . . 116
E.2 Non-associative flow rule . . . 118
E.3 Deviatoric hardening or softening . . . 120

List of Figures

1.1.1 Failure mechanisms of flood embankments (Bakkenist, 2012).A: Run-over; B: Wave over-topping; C:Macro-instability inner slope; D: Sliding; E: Macro-instability outer slope; F: Micro-instability; G:Piping; H: Outer slope erosion; I: Foreshore erosion; J: Excessive settlement ;K: Ice damage; L: Ship collision 14
1.1.2 Visualisation of slope instability with a circular failure surface (Kremer, Van der Meer, Niemeijer, Koehorst, & Calle, 2001) 15
1.1.3 LiftVan limit equilibrium method (Ministerie van Infrastructuur en Milieu, 2016).1:Water level; 2: Dike body; 3:Phreatic surface; 4:Horizontal dike section; 5:Sand layer; 6:Groundwater flow; 7:Water pressures 16
1.3.1 Active, Direct and Passive shearing in the failure surface of an embankment (Ministerie van Infrastructuur en Milieu, 2016). 18
1.3.2 Stress-Strain curve for a typical CRS test. The horizontal line at point A corresponds to the strain at in-situ initial vertical effective stress σ'_{vi} and point B is the preconsolidation stress σ'_p (Ministerie van Infrastructuur en Milieu, 2016). 19
1.3.3 Correlations between the undrained shear strength ratio S and the overconsolidation ratio (Ministerie van Infrastructuur en Milieu, 2016). 19

2.1.1 Critical state line and Critical state parameter M 21
2.1.2 Critical state line and Normal Compression line according to the Modified Cam Clay model 21
2.1.3 Typical behaviour of clay in a drained shear test initially on the dry and wet side of the Critical state (Atkinson et al., 1993). 22
2.1.4 Behaviour of an OC and NC under drained conditions at constant p'(Atkinson et al., 1993). 22
2.1.5 Behaviour of an OC and NC under undrained conditions (Atkinson et al., 1993). . 22
2.2.1 Shapes of failed specimens in a triaxial test (Ehrgott, 1971) 24
2.2.2 Typical deformation mechanisms of Gorinchem Clay tested in undrained triaxial from the wet side 25
2.2.3 Typical deformation mechanisms of Gorinchem Clay tested in undrained triaxial from the dry side 26
2.2.4 Possible failure mechanisms in an idealised Direct Simple Shear test for (a) horizontal failure surface and (b) vertical failure surface (Hanzawa, Nutt, Lunne, Tang, & Long, 2007) 27
2.2.5 Typical deformation mechanisms of Gorinchem Clay tested in Undrained Triaxial Extension from the wet side 28
2.3.1 Failure surfaces in the deviatoric plane (Georgiadis, Potts, & Zdravkovic, 2004) . 29
2.3.2 Effective stress paths for drained over-consolidated (D-OC), drained normally consolidated (D-NC), undrained over-consolidated (U-OC) soils and undrained normally consolidated (U-NC) soils. 30
2.3.3 Idealised normalised shear stress versus shear strain for triaxial compression, direct simple shear and triaxial extension tests under plain strain, as in (Ladd, 1991) . . 30
2.3.4 Idealised behaviour in the p'q space and corresponding response in the void ratio space according to the Modified Cam Clay model (Wroth, 1984) 31

2.3.5 Idealised sample behaviour in an undrained triaxial test in the void ratio space. EOC: end of consolidation, EOU: end of unloading. 32
2.3.6 Idealised sample behaviour in a drained triaxial test in the void ratio space. EOC: end of consolidation, EOU: end of unloading. 32

3.0.1 Locations of sampled dike sections 33
3.0.2 Location of samples in dike section TG321 34
3.0.3 Location of samples in dike section TG396 34
3.0.4 Location of samples in dike section TG422-421 34
3.0.5 Soil Classification and Cross-section at dike section TG321 35
3.0.6 Soil Classification and Cross-section at dike section TG396 35
3.0.7 Soil Classification and Cross-section at dike section TG422 35
3.1.1 Sand, silt, clay, and organic content of the samples tested in the triaxial apparatus 36
3.1.2 Casagrande Plasticity chart for Triaxial Compression and DSS tested samples . . 36
3.2.1 Coefficient of earth pressure at rest K_0 to be considered for triaxial tests 37

4.1.1 Unexpected behaviour of undrained tests showing excessive softening and no convergence towards a Critical State line 43
4.1.2 Unexpected behaviour of undrained tests showing a non linear elastic stress path from the dry side and an initial increasing confining pressure on the wet side . . . 43
4.1.3 Unexpected behaviour of drained tests showing post peak softening and varying stiffness for normally consolidated samples 44
4.1.4 Unexpected behaviour of undrained tests showing continuous excess pore pressure development 44
4.1.5 Normalised deviatoric stress and stress ratio as a function of the wet volumetric weight at 10% axial strain 45
4.1.6 Normalised deviatoric stress and stress ratio as a function of the wet volumetric weight at 15% axial strain 45
4.1.7 Normalised deviatoric stress and stress ratio as a function of the wet volumetric weight at 20% axial strain 46
4.1.8 Normalised deviatoric stress and stress ratio as a function of the wet volumetric weight at 25% axial strain 46
4.1.9 Normalised deviatoric stress and stress ratio as a function of Plasticity Index at 10% axial strain 47
4.1.10 Normalised deviatoric stress and stress ratio as a function of Plasticity Index at 15% axial strain 47
4.1.11 Normalised deviatoric stress and stress ratio as a function of Plasticity Index at 20% axial strain 48
4.1.12 Normalised deviatoric stress and stress ratio as a function of Plasticity Index at 25% axial strain 48
4.1.13 Stress ratio η as a function of the wet volumetric weigth. 49
4.1.14 Excess pore pressures as a function of the wet volumetric weigth. 50
4.1.15 Stress ratio η as a function of the Plasticity Index. 51
4.1.16 Excess pore pressures as a function of the Plasticity Index. 52
4.1.17 Stress ratio η as a function of the Clay content from the dry side. 53
4.1.18 Excess pore pressures as a function of the Clay content from the dry side. 53
4.1.19 Stress ratio η as a function of the Organic content from the dry side. 54
4.1.20 Excess pore pressures as a function of the Organic content from the dry side. . . . 54
4.1.21 Stress ratio η as a function of the Silt content from the dry side. 55
4.1.22 Excess pore pressures as a function of the Silt content from the dry side. 55
4.2.1 Preliminary DSS results for normally consolidated conditions 56
4.2.2 Preliminary DSS results for over-consolidated conditions 56
4.3.1 Preliminary undrained Triaxial Extension results 57

4.4.1 Normalised stress-strain of Triaxial Compression, DSS and Triaxial Extension tests for volumetric weights between 14 and 16 kN/m^3 . . . 58
4.4.2 Normalised stress-strain of triaxial compression, DSS and triaxial extension tests for volumetric weights between 16 and 17.5 kN/m^3 . . . 59
4.4.3 Normalised stress-strain of triaxial compression, DSS and triaxial extension tests for volumetric weights between larger than 17.5 kN/m^3 . . . 59
4.5.1 Correlation between parameters a and b versus wet volumetric weight . . . 60
4.5.2 Pre-consolidation pressures Triaxial Compression test determined from CRS and oedometer tests . . . 61
4.5.3 Pre-consolidation pressures DSS test determined from CRS and oedometer tests . 61

5.2.1 Results Triaxial compression tests for matched Plasticity Index 38% . . . 64
5.2.2 Results Triaxial compression tests for matched Plasticity Index 44% . . . 64
5.2.3 Results Triaxial compression tests for matched Plasticity Index 47% . . . 65
5.3.1 Results Triaxial compression tests for matched Plasticity Index 50% . . . 67
5.3.2 Results Triaxial compression tests for matched Plasticity Index 56% . . . 67
5.3.3 Results Triaxial compression tests for matched Plasticity Index 60% . . . 68
5.3.4 Results Triaxial compression tests for matched Plasticity Index 69% . . . 68
5.3.5 Asymptotic behaviour of Gorinchem clay, fibrous peat and glacial till in undrained triaxial compression. Black: test data; Red: expected behaviour. Test data for Gorinchem clay tested from the wet side shows significant 'test effects'. . . . 69
5.4.1 Undrained shear strength for samples of Similar Plasticity indexes (40%) and pre-consolidation pressure . . . 70
5.4.2 Undrained shear strength for samples of Similar Plasticity indexes (50%) and pre-consolidation pressure . . . 70

6.1.1 elastic-perfectly plastic behaviour (Wood, 2014) . . . 73
6.1.2 Visualisation of strain softening mechanism for undrained conditions using a shrinking yield surface according to the Structured Cam-clay model. 1,2,3: successive yield surfaces where 1 is the yield surface of the intact structured clay, 3 the yield surface for a fully remoulded clay and 2 an intermediate state . . . 76
6.1.3 Visualisation of strain softening mechanism for undrained normally consolidated conditions using a rotational hardening rule and destructuration. 1: yield surface of the intact material, 2: rotated yield surface, 3: rotated and destructed yield surface. . . . 77
6.1.4 Stress path for non-associative flow induced strain softening for undrained normally consolidated conditions. (a): elliptical shaped yield locus smaller than the plastic potential locus, (b): tear-drop shaped yield locus . . . 77
6.1.5 Stress path for non-associative flow and tear-drop shaped yield locus inducing strain softening. (a): undrained over-consolidated conditions (TC), (b): undrained normally consolidated conditions (TE) . . . 77
6.2.1 Comparison of the stress ratio reach for over-consolidated and normally consolidated conditions on similar samples. $TG321. + 017\_B\_BUT\_M019 - a$: typical undrained normally consolidated test showing excessive softening; $TG421. + 093\_B\_MBIB\_mo - 13c$: drained over-consolidated test; $TG421.+094\_B\_BUT\_mo - 19b$: good quality undrained normally consolidated test; $TG421.+093\_B\_MBIB\_mo - 12b$: slightly over-consolidated undrained test . . . 80
6.3.1 Considered tests to be modelled . . . 81
6.3.2 Shapes of the proposed plastic potential and yield surface . . . 82
6.3.3 Experimental results of test TG321.+017_B_BUT_M019-a and simulations using the MCC model, a non-associative flow rule and a non-associative flow rule with distortional hardening. . . . 83

6.3.4 Experimental results of test TG422.+005_B_MBIB_mo-19a and simulations using the MCC model, a non-associative flow rule and a non-associative flow rule with distortional hardening. 84
6.3.5 Experimental results of test TG421.+093_B_MBIB_mo-20a and simulations using the MCC model, a non-associative flow rule and a non-associative flow rule with distortional hardening. 84
6.3.6 Drained and undrianed stress path and yield point for MCC model and tear-drop shaped yield locus for non-associative flow rule. a: MCC shaped yield locus, b: tear drop shaped yield locus, a': MCC shaped yield locus at the pre-consolidation pressure, b': tear drop shaped yield locus at the pre-consolidation pressure. 85
6.3.7 Triaxial Compression tests of samples with Plasticity Index 47% ± 5% and MCC simulation where λ=0.14, κ=0.01 and M=1.65 85
6.3.8 Triaxial Compression tests of samples with Plasticity Index 47% ± 5% and non-associative flow rule simulation where λ=0.14, κ=0.01, M_g=1.65, M_f=1.4, χ_g=0.9, χ_f=0.4 86
6.3.9 Triaxial Compression tests of samples with Plasticity Index 47% ± 5% and non-associative flow rule simulation where λ=0.14, κ=0.01, M_g=1.65, M_f=1.4, χ_g=0.9, χ_f=0.4, D_0=-1 and D_1=30 86
6.3.10 Shapes of the plastic potential for χ_g=2.0, 0.9 and 0.4 87
6.3.11 Sensitivity of parameter χ_g on the stress path simulation for undrained normally consolidated conditions 88
6.3.12 Sensitivity of parameter χ_g on the stress path simulation for undrained over-consolidated conditions 88
6.4.1 Triaxial Extension experimental stress path for undrained conditions and simulated results 89

A.0.1 Silt content of samples tested in Triaxial Compression 97
A.0.2 Clay content of samples tested in Triaxial Compression 98
A.0.3 Organic content of samples tested in Triaxial Compression 98
A.0.4 Sand content of samples tested in Triaxial Compression 99

B.0.1 Triaxial test stress Paths for dike section 7h 100
B.0.2 Triaxial test stress Paths for dike section 10b 101
B.0.3 Triaxial test stress Paths for dike section 12g 101
B.0.4 Triaxial test stress Paths for dike section 7h 102
B.0.5 Triaxial test stress Paths for dike section 10b 102
B.0.6 Triaxial test stress Paths for dike section 12g 103
B.0.7 Normalised undrained shear Strength S in Triaxial Compression 103
B.0.8 DSS test stress Paths for dike section 7h 104
B.0.9 DSS test stress Paths for dike section 10b 104
B.0.10 DSS test stress Paths for dike section 12g 105
B.0.11 DSS test stress Paths for dike section 7h 105
B.0.12 DSS test stress Paths for dike section 10b 106
B.0.13 DSS test stress Paths for dike section 12g 106
B.0.14 Normalised undrained shear Strength S in DSS 107

C.0.1 CRS test results for dike section 7h 108
C.0.2 CRS test results for dike section 7h 109
C.0.3 CRS test results for dike section 7h 110

D.0.1 Parameter a versus Plasticity Index 111
D.0.2 Parameter b versus Plasticity Index 112
D.0.3 Parameter a versus clay content 112

D.0.4 Parameter b versus clay content . . . 113
D.0.5 Parameter a versus silt content . . . 113
D.0.6 Parameter b versus silt content . . . 114
D.0.7 Parameter a versus organic content . . . 114
D.0.8 Parameter b versus organic content . . . 115

E.1.1 MCC analysis parameter Mg. . . . 116
E.1.2 MCC analysis parameter λ. . . . 117
E.1.3 MCC analysis parameter κ. . . . 117
E.1.4 MCC analysis parameter ν. . . . 118
E.1.5 MCC analysis parameter e_0. . . . 118
E.2.1 Non-associative flow rule analysis parameter M_f. . . . 119
E.2.2 Non-associative flow rule analysis parameter $\varkappa_g$ for $M_f > M_g$. . . . 119
E.2.3 Non-associative flow rule analysis parameter $\varkappa_f$ for $M_f > M_g$. . . . 120
E.3.1 Softening parameter analysis D_0. . . . 120
E.3.2 Softening parameter analysis D_1. . . . 121
E.3.3 Results Triaxial compression tests for matched Plasticity Index 23% . . . 122
E.3.4 Results Triaxial compression tests for matched Plasticity Index 34% . . . 122
E.3.5 Results Triaxial compression tests for matched Plasticity Index 42% . . . 123
E.3.6 Results Triaxial compression tests for matched Plasticity Index 43% . . . 123
E.3.7 Results Triaxial compression tests for matched Plasticity Index 44% . . . 124
E.3.8 Results Triaxial compression tests for matched Plasticity Index 50% . . . 124
E.3.9 Results Triaxial compression tests for matched Plasticity Index 52% . . . 125
E.3.10 Results Triaxial compression tests for matched Plasticity Index 54% . . . 125
E.3.11 Results Triaxial compression tests for matched Plasticity Index 56% . . . 126
E.3.12 Results Triaxial compression tests for matched Plasticity Index 60% . . . 126
E.3.13 Results Triaxial compression tests for matched Plasticity Index 64% . . . 127
E.3.14 Results Triaxial compression tests for matched Plasticity Index 69% . . . 127
E.3.15 Results Triaxial compression tests for matched Plasticity Index 77% . . . 128

List of Symbols and abbreviations

Symbols

S_u:	Undrained shear strength
S:	Normally consolidated Undreained Shear Strength ratio
γ_{sat}:	Saturated volumetric weight
σ'_{vi}:	Current effective vertical stress
σ'_v:	Effective vertical stress
σ'_p,p_c:	Pre-consolidation stress
σ_1:	Major principle stress
σ_3:	Minor principle stress
OCR:	Over-Consolidation Ratio
m:	SHANSHEP strength exponent
κ,a:	Slope of the isotropic unloading/reloading line
λ,b:	Slope of the isotropic normal compression line
M:	Slope Critical State line
p':	Mean effective stress
q:	Deviatoric stress
η:	Stress ratio
ϕ'_{cs}:	Critical State friction angle
$\phi'_{mob,tc}$:	Mobilised friction angle for axisymmetric conditions
$\phi'_{mob,ps}$:	Mobilised friction angle for plain-strain conditions
Δu:	Excess pore pressures
τ:	Shear stress
τ_c:	Shear stress in Triaxial Compression
τ_d:	Shear stress in Direct Simple Shear
τ_e:	Shear stress in Triaxial Extension
K_0:	Coefficient of earth pressure at rest
$(\frac{\tau}{\sigma'_{vc}})_{ps}$:	Normalised shear stress for plain strain conditions
$\gamma\%$:	Shear strain
ϵ_a:	Axial strain
υ:	Specific volume
υ_0:	Initial specific volume
υ_κ:	Reference specific volume
e:	Void ratio
e_0:	Initial void ratio
V:	Current sample volume
V_0:	Initial sample volume
p_0:	Initial confining pressure at the beginning of shearing
p_{eq}:	Equivalent confining pressure
$\boldsymbol{\sigma}$:	Stress vector
$\boldsymbol{D}$:	Elastic stiffness matrix
$\boldsymbol{D}^{ep}$:	Elasto-plastic matrix

$\boldsymbol{\epsilon}$:	Total strain vector
ν:	Poisson ratio
E:	Young modulus
K:	Bulk modulus
G:	Shear modulus
ϵ_p:	Volumetric strain
ϵ_q:	Deviatoric/distortional strain
ϵ_1:	Total strains in principle stress direction
ϵ_3:	Total strains in minor stress direction
$\boldsymbol{\epsilon^e}$:	Elastic strain vector
$\boldsymbol{\epsilon^p}$:	Plastic strain vector
λ:	Plastic multiplier
f:	Yield function
g:	Plastic potential function
χ:	Hardening parameter
H:	Plastic modulus
M_g:	Critical State stress ratio
M_f:	Plastic potential size parameter
χ_g:	Plastic potential shape factor
χ_f:	Yield locus shape factor
D:	Deviatoric hardening function
D_0, D_1:	Coefficients of the deviatoric hardening

Abbreviations

SHANSEP: Stress History and Normalised Soil Engineering Properties
TC: Triaxial Compression Test
DSS: Direct Simple Shear Test
TE: Triaxial Extension Test
CRS: Constant rate of Strain test
NC, nc: Normally consolidated conditions
OC, oc: Over-consolidated conditions
U: Undrained condition
D: Drained conditions
NCL, VCL: Normally Consolidated Line, Virgin Compression Line
CSL: Critical State Line
cs: Critical State
MCC: Modified Cam-Clay model
EOC: End Of Consolidation
EOU: End Of Unloading
PI: Plasticity Index
h/d: Sample height over diameter ratio Triaxial test

Introduction

Background and motivation

Two thirds of the Dutch territory are susceptible to flood damages: flood defences have been built since the Middle-ages to result in the present day in over 3600 kilometres of primary dikes and 14 000 kilometres of regional dikes. These flood defences are continuously updated against inland settlement, newly discovered failure mechanisms and more recently against the sea level rise, river discharge, intensity of storms, precipitation and drought. The vast majority of the flood protection is guaranteed by earth embankments built on soft holocenic deposits of sand, peat, and organic and silty clays. The macro-stability of such constructions has always been a challenge for Dutch geotechnical engineers: on the one hand these constructions require to be safe and reliable although they require working with difficult and sometimes unpredictable materials, and one the other hand need to be designed cost-effectively due to the magnitude of the investments required to maintain such level of flood protection. As an illustration, the price to update a two meter high earth embankment may vary between 1 to 2 million Euro per kilometre (Stoop, 2010), and the annual cost of maintaining the existing flood defence system reaches 1.4 billion Euro.

The macro-stability analysis of dikes is often debated and has changed drastically over the years. Most recent update dates from 2017, where the fundamental macro-stability analysis has been changed from an effective strength approach restricted by small deformations (2-5%) to an undrained strength approach applied to larger deformations according to the principles of Critical State Soil mechanics. The new guidelines however drastically changed the perception of Dutch engineers towards the stability of dikes since the new assessment would require major changes on flood defences which have been withstanding storms and high water levels for decades not to mention centuries. Additionally, it has been shown over the years in several studies that the strength of soils such as peats was highly underestimated. A certain level of apprehensiveness towards the new norms has therefore appeared in the eyes of many geotechnical engineers and the governing bodies for which clarity and better regulations are required.

In this Master thesis, the assessment of strength parameters of the dike stability reinforcement project between Gorinchem and Waardenburg in the South west of the Netherlands is studied as a case study towards either the confirmation of the current norms or towards a more optimised and less conservative choice of the strength parameters. This study was performed with the contribution and under supervision of Delft University of Technology and Royal Haskoning DHV. The structure of this thesis is as follows: first, a literature study is performed on the strength parameters assessment in chapter 1, the principles of the Critical State Soil Mechanics and the difficulties encountered in the determination of the strength parameters from laboratory tests in chapter 2. The laboratory results are then exploited in chapters 3 to 5. The next chapters focus on a more fundamental understanding of the considered material consisting of modelling the material behaviour in chapter 6. The conclusions and discussions on the findings are to be found in chapter 7, whilst the recommendations for future work and practices to be adopted in the assessment of strength parameters are shown in chapter 8.

Research objectives and questions

The main objective of this Master thesis is to better assess the strength parameters from laboratory testing in the evaluation of the macro-stability of flood embankments according to the recently introduced Dutch norms, and to better understand the general behaviour of the considered material in different laboratory tests. The following research questions where hence formulated:

- Is the strain softening experienced in the laboratory tests a result of the limitations of the tests at large displacements or is the softening true material behaviour?
- What are the limitations of the Classical Critical State Soil mechanics and hence the SHANSEP method if applied to field scenario's?
- Is the determination of Critical State strength parameters according to the 2017 Dutch norms applicable on Gorinchem Clay?
- Can the use of an isotropic non-associative elasto-plastic constitutive model with volumetric and deviatoric hardening or softening be used to model the behaviour of the material in question?
- How can the difficulties encountered in determining the parameters of the SHANSEP model from laboratory tests be remedied?

Chapter 1

Dike Design in the Netherlands

In this chapter, the general flood embankment design considerations and strength assessment are explained in section 1.1, with emphasis on the macro-stability of dikes. The pre-2017 macro-stability strength assessment and its limitations are discussed in section 1.2 whereas the current approach is explained in section 1.3.

1.1 Overview general design and macro-stability

The design of flood embankment is to be performed according to all the known failure mechanisms illustrated in figure 1.1.1 and loads such as hydraulic loads, traffic loads, soil self-weight and wind (Ministerie van Infrastructuur en Milieu, 2016). Biological (animal hollows) and climatic alterations (drought cracks) are also to be considered (Ministerie van Infrastructuur en Milieu, 2016). The aim of this study is to assess the macro-stability of a flood embankment i.e. case C and E in figure 1.1.1.

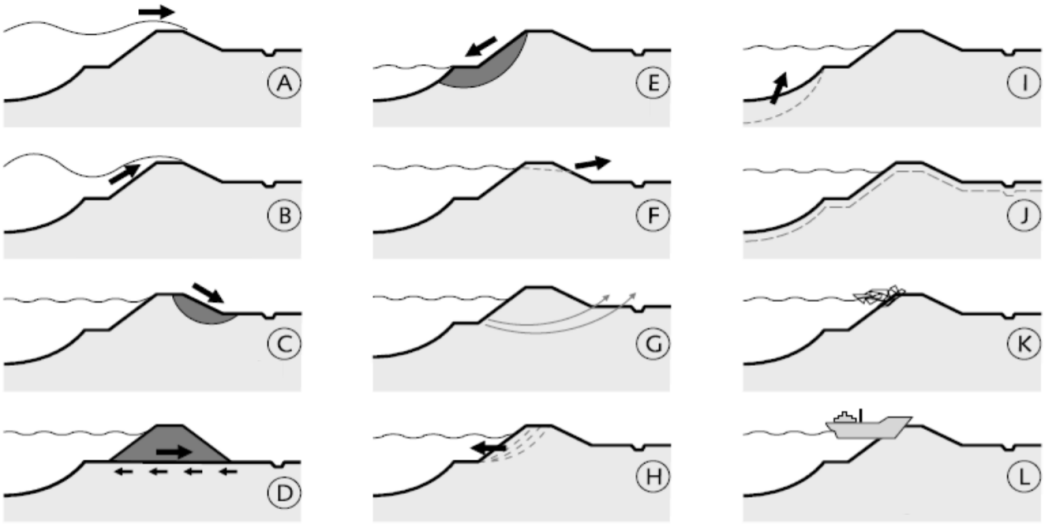

Figure 1.1.1: Failure mechanisms of flood embankments (Bakkenist, 2012).A: Run-over; B: Wave over-topping; C:Macro-instability inner slope; D: Sliding; E: Macro-instability outer slope; F: Micro-instability; G:Piping; H: Outer slope erosion; I: Foreshore erosion; J: Excessive settlement ;K: Ice damage; L: Ship collision

The macro-stability of a dike corresponds to the resistance of slope failure for both the hinterland and river or sea side. Besides the available strength of the dike body and soil underneath the dike, the macro-stability of a flood embankment is determined by the hydraulic boundary conditions. For a high water level, the available strength of the soil is reduced due to the rise of the

phreatic surface lowering the effective stresses in the soil (Ministerie van Infrastructuur en Milieu, 2016). In addition, the high water level may induce heave and bursting: this situation occurs when the stratigraphy consists of a non-permeable layer (clay) on top of a very permeable layer (sand) (Van Baars & Van Kempen, 2009), which is characteristic of most flood embankment scenario's in The Netherlands (Den Haan & Kruse, 2007). This phenomenon has the effect of further reducing the strength of the overall dike by affecting the strength at the toe of the embankment. For this scenario, the macro-stability towards the hinterland is critical (Ministerie van Infrastructuur en Milieu, 2016).
For a lowering water level, the previously induced pore pressures dissipate at a much slower rate than the water level does due to the low permeability of the dike material. As a consequence, the available strength of the material is similar, however the lowering of the water level causes the dike to load back to its non-buoyant self weight. In this case the macro-stability outside of the dike is critical (Ministerie van Infrastructuur en Milieu, 2016).
In the current norms, the macro-stability of an embankment is to be evaluated according to limit equilibrium methods. Several methods exist and each method may not give the most critical failure surface (Ministerie van Infrastructuur en Milieu, 2016). The guidelines therefore recommend to evaluate the macro-stability of the dike for each method and to consider the most critical case. The methods consist of the Bishop method, the Spencer-Van der Meij method and LiftVan method. In the Bishop method, the failure surface is assumed to be circular (see figure 1.1.2) and the equilibrium analysis is performed for vertical forces only (Ministerie van Infrastructuur en Milieu, 2016). For the Spencer-Van der Meij method, the failure surface may not be circular and the horizontal forces between slices are also considered (Ministerie van Infrastructuur en Milieu, 2016). In the LiftVan method, the failure surface is composed of two circular surfaces (active and passive) and a horizontal segment as shown in figure 1.1.3.
The input strengths in the slope stability analysis are the undrained shear strengths and are to be determined from laboratory tests (Ministerie van Infrastructuur en Milieu, 2016). Such tests are time consuming and expensive, they can therefore only produce a coarse mapping of the shear strength of the soil profile and overall dike project. These tests are therefore used to calibrate the parameters of the SHANSEP model described in section 1.3.1. These parameters can then be used to determine the undrained shear strength based on Cone Penetration test (CPT) measurements (Ministerie van Infrastructuur en Milieu, 2016). The use of the CPT enables to evaluate the strength of the soil along the whole soil profile and at many locations.

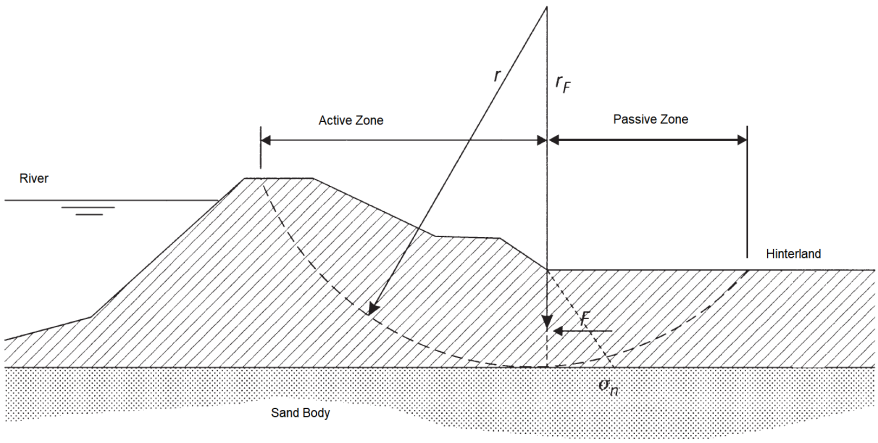

Figure 1.1.2: Visualisation of slope instability with a circular failure surface (Kremer et al., 2001)

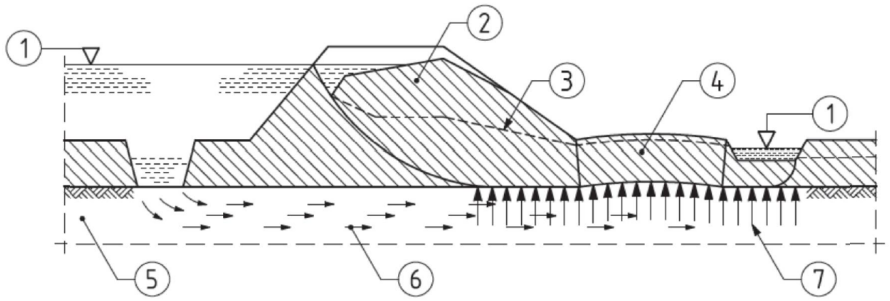

Figure 1.1.3: LiftVan limit equilibrium method (Ministerie van Infrastructuur en Milieu, 2016).1:Water level; 2: Dike body; 3:Phreatic surface; 4:Horizontal dike section; 5:Sand layer; 6:Groundwater flow; 7:Water pressures

1.2 The 'traditional' macro-stability strength assessment and limitations

The 'traditional' dike macro-stability analysis in the Netherlands is based on the Mohr-Coulomb model with an effective strength approach: the strength parameters (c and ϕ') are determined from drained triaxial tests for strain levels of 2 to 5% along estimated pore pressures (Stoop, 2010). In the engineering practice, this introduces a degree of variability in the strength parameter definition for limit equilibrium macro-stability analysis from one project to another, however engineers tend to stick to strength parameters at 2% strain by means of precaution which as a consequence leads to over-conservative design parameters (Stoop, 2010).
This approach is applied for cases exhibiting small strains, however for a structure inducing a large change of geometry and displacements, the stress redistribution and experienced strains produces so called pre-shearing (van Duinen, 2014; Zdravković & Jardine, 2001), where a soil element at the toe of the dike experiences significant stress rotation and shearing. This aspect causes in case of the 'traditional' methods an underestimation of the shear strength for normally consolidated conditions for multi-stage structures (Zwanenburg, 2016). For over-consolidated conditions, the available undrained shear strength decreases once the experienced strains have passed the peak strength. In this case, the undrained shear strength is over-estimated (Ministerie van Infrastructuur en Milieu, 2016).
Another issue with the 'traditional' strength parameter assessment concerns the strain mode of the embankment (Ladd, 1991): the peak shear strength of different soils does not necessarily occur for the same strains in a macro-stability analysis of a dike due to differences in soil types, stress history, stress conditions and direction of principle stress. Peak strengths along the failure surface therefore do not necessarily occur at the same strain level, which results in an over-estimation of the shear strength (Ladd, 1991).
For the cases in which the undrained behaviour is governing (clay and peat), shear induced pore pressures considerably affect the shear stress the soil can endure without failing, which is not taken into account with a Mohr-Coulomb and effective stress approach (Zwanenburg, 2016). These limitations called for an improved method in selecting strength parameters for the macro-stability of water retaining ground constructions. It has furthermore been recognised that the failure of dikes is better represented and safer for undrained conditions (Ministerie van Infrastructuur en Milieu, 2016).

1.3 Current Dutch macro-stability assessment: Undrained Critical State strengths

In 2016, the Dutch Ministry of Infrastructure and Environment published new guidelines and regulations for assessing the macro-stability of water retaining ground constructions for the year 2017. These new regulations are meant to answer the shortcomings of the previous macro-stability methods as previously illustrated. In this section, the principles of the stability assessment are introduced and the strength parameter determination are explained.

1.3.1 Principles of critical state soil mechanics and SHANSEP method

The main changes in the water retaining ground construction regulations of 2017 concern the drainage conditions and soil model to be considered: soils are to be modelled according to the Critical State Soil Mechanics and soils which feature low permeability (peats and clays) are to be modelled under undrained conditions whereas soils with high permeability (sand) are to be modelled under drained conditions (Ministerie van Infrastructuur en Milieu, 2016). Additionally, the principles of active, direct and passive shearing according for strain mode developed by Ladd (1991) are to be considered for the concerned sections of the failure surface (see figure 1.3.1), that is: parameters from triaxial compressions tests (TC) are to be determined for the active zone, direct simple shear (DSS) test for the direct shear zone and triaxial extension (TE) for the passive zone.

The critical state of a soil is the concept that a soil will reach a constant state when distorted sufficiently for which the soil flows as a frictional fluid (Schofield & Wroth, 1968) and has strain independent shear strength. The critical state is independent of the initial states and is soil specific (Atkinson et al., 1993; Lupini, Skinner, & Vaughan, 1982), and is independent of pre-shearing (Ministerie van Infrastructuur en Milieu, 2016). Physically speaking, the critical state is achieved when the soil remains at constant volume whilst shearing and is associated with the turbulent flow of the soil particles (Atkinson et al., 1993). This is equivalent to reaching constant plastic volumetric strains whilst the deviatoric plastic strains increase steadily, since the strain hardening or softening of the soil is plastic volumetric strain dependent only (Wood, 2014). By strain hardening or softening it is implied the material's strength increases or decreases whilst it is sheared. For sands and generally soils with rotund particles, the critical state corresponds to the residual state (Atkinson et al., 1993). This isn't the case for clays which consist of flat particles and develop laminar flow when the orientation of these flat grains have become parallel: the residual state can then be significantly different than the critical state (Atkinson et al., 1993). The critical state model inherently describes the behaviour of the soil and links the shear strength with compression, dilation, changes of volume and shear induced pore pressures in terms of effective stresses and stress history (Ministerie van Infrastructuur en Milieu, 2016).

The SHANSEP model (Stress History and Normalised Soil Engineering Properties) was therefore introduced in order to determine the undrained shear stress of a soil according to the critical state theory (Ministerie van Infrastructuur en Milieu, 2016). The method is based on the Cam-Clay model, which states that there is a logarithmic relationship for the change in void ratio in isotropic compression and unloading (Atkinson et al., 1993). One of the assumptions made for the Cam-Clay model is that mechanically over-consolidated behaviour represents all preconsolidation pressure mechanisms (i.e. plastic volumetric strains), which can induce errors with highly structured, sensitive clays and naturally cemented deposits (Ladd, 1991). This also applies to sand and silt rich clays, including löss and boulder clays, in the case of typical Dutch soils (Ministerie van Infrastructuur en Milieu, 2016). The SHANSEP model can only be applied to fairly regular deposits for which a well-defined stress-history can be obtained, the method is therefore not advised if random clay deposits are encountered (Ladd & Foott, 1974). The method also features limitations near the top of a highly desiccated 'drying crust' due to weathering and the difficulty involved in determining the OCR in that region (Ladd & Foott, 1974). Other effects which are not considered in the Cam-Clay model include anisotropic behaviour, creep, destructuration and softening (Wheeler,

Näätänen, Karstunen, & Lojander, 2003),(Knabe, 2010).
The undrained shear strength is described by the SHANSEP model by equation 1.3.1 (Ladd, 1991), where S is a friction parameter and corresponds to the normally consolidated (i.e. OCR=1) undrained shear strength ratio as given by equation 1.3.2. Parameter m relates the contribution of the OCR to the undrained shear strength. Parameter m can also be determined according to equation 1.3.3 where λ is the slope of the virgin compression line in logarithmic scale and κ the slope in unloading-reloading in logarithmic scale also (Ladd, 1991). Equation 1.3.3 is equivalent to $m = 1 - \frac{a}{b}$ using the Dutch parameter nomenclature (Ministerie van Infrastructuur en Milieu, 2016).

$$S_u = S\sigma'_{vi}OCR^m \tag{1.3.1}$$

$$S = (\frac{S_u}{\sigma'_{vi}})_{nc} \tag{1.3.2}$$

$$m = 1 - (\frac{\kappa}{\lambda}) = 1 - (\frac{a}{b}) \tag{1.3.3}$$

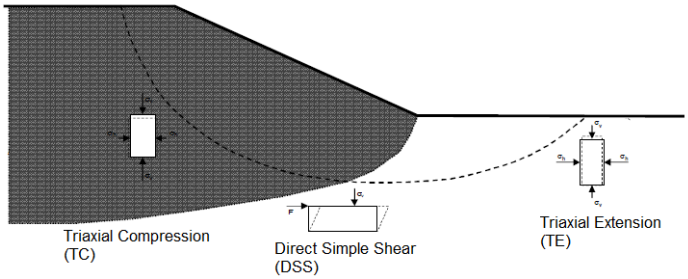

Figure 1.3.1: Active, Direct and Passive shearing in the failure surface of an embankment (Ministerie van Infrastructuur en Milieu, 2016).

1.3.2 Parameter selection according to the new Dutch guidelines

The Ministery of Infrastucture and Environment (2017) prescribes determining parameter S at critical state which corresponds to strain levels of 25% in a triaxial setup for clay and sand and 40% for peat in direct simple shear test. Since S is a parameter for normally consolidated soil, the undrained consolidated Triaxial test (TC) or undrained direct simple shear test (DSS) need to be performed on normally consolidated samples, for which the preconsolidation pressure is to be determined from a constant rate of Strain cell test (CRS test) and taken at point B as shown in figure 1.3.2. The downside of this method is that because of the high preconsolidation pressure, the sample's fabric may be altered and could well result in a loss of strength. On the other hand, point A is to be taken as the preconsolidation pressure when the parameter is used to determine the undrained shear strength with the SHANSEP formulation (equation 1.3.1). Point B corresponds to conditions of purely normal consolidation and is therefore a guarantee to have a purely normally consolidated sample in the triaxial or DSS apparatus, whereas point A is within the transition zone between normally and over-consolidated conditions and is therefore more conservative in determining the undrained shear strength from the over-consolidation ratio.
Parameter S can also be determined for over-consolidated samples by determining the over-consolidated undrained shear strength ratio following the same procedure as for a normally consolidated sample and reaching the expected vertical effective stress rather than the preconsolidation stress. The normally consolidated undrained shear strength ratio can then be determined by correlating results from the over-consolidated undrained shear strength with the over-consolidation ratio (OCR), as reported in figure 1.3.3. Since the tests may have to be conducted at low pressures, the inaccuracies of the measuring apparatus is more pronounced than for higher pressures. Also, several

samples are required for this method in order to perform a proper correlation, since each specific sample may have a slightly different S value, as shown figure 1.3.3.
Parameter m is to be determined in a CRS test in which parameters λ and κ can be determined. Similarly to the method to determine parameter S on the over-consolidated side, m can also be determined by back calculating the undrained shear strength of an over-consolidated soil using equation 1.3.1(Ministerie van Infrastructuur en Milieu, 2016). The results of both methods are slightly different (Ministerie van Infrastructuur en Milieu, 2016), and the current guidelines prescribe the first method as the method to determine the relevant strength parameters.

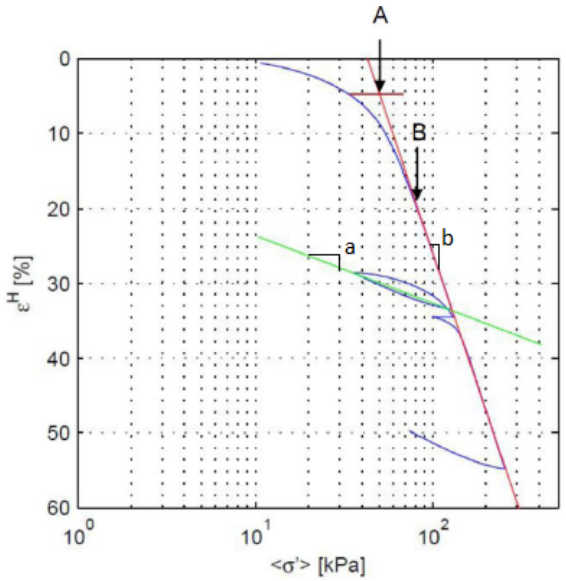

Figure 1.3.2: Stress-Strain curve for a typical CRS test. The horizontal line at point A corresponds to the strain at in-situ initial vertical effective stress σ'_{vi} and point B is the preconsolidation stress σ'_p (Ministerie van Infrastructuur en Milieu, 2016).

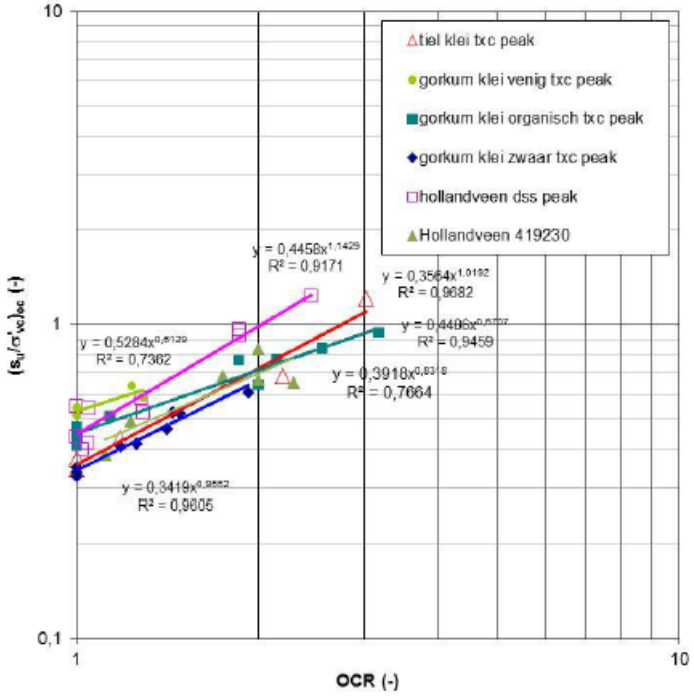

Figure 1.3.3: Correlations between the undrained shear strength ratio S and the overconsolidation ratio (Ministerie van Infrastructuur en Milieu, 2016).

Chapter 2

Classical Critical state soil mechanics and experimental practices

The first concepts of Critical state soil mechanics were introduced in 1.3.1. In this section, the concept is elaborated on further and the current practices in determining the Critical State parameters are explained. The use of laboratory equipment to determine these parameters comes with several issues, which are developed for each of the required laboratory tests in the parameter assessment according to the 2017 Dutch guidelines. Finally, a strategy is suggested in order to determine the parameters with better reliability and understanding.

2.1 Critical State fundamentals

The typical behaviour of a normally consolidated and overconsolidated clay sheared drained is given in figure 2.1.3. Normally consolidated and slightly over-consolidated soils are said to be on the 'Wet side' of Critical State whereas heavily over-consolidated soil are said to be on the 'Dry side' of Critical State (Atkinson et al., 1993). Figure 2.3(a) shows that soil on the Wet side of its Critical State features shear hardening, i.e. the soil becomes harder to shear at larger strains. The cause of shear hardening can be understood from figure 2.3(c) and 2.3(d) where the soil is compressing and therefore increasing the interlocking of the soil particles. In the case of a soil on the Dry side of its Critical State, the soil will initially harden and compress until reaching a peak shear strength after which the soil softens and dilates. The terminology 'Dry side' and 'Wet side' comes from the volumetric behaviour of the soil during shearing: a contractive soil will expel water during drained loading (i.e. wet) whereas a dilative soil will not (i.e. dry). During an undrained test, volume changes are not permitted since the pore water cannot flow out of the sample, instead positive excess pore water pressures develop for a soil on the wet side of Critical State or negative excess pore water pressures if on the dry side of critical.

According to the Critical State principle, the same soil will reach the same Critical State Line (CSL) regardless of its overconsolidation ratio and drainage conditions although the critical state strength is different, as show figures 2.4(a) and 2.5(a). The slope of the critical state line in compression tests (2.1.1) is given by the critical state parameter M given in equation 2.1.1 where $\phi_{cs}^{'}$ is the friction angle at critical state (Atkinson et al., 1993). Like the critical state strength, the critical state friction angle is unique to each soil. The soil on the Dry side of Critical state again reaches a peak strength before softening to the Critical State. In figure 2.4(a) the stress path is a function of q only for drained conditions as no shear induced pore pressure are generated, unlike shearing under undrained conditions as is shown in figure 2.5(a). In the υp' space, soils sheared undrained remain at constant specific volume υ since the volume change prevention is converted to excess pore pressure development (see figure 2.5(b)). Figure 2.4(b) shows that drained shearing is only a function of the specific volume υ, this is true only at constant p' shearing, which is not necessarily the case in most soil testing procedures. In the case of a normally consolidated soil and therefore on the Wet side, the initial state is on the Normally Consolidated line (NCL). If the

specific volume (or void ratio) is plotted as a function of the logarithm of the mean normal stress p, the NCL and CSL are linear and parallel lines according to the Modified Cam-Clay model (MCC) as shown in figure 2.1.2.

The critical state can additionaly be determined in an undrained triaxial test based on the excess pore pressure development: given that at Critical State the deviatoric stress to mean effective confining stress ratio (q/p') is a constant, so must also be the excess pore pressures as shown in equation 2.1.2. In incremental form (equation 2.1.3), the incremental deviatoric stress to mean incremental effective confining stress ratio must be zero and so must be the incremental pore pressures.

$$M = \frac{6\sin(\phi'_{cs})}{3 - \sin(\phi'_{cs})} \tag{2.1.1}$$

$$\frac{q}{p'} = \frac{q}{p-u} = \frac{\sigma_1 - \sigma_3}{\frac{\sigma_1 + 2\sigma_3}{3} - u} \tag{2.1.2}$$

$$\frac{dq}{dp'} = \frac{dq}{dp - du} = \frac{d\sigma_1 - d\sigma_3}{\frac{d\sigma_1 + 2d\sigma_3}{3} - du} \tag{2.1.3}$$

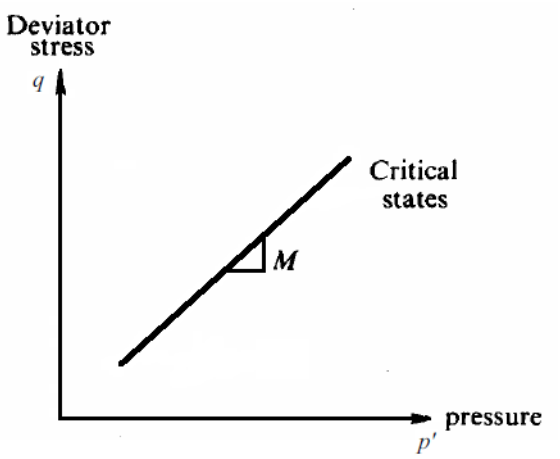

Figure 2.1.1: Critical state line and Critical state parameter M

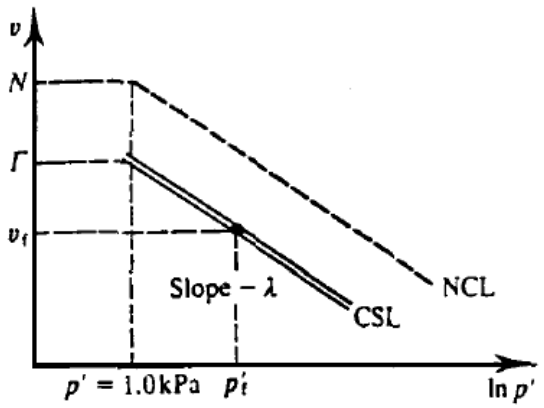

Figure 2.1.2: Critical state line and Normal Compression line according to the Modified Cam Clay model

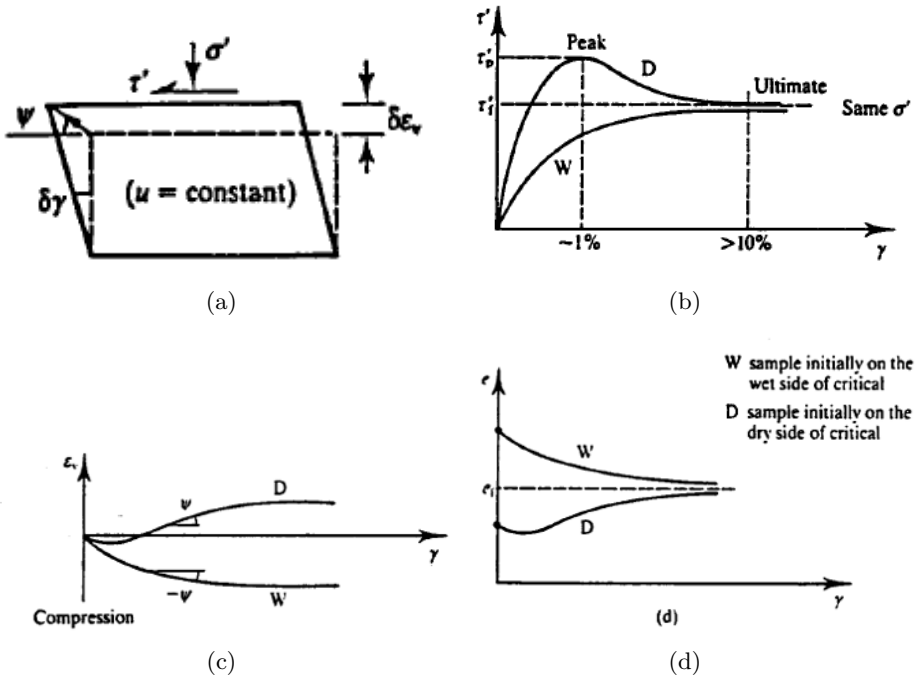

Figure 2.1.3: Typical behaviour of clay in a drained shear test initially on the dry and wet side of the Critical state (Atkinson et al., 1993).

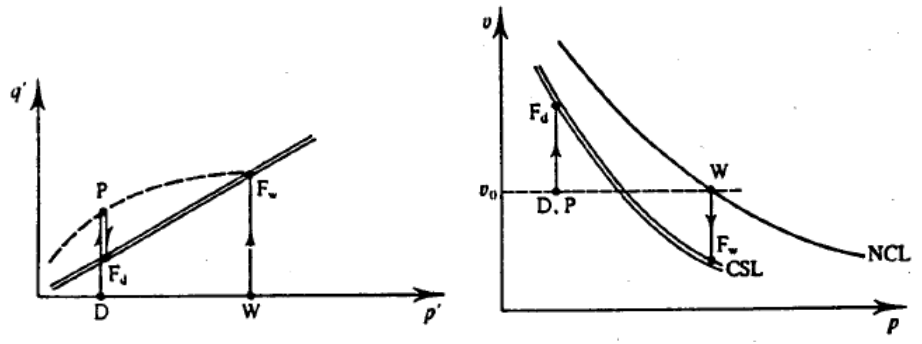

Figure 2.1.4: Behaviour of an OC and NC under drained conditions at constant p'(Atkinson et al., 1993).

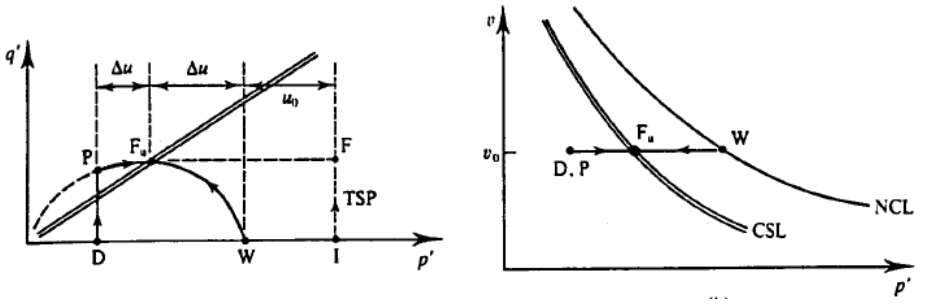

Figure 2.1.5: Behaviour of an OC and NC under undrained conditions (Atkinson et al., 1993).

2.2 Determining Critical State in practice

The 2017 Dutch guidelines recommend determining the Critical state parameters for Triaxial Compression, Direct Simple Shear and Triaxial Extension in order to comply with the strain compatibility and ADP method developed by Ladd (1991). The specific conditions and issues of these tests are hereby developed.

2.2.1 Determining the Critical State for soft soil using the Triaxial test

In practice it often appears to be tricky to find the critical state using typical triaxial apparatus for a soft soil such as clay or peat: the imposed boundary conditions from the end restraints in the Triaxial apparatus causes stress and strain non-homogeneities as was demonstrated by Chatzis (2018) and Muraro (2019). The friction at the sample-porous stone interface in the triaxial apparatus causes the formation of so-called 'dead wedges' in which the deformations are restricted compared to the free failure surface, in addition to reducing the free failure zone of the sample. As axial strains increase, the dead zones may merge and force lateral expansion around the perimeter of the sample (Muraro, 2019). These effects are expected to be of increasing relevance for high frictional and compressible materials. For a soil on the dry side, thin distinct discontinuities and slip surfaces may develop, in which the soil is subjected to intense shearing and is able to change volume (Atkinson et al., 1993). The resulting non-homogeneity of shear strains and volumetric strains of the tested soil sample causes the test to be unreliable due to the difficulties in determining the specific volume in and around the slip surfaces for a drained test. This is especially true if deformations are measured externally (Wood, 2014) which is often the case in standard laboratory tests. In an undrained test, the stress inhomogeneity causes additional excess pore pressure development, especially for a highly over-consolidated soil sample where the stresses and deformations are concentrated at the discontinuities formed whilst shearing the material. On the other hand, a soft soil on the wet side of critical or lightly over-consolidated tends to locally compress on straining and harden the material by draining excess pore water in the case of a drained test (Atkinson et al., 1993). This again causes issues in determining the specific volume of the segment of soil at critical state. For an undrained test, the stress-inhomogeneity causes local pore pressure accumulation which reduces the strength of the tested sample. In order to reduce the effects of the porous stone friction, soil samples prepared to be tested in triaxial setups are made long and slender.

The main assumption made for an undrained test is the constant water content or void ratio within the sample. Local drainage can however still occur from the intense shearing zones to the less intense sheared zones and vice versa, which in terms can result in false interpretation of the laboratory results (Atkinson et al., 1993). For clays this assumption is even more problematic since the effects of undrained creep are completely neglected in addition to the fact that strain rates are often minimized as these result in more conservative measurements of the shear strength. For undrained conditions, the measurement of excess pore-pressures can be unreliable as the external measurement is often an average on the overall sample, especially for soils on the dry side which have very localised shear zones.
The results are even more problematic for larger strain levels, where the stress and strain non-uniformities are magnified: the accumulation of deformations causes greater uncertainties in determining the cross-sectional area on which the loads are applied to as illustrated in 2.2.1. The consequences for a discontinuous sheared sample (highly over-consolidated sample) is an under-estimation of the applied deviatoric stress due to cross-sectional reduction and an over-estimation of the deviatoric stress for a bulging sample. This effect of bulging is furthermore accentuated by the long and slender nature of the sample. As shown by Chatzis (2018) and as implemented in the Dutch guidelines, the dimensions of the sample are optimised in order to reduce these effects. At very large axial strains (larger than 20 %) soft soil samples tested from the wet side have been witnessed to first bulge (figure 2.2(a)), therefore increasing the cross-sectional area on which the normal load is applied, followed by the formation of discontinuities along the sample at the pe-

riphery of the loading pistons causing a cross-sectional reduction of the sample as shown in figure 2.2(b). The discontinuities formed under these conditions are generally not of the same nature as the formation of discontinuities for highly over-consolidated conditions as shown in figure 2.2(c) where the discontinuities does not protrude deeply within the sample as opposed to figure 2.3(b) for a highly over-consolidated sample. Highly over-consolidated clays tested under undrained conditions are generally observed to either feature strong crossing discontinuities (figure 2.3(a)) or single discontinuities (figure 2.3(c)). Lightly over-consolidated clay samples tend to have a mixed failure mechanism showing both bulging and the formation of discontinuities 2.3(d) altough some may only produce bulging.
In order to remedy against these issues, many techniques have been used in (Ehrgott, 1971) and for peats in (Muraro, 2019) to correct for the cross-sectional changes during testing, however the choice of the correct method to be used is highly dependent on the stress history, compressibility, dimensions, deformation mode and strain level of the tested sample. Another aspect is the strain rate which is chosen for during undrained shearing: higher strain rates result in larger shear strengths for the same tested material by up to 10% per strain rate order of magnitude (Sheahan, Ladd, & Germaine, 1996; Zhu & Yin, 2000; Gens, 1982). To remedy against this issue, the current guidelines recommend using an axial strain rate of 1% per hour or lower should the permeability of the material be very low (Ministerie van Infrastructuur en Milieu, 2016).

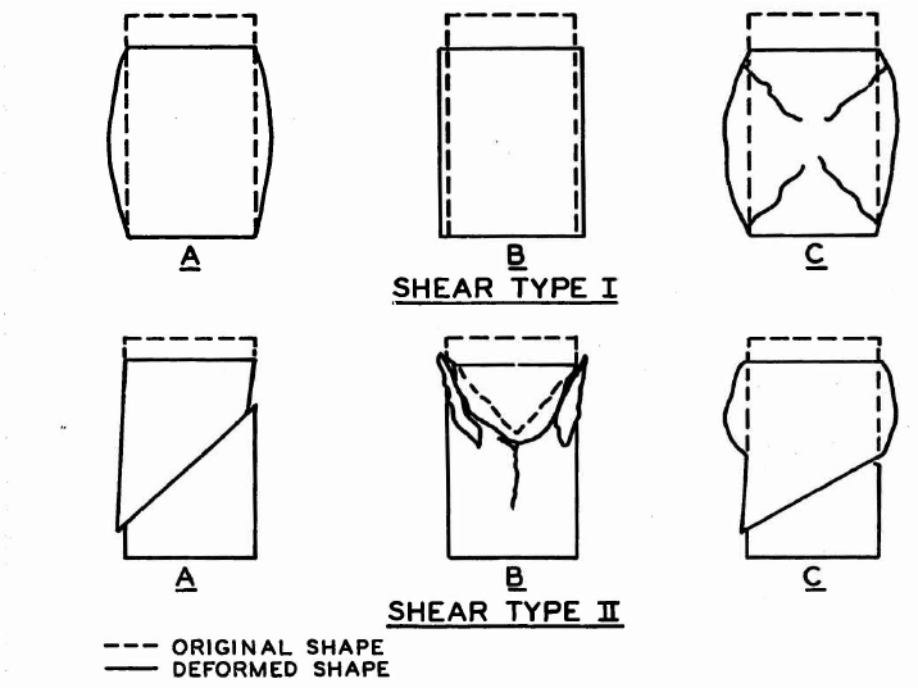

Figure 2.2.1: Shapes of failed specimens in a triaxial test (Ehrgott, 1971)

(a) Sample TG421.+094_B_BUT_mo-19b featuring sample bulging

(b) Sample TG421.+094_B_BITA_mo-16a featuring sample bulging and formation of discontinuities

(c) Sample cross-section TG421.+094_B_BITA_mo-16a featuring sample bulging and formation of discontinuities

Figure 2.2.2: Typical deformation mechanisms of Gorinchem Clay tested in undrained triaxial from the wet side

(a) Sample TG421.+093_B_MBIB_mo-11b featuring the formation of discontinuities

(b) Sample cross-section TG421.+093_B_MBIB_mo-11b featuring the formation of discontinuities

(c) Sample TG421.+094_B_BUK_mo-25b featuring the formation of a single discontinuity

(d) Sample TG421.+093_B_MBIB_mo-15b featuring bulging and the formation of discontinuities

Figure 2.2.3: Typical deformation mechanisms of Gorinchem Clay tested in undrained triaxial from the dry side

2.2.2 Determining the Critical State for soft soil using the Direct simple shear (DSS) test

The Direct simple shear (DSS) test was introduced in as an improvement of the highly non-homogenous Direct shear test (DST) to simulate shearing along a horizontal plane (Ladd & DeGroot, 2003). Although the DSS has been reported to predict very reasonable estimates of the undrained shear strength for some soils (Ladd & DeGroot, 2003), in practice it may be tricky to determine the critical state for soft soils. Indeed, the DSS test features considerable strain non-homogeneities (Dounias & Potts, 1993; Grognet, 2011; Ladd & DeGroot, 2003; Hanzawa et al., 2007), excessive strain softening beyond 10 to 15% shear strain (Ladd & DeGroot, 2003), in addition to the fact that the rupture type is dependent on the stiffness of the vertical sides of the DSS apparatus (Budhu, 1984). Tejchman and Bauer (2005) additionally showed the shear zones of the tested sample at failure are wider and less intense at the external vertical boundaries than at the center of the sample, which is to some extend similar to stress and deformations inhomogeneities in the triaxial compression test shown in (Muraro, 2019) and (Chatzis, 2018) although the shear zone in the DSS is slightly tilted. One of the main disadvantages with the DSS apparatus is lack

of measurable variables, such as the direction of principle stress, giving a complete understanding of the stress state in the sample (Boylan & Long, 2008). Another drawback of the DSS apparatus regards the assumption of a horizontal failure mechanisms itself, as the failure mechanism may occur as a translation along horizontal or vertical planes as shown in figure 2.2.4. The failure mechanism which features the least resitance is generally the along the vertical plane and a soil element will tend to fail along the path of least resistance (Hanzawa et al., 2007).

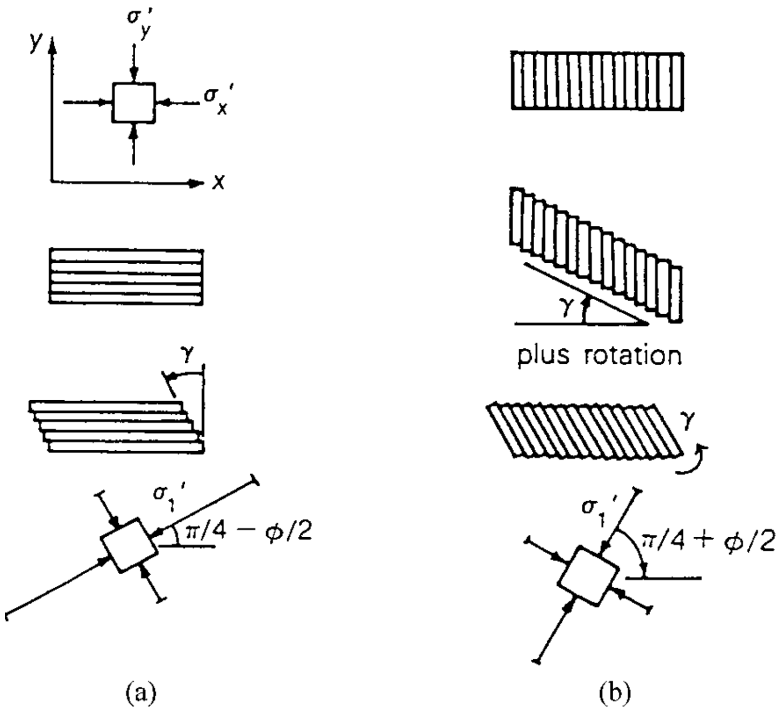

Figure 2.2.4: Possible failure mechanisms in an idealised Direct Simple Shear test for (a) horizontal failure surface and (b) vertical failure surface (Hanzawa et al., 2007)

2.2.3 Determining the Critical State for soft soil using the Triaxial Extension test

The Triaxial Extension test has similar issue in terms of stress non-homogeneity and deformations as the Triaxial Compression test discussed in section 2.2.1. Although the effects of end restraints has been studied for sand in Triaxial Extension (Wu & Kolymbas, 1991; Yamamuro & Lade, 1995; P. V. Lade & Wang, 2012; P. Lade, Yamamuro, & Skyers, 1996), very little is known about the effects of the boundary condition on fine grained materials. Wu and Kolymbas (1991) showed on sand that factors such as the inhomogeneous deformation and the effects of the rubber membrane have a larger effect on the results in Extension than Compression. The deformations in Triaxial Extention cause severe necking as shown in figure 2.2.5, which causes uncertainties in determining the true deviatoric stress experienced by the sample at large strains especially.

(a) test 2-102_13

(b) test 15-102_31

Figure 2.2.5: Typical deformation mechanisms of Gorinchem Clay tested in Undrained Triaxial Extension from the wet side

2.3 Strategy to find the Critical State

Due to the experienced uncertainties in determining the critical state using the available methods, an experimental strategy was required to narrow down the uncertainty and converge towards the true Critical State strength parameters and Critical State Line of the encountered soils.

The first step was to perform overconsolidated and normally consolidated undrained tests to approach the critical state from the dry and wet side. The second step was to approach the critical state line using drained tests: although the strength parameters have to be determined for undrained conditions as conform to the guidelines, the critical state line is the same for undrained and drained conditions due to the uniqueness of the critical state friction angle. The expected idealised stress paths in the deviatoric stress to mean effective stress space are represented in figure 2.3.2. The results can further be represented in the stress ratio η to axial strain space

and the excess pore pressure to axial strain space: both the stress ratio and excess pore pressures should converge towards a constant at a certain axial strain for both OC and NC tests. The main idea in using these different stress and strain representation is to dismiss test features in order to better understand the soil's true behaviour.

The outcomes of the critical state undrained shear strength of TC, DSS and TE are expected to be similar (Mayne, 1985; Prevost, 1979) and therefore are worth comparing although differences are to be expected since each method imposes different loading conditions, boundary conditions, strain rates and initial stress states (Mayne, 1985; Ladd, 1991). Additionally, the direction of major principle stress in a Triaxial Compression test is in the direction of the moving piston (vertical) and horizontal in Triaxial Extension, whereas the major principle stress in a DSS test is allowed to rotate freely as the test is executed, resulting in different undrained shear strengths for a cross-anisotropic soil (Abelev & Lade, 2004). The second step is therefore to compare the triaxial (compression and extension) and DSS results in order to better understand the material behaviour and test specific features. The DSS Critical State undrained shear strength is expected to be of intermediate strength between the undrained shear strength from TC and TE (Mayne, 1985), and the strength discrepancy between a Triaxial compression test, DSS and triaxial extension test are expected to reduce at high plasticity indexes for normally consolidated clays and silts (Ladd, 1991; Mayne, 1985). In order to compare the TC to the DSS results for different stress states, the normalised shear strength for Triaxial Compression for plane strain conditions is determined according to equation 2.3.1 (Koutsoftas & Ladd, 1985), where $\phi'_{mob,ps}$ is given in equation 2.3.2 assuming a Matsuoka-Nakai failure criterion (Wroth, 1984) (see figure 2.3.1). The axial strain can be converted in terms of shear strain according to equation 2.3.3 (Ladd & DeGroot, 2003).

$$(\frac{\tau}{\sigma'_{vc}})_{ps} = \frac{q \cos \phi'_{mob,ps}}{2\sigma'_{vc}} \tag{2.3.1}$$

$$\phi'_{mob,ps} = \frac{9}{8}\phi'_{mob,tc} \tag{2.3.2}$$

$$\gamma = 1.5\epsilon_a \tag{2.3.3}$$

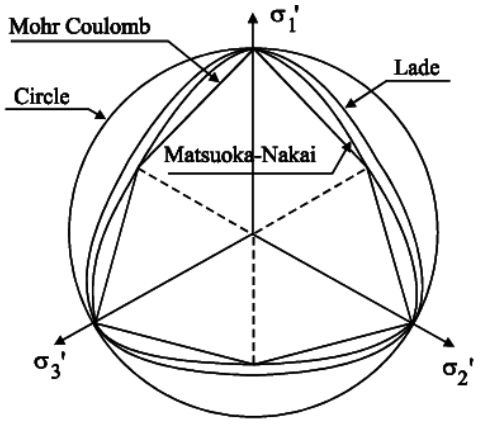

Figure 2.3.1: Failure surfaces in the deviatoric plane (Georgiadis et al., 2004)

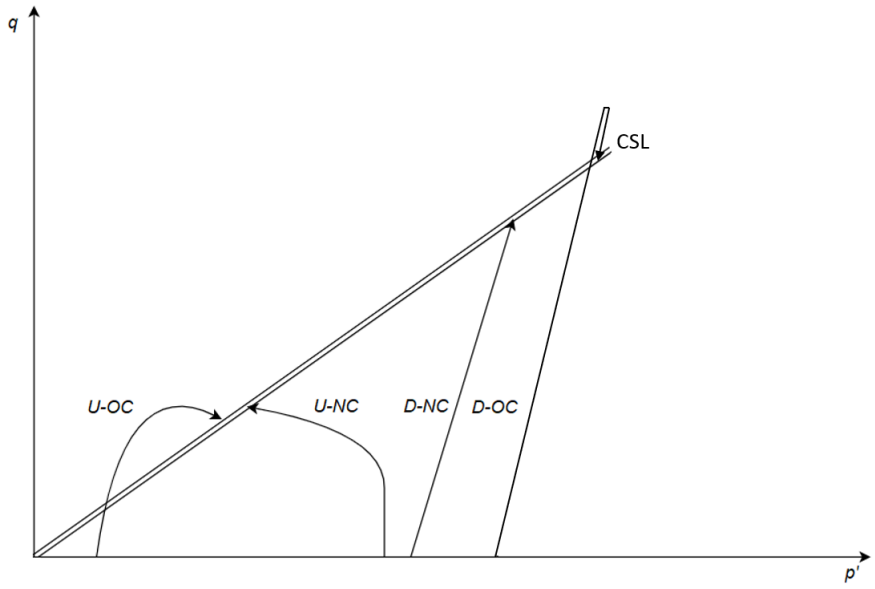

Figure 2.3.2: Effective stress paths for drained over-consolidated (D-OC), drained normally consolidated (D-NC), undrained over-consolidated (U-OC) soils and undrained normally consolidated (U-NC) soils.

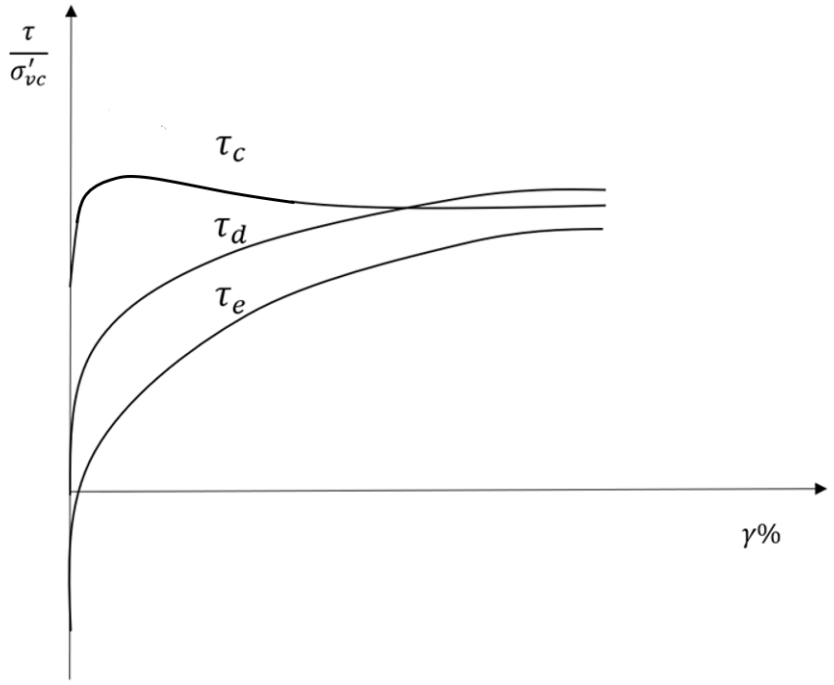

Figure 2.3.3: Idealised normalised shear stress versus shear strain for triaxial compression, direct simple shear and triaxial extension tests under plain strain, as in (Ladd, 1991)

.

The triaxial data can further be exploited according to the void ratio in the sample during testing as explained in section 2.1. This analysis can be extended by plotting the results as a function of axial strains and the confining pressure to equivalent confining pressure ratio where the equivalent confining pressure is defined as the pressure on the normal consolidation line at the same void ratio as that of the soil in a different state (Hvorslev, 1937). This ratio is expected to be a constant as the critical state line is assumed to be parallel to the virgin compression line and is expected to be quasi-equal to 2 (Wroth, 1984) as conform to the modified Cam-Clay model

and Classical Critical State theory (see figure 2.3.4). The idealised sample behaviour in the void ratio space is given in figure 2.3.5 and figure 2.3.6 for undrained and drained conditions respectively. The equivalent confining pressure can then be determined according to equations 2.3.4 for undrained normally consolidated conditions, 2.3.5 for undrained over-consolidated conditions, 2.3.6 for drained normally consolidated conditions and 2.3.7 for drained over-consolidated conditions, where b is the slope of the Normal Compression Line (NCL).

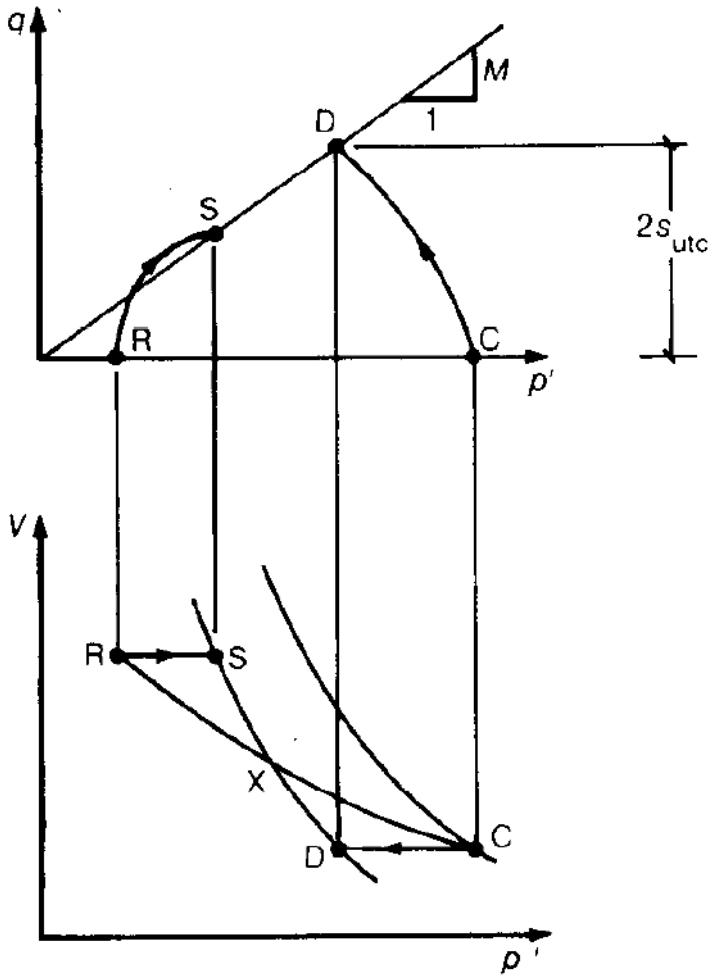

Figure 2.3.4: Idealised behaviour in the p'q space and corresponding response in the void ratio space according to the Modified Cam Clay model (Wroth, 1984)

.

$$p_{eq} = p_0 \tag{2.3.4}$$

$$p_{eq} = p_0 OCR(1-b) \tag{2.3.5}$$

$$p_{eq} = p_0 - \frac{e - e_0}{b} \tag{2.3.6}$$

$$p_{eq} = p_0 OCR(1-b) - \frac{e - e_0}{b} \tag{2.3.7}$$

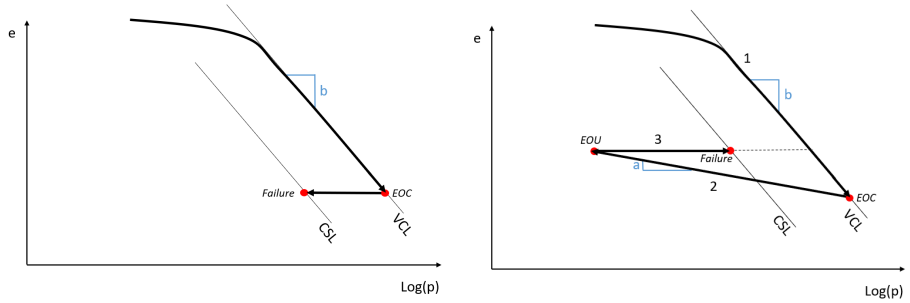

(a) undrained behaviour from the wet side (b) undrained behaviour from the dry side

Figure 2.3.5: Idealised sample behaviour in an undrained triaxial test in the void ratio space. EOC: end of consolidation, EOU: end of unloading.

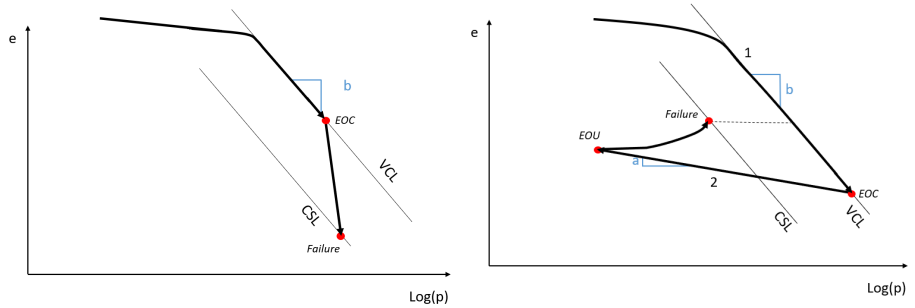

(a) drained behaviour from the wet side (b) drained behaviour from the dry side

Figure 2.3.6: Idealised sample behaviour in a drained triaxial test in the void ratio space. EOC: end of consolidation, EOU: end of unloading.

Chapter 3

Data overview and testing procedures

Laboratory tests were performed on samples at several detphs of the considered geotechnical unit at three different locations (figures 3.0.2 to 3.0.4) within the project boundaries (figure 3.0.1). The laboratory tests were mainly performed on the clayey layers as shown in figures 3.0.5 to 3.0.7, which show the stratigraphy and classification at these three locations. In the sample reference, TG stands for Tiel-Gorinchem, the first set of numbers to the hectometre marker of the dike section, followed by the distance in meters from this hectometer marker. The position of the sample normal to the dike is given by a set of letters as given in table 3.0.1 whereas the three numbers after the M refers to the core number which is divided again in intervals a,b and c. For each dike section several laboratory tests were performed on the core sections. These include Triaxial Compression tests (TC), Direct Simple Shear tests (DSS), Constant Rate of Strain tests (CRS), Oedometer tests and additional material property and index tests to determine the Atterberg limits, grain size distribution, volumetric weights and void ratio of the tested sample. These laboratory tests were performed by two Dutch geotechnical laboratories Inpijn Blokpoel Ingenieurs and Wierstema & Partners, where each laboratory performed the aforementioned tests on separate dike sections. In addition, Triaxial Extension (TE) tests were performed by the research institute Deltares.

Table 3.0.1: Sample denomination

MBIB	BUTA	BUT	BUK	AL	BIT	BITA
crest	outer slope	outer toe	outer crest	hinterland	inner toe	inner slope

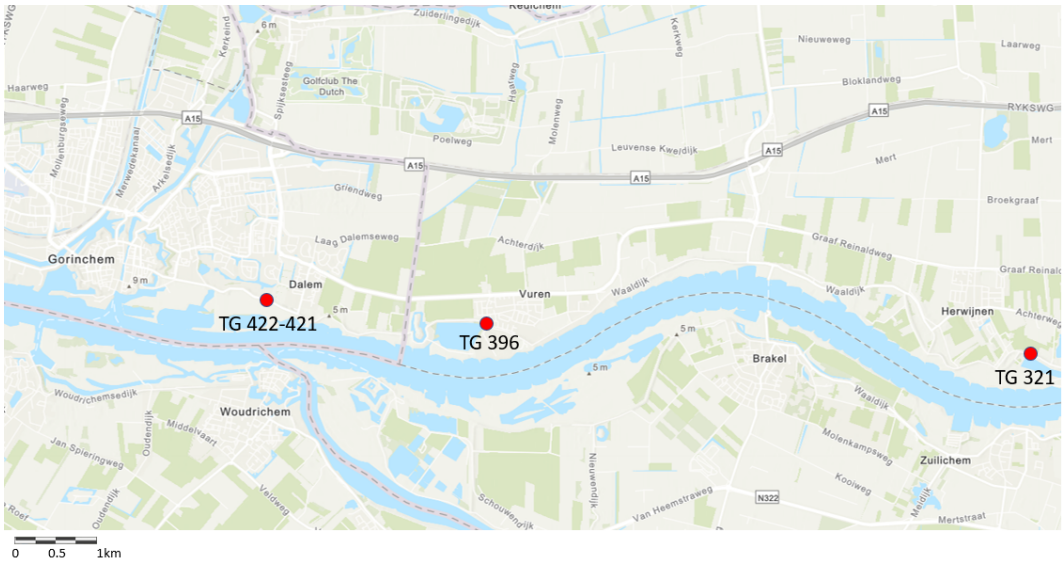

Figure 3.0.1: Locations of sampled dike sections

.

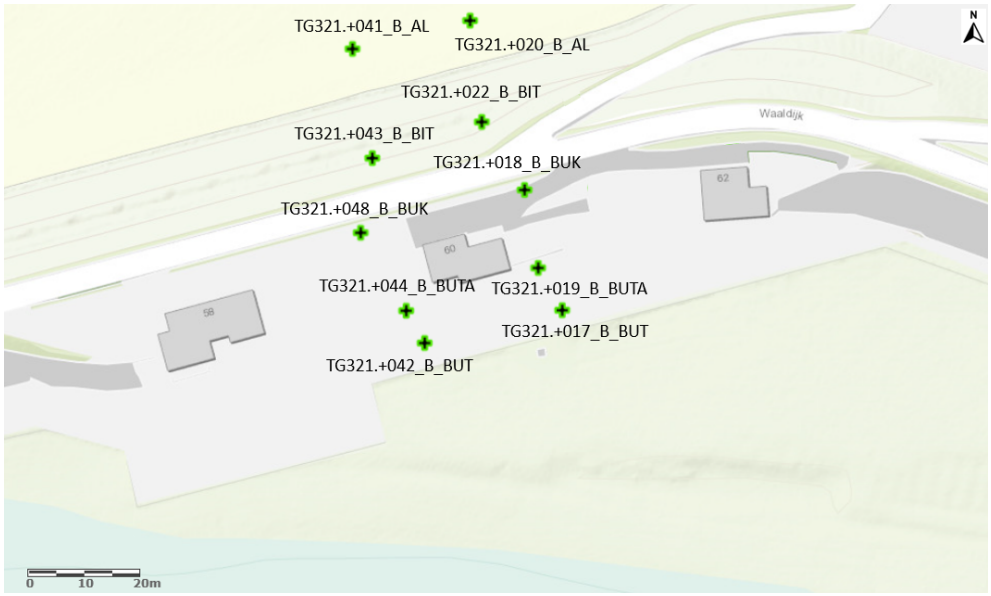

Figure 3.0.2: Location of samples in dike section TG321

.

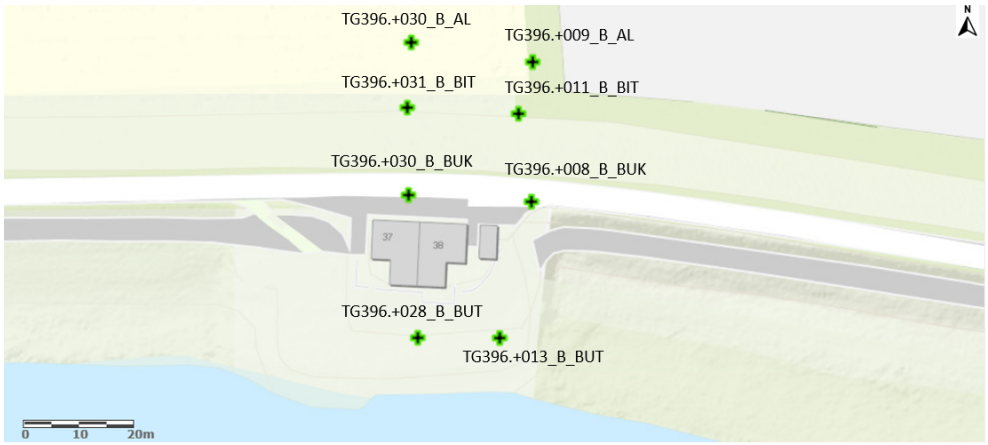

Figure 3.0.3: Location of samples in dike section TG396

.

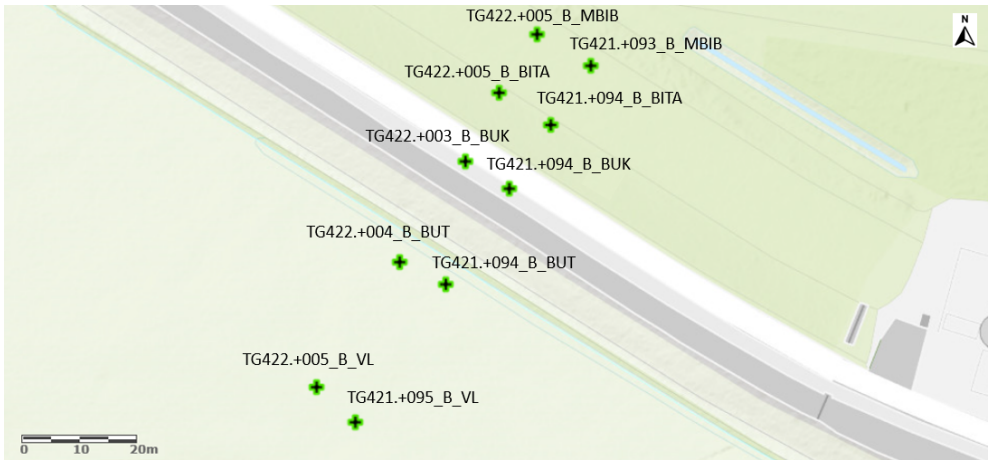

Figure 3.0.4: Location of samples in dike section TG422-421

.

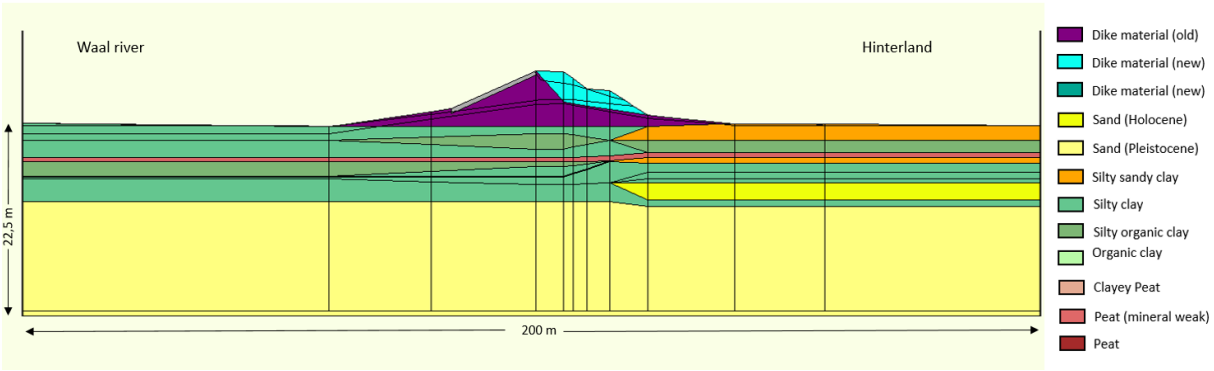

Figure 3.0.5: Soil Classification and Cross-section at dike section TG321

.

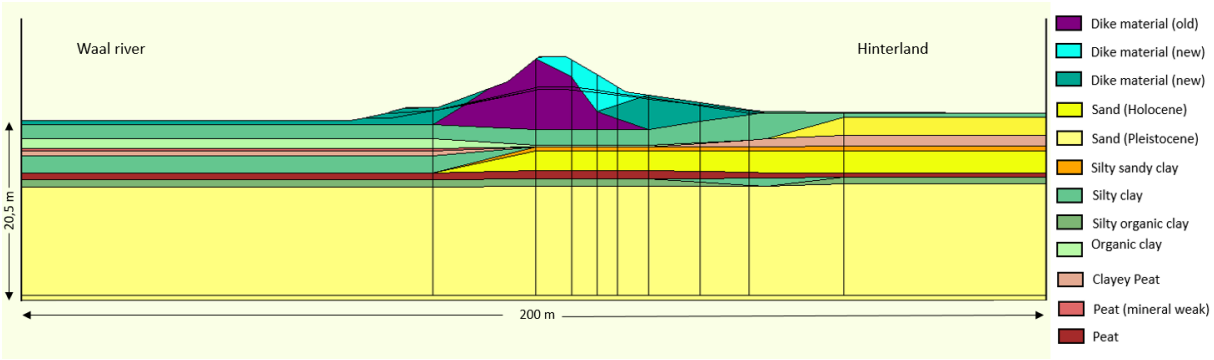

Figure 3.0.6: Soil Classification and Cross-section at dike section TG396

.

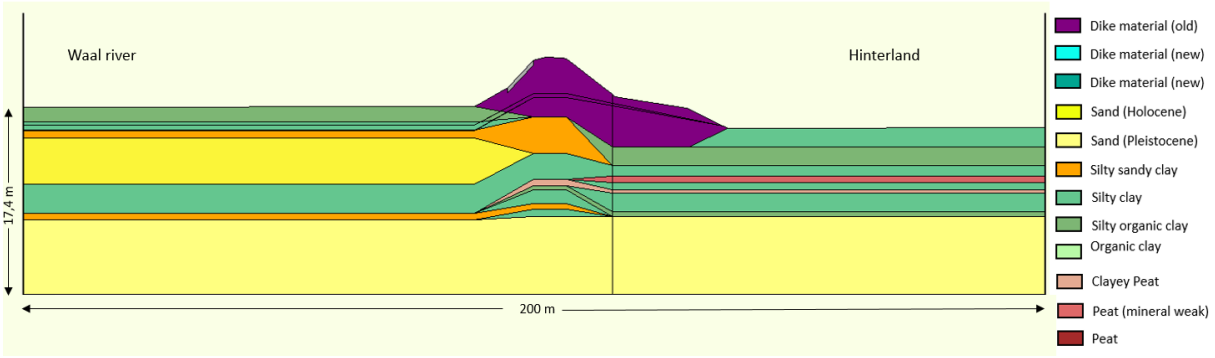

Figure 3.0.7: Soil Classification and Cross-section at dike section TG422

.

3.1 Material properties

The grain size distribution and classification were determined for the samples tested in the Triaxial Compression tests of dike section TG422 (see figure 3.1.1). The grain size distribution and classification show that the Gorinchem Clay is in reality (in most cases) a silt dominated soil ranging from 20 to 70% and a mean of 56% with clay fraction ranging from 0 to 40% and a mean of 24%, organic content ranging from 5 to 42% with a mean of 12% and a sand fraction from 1 to 54% with a mean of 8%. The volumetric weights of the samples were determined for all of the Triaxial (compression and extension) and DSS tests. The Atterberg limits were determined for both the Triaxial Compression tests and DSS tests. The Casagrande Plasticity chart for the Triaxial

Compression and DSS tested samples are given in figure 3.1.2. The Atterberg limits are usually determined on clays without organic content, however the inclusion of organic matter increases the Plasticity index (Zentar, Abriak, & Dubois, 2009) resulting in particularly large Plasticity Indexes.

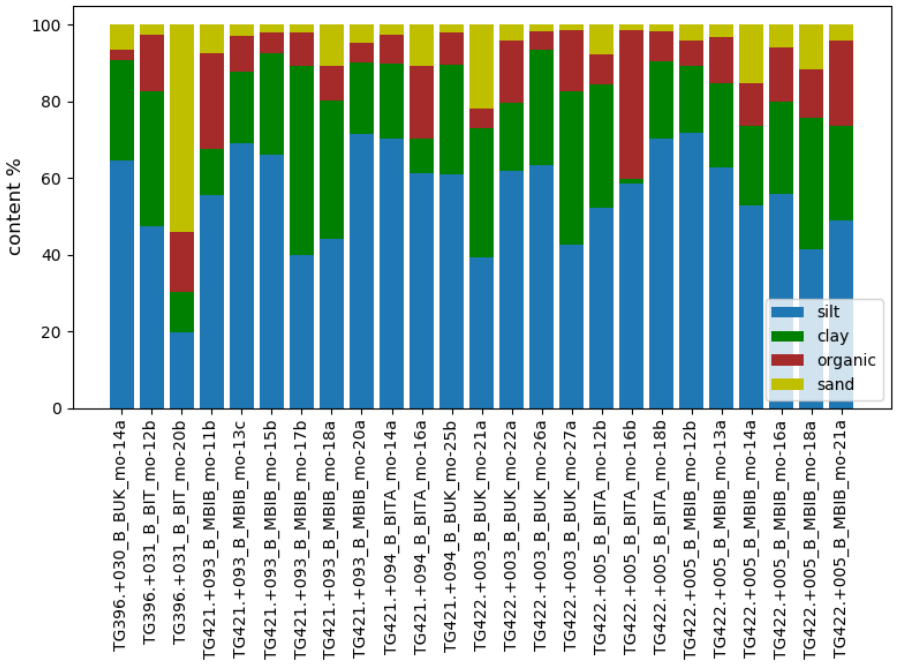

Figure 3.1.1: Sand, silt, clay, and organic content of the samples tested in the triaxial apparatus

.

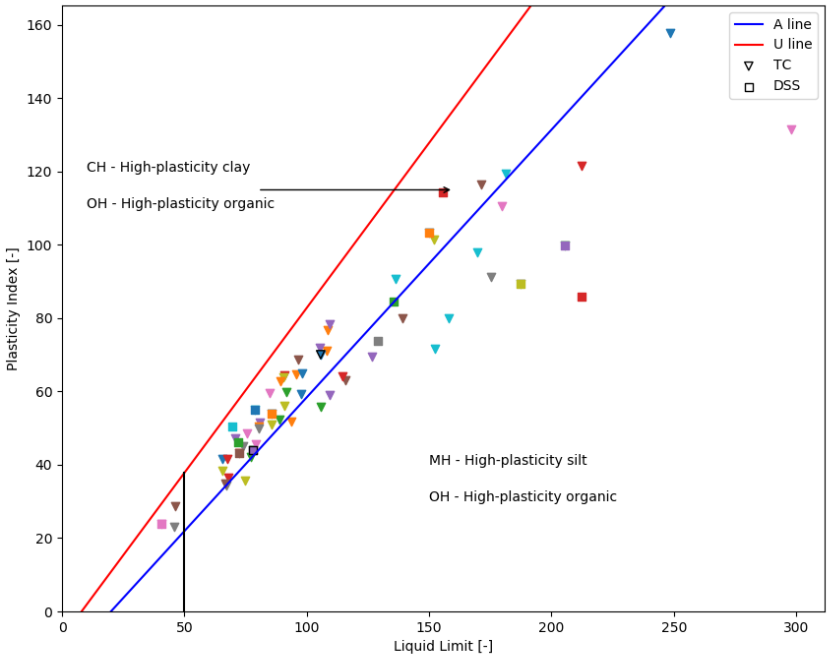

Figure 3.1.2: Casagrande Plasticity chart for Triaxial Compression and DSS tested samples

.

3.2 Triaxial Compression tests

The Triaxial Compression tests were performed for samples of initial heights of 100 mm and initial diameter of 50 mm. The samples were first isotropically consolidated with a back pressure of 300 kPa and then brought to K_0 conditions in the case of normally consolidated tests (anisotropic consolidation). The consolidation was performed within three days to limit the effects of creep, or when the excess pore pressures didn't exceed 1 kPa within 10 minutes after the drainage valves are closed (Ministerie van Infrastructuur en Milieu, 2016). As specified by the current Dutch guidelines, samples with height to diameter ratio lower than 1.8 and larger than 2.2 after consolidation were considered as non-conform tests in order to limit the effects described in section 2.2.1. The coefficient of earth pressure at rest K_0 was chosen as 0.35 for volumetric weights lower than 14 kN/m^3 and 0.45 for volumetric weights higher than 14 kN/m^3 as is specified in the current norms. For over-consolidated conditions the K_0 values were determined according figure 3.2.1 (Ministerie van Infrastructuur en Milieu, 2016). The samples then were brought to failure at strain rates ranging from 0.3 to 1.0 % axial strain per hour according to the required consolidation period as specified in NEN 5117 (Ministerie van Infrastructuur en Milieu, 2016). A correction for the effects of drainage strips and the membrane was applied using gelatine cores sheared to the same axial strain as the real tests following (Greeuw, Adel, Schapers, & Haan, 2001): the measured shear strength of the gelatine and drainage strips is later subtracted from the test measurements. The heights and diameters of the samples at the end of consolidation were measured and photographs of the failed samples were taken, for which the failure mode was determined. The initial void ratio was determined prior to the test and estimates of the void ratio for each loading stage were provided based on the measurements of expelled or absorbed pore water. The test properties of each tested sample are given in tables 3.2.1 to 3.2.3.

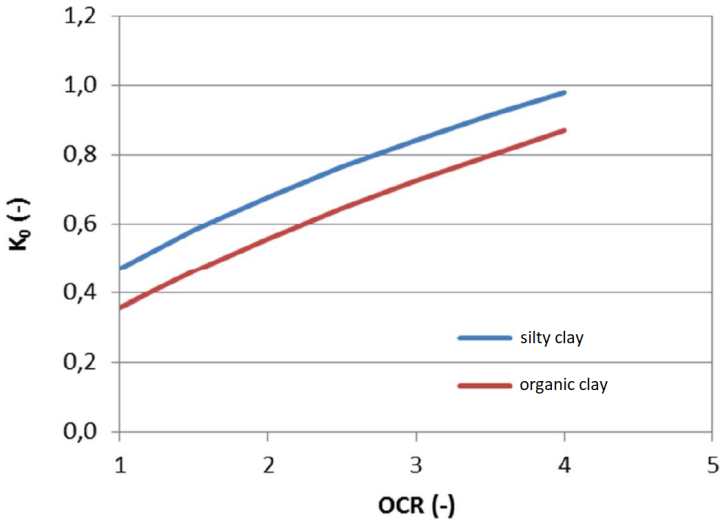

Figure 3.2.1: Coefficient of earth pressure at rest K_0 to be considered for triaxial tests

Table 3.2.1: Triaxial compression test properties of samples from dike section 7h

Name test	Test type	OCR [-]	Test validity	Failure mode	K0 [-]	Strain rate [%/hour]	PI %
TG321.+017_B_BUT_M011-a	U-NC	1	False Test	/	0.35	0.14	103
TG321.+017_B_BUT_M014-a	U-OC	3.0	False Test	O/	0.93	1.02	/
TG321.+017_B_BUT_M015-a	U-NC	1	OK Test	O	0.45	0.96	76
TG321.+017_B_BUT_M017-a	U-NC	1	False Test	O	0.35	0.34	99
TG321.+017_B_BUT_M018-a	U-NC	1	OK Test	O	0.45	1.03	43
TG321.+017_B_BUT_M019-a	U-NC	1	OK Test	O	0.45	0.99	51
TG321.+017_B_BUT_M020-a	U-NC	1	False Test	O/	0.35	0.95	116
TG321.+018_B_BUK_M007-a	U-NC	1	False Test	O/	0.45	0.99	23
TG321.+018_B_BUK_M021-a	U-NC	1	False Test	O	0.35	0.97	89
TG321.+018_B_BUK_M025-a	U-OC	3.9	OK Test	X	0.88	1.03	/
TG321.+019_B_BUTA_M016-a	U-NC	1	OK Test	O	0.45	1.04	56
TG321.+019_B_BUTA_M018-a	U-OC	3.8	OK Test	O/	0.86	0.95	/
TG321.+019_B_BUTA_M019-a	U-NC	1	False Test	O	0.45	1.0	71
TG321.+019_B_BUTA_M020-a	U-NC	1	OK Test	O	0.45	0.99	41
TG321.+019_B_BUTA_M021-a	U-OC	3.8	OK Test	X	0.88	0.95	71
TG321.+019_B_BUTA_M022-a	U-OC	3.4	False Test	O/	0.94	1.0	55
TG321.+020_B_AL_M005-a	U-NC	1	OK Test	O	0.45	0.99	64
TG321.+020_B_AL_M008-a	U-NC	1	OK Test	O	0.45	1.0	47
TG321.+020_B_AL_M012-a	U-NC	1	OK Test	O	0.45	1.0	68
TG321.+022_B_BIT_M013-a	U-NC	1	OK Test	O	0.45	1.01	59
TG321.+022_B_BIT_M017-a	U-NC	1	OK Test	O	0.42	0.98	34
TG321.+022_B_BIT_M019-a	U-OC	nan	False Test	O/	0.96	1.01	63
TG321.+022_B_BIT_M021-a	U-NC	1	False Test	O	0.45	0.94	54
TG321.+022_B_BIT_M023-a	U-NC	1	OK Test	O	0.45	0.61	54
TG321.+022_B_BIT_M024-a	U-OC	3.2	OK Test	O/	0.96	0.95	62
TG321.+041_B_AL_M007-a	U-NC	1	OK Test	O	0.45	0.97	59
TG321.+041_B_AL_M008-a	U-OC	2.4	False Test	O/	0.89	1.02	121
TG321.+041_B_AL_M012-a	U-NC	1	False Test	O	0.45	0.58	78

O: bulging; /:single discontinuity; X: several discontinuities
U: Undrained Test; D: Drained Test

Table 3.2.2: Triaxial compression test properties of samples from dike section 10b

Name test	Test type	OCR [-]	Test validity	Failure mode	K0 [-]	Strain rate [%/hour]	PI %
TG396.+028_B_BUT_M013-a	U-NC	1	False Test	O/	0.35	0.53	/
TG396.+028_B_BUT_M022-b	U-OC	3.3	False Test	/	0.93	1.02	/
TG396.+030_B_AL_M018-a	U-NC	1	False Test	O	0.35	0.51	/
TG396.+030_B_BUK_mo-14a	U-NC	1	False Test	O	0.45	0.76	28
TG396.+030_B_BUK_mo-28b	U-NC	1	False Test	O	0.44	0.23	131
TG396.+030_B_BUK_mo-29a	U-OC	3.5	OK Test	/	0.84	0.79	91
TG396.+031_B_BIT_mo-12b	U-NC	1	False Test	O/	0.47	0.37	101
TG396.+031_B_BIT_mo-20b	U-NC	1	False Test	O/	0.46	0.25	97

O: bulging; /:single discontinuity; X: several discontinuities
U: Undrained Test; D: Drained Test

Table 3.2.3: Triaxial compression test properties of samples from dike section 12g

Name test	Test type	OCR [-]	Test validity	Failure mode	K0 [-]	Strain rate [%/hour]	PI %
TG421.+093_B_MBIB_mo-11b	U-OC	3.4	OK Test	X	0.83	0.96	157
TG421.+093_B_MBIB_mo-12b	U-OC	3.4	OK Test	O/	0.94	0.78	50
TG421.+093_B_MBIB_mo-13c	D-OC	4.9	OK Test	O	0.92	0.48	52
TG421.+093_B_MBIB_mo-15b	U-OC	3.7	OK Test	O/	0.96	0.36	41
TG421.+093_B_MBIB_mo-17b	U-OC	3.6	OK Test	OX	0.96	0.6	72
TG421.+093_B_MBIB_mo-18a	U-OC	3.5	OK Test	O/	0.86	0.96	63
TG421.+093_B_MBIB_mo-20a	D-OC	3.8	OK Test	OX/	0.94	0.78	48
TG421.+094_B_BITA_mo-13a	U-NC	1	OK Test	O	0.45	0.67	50
TG421.+094_B_BITA_mo-14a	U-NC	1	False Test	O	0.44	0.94	35
TG421.+094_B_BITA_mo-16a	U-NC	1	False Test	O	0.41	0.14	79
TG421.+094_B_BUK_mo-25b	U-OC	3.5	OK Test	/	0.97	0.4	59
TG421.+094_B_BUK_mo-26a	U-OC	3.7	OK Test	OX	0.97	0.6	64
TG421.+094_B_BUT_mo-19b	U-NC	1	OK Test	O	0.45	0.87	44
TG422.+003_B_BUK_mo-20b	U-OC	3.6	False Test	OX	0.97	0.96	/
TG422.+003_B_BUK_mo-21a	U-OC	3.6	OK Test	X	0.94	0.9	36
TG422.+003_B_BUK_mo-22a	U-OC	3.7	OK Test	X	0.85	0.96	69
TG422.+003_B_BUK_mo-26a	U-OC	3.6	OK Test	O	0.97	0.3	34
TG422.+003_B_BUK_mo-27a	U-OC	3.5	OK Test	X	0.96	0.36	45
TG422.+004_B_BUT_mo-15b	U-NC	1	OK Test	O	0.45	0.95	23
TG422.+005_B_BITA_mo-12b	D-NC	1	OK Test	O	0.33	0.71	50
TG422.+005_B_BITA_mo-15a	U-NC	1	False Test	O	0.46	0.9	/
TG422.+005_B_BITA_mo-16b	U-NC	1	False Test	O	0.45	0.34	119
TG422.+005_B_BITA_mo-18b	U-NC	1	False Test	O	0.45	0.8	64
TG422.+005_B_BITA_mo-20b	D-NC	1	OK Test	O	0.45	0.59	51
TG422.+005_B_MBIB_mo-12b	U-NC	1	False Test	O	0.44	0.85	42
TG422.+005_B_MBIB_mo-13a	U-OC	3.3	OK Test	O	0.93	0.95	64
TG422.+005_B_MBIB_mo-14a	U-OC	3.5	OK Test	O	0.94	0.36	59
TG422.+005_B_MBIB_mo-16a	U-NC	1	False Test	O	0.48	0.93	79
TG422.+005_B_MBIB_mo-18a	U-OC	3.6	OK Test	O	0.86	0.36	110
TG422.+005_B_MBIB_mo-19a	U-OC	3.5	OK Test	OX	0.94	0.96	45
TG422.+005_B_MBIB_mo-20a	U-NC	1	OK Test	OX	0.35	0.64	38
TG422.+005_B_MBIB_mo-21a	U-OC	3.6	OK Test	O	0.94	0.96	90
TG422.+005_B_VL_mo-20a	U-NC	1	False Test	X	0.46	0.79	70

O: bulging; /:single discontinuity; X: several discontinuities
U: Undrained Test; D: Drained Test

3.3 Direct Simple Shear (DSS) tests

The Direct Simple Shear tests were performed according to ASTM norm (D6528-17, 2017). The samples were consolidated for at least the time required to reach 90% consolidation (from 16 to 69 hours). Over-consolidated samples were replicated using the SHANSEP consolidation method (Ministerie van Infrastructuur en Milieu, 2016) which involves consolidating the sample to its estimated pre-consolidation pressure, unloading the sample to the desired vertical stress and allowed to consolidate again for four hours. The current norms recommend a shear strain rate of 5%/hour and a maximum of 8%/hour. The shear strain rate as executed by the laboratories vary between 4.1 and 6.9 %/hour. The properties of each test are given in table 3.3.1.

Table 3.3.1: Direct Simple Shear test properties of samples from dike section 7h, 10b and 12g

Name test	Test type	OCR	PI %	Strain rates [%/hour]
TG321.+017_B_BUT_M011-a	U-NC	1	103	6.75
TG321.+017_B_BUT_M014-a1	U-NC	1	84	6.5
TG321.+017_B_BUT_M014-a2	U-OC	4.0	84	6.55
TG321.+017_B_BUT_M016-a1	U-NC	1	114	6.75
TG321.+017_B_BUT_M016-a2	U-OC	2.5	114	6.76
TG321.+017_B_BUT_M017-a	U-NC	1	99	6.74
TG321.+017_B_BUT_M018-a	U-NC	1	43	6.75
TG321.+018_B_BUK_M007-a	U-NC	1	23	6.76
TG321.+018_B_BUK_M020-a1	U-OC	1	73	6.72
TG321.+018_B_BUK_M020-a2	U-OC	4.0	73	6.91
TG321.+018_B_BUK_M021-a1	U-NC	1	89	6.69
TG321.+018_B_BUK_M021-a2	U-OC	2.5	89	6.69
TG321.+019_B_BUTA_M016-a	U-NC	1	/	6.64
TG321.+022_B_BIT_M015-a	U-NC	1	50	6.76
TG321.+022_B_BIT_M021-a	U-NC	1	54	5.06
TG321.+022_B_BIT_M023-a	U-NC	1	54	6.79
TG396.+009_B_AL_M010-a	U-NC	1	/	6.83
TG396.+013_B_BUT_M012-a	U-NC	1	/	6.76
TG396.+013_B_BUT_M013-b	U-NC	1	/	6.75
TG396.+013_B_BUT_M014-a	U-NC	1	/	6.76
TG396.+028_B_BUT_M011-a	U-NC	1	/	6.74
TG396.+028_B_BUT_M012-a	U-NC	1	/	6.77
TG396.+028_B_BUT_M020-a	U-NC	1	/	6.75
TG396.+030_B_AL_M018-a	U-NC	1	/	6.74
TG396.+030_B_BUK_M014-b	U-NC	1	/	6.76
TG396.+030_B_BUK_M019-a	U-NC	1	/	6.73
TG396.+030_B_BUK_M028-c	U-NC	1	/	6.69
TG396.+031_B_BIT_M020-c	U-NC	1	/	6.73
TG396.+031_B_BIT_mo-08a	U-NC	1	46	4.1
TG396.+031_B_BIT_mo-12c	U-NC	1	85	4.9
TG421.+094_B_BUT_mo-19b	U-NC	1	44	4.6

3.4 Triaxial Extension tests

The Triaxial Extension tests were performed by research Institude Deltares on samples of heights and diameters prior to consolidation of 67 mm and 108 to 123 mm respectively. The samples were consolidated and then brought to K_0 conditions in the same fashion as the triaxial compression tests as described in section 3.2. The samples were brought to failure at constant cell pressure by decreasing the vertical pressure at axial rate varying from 0.4 to 1.0 %/hour. The tests were then corrected for the effects of drainage strips and the membrane in the same fashion as described in section 3.2. The validity of the tests regarding the sample dimensions was determined according to the same criterion as used for Triaxial Compression tests.

Table 3.4.1: Triaxial Extension test properties

Name test	Test type	Test validity	Failure mode	K0 [-]	Strain rates [%/hour]
05-102_26	U-NC	False Test	><	0.47	-1.0
15-102_31	U-NC	OK Test	><	0.51	-0.5
2-102_13	U-NC	False Test	><	0.5	-1.0
4-2-102_24	U-NC	False Test	><	0.5	-0.4
4-102_16	U-NC	False Test	><	0.51	-0.4

><: local necking

3.5 Constant Rate of Strain (CRS) and Oedometer tests

The Constant Rate of Strain (CRS) and Oedometer tests were used in this project to determine the pre-consolidation pressure and parameters a and b (or λ and κ in the classical Critical State soil mechanics). For the CRS tests, the Dutch guidelines recommend saturating the sample at 2 kPa, loading to four times the in-situ vertical pressure, unloading back to two times the in-situ vertical pressure and reloading to six times the in-situ vertical pressure. Axial strain rates from

0.1 to 0.5% per hour were used, and were lowered in the next step of loading/unloading in case the pore pressure to vertical stress ratio exceeded 15%. The Dutch practice for the oedometer test is to load the sample with nine steps when the in-situ vertical stress is less than 50 kPa, where the steps are respectively 0.25, 0.5, 1, 2, 4, 2, 4, 8 and 16 times the in-situ vertical stress. For in-situ vertical pressures exceeding 50 kPa, eight steps are used as follows: 0.25, 0.5, 1, 2, 4, 2, 4, 10 times the in-situ vertical stress. The unloading reloading section of the test is fitted by a line where its slope determines the value of parameter a. Parameter b is taken as the slope of the virgin compression line. The pre-consolidation pressure was taken as the pressure on the virgin compression line corresponding to the axial strains of the in-situ pressure as prescribed by the Dutch guidelines (Ministerie van Infrastructuur en Milieu, 2016).

Chapter 4

Preliminary results

The preliminary results of the laboratory tests on the Gorinchem Clay are shown and discussed in this chapter. The results in Triaxial Compression, DSS and Triaxial Extension are to be found in respectively in sections 4.1 to 4.3. The combined results expressed in shear strain and shear stress are discussed in section 4.4. Finally, the results of parameters a,b and the pre-consolidation stress are shown in section 4.5.

4.1 Preliminary results of the Triaxial Compression tests

4.1.1 Unexpected behaviour of the soil

The preliminary results show some inconsistencies with regards to the expected behaviour of the soil at Critical State and in the process leading towards it. Indeed in figure 4.1.1 where two samples on the wet side were tested undrained, the stress path initially shows a very large stiffness unlike the curved stress paths described by Atkinson et al. (1993), Wood (2014) or Schofield and Wroth (1968). In figure 4.1.2 the sample on the wet side features increasing confining pressure in its early stage of shearing in contrast to the decrease in confining pressure due to build-up of excess pore pressures as would normally be expected. The samples in figure 4.1.1 thereafter soften in an apparent liquefaction fashion and reach a peak stress ratio.
In many examples (Sheahan et al., 1996; Muraro, 2019), the post stress ratio peak response shows strain softening or hardening along the Critical State line or peak stress ratio, which isn't the case for the tests in figure 4.1.1. According to the Dutch guidelines, the Critical State undrained shear strength for peat and clay is reached at 25% axial strain, however for these two tests the undrained shear strength at 25% axial strain is lower than the deviatoric stress at anisotropic consolidation conditions. The excess pore pressure development shown in figure 4.1.4 is also problematic as both samples tested from the dry and the wet rarely show excess pore pressures reaching steady state. The general trend for the normally consolidated samples is that around 10% axial strain, the excess pore pressures increase at a constant rate. This tendency is particularly true for very silty and organic samples. For the over-consolidated samples, the general trend is that for low over-consolidation ratio's (lower than 3.0) the pore pressures do reach steady state and they do so at low axial strains (around 5%), which is expected as the void ratio at low OCR is close to the Critical State void ratio. For large OCR's, the tests can feature continuously increasing, post-peak continuous decreasing or oscillating excess pore pressures without any particular trend although these effects are most probably related to the difficulties of performing a test at low confining pressures.
The normally consolidated drained tests in figure 4.1.3 show in one case post-peak softening after 1% axial strain without a clear reach of steady state and in the other case a continuously hardening material (as would be expected) however with varying stiffnesses and a possible steady state at 15% axial strain.
These observations raise the question whether the observed strain softening is a result of true

material behaviour, in which case the undrained shearing produces considerably large strength degradation of the material, or whether the observed strain softening is a manifestation of the limitations of the laboratory testing equipment on soft soils as was discussed in chapter 2.2, in which case the material and test behaviour produces considerable 'apparent' strain softening.

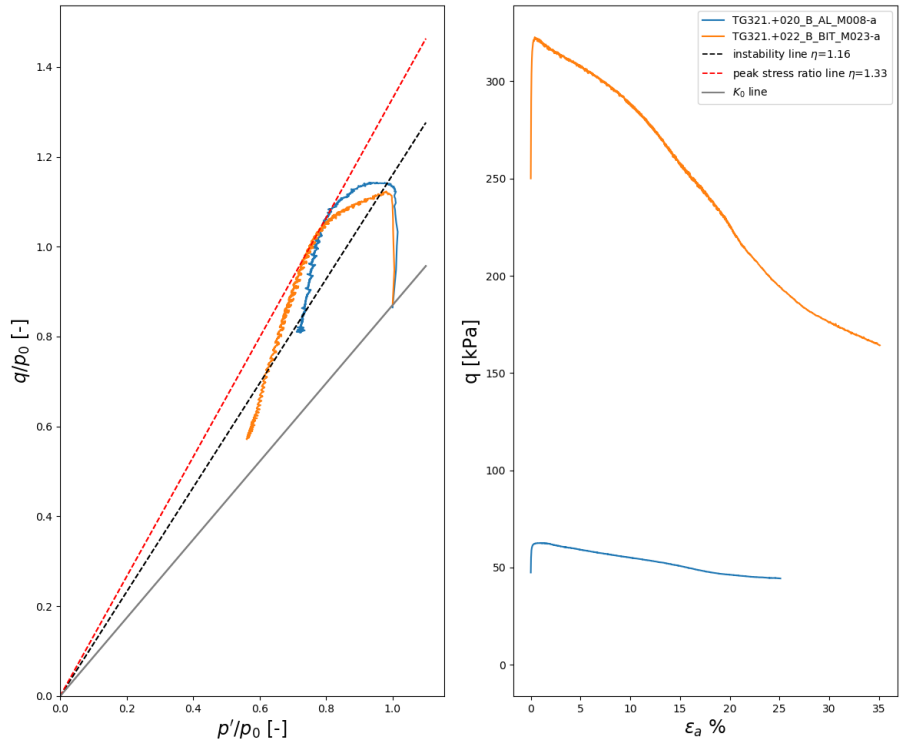

Figure 4.1.1: Unexpected behaviour of undrained tests showing excessive softening and no convergence towards a Critical State line

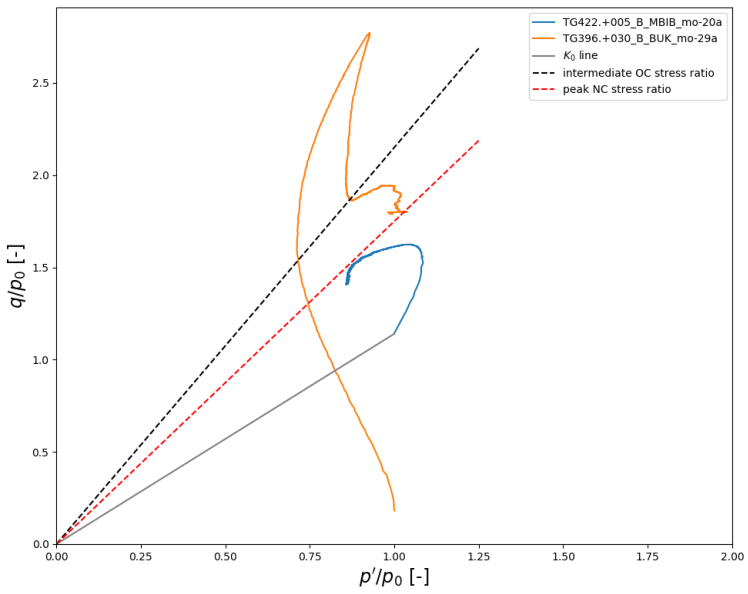

Figure 4.1.2: Unexpected behaviour of undrained tests showing a non linear elastic stress path from the dry side and an initial increasing confining pressure on the wet side

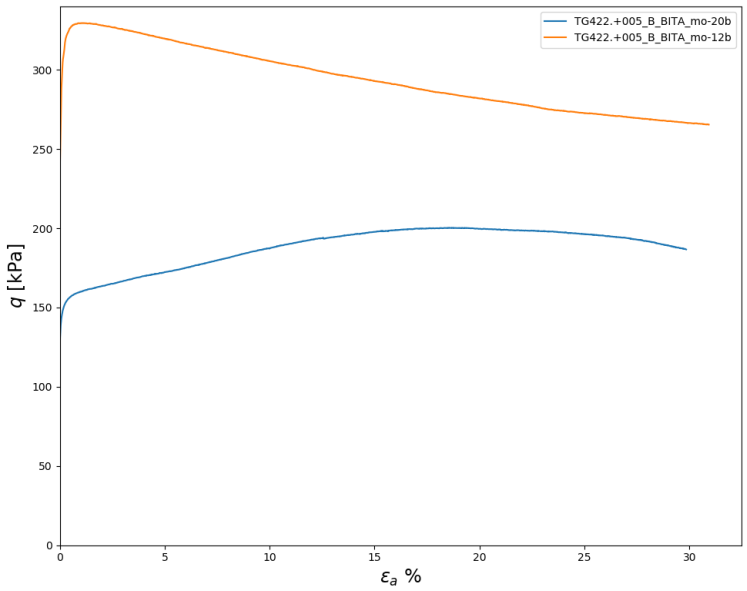

Figure 4.1.3: Unexpected behaviour of drained tests showing post peak softening and varying stiffness for normally consolidated samples

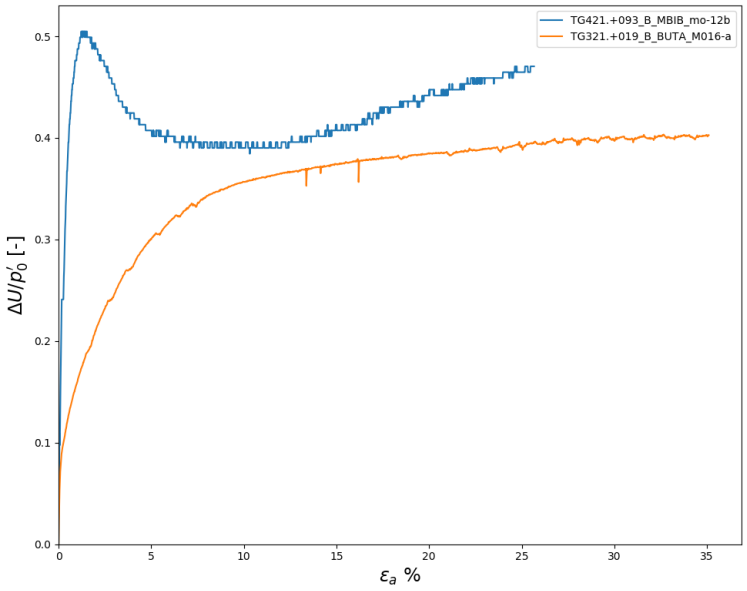

Figure 4.1.4: Unexpected behaviour of undrained tests showing continuous excess pore pressure development

4.1.2 Strain based correlations

In figures 4.1.5 to 4.1.8 the undrained shear strength and stress ratio at respectively 10, 15, 20 and 25% axial strain are given as a function the wet volumetric weight and figures 4.1.9 to 4.1.12 as a function of the Plasticity Index, recalling the guideline recommendation of 25% axial strain to reach Critical State. The wet volumetric weight and the Plasticity Index are two parameters for which a correlation with the undrained shear strength and the stress ratio (or by back-calculating the friction angle) is expected (Ladd, 1991). The results however show little to no correlation for either parameter at the considered axial strains in addition to the fact that the least mean square fit of the data is very poor.

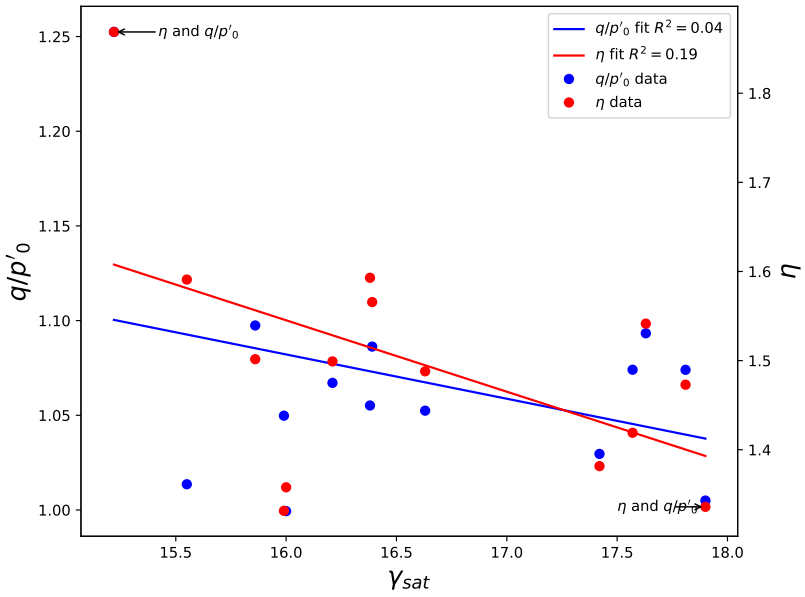

Figure 4.1.5: Normalised deviatoric stress and stress ratio as a function of the wet volumetric weight at 10% axial strain

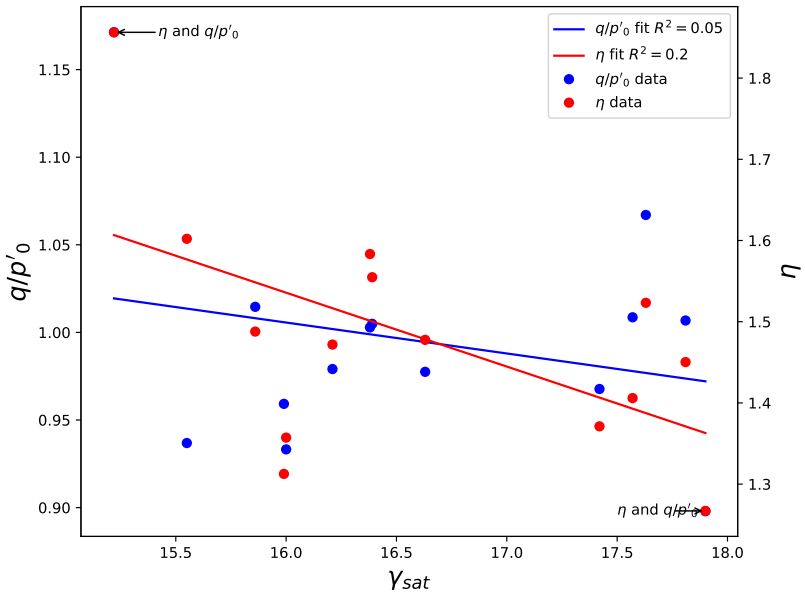

Figure 4.1.6: Normalised deviatoric stress and stress ratio as a function of the wet volumetric weight at 15% axial strain

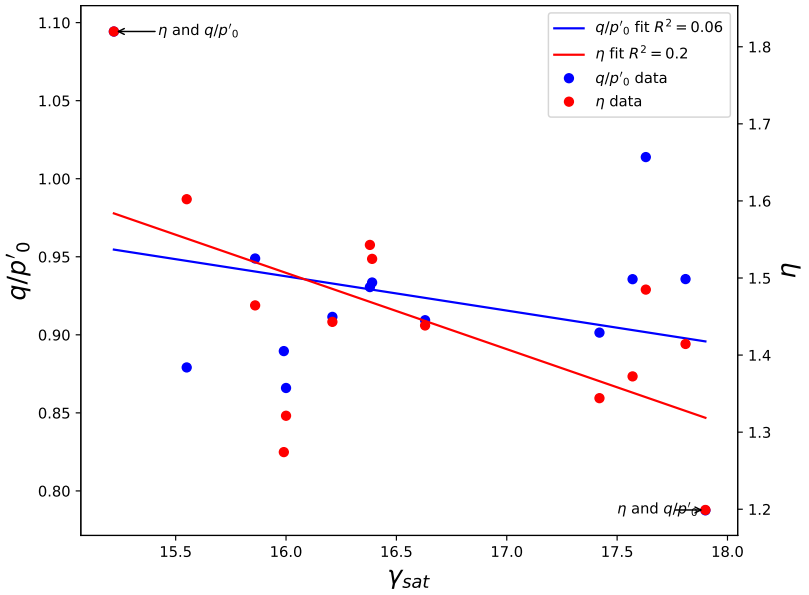

Figure 4.1.7: Normalised deviatoric stress and stress ratio as a function of the wet volumetric weight at 20% axial strain

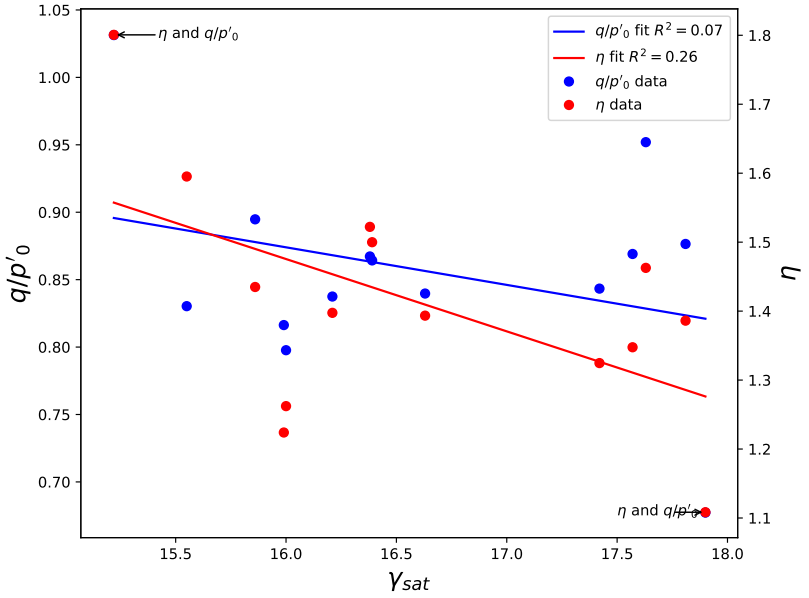

Figure 4.1.8: Normalised deviatoric stress and stress ratio as a function of the wet volumetric weight at 25% axial strain

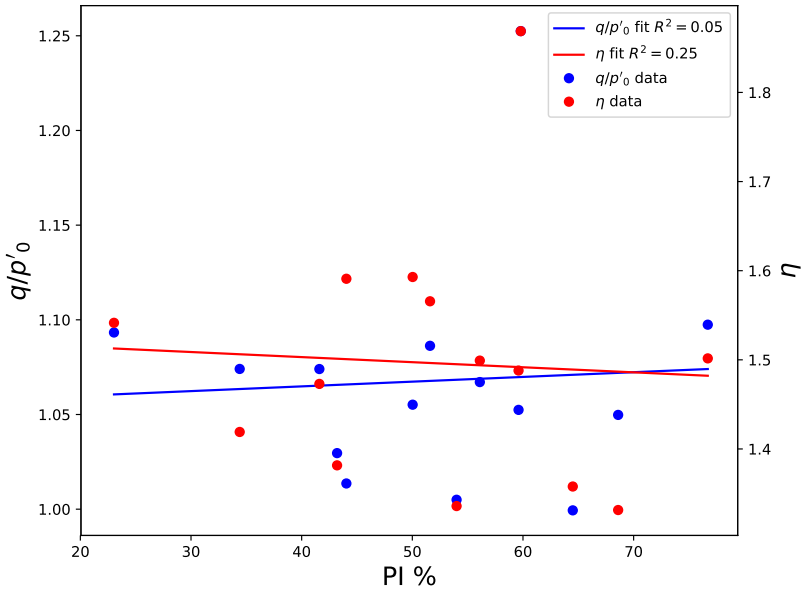

Figure 4.1.9: Normalised deviatoric stress and stress ratio as a function of Plasticity Index at 10% axial strain

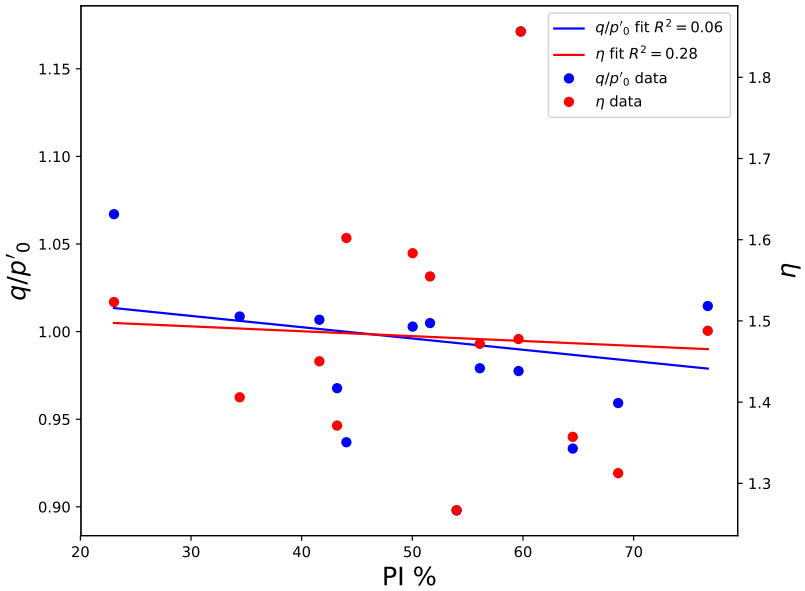

Figure 4.1.10: Normalised deviatoric stress and stress ratio as a function of Plasticity Index at 15% axial strain

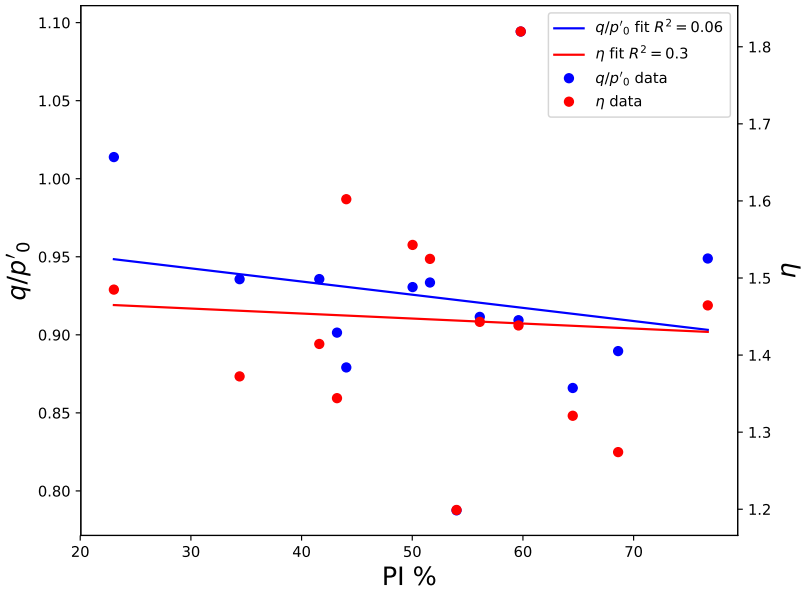

Figure 4.1.11: Normalised deviatoric stress and stress ratio as a function of Plasticity Index at 20% axial strain

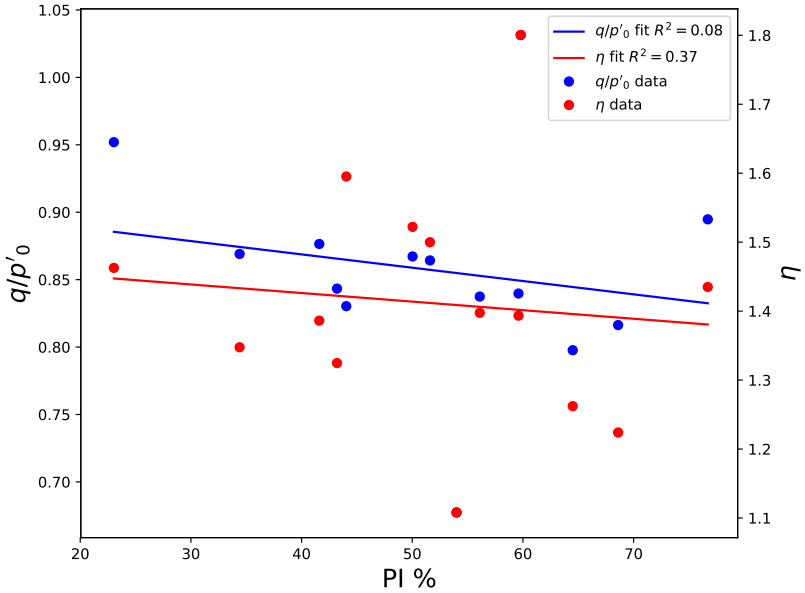

Figure 4.1.12: Normalised deviatoric stress and stress ratio as a function of Plasticity Index at 25% axial strain

4.1.3 Stress Path trends of the results in soil parameters and classification

The stress ratio and excess pore pressure development are given in figures 4.1.13 to 4.1.22 for intervals of wet volumetric weight, plasticity index and classification (clay, silt and organic content). The classification based trends could not be performed for normally consolidated conditions due to the lack of classification data for these tests. The results show very little trend with the soil parameters or classification, especially for the test on normally consolidated samples. Some trend can be distinguished in the stress ratio for over-consolidated conditions (figure 4.13(a)) which decreases with decreasing organic content and increasing with wet volumetric weight. In figure

4.16(b) it is observed that continuously increasing excess pore pressure occurs mainly for high Plasticity indexes (higher than 40%). Since the plasticity index is mainly, for this specific soil, correlated to the organic content it can be concluded that the constant increase in excess pore pressures is a feature of tests on organic rich soils.

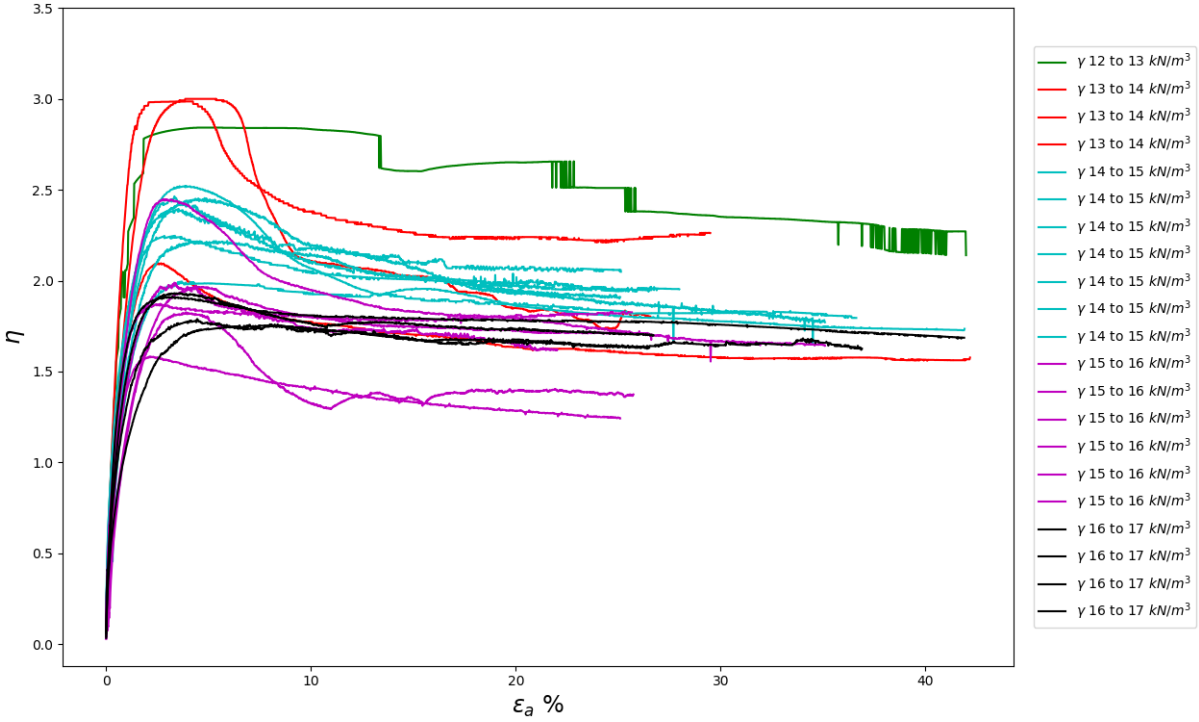

(a) undrained behaviour from the dry side

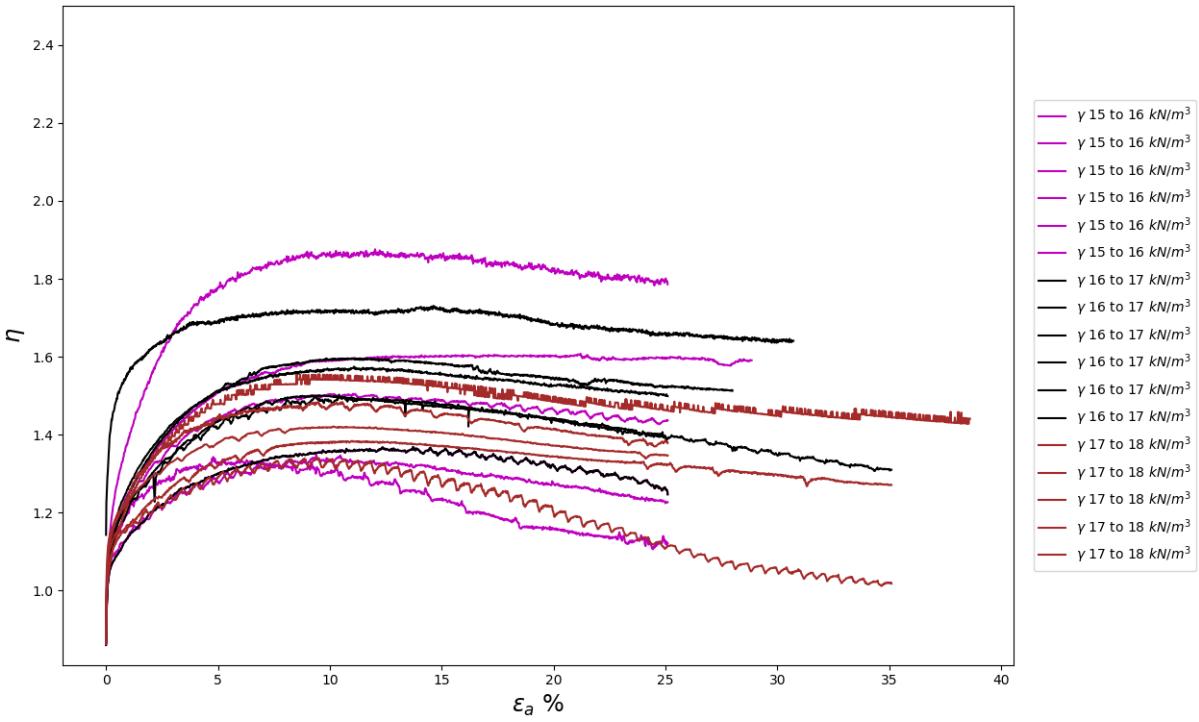

(b) undrained behaviour from the wet side

Figure 4.1.13: Stress ratio η as a function of the wet volumetric weigth.

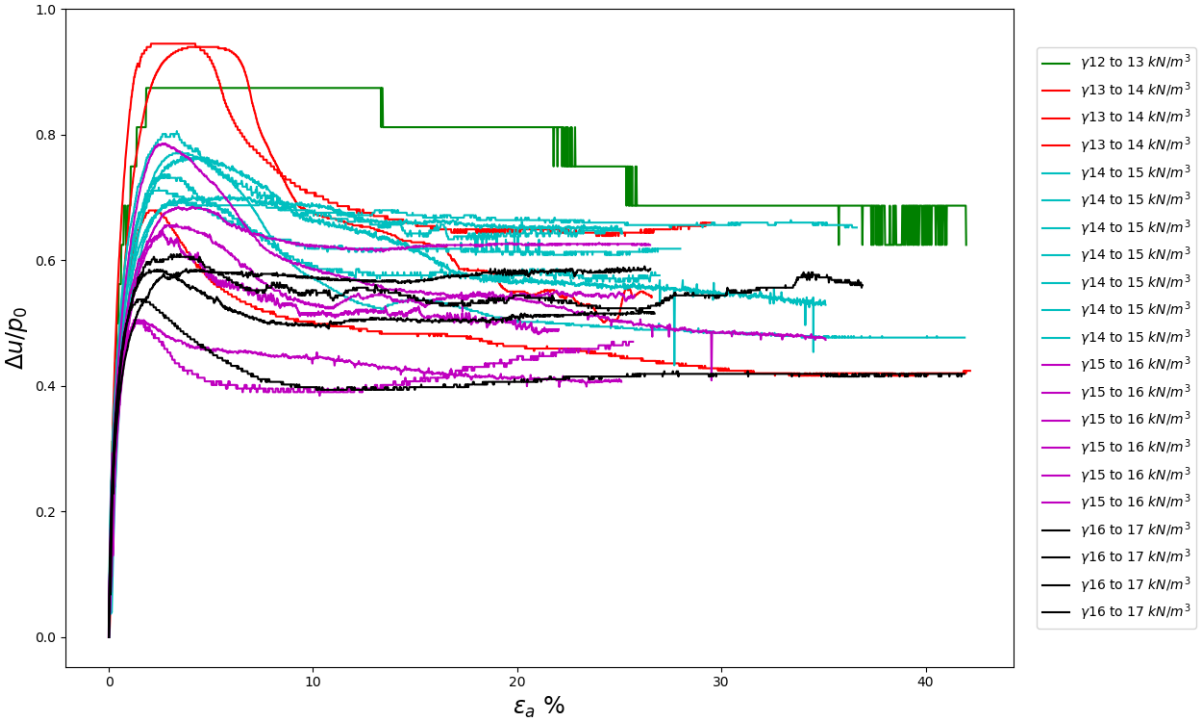

(a) undrained behaviour from the dry side

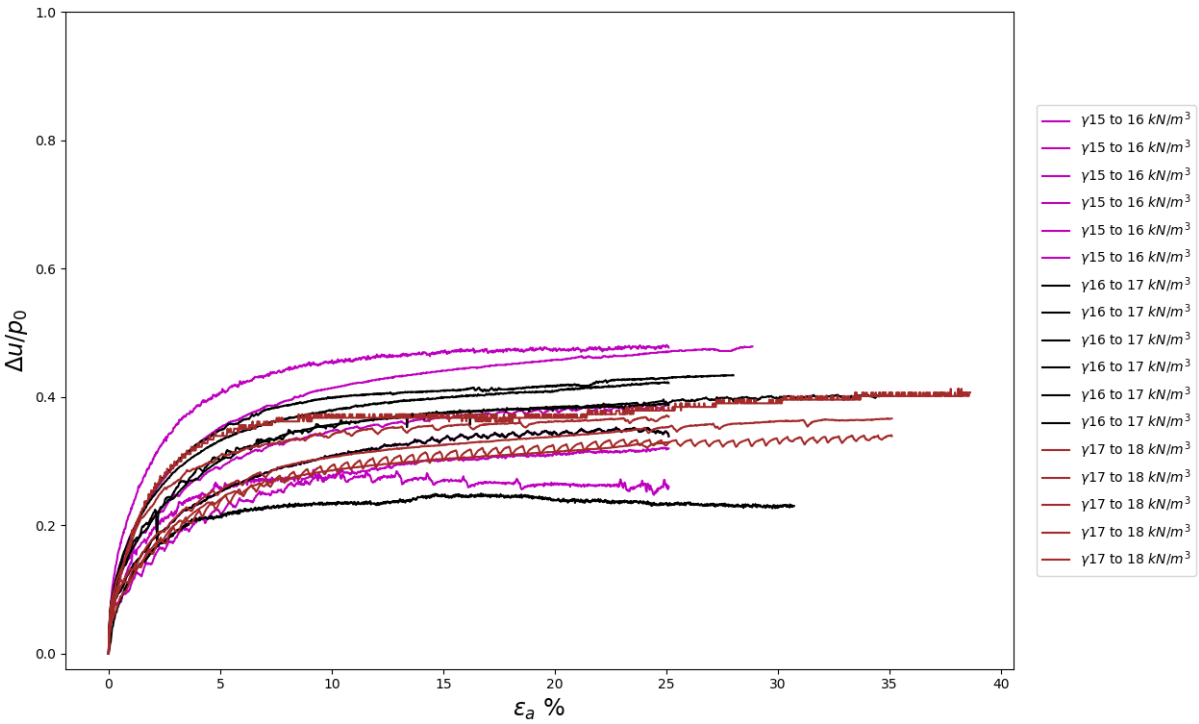

(b) undrained behaviour from the wet side

Figure 4.1.14: Excess pore pressures as a function of the wet volumetric weigth.

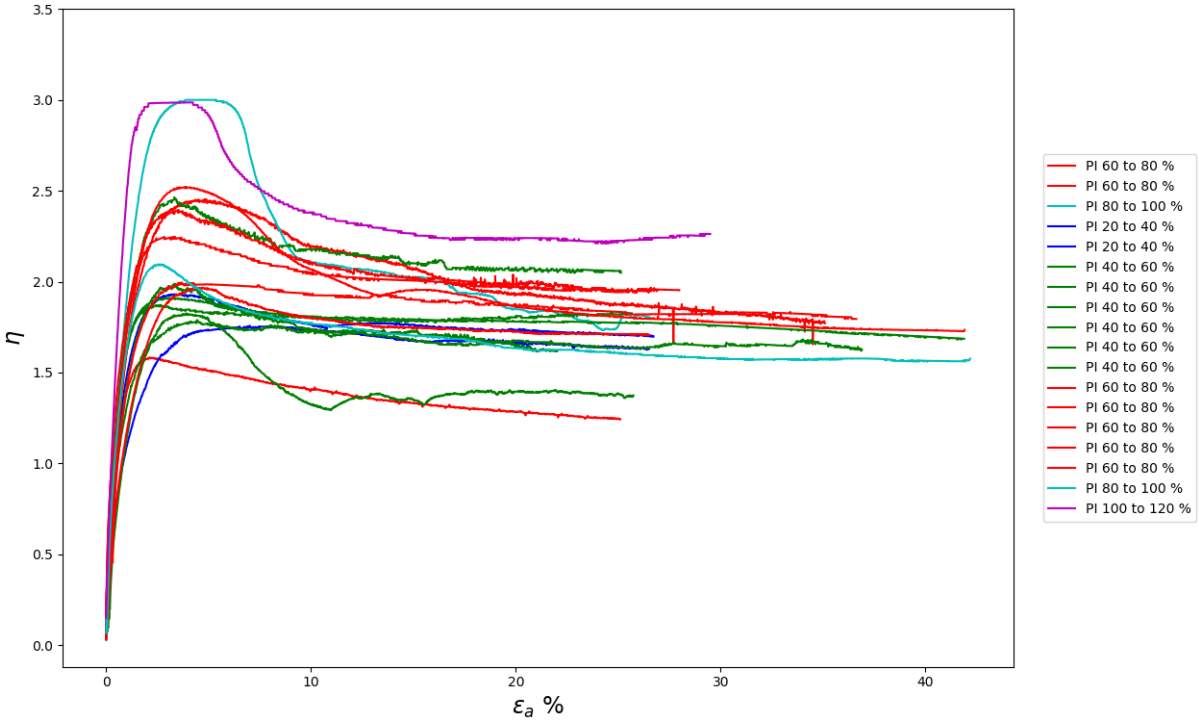

(a) undrained behaviour from the dry side

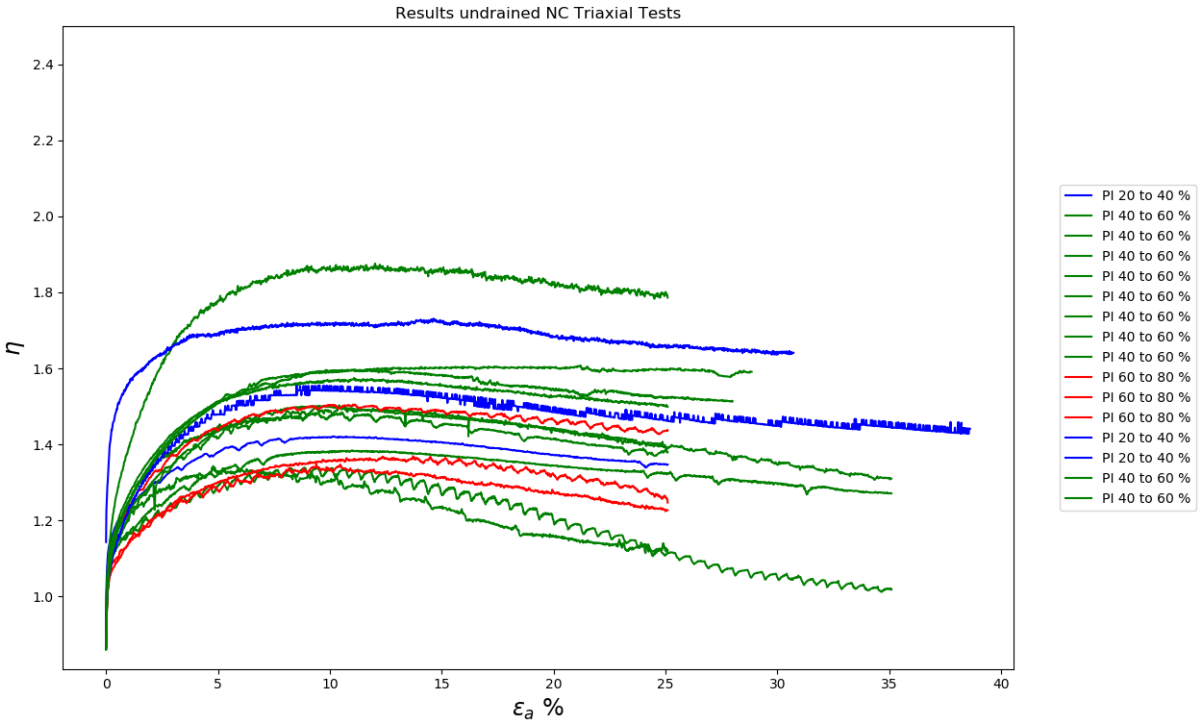

(b) undrained behaviour from the wet side

Figure 4.1.15: Stress ratio η as a function of the Plasticity Index.

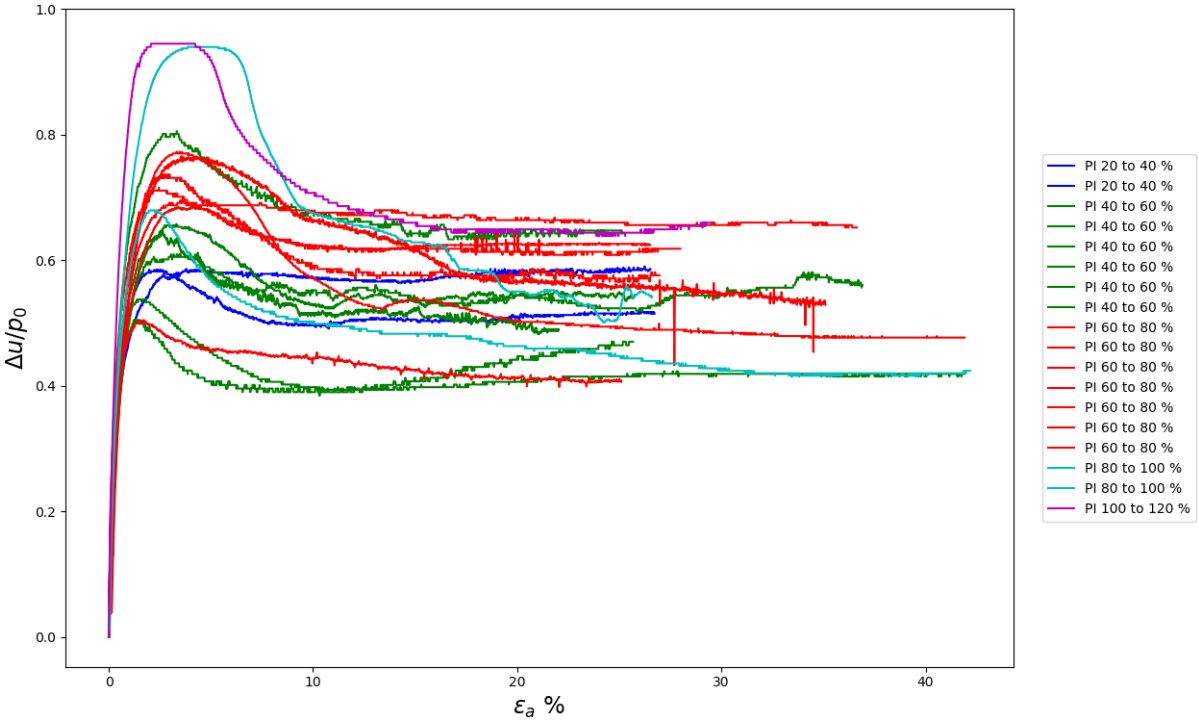

(a) undrained behaviour from the dry side

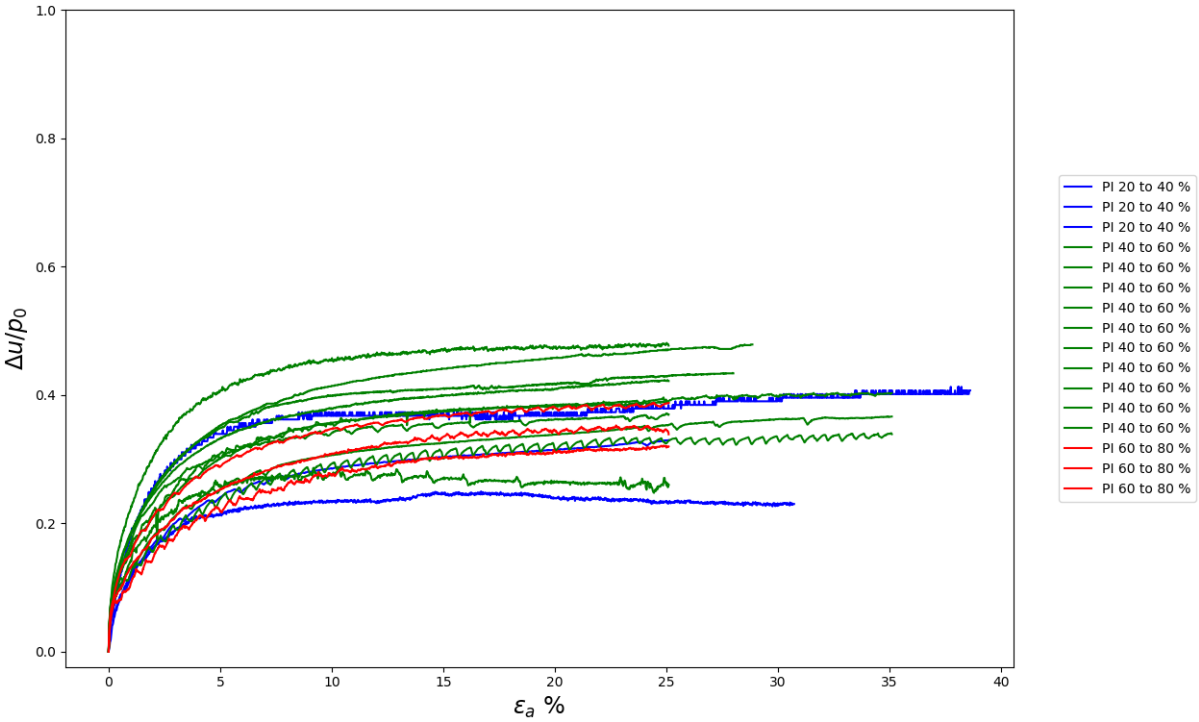

(b) undrained behaviour from the wet side

Figure 4.1.16: Excess pore pressures as a function of the Plasticity Index.

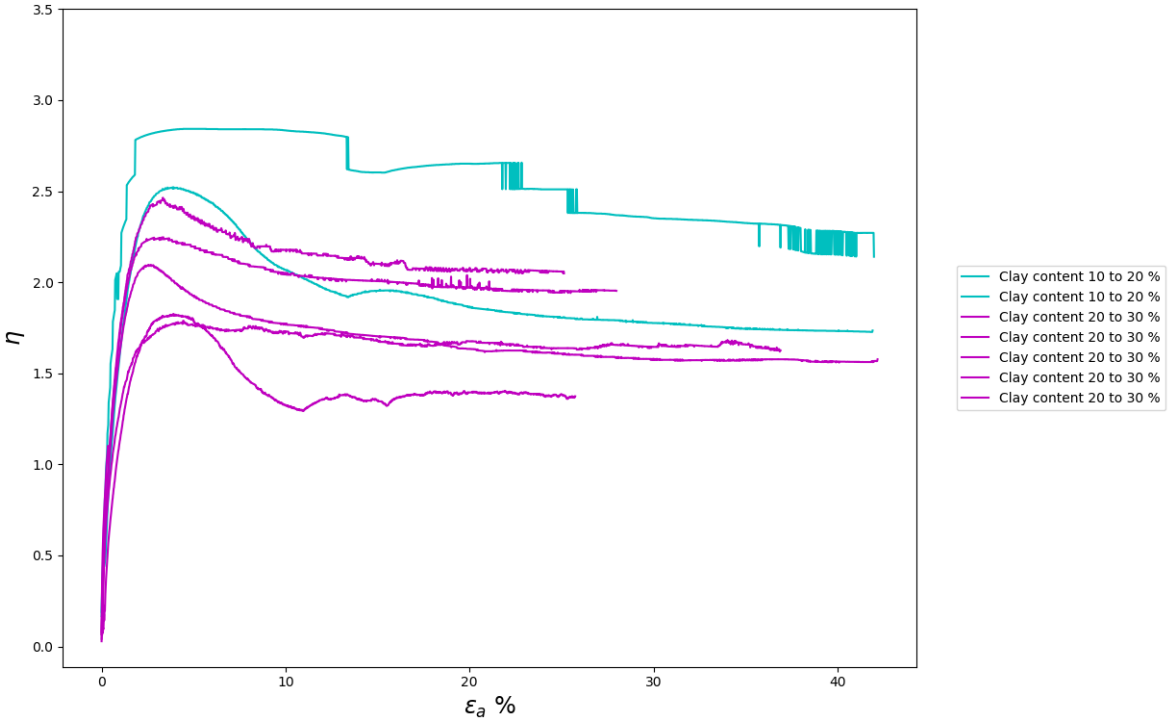

Figure 4.1.17: Stress ratio η as a function of the Clay content from the dry side.

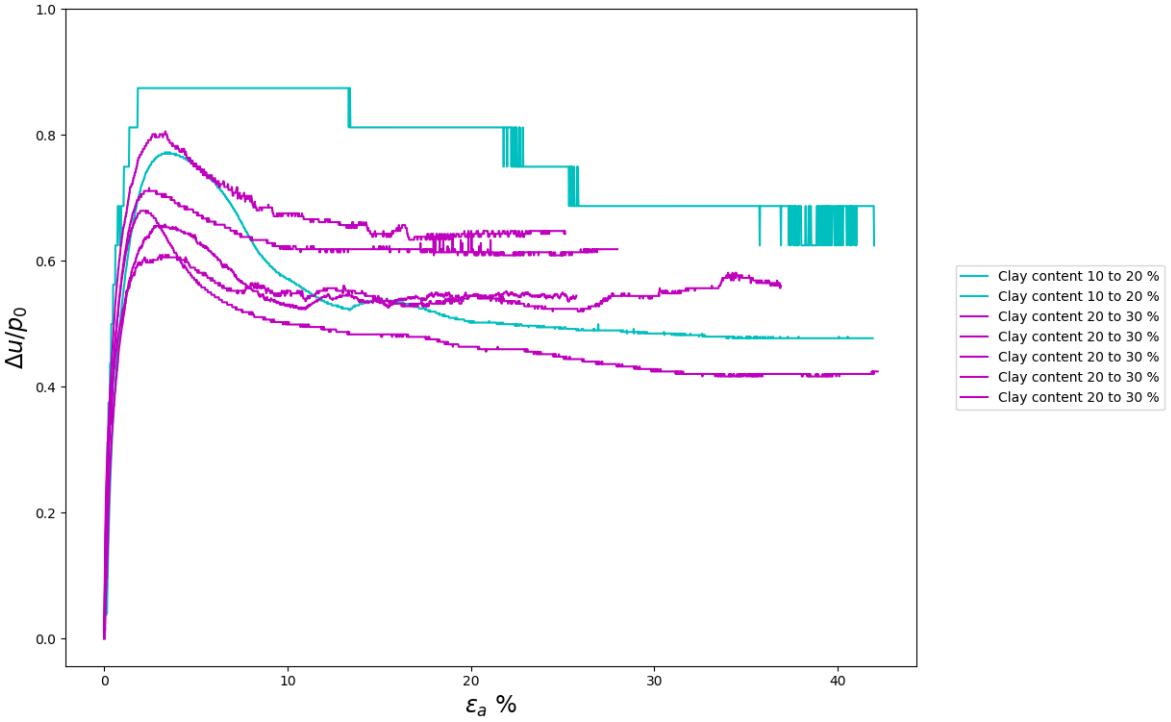

Figure 4.1.18: Excess pore pressures as a function of the Clay content from the dry side.

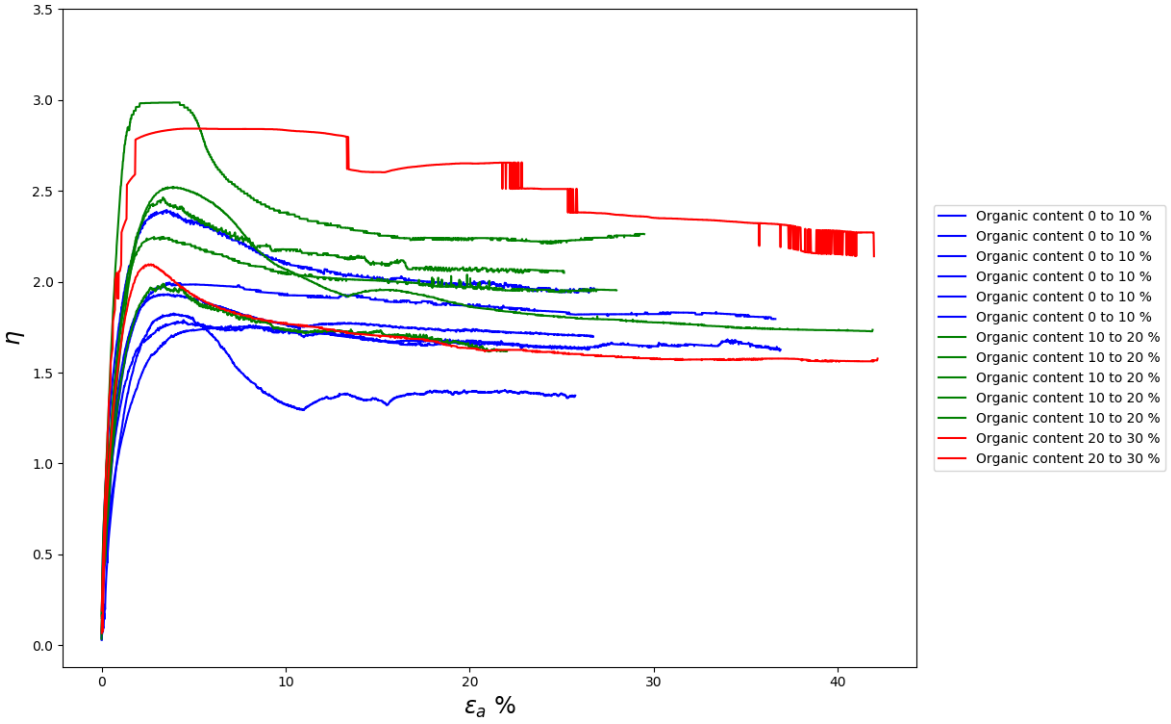

Figure 4.1.19: Stress ratio η as a function of the Organic content from the dry side.

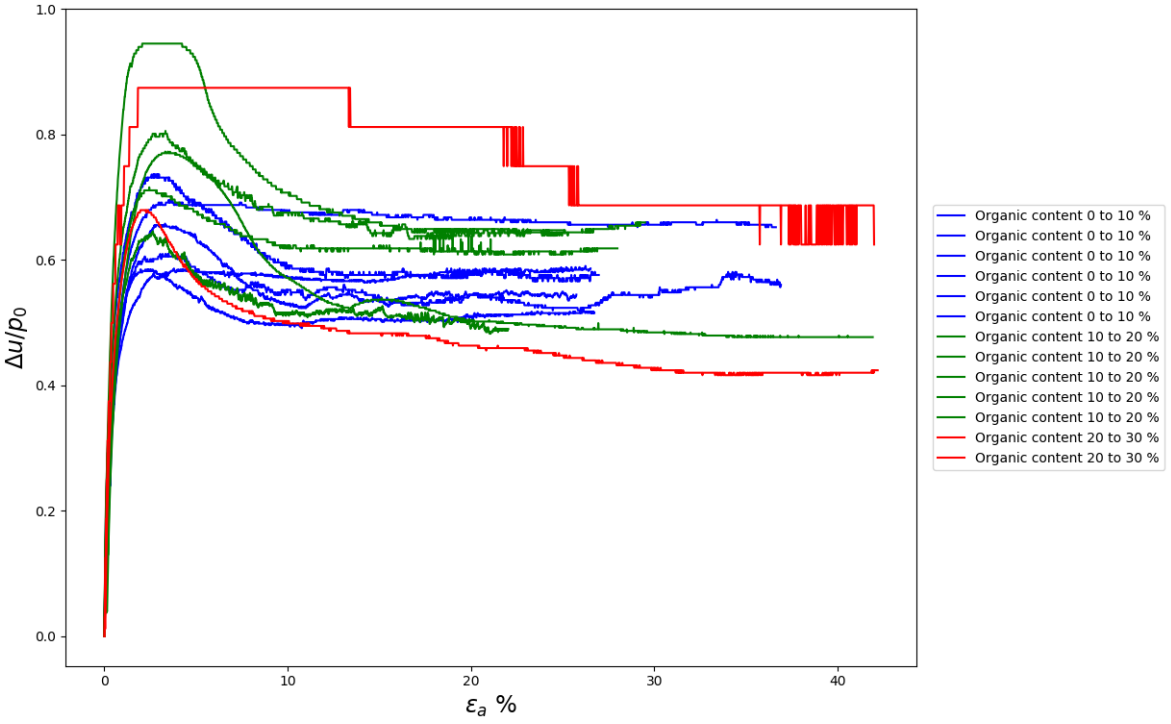

Figure 4.1.20: Excess pore pressures as a function of the Organic content from the dry side.

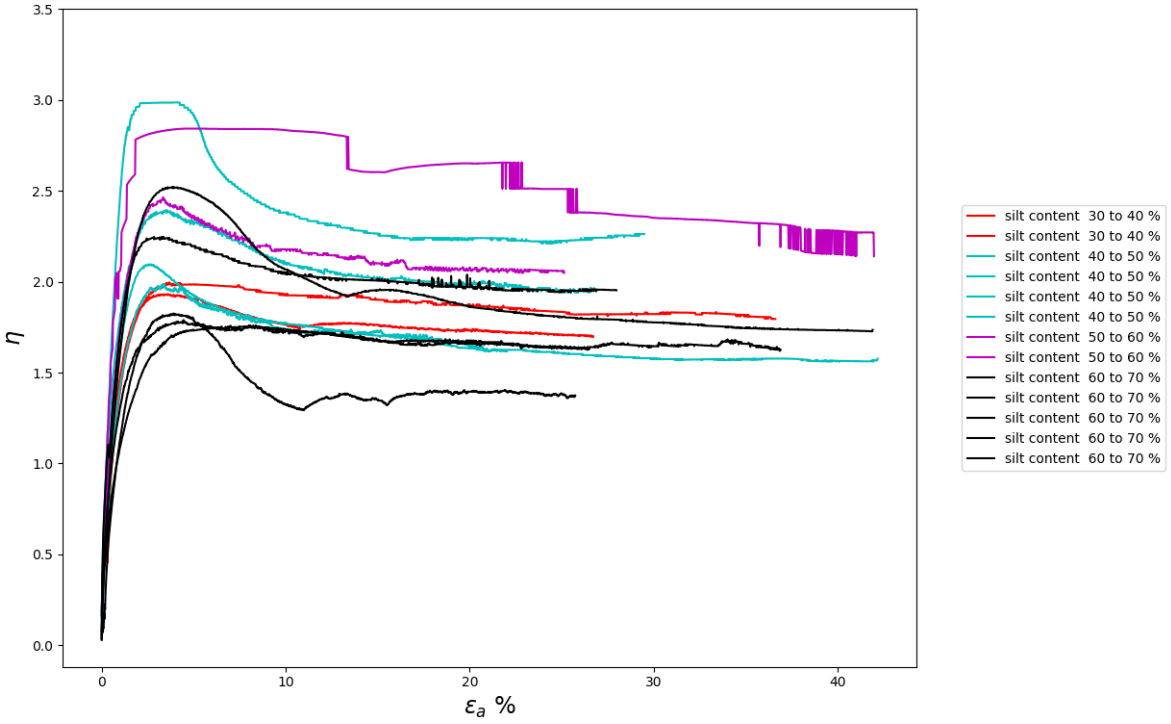

Figure 4.1.21: Stress ratio η as a function of the Silt content from the dry side.

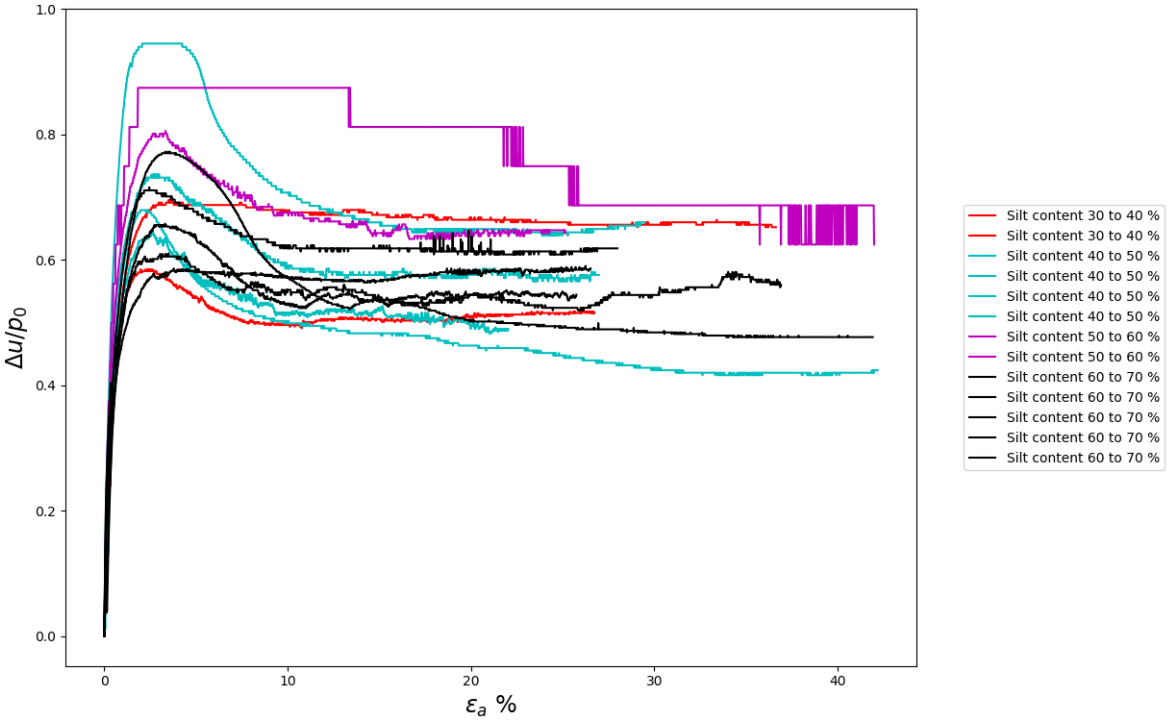

Figure 4.1.22: Excess pore pressures as a function of the Silt content from the dry side.

4.2 Preliminary results of the Direct Simple Shear tests

In figures 4.2.1 and 4.2.2, results of several DSS tests are given for normally consolidated and over-consolidated conditions respectively where the results again show ongoing strain softening without an asymptotic reach of what could be considered to be Critical State line. It is known the DSS apparatus may produce excessive strain softening beyond 10 to 15% shear strain (Ladd & DeGroot, 2003), although the results start showing shear softening from 15 to in some cases 25% shear strain. The current guidelines state the Critical State conditions are to be reached at 40% shear strain in DSS: this again does not conform with the traditional understanding of the Critical State soil mechanics post peak softening is not expected to occur for a soil tested under normally consolidated conditions in the DSS apparatus.

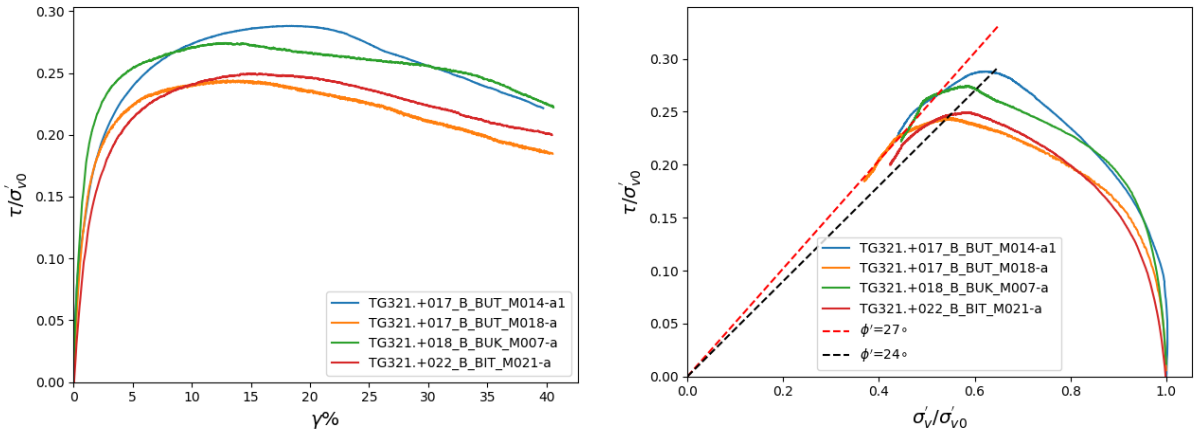

Figure 4.2.1: Preliminary DSS results for normally consolidated conditions

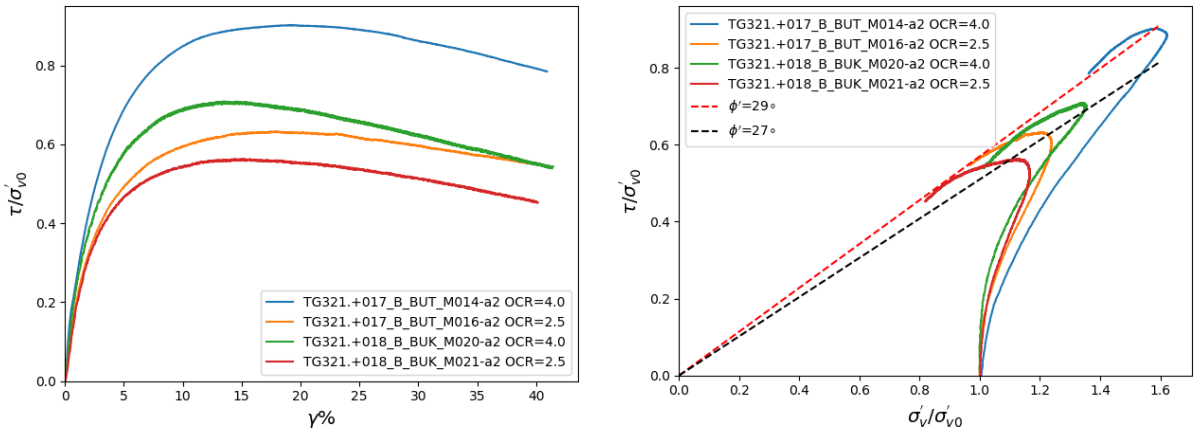

Figure 4.2.2: Preliminary DSS results for over-consolidated conditions

4.3 Preliminary results of the Triaxial Extension tests

The preliminary results of the Triaxial Extension tests are given in figure 4.3.1. The results show again strain softening beyond 10-15 % axial strain and large discrepancies in the peak stress ratio and normalised undrained shear strength. Amongst similar materials (similar volumetric weights), the results shows a clear dependency on the height to diameter ratio after consolidation: for Gorinchem clay between 14 and 14.5 kN/m^3, the normalised shear strength and stress ratio is lower for lower sample height to diameter ratio's.

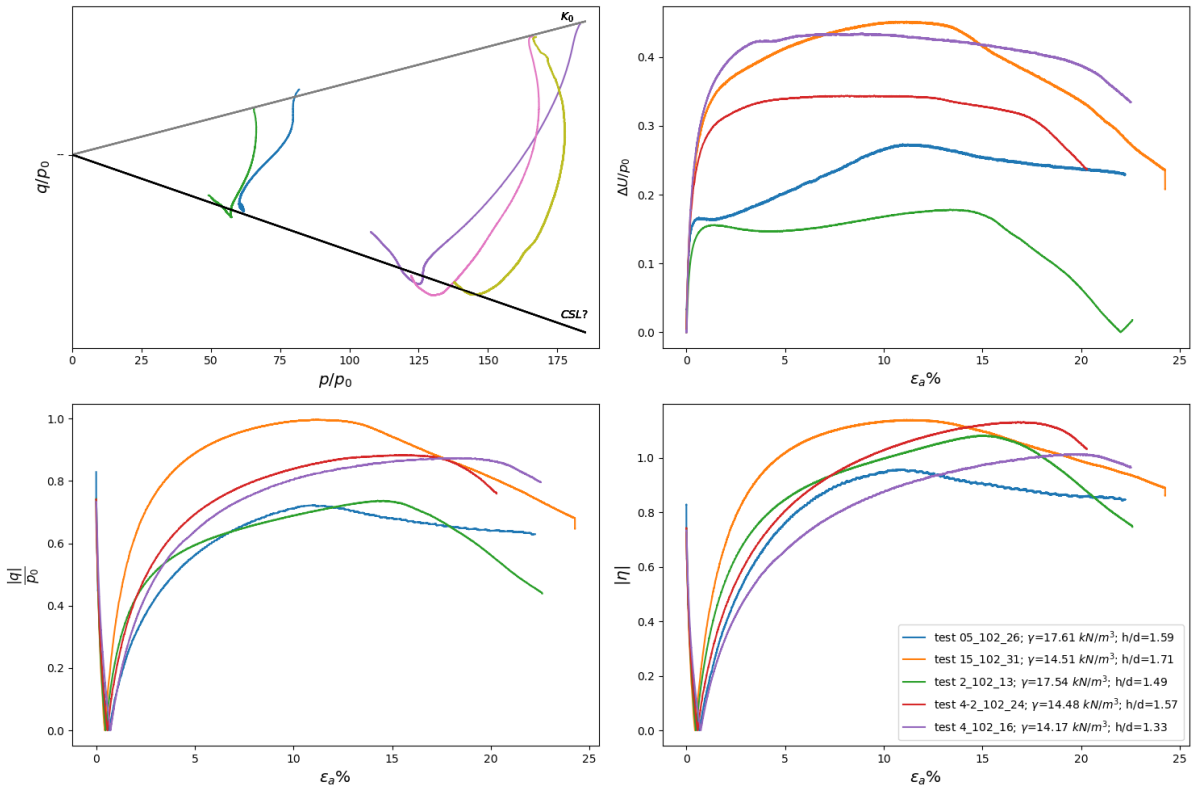

Figure 4.3.1: Preliminary undrained Triaxial Extension results

4.4 Combined preliminary results in Triaxial Compression, Direct Simple Shear and Triaxial Extension

The approach in the Dutch guidelines of determining the macro-stability of an embankment is based on the strain mode of the different sliding sections of the dike (ADP method (Ladd, 1991)). According to this method, the shear strain versus shear stress of soils tested in Triaxial Compression, Direct Simple Shear and Triaxial Extension can be expressed together as previously explained in section 2.3. It is expected that the results of the different tests expressed in this fashion to be slightly different and the result of the undrained shear strength in Triaxial Compression should approximately equate the average of the strengths in DSS and Triaxial Extension, where the strength in DSS is highest and Triaxial Extension the lowest (Ladd, 1991). In addition, the normalised undrained shear strength ratio in TC, DSS and TE are expected to be of much closer magnitude with increasing Plasticity Index (Ladd, 1991), and the expected value for the normalised shear strength for this soil is 0.3 (Ministerie van Infrastructuur en Milieu, 2016).

The first results of the tests at the project show some inconsistencies regarding these observations: for volumetric weights between 14 and 16 kN/m^3 in figure 4.4.1, the mean normalised undrained shear strength ratio's of the DSS and Extension tests are closely matched (2% relative difference from DSS at 15% shear strain) but significantly lower in Compression (10% relative difference from DSS at 15% shear strain). For volumetric weights in the 16 to 17.5 kN/m^3 range (figure 4.4.2), the mean normalised shear stress in Triaxial Compression exceeds the normalised shear stress in DSS by up to 20% at 15% shear strain. For volumetric weights larger than 17.5 kN/m^3 (figure 4.4.3), again the tests in Compression exceed the test in DSS (20% relative difference from DSS at 15% shear strain) however the Extension test results in much lower normalised shear strength (10% relative difference from DSS at 15% shear strain) in contrast to the results for volumetric weights between 14 and 16 kN/m^3 in figure 4.4.1. The results are additionally considerably lower

than the expected normalised shear strength of 0.3 at the shear strains prescribed by Ministerie van Infrastructuur en Milieu (2016). In section 4.3 the results showed to be sensitive to the height to diameter ratio measured after consolidation, more specifically low height to diameter samples results in lower stress ratio's and undrained shear strengths. The low outcome on Triaxial Extension tests in combined results for volumetric weights larger than 17.5 kN/m^3 is most probably an indication that the height to diameter ratio in the two Extension tests performed within this interval (1.59 and 1.49) are too small and therefore introduce too many boundary effects.
The results additionally show a large spread around the mean, especially in DSS for all ranges. The nature of the soil shows the Plasticity Index is inversely proportional to the volumetric weight: the results show no correlation between the measured undrained shear strength of the different tests and the Plasticity Index as opposed to the findings of Ladd (1991).

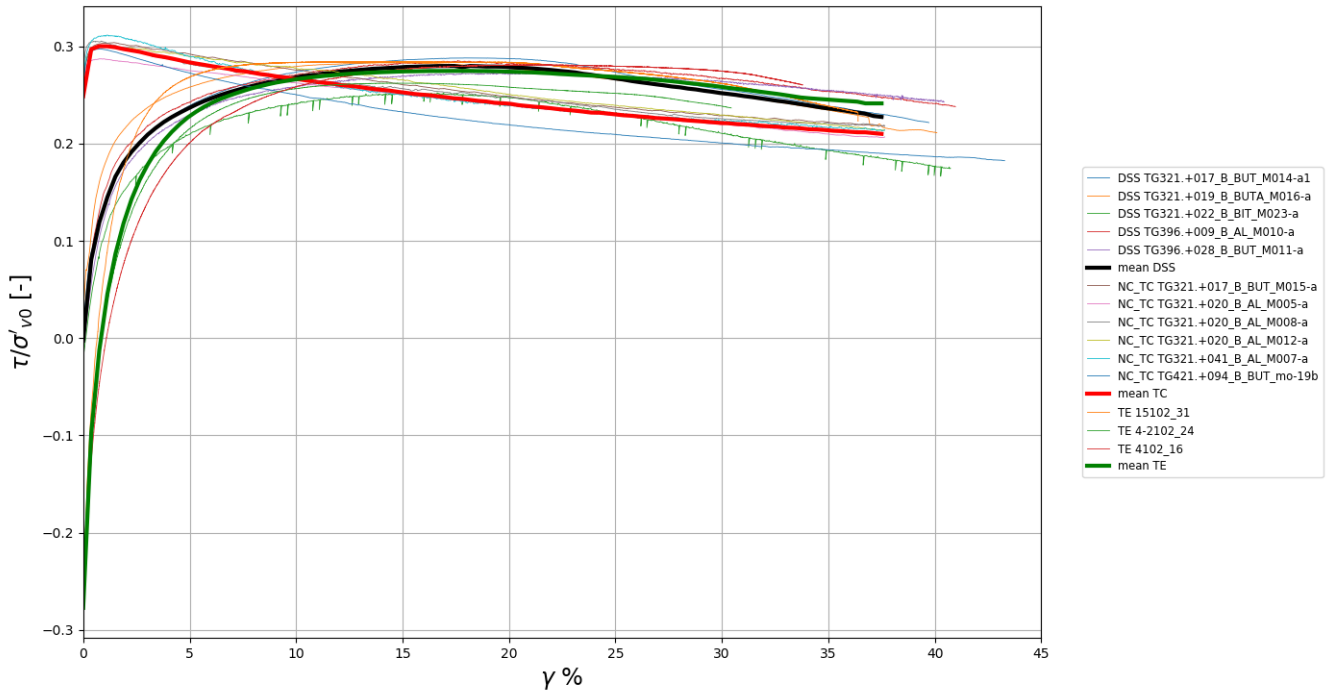

Figure 4.4.1: Normalised stress-strain of Triaxial Compression, DSS and Triaxial Extension tests for volumetric weights between 14 and 16 kN/m^3

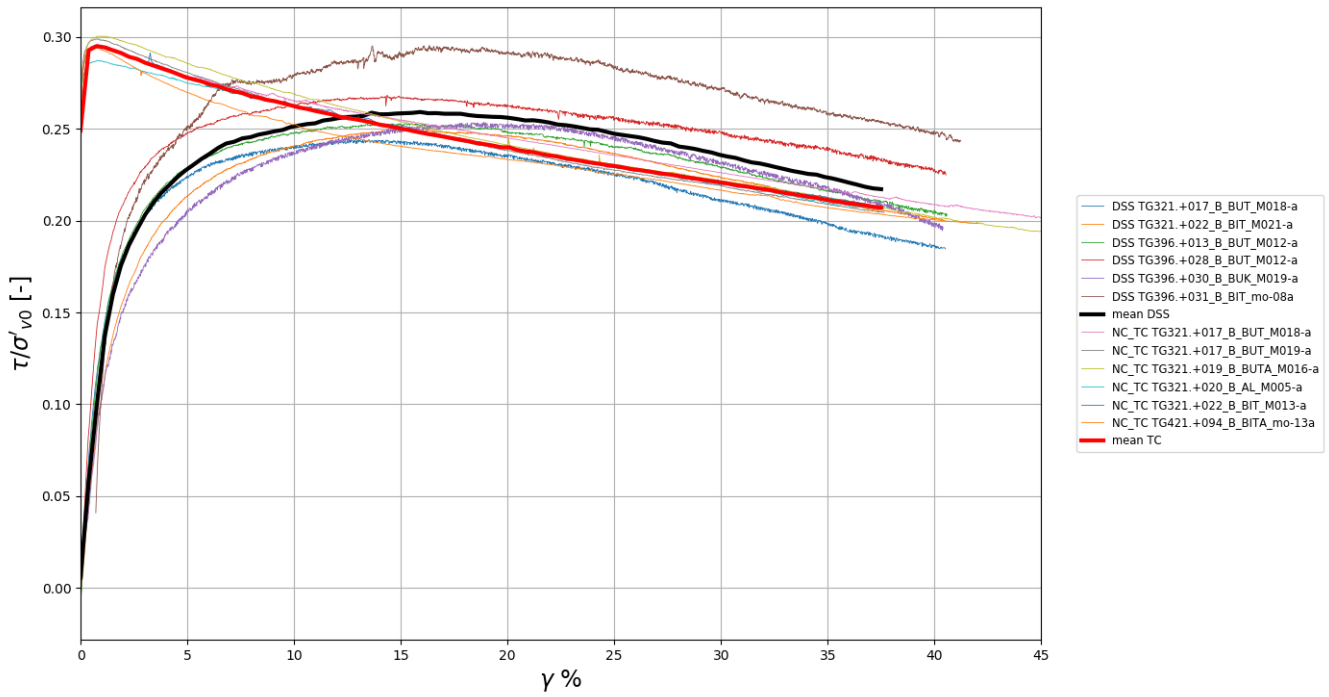

Figure 4.4.2: Normalised stress-strain of triaxial compression, DSS and triaxial extension tests for volumetric weights between 16 and 17.5 kN/m^3

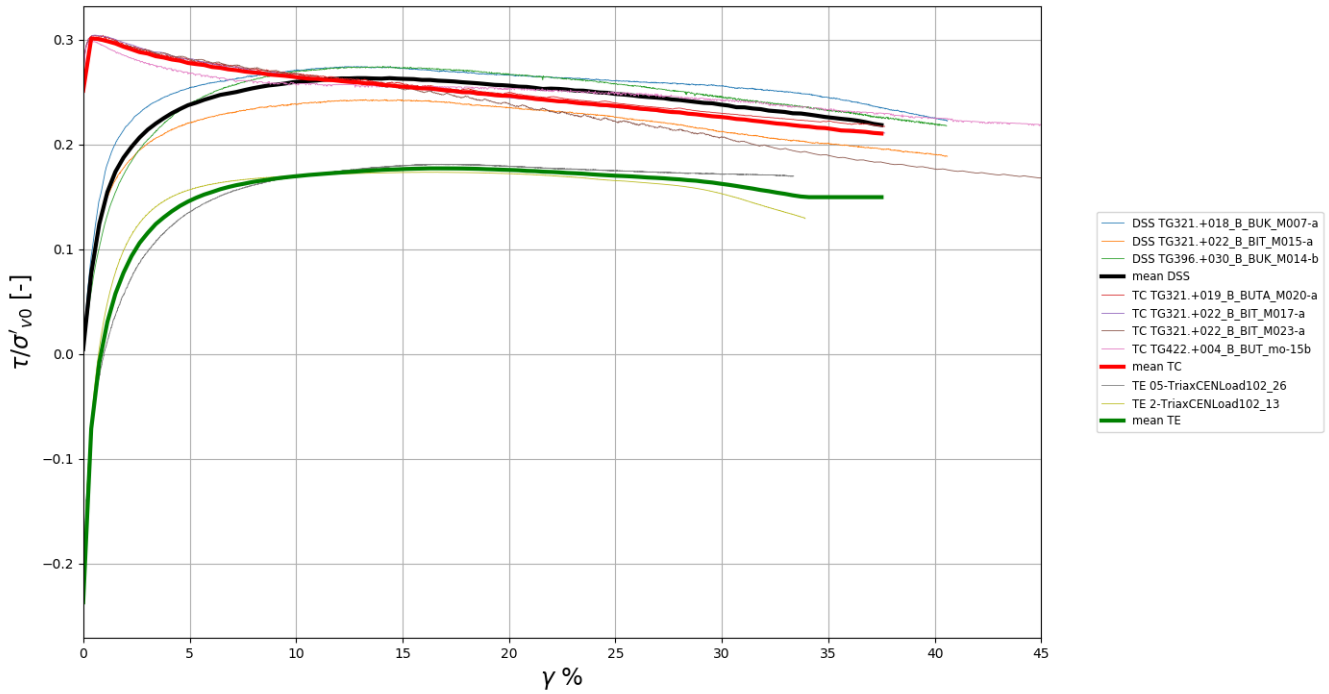

Figure 4.4.3: Normalised stress-strain of triaxial compression, DSS and triaxial extension tests for volumetric weights between larger than 17.5 kN/m^3

4.5 Preliminary results of the Constant Rate of Strain test (CRS) and Oedometer test

Parameters a and b were determined from CRS tests and the results were correlated to the wet volumetric weight as shown in figure 4.5.1. The wet volumetric weight showed to correlate very well with parameter b and slightly less so for parameter a, although this is most probably related to the measurement errors being magnified for small deformation measurements. These two correlations were used to determine parameters a and b of the samples tested in Triaxial Compression and Extension. It was in addition shown that parameters a and b are mostly related to the organic and clay content of the soil.
The pre-consolidation pressure of the tested samples were determined from both CRS and oedometer tests. The results of the pre-consolidation pressures for the Triaxial Compression and DSS tests are given in figures 4.5.2 and 4.5.3.

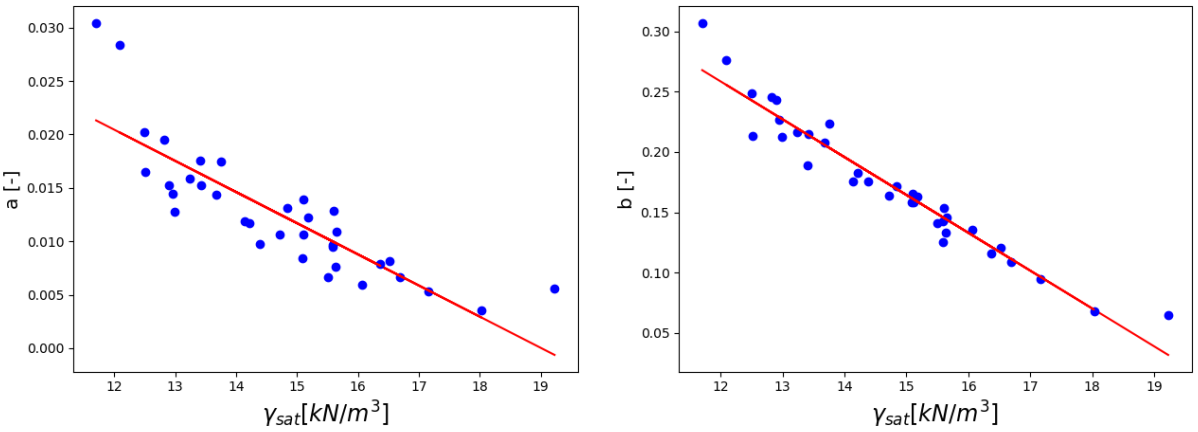

Figure 4.5.1: Correlation between parameters a and b versus wet volumetric weight

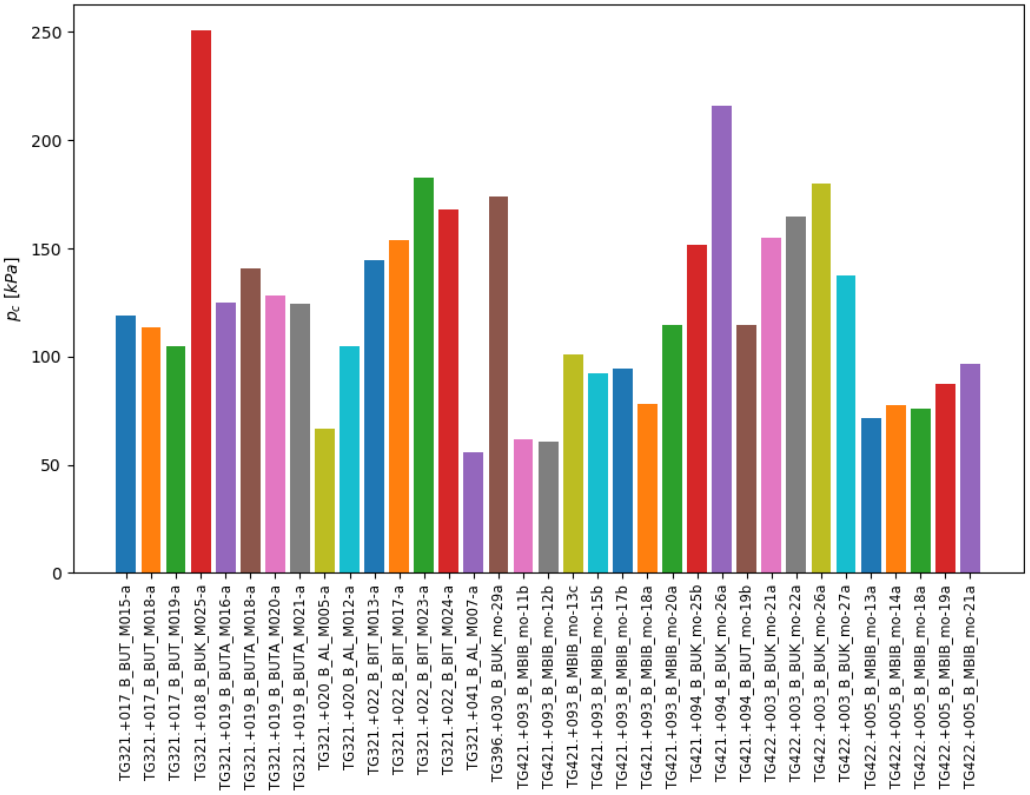

Figure 4.5.2: Pre-consolidation pressures Triaxial Compression test determined from CRS and oedometer tests

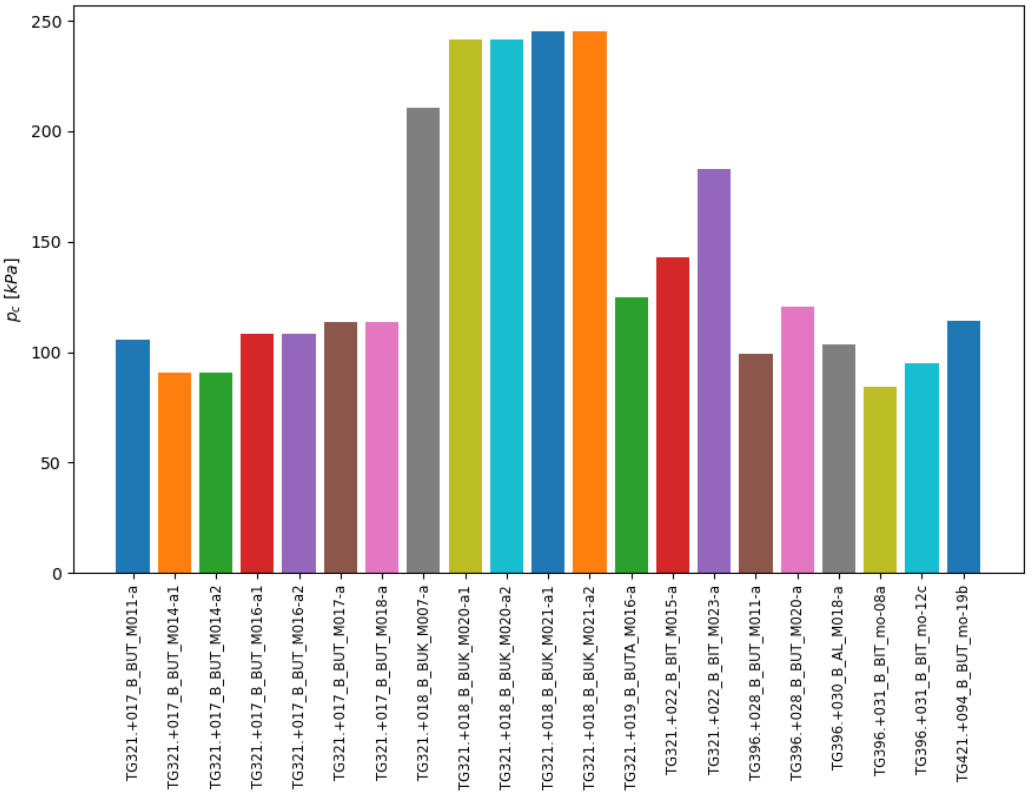

Figure 4.5.3: Pre-consolidation pressures DSS test determined from CRS and oedometer tests

Chapter 5

Extended Results

The previous analysis showed that no conclusions could be drawn on the general behaviour of the soil and the general correlations which can be expected across the different samples. In this section, similar samples are matched based on index tests which give an indication of the behaviour of the soil in order to better understand the behaviour of one particular material according to different boundary conditions, stress history and throughout the confining pressures encountered for the construction of a river embankment. First, the method for matching these samples is described in section 5.1, after which the reasoning for removing outliers is explained in section 5.2. In section 5.3, the limitations of the classical Critical State Soil mechanics based on these results are discussed, as well as the effects which are specific to the laboratory tests and equipment and therefore do not correspond to the true material behaviour.

5.1 Matching samples of equal properties

The next step is to perform the analysis on (close to) identical samples tested under different conditions and stress levels in order to better understand the behaviour of one particular soil composition across the range of stress levels encountered for this project.
As mentioned in section 3.1, the soil is composed of varying amounts of clay, silt, organic material and sand. The volumetric weight is often used to differentiate soils from each other, however different combinations of soil composition and in-situ confinement can result in the same measured volumetric weight due to the variability in soil composition. Additionally, the range of stress levels encountered in the field means the volumetric weights would require to be adjusted according to the void ratio (stress level dependent) which is in turn dependent of the decomposition of the organic matter (Hobbs, 1987). The decomposition of the organic matter is itself again dependent on the stress history and depth of the deposit. The use of volumetric weights to differentiate samples is therefore tedious and potentially unreliable due to the many variables. The Atterberg limits and more particularly the Plasticity Index offer a good alternative since the tests are performed on completely remoulded samples, therefore inhibiting any effect of structure, and give a good indication of the plastic behaviour of the soils as shown by Ladd (1991) and Nakase, Kamei, and Kusakabe (1988).
The method which was adopted is the following: the tested samples were matched based on equal Plasticity Index and soil classification (if these properties are known) albeit with the addition of a threshold tolerance. The use of a tolerance to match different samples accounts for the natural heterogeneity within the soil sample, yet this method may be problematic for soils near the turning point between characteristic soils: organic soils with organic contents as low as 27.5% may still behave like a peat (Hobbs, 1987) and the soil in question would be classified from a silty clay to clayey peat (Den Haan & Kruse, 2007). The turning point between peat and clay behaviour can occur at different organic contents according to the morphology of the soil and can therefore not easily be predicted (Hobbs, 1987). The choice of the threshold tolerances for the Plasticity Index and the soil classification is therefore key in this analysis: a low threshold can result in

too few results to perform a convincing analysis and too high threshold could feature soil samples with different behaviour. The chosen threshold tolerances used in this analysis were 5% for the Plasticity Index and Classification.
Samples tested in the triaxial test for which the soil classification wasn't determined were considered as outliers whenever their behaviour was considered too different to the behaviour of the tests of matched composition. The removal of outliers is further detailed in section 5.2.
The general trend of the matched results show a large band in the stress ratio and p_{eq}/p ratio reached at steady state pore pressure development. For both cases, there is a clear distinction between the type of test and stress history of the sample. The p_{eq}/p ratio shows a band between the results which is more predominant for over-consolidation conditions: samples shearing undrained from the wet side reach values of 1.5 at 10% strain whilst if sheared from the dry side this ratio reaches values of 2 to almost 4. This ratio increases with the OCR of the sample. A possible explanation for this aspect is the presence of large discontinuities in which the constant void ratio cannot be guaranteed for undrained tests and the development of non-uniform excess pore-pressures as previously developed in 2.2.1. The expected p_{eq}/p ratio is expected to be reached at steady state and closely equate 2.0 according to the classical Critical State Soil mechanics (Wroth, 1984). In this dataset, only the drained tests on over-consolidated samples and low over-consolidated samples sheared undrained appear to reach this expected value.

5.2 Outlier removal

The matching of samples of similar plasticity indexes results in some considerations regarding outliers: again, this method does not ensure perfectly identical soil samples, in terms of classification, to be matched. The tests which were considered outliers were either proven to be faulty or their behaviour was proven to differ too much from the other tests which similar boundary conditions. The latter only applies to the samples for unknown soil classification. Sample TG422.+005_B_MBIB_mo-20a was matched in figure 5.2.1, however its behaviour clearly deviates from the other normally consolidated samples. The test shows increasing confining pressures in its early stage of shearing and the equivalent confining pressure to current confining pressure ratio doesn't reach values similar to the other normally consolidated samples. In addition, the sample fails at lower axial strains than the other undrained tests sheared from the wet side and above all at axial strains slightly lower than what would be expected.
In figure 5.2.2, sample TG321.+020_B_AL_M008-a shows in the $e - log(p')$ space that the initial void ratio is considerably lower than the initial void ratio of sample TG421.+094_B_BUT_mo-19b although its initial confining pressure is almost double the initial confining pressure of test TG321.+020_B_AL_M008-a. In addition, the test reached at the end of the test confining pressures higher than expected and the typical band width between the results of soils tested from the dry and wet side is not observed. The equivalent confining pressure to current confining pressure ratio also doesn't reach the typical values expected from the general behaviour.
Another consideration is the presence of faulty tests: both laboratories which have performed the triaxial tests have reported many tests failed prematurely during consolidation or right after. In the latter case, it may not always be obvious whether the test is faulty and might be considered as a well executed test of weaker material. For test TG422.+005_B_BITA_mo-12b shown in figure 5.2.3, the results show a peak stress ratio at strain levels of 1% whilst axial strain of at least 10% are expected for drained test performed from the wet side (Atkinson et al., 1993). The equivalent confining pressure to current confining pressure ratio also doesn't reach the the expected values. In this test, the excessive strain softening is clearly a result of premature failure of the sample. Additionally, both tests TG321.+020_B_AL_M008-a and TG422.+005_B_BITA_mo-20b were considered as outliers due to the low stress ratio's reached during the test.

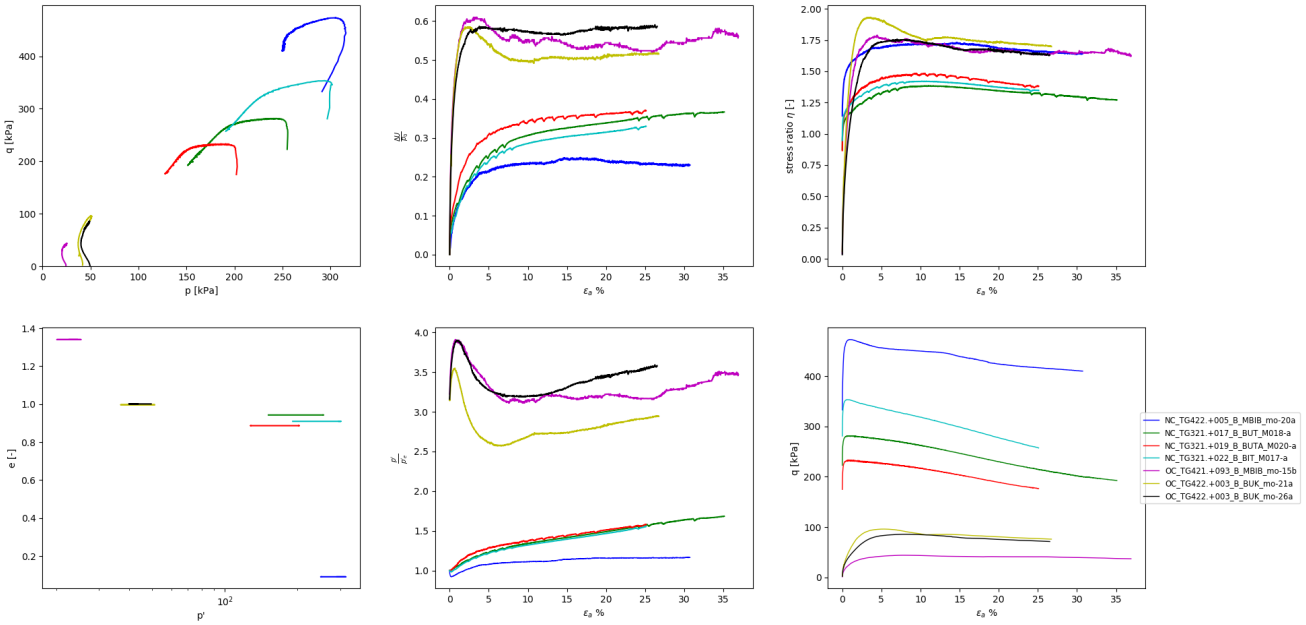

Figure 5.2.1: Results Triaxial compression tests for matched Plasticity Index 38%

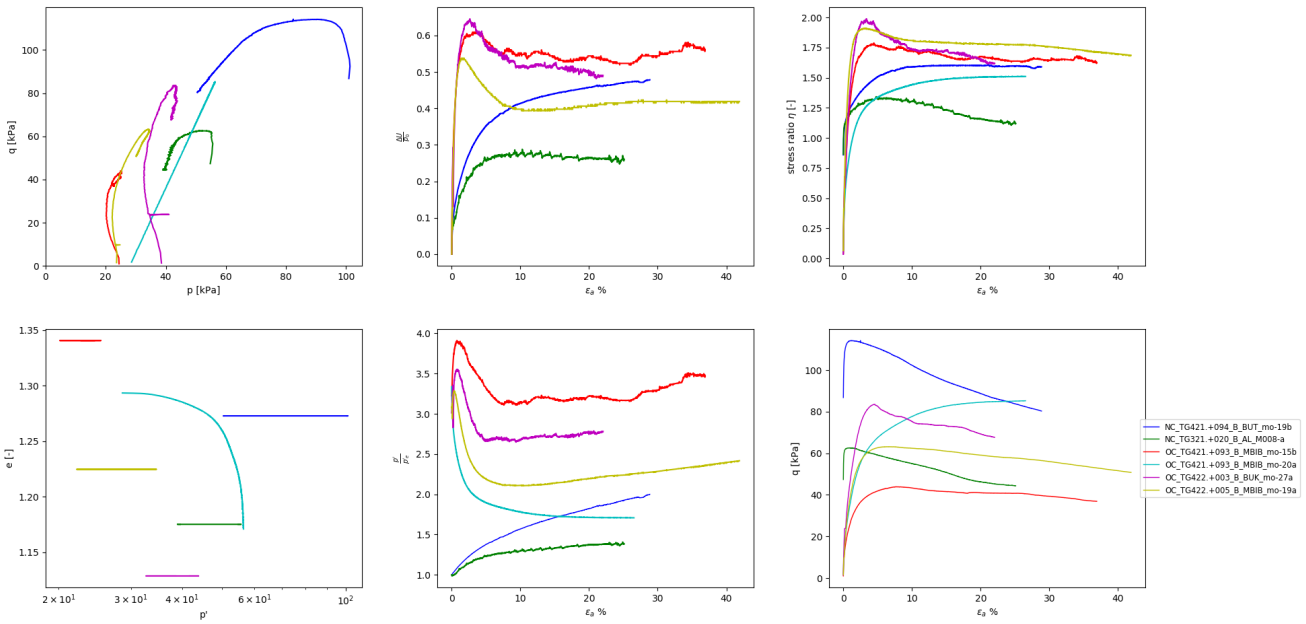

Figure 5.2.2: Results Triaxial compression tests for matched Plasticity Index 44%

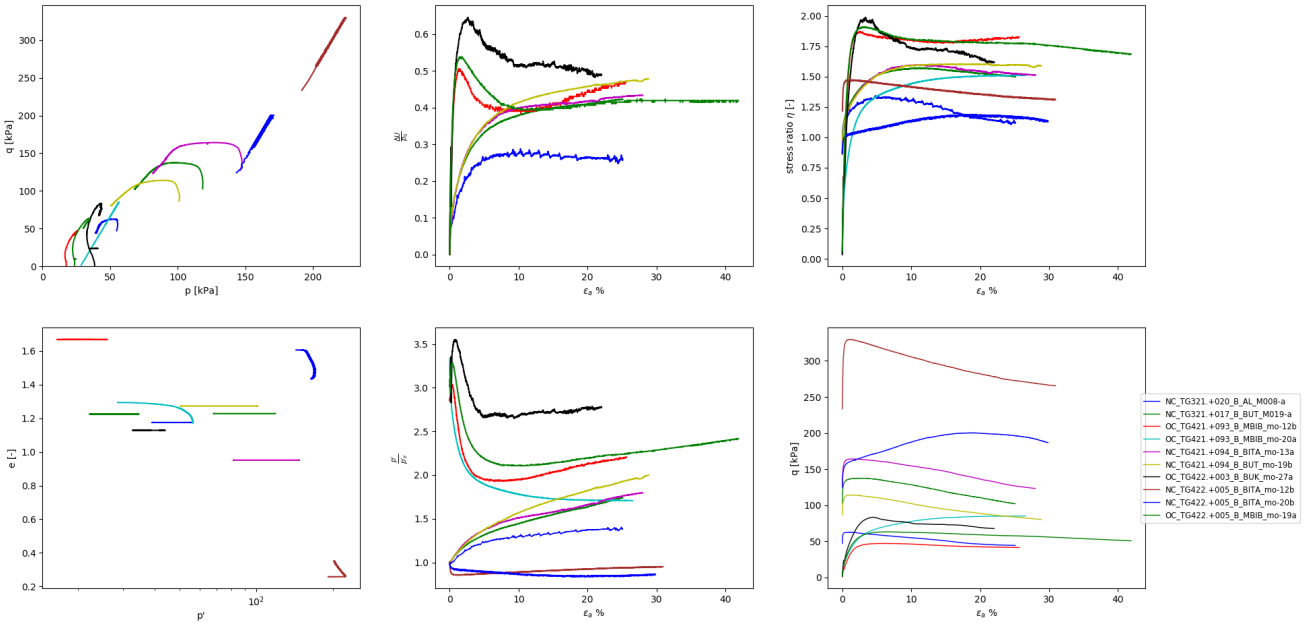

Figure 5.2.3: Results Triaxial compression tests for matched Plasticity Index 47%

5.3 Limitations of the Classical Critical State theory in explaining the test results

In figures 5.3.1 to 5.3.4, examples of the matches results are shown for respective Plasticity Indexes of 47, 56, 60 and 69 % respectively. The results again show inconsistencies with the Classical Critical State theory: the post peak stress ratio of the undrained over-consolidated tests is in almost every case always higher than the stress ratio of the undrained normally consolidated tests. The same is true for the drained tests (see figure 5.3.1). Amongst similar normally consolidated samples tested in an undrained test, there is a tendency of the stress ratio to be dependent on the initial confining pressure where the steady state stress ratio decreases with increasing initial confining pressure. This trend is also noticeable amongst the over-consolidated samples. In fact, one can argue whether the differences observed occur due the different test boundary conditions and sample stress history resulting in different results regardless of the initial confining stress, or whether this is a manifestation of the initial confining stress dependency of the undrained shear strength and Critical State friction as shown by Casey and Germaine (2013) and Abdulhadi, Germaine, and Whittle (2012). The latter was shown to be significant for large ranges of initial confining pressures (100 kPa to 10 MPa), which would imply the effects on the stress levels considered for this macro-stability assessment would be minimal, however Casey and Germaine (2013) showed the stress dependency of the Stress ratio increases with increasing soil liquid limit which is the case for Gorinchem clay.s

The differences occurring in the void ratio space or p_e/p space also deviate significantly from the Classical Critical State theory: the results show a significant bandwidth between the outcomes of the test according to the drainage conditions and stress history, where the results should reach the same Critical State Line (void ratio space) or p_e/p ratio of 2.0 according to the Classical Critical State theory and Modified Cam-Clay soil model. In figure 5.3.1, the normal compression line (NCL) was drawn and attempts of CSL are proposed. The results appear to be consistent for the undrained normally consolidated tests and drained over-consolidated tests, however the attempted Critical State Lines feature a significant bandwidth. The undrained over-consolidated tests seem to less reliable in the void ratio space which can be explained by the distinct shear zone developed samples tested undrained from the dry side, as was discussed in section 2.2.1. In

figures 5.3.2 to 5.3.4, the determination of the CSL line was less successful. A p_e/p ratio of 2.0 corresponds to a symmetric ellipse as the shape of the yield surface. The results may suggest the p_e/p ratio to be different than 2.0 in which case the Modified Cam-Clay is not a suitable soil model to replicate the behaviour of this particular soil. Another cause of such discrepancy, and particularly relevant for Dutch soils (Ministerie van Infrastructuur en Milieu, 2016), is creep: should the soil sample have featured creep during the onset from consolidation to undrained shearing and during undrained shearing (Atkinson et al., 1993), the estimations of the void ratio and equivalent confining pressure would lean towards a p_e/p ratio smaller than 2.0 following a traditional Isotach model (Imai, Tanaka, & Saegusa, 2003).
The results show most tests on normally consolidated samples feature increasing excess pore pressures up to 10% axial strain after which the excess pore pressures increase at constant rate. The stress ratio of most undrained tests on NC samples remain constant beyond 10% axial strain. Similar effects and conclusions were noted by Głuchowski, Soból, Szymański, and Sas (2019) albeit with monotonically decreasing excess pore pressures once the critical state undrained shear strength was reached. The Classical Critical State theory does not predict either post critical state strain softening or hardening due to additional post critical state excess pore pressure development. This softening also cannot be considered to be a steady reach of the residual state as the residual strength of the soil is only expected to occur at much large strains (Lupini et al., 1982).

In most of the literature (Głuchowski et al., 2019; Nakase & Kamei, 1983; Sheahan et al., 1996; J. Liu, Wang, Zhang, Yang, & Zhang, 2019; Abelev & Lade, 2004), the post Critical State strain softening or hardening for clays or peats in undrained tests occur at constant stress ratio M, in other words the stress path follows the Critical State line in the $p'q$ space. In most of the results of Gorinchem clay for undrained normally consolidated conditions, the stress path 'plunges' and deviates away from a potential Critical State line in a drastic fashion as in figure 4.1.1, or in a moderate fashion as is observed for most cases (figures 5.3.2, 5.3.3, 5.3.4), although this behaviour does not occur necessarily for all the samples which were matched previously. These effects can be explained by the issues of performing large strain triaxial compression tests on soft soils as previously discussed in 2.2.1, and may indicate the Critical State conditions are not reached reliably. This behaviour therefore does not necessarily correspond to the in-situ material behaviour. These results and the results from Muraro (2019); Głuchowski et al. (2019); J. Liu et al. (2019) and particularly the results from Gens (1982) and Sheahan et al. (1996) show the Critical State conditions for soft soils are reached in an asymptotic fashion as shown in figure 5.3.5 rather than the common understanding from the Classical Critical State soil mechanics. This explains some degree of strain softening although not to the extend as for an undrained shear strength at 25% axial strain as recommended in the guidelines. The cause of the excessive softening is most probably a consequence of extensive 'testing effects' due to the high plasticity of Gorinchem clay, as opposed to the tested Boston Blue Clay (Sheahan et al., 1996) and Lower Cromer Glacial Till (Gens, 1982) for which plasticity indexes of 24% and 12% respectively.
The asymptotic reach of the Critical State line and ongoing strain softening mean the choice for the undrained Critical State shear strength as a steady state parameter is not ideal when assessing strength parameters for this particular material and requires an alternative strength assessment in accordance with the experimental results. Many of the observations which do not conform to the traditional Critical State Soil mechanics and Cam-Clay models can be attributed to the fact that fully remoulded soil samples were used in the development of these theories and are therefore limited for intact soils (Graham & Li, 1985). Some of the observed inconsistencies and spread in the results may however be caused by the use of slightly different strain rates between the matched samples.

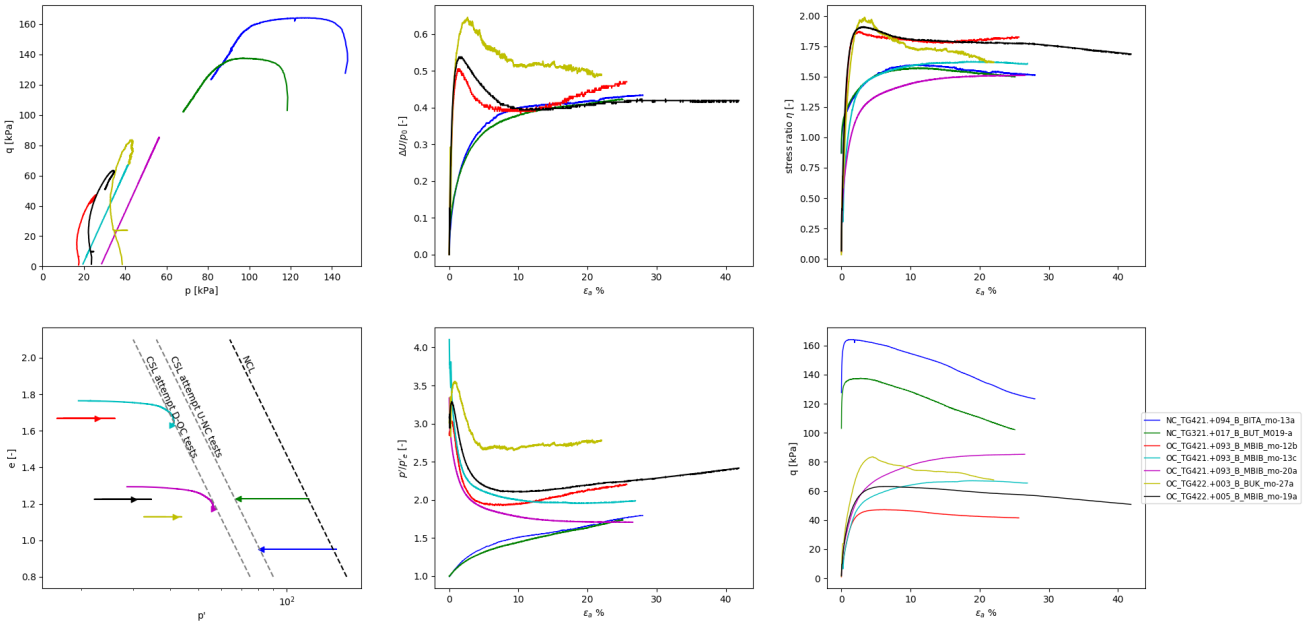

Figure 5.3.1: Results Triaxial compression tests for matched Plasticity Index 50%

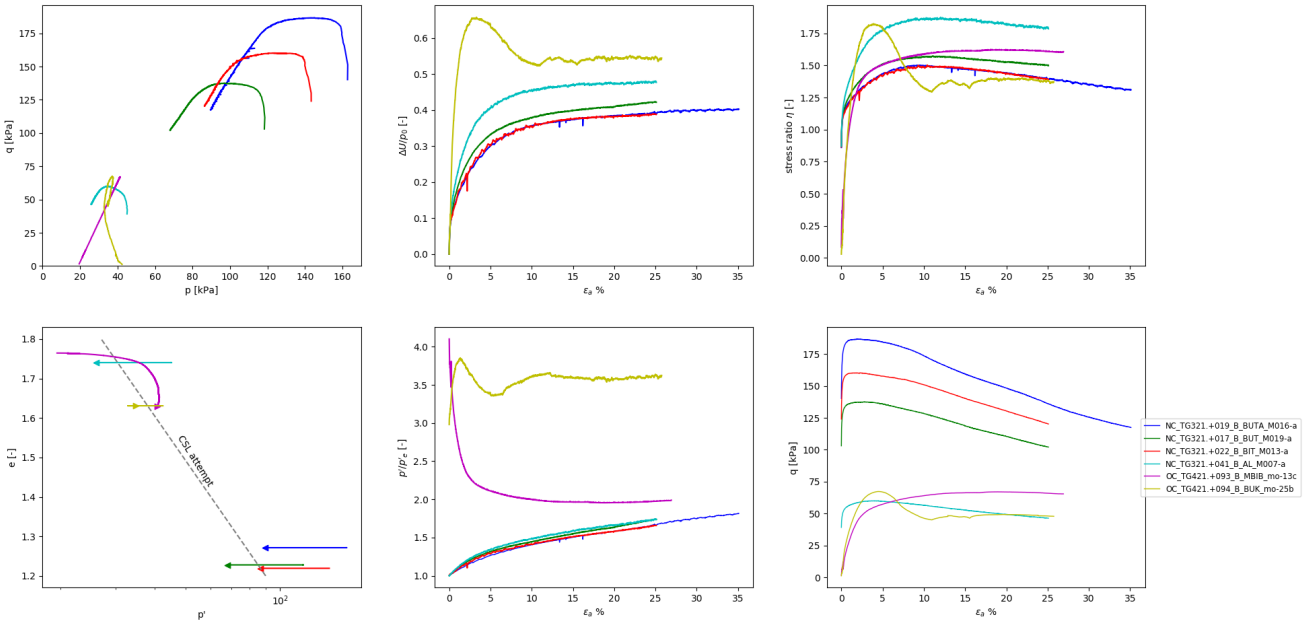

Figure 5.3.2: Results Triaxial compression tests for matched Plasticity Index 56%

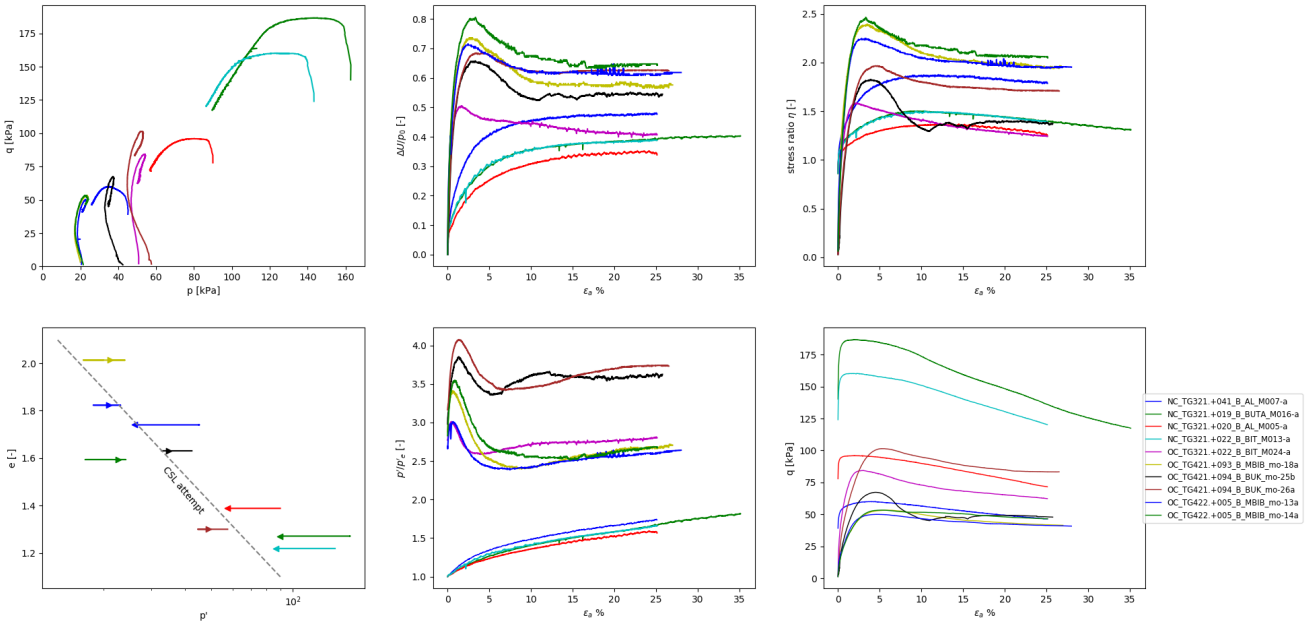

Figure 5.3.3: Results Triaxial compression tests for matched Plasticity Index 60%

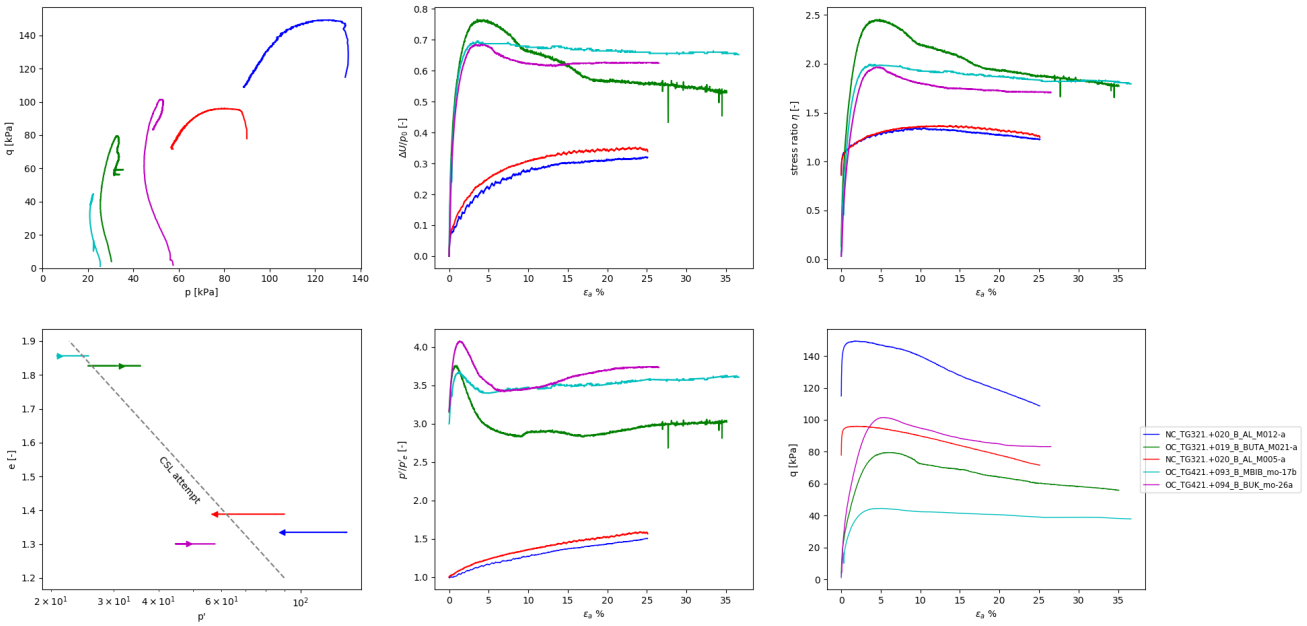

Figure 5.3.4: Results Triaxial compression tests for matched Plasticity Index 69%

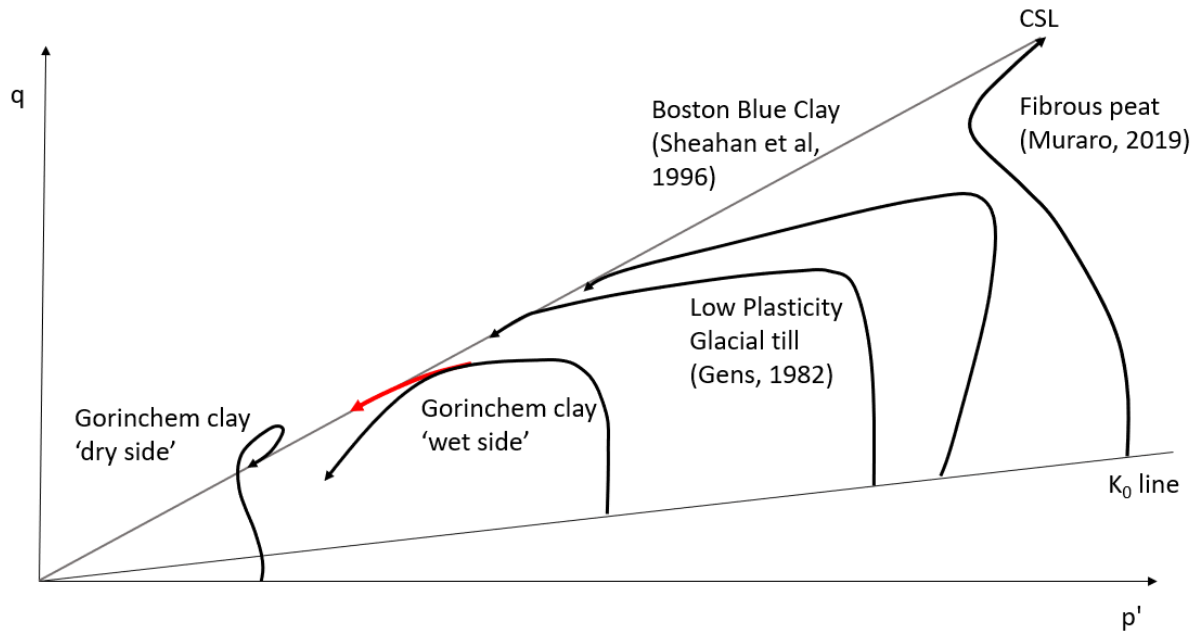

Figure 5.3.5: Asymptotic behaviour of Gorinchem clay, fibrous peat and glacial till in undrained triaxial compression. Black: test data; Red: expected behaviour. Test data for Gorinchem clay tested from the wet side shows significant 'test effects'.

5.4 Normally consolidated undrained stress path in DSS and Triaxial Compression for matching samples

The TC and DSS tests were matched based on similar initial confining pressures for normally consolidated conditions with a maximum threshold of 25 kPa and based on Plasticity Index in the same fashion as in section 5.1. The matched samples tested in TC and DSS are shown in figures 5.4.1 and 5.4.2 with the corresponding shear strain of the Triaxial Compression test at which the Critical State was reached.
The results show the that that peak stress ratio in Triaxial Compression occurs close to the peak stress ratio in DSS at 12 to 15 % shear strain. The post peak stress ratio response in DSS shows again excess strain softening confirming the excessive softening experienced with this test beyond 10 to 15% axial strain as expressed by Ladd and DeGroot (2003). Additionally, the results show the results in DSS significantly decrease from low to high confining pressures (up to 20%).

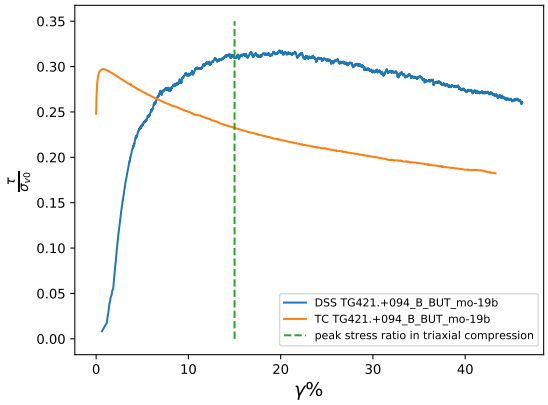

(a) 155 kPa

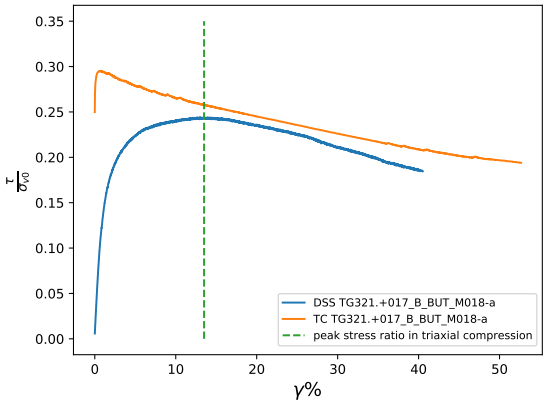

(b) 400 kPa

Figure 5.4.1: Undrained shear strength for samples of Similar Plasticity indexes (40%) and pre-consolidation pressure

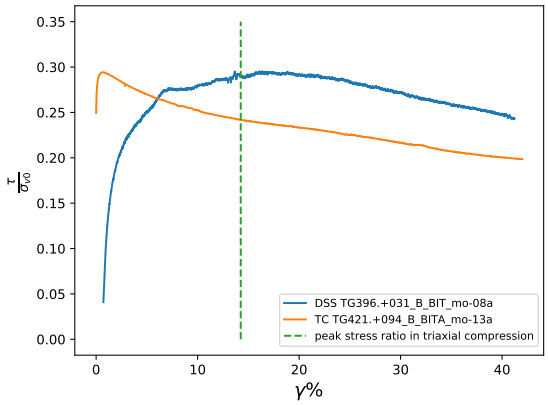

(a) 240 kPa

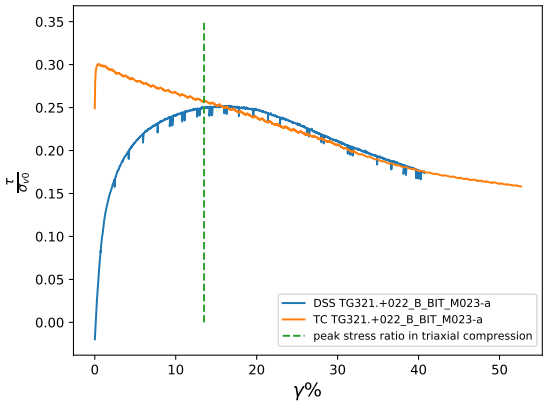

(b) 454 kPa

Figure 5.4.2: Undrained shear strength for samples of Similar Plasticity indexes (50%) and pre-consolidation pressure

Chapter 6

Modelling the behaviour of the soil in Triaxial tests

As was discussed in chapter 5, the Classical Critical State soil mechanics and Cam-Clay models show considerable limitations in predicting the behaviour of intact samples of Gorinchem Clay. This soil therefore requires an alternative strength assessment approach and a more advanced constitutive soil model. In this section, the general constitutive models developed to model the behaviour of soil are described according to Wood (2014), from the most basic elastic models to the full elasto-plastic models in section 6.1. The constitutive model used in this thesis, which is able to model non-associative flow and deviatoric effects, is then introduced and used to reproduce the behaviour of the Triaxial Compression tests in section 6.2 and in Triaxial Extension in section 6.4.

6.1 On the behaviour of soils

6.1.1 Elastic models

The most basic stress strain relationship which can be used in constitutive modelling is the elastic model according to Hookes's law, which states that the stress increment $\delta\sigma$ and strain increment $\delta\epsilon$ are proportional by the stiffness matrix (equation 6.1.1). In a three dimensional space, the stress increment, strain increment and stiffness matrix can be expressed respectively as shown in equation 6.1.2,6.1.3 and 6.1.4, where E is the Young's modulus and ν the Poisson ratio. Equation 6.1.1 can be expressed in terms of the deviatoric stress and mean normal stress in a triaxial space as shown in equation 6.1.5 where K is the Bulk modulus and G the Shear Modulus, whilst the volumetric strain increment $d\epsilon_v$ and the deviatoric strain increment $d\epsilon_q$ given in equations 6.1.6 and 6.1.7. The elastic model is a simple to use model however its use is limited to the small strain domain as the predictions from the elastic model overestimate the material stiffness. In addition, the criterion for failure is somewhat vague as the limiting factor is a strain threshold rather than a physical feature. Nonetheless, the elastic model constitutes the basis for the more advanced constitutive models able to feature plastic behaviour of the soil.

$$d\boldsymbol{\sigma} = \boldsymbol{D} d\boldsymbol{\epsilon} \tag{6.1.1}$$

$$d\boldsymbol{\sigma} = \begin{bmatrix} d\sigma_{xx} & d\sigma_{yy} & d\sigma_{zz} & d\sigma_{xy} & d\sigma_{yz} & d\sigma_{zx} \end{bmatrix}^T \tag{6.1.2}$$

$$d\boldsymbol{\epsilon} = \begin{bmatrix} d\epsilon_{xx} & d\epsilon_{yy} & d\epsilon_{zz} & d\gamma_{xy} & d\gamma_{yz} & d\gamma_{zx} \end{bmatrix}^T \tag{6.1.3}$$

$$\boldsymbol{D} = \frac{E}{(1+\nu)(1-2\nu)} \begin{bmatrix} 1-\nu & \nu & \nu & 0 & 0 & 0 \\ \nu & 1-\nu & \nu & 0 & 0 & 0 \\ \nu & \nu & 1-\nu & 0 & 0 & 0 \\ 0 & 0 & 0 & \frac{1}{2}-\nu & 0 & 0 \\ 0 & 0 & 0 & 0 & \frac{1}{2}-\nu & 0 \\ 0 & 0 & 0 & 0 & 0 & \frac{1}{2}-\nu \end{bmatrix} \tag{6.1.4}$$

$$\begin{bmatrix} dp \\ dq \end{bmatrix} = \begin{bmatrix} K & 0 \\ 0 & 3G \end{bmatrix} \begin{bmatrix} d\epsilon_p \\ d\epsilon_q \end{bmatrix} \tag{6.1.5}$$

$$d\boldsymbol{\epsilon_p} = d\epsilon_1 + 2d\epsilon_3 \tag{6.1.6}$$

$$d\boldsymbol{\epsilon_q} = \frac{2}{3}(d\epsilon_1 - d\epsilon_3) \tag{6.1.7}$$

6.1.2 The elastic-perfectly plastic model, an introduction to yield criterion and plastic potential

As seen in section 2.1 most soils develop volume changes when they are subjected to shear stresses. The Critical State concept states that the soil reaches a constant volume and therefore constant shear stress when sheared to large enough strains. The elastic-perfectly plastic model therefore constitutes the first model capable of reproducing this particular aspect of the behaviour of soils. In the elastic-perfectly plastic model, the elastic strains (recoverable) have to be distinguished from the plastic strains (irrecoverable) as in equation 6.1.8, where ϵ^e are the elastic strains and ϵ^p are the plastic strains. The elastic strain increment occurs when there is a change in stress $\delta\sigma$ according to equation 6.1.9, where D is the elastic stiffness matrix. The main assumption in the elastic-perfectly plastic model is that upon shearing, initially only elastic strains occur until an elastic boundary called the yield surface, after which only plastic strains occur and the material deforms at constant shear stress. This behaviour is represented in figure 6.1.1. The perfect plasticity after the yield condition implies that the yield condition is a failure condition and that the stress state cannot go beyond the yield surface. The yield function f is introduced in equation 6.1.10 to represent this behaviour, for which the plastic strain increment $\delta\epsilon^p$ occurs when the stress state lies on the yield surface during incremental loading as shown in equation 6.1.11. This feature is called the consistency condition.

The plastic strains can be determined by introducing the plastic potential function $g(\sigma)$ which can be evaluated by the current stress state as shown in equation 6.1.12. λ is the plastic multiplier which is equal to zero for purely elastic behaviour and non-zero for plastic behaviour. Substituting equation 6.1.12 in equation 6.1.8 and 6.1.9 yields equation 6.1.13. Combining equations 6.1.11 and 6.1.13, the plastic multiplier can be expressed as equation 6.1.14 and the full elastic-perfectly plastic relationship can be expressed as equation 6.1.15, where D^{ep} is the elastic-plastic stiffness matrix. In the classical plasticity theory, the plastic potential function g equates the yield function f, also known as the associative flow rule or normality which implies that the strain increment vectors are normal to the yield surface of the current stress state. To resume, when the plastic potential is lower than the yield surface, the yield function and plastic potential are non-zero which implies only elastic strains occur (such case occurs during an unloading-reloading event) whist the strains are solely plastic once the potential function has reached the yield surface.

The elastic-perfectly plastic model features a physical description of failure, in doing so however, the model neglects that fact that plastic deformation also occur at the pre-failure stage. This aspect is tackled by the elasto-plastic model in the next section.

$$d\boldsymbol{\epsilon} = d\boldsymbol{\epsilon^e} + d\boldsymbol{\epsilon^p} \tag{6.1.8}$$

$$d\boldsymbol{\sigma} = \boldsymbol{D} d\boldsymbol{\epsilon}^{\boldsymbol{e}} \tag{6.1.9}$$

$$f(\boldsymbol{\sigma}) = 0 \tag{6.1.10}$$

$$df(\boldsymbol{\sigma}) = (\frac{\partial f}{\partial \boldsymbol{\sigma}})^T d\boldsymbol{\sigma} = 0 \tag{6.1.11}$$

$$d\boldsymbol{\epsilon}^{\boldsymbol{p}} = \lambda \frac{\partial g}{\partial \boldsymbol{\sigma}} \tag{6.1.12}$$

$$d\boldsymbol{\sigma} = \boldsymbol{D} d\boldsymbol{\epsilon} - \lambda \boldsymbol{D} \frac{\partial g}{\partial \boldsymbol{\sigma}} \tag{6.1.13}$$

$$\lambda = \frac{\frac{\partial f}{\partial \boldsymbol{\sigma}}^T \boldsymbol{D} d\boldsymbol{\epsilon}}{\frac{\partial f}{\partial \boldsymbol{\sigma}}^T \boldsymbol{D} \frac{\partial g}{\partial \boldsymbol{\sigma}}} \tag{6.1.14}$$

$$d\boldsymbol{\sigma} = \left[\boldsymbol{D} - \frac{\boldsymbol{D} \frac{\partial g}{\partial \boldsymbol{\sigma}} \frac{\partial f}{\partial \boldsymbol{\sigma}}^T \boldsymbol{D}}{\frac{\partial f}{\partial \boldsymbol{\sigma}}^T \boldsymbol{D} \frac{\partial g}{\partial \boldsymbol{\sigma}}} \right] d\boldsymbol{\epsilon} = \boldsymbol{D}^{ep} d\boldsymbol{\epsilon} \tag{6.1.15}$$

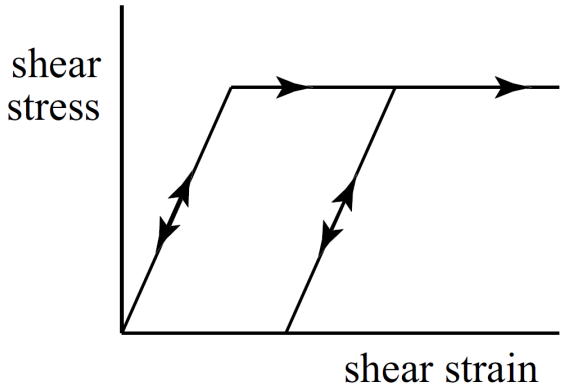

Figure 6.1.1: elastic-perfectly plastic behaviour (Wood, 2014)

6.1.3 Elasto-plastic models

The elasto-plastic models have the ability of reproducing the pre-failure non-linearity by introducing a hardening yield function. The model essentially still features the basic framework of the elastic-perfectly plastic model with the addition of a growing yield surface, thus resulting in plastic strains during the pre-failure stage. The failure definition is identical to the failure definition in the elastic-perfectly plastic model. The hardening as a result of plastic strains can be illustrated physically with an over-consolidated soil sheared undrained: the over-consolidation causes irreversible volumetric strains causing the elastic region to increase and upon undrained reloading of the material causes failure to occur at larger stress levels than the normally consolidated soil. The addition of the hardening feature requires an additional equation which describes how much hardening occurs for every increment of plastic strains. The elasto-plastic model therefore requires four parts: an expression for the elastic response of the elastic deformations, a yield criterion which specifies the boundary of pure elastic behaviour, a flow rule which specifies the mechanism of plastic deformation and a hardening rule which links the change in size of the yield surface with plastic deformations. The description of the elastic deformations and the flow rule can be performed with the same expressions as in the elastic-perfectly plastic model. The introduction of plastic hardening requires the modification of the yield criterion to be a function of the hardening

parameter χ, where the yield is given by equation 6.1.16. Again the stress state cannot surpass the yield surface, the consistency condition can therefore be expressed as equation 6.1.17. The hardening parameter is itself a function of the amount of plastic strains $\chi = \chi(\epsilon^p)$, equation 6.1.17 can therefore be written as equation 6.1.18 using the same flow rule expression as in equation 6.1.12. Equation 6.1.18 can then we written as equation 6.1.19 where H is the plastic modulus defined in equation 6.1.20. The full elasto-plastic relationship can then be expressed as equation 6.1.21

$$f(\boldsymbol{\sigma}, \chi) = 0 \tag{6.1.16}$$

$$df = \frac{\partial f}{\partial \boldsymbol{\sigma}}^T d\boldsymbol{\sigma} + \frac{\partial f}{\partial \chi} d\chi = 0 \tag{6.1.17}$$

$$\frac{\partial f}{\partial \boldsymbol{\sigma}}^T d\boldsymbol{\sigma} + \lambda \frac{\partial f}{\partial \chi} \frac{\partial \chi}{\partial \boldsymbol{\epsilon^p}} \frac{\partial g}{\partial \boldsymbol{\sigma}} = 0 \tag{6.1.18}$$

$$\frac{\partial f}{\partial \boldsymbol{\sigma}}^T d\boldsymbol{\sigma} + H\lambda \tag{6.1.19}$$

$$H = -\frac{\partial f}{\partial \chi} \frac{\partial \chi}{\partial \boldsymbol{\epsilon}^p}^T \frac{\partial g}{\partial \boldsymbol{\sigma}} \tag{6.1.20}$$

$$d\boldsymbol{\sigma} = \left[\boldsymbol{D} - \frac{\boldsymbol{D} \frac{\partial g}{\partial \boldsymbol{\sigma}} \frac{\partial f}{\partial \boldsymbol{\sigma}}^T \boldsymbol{D}}{\frac{\partial f}{\partial \boldsymbol{\sigma}}^T \boldsymbol{D} \frac{\partial g}{\partial \boldsymbol{\sigma}} + H} \right] d\boldsymbol{\epsilon} = \boldsymbol{D}^{ep} d\boldsymbol{\epsilon} \tag{6.1.21}$$

6.1.4 The modified Cam-Clay model

The modified Cam-Clay model is the first hardening plastic model which has been adopted to model the behaviour of soils. It also forms the basis for most soil models including the non-associated elasto-plastic model used later in this thesis. The basic concepts of the modified Cam-Clay model were introduced in sections 2.1. The elastic volumetric response is characterised by equation 6.1.22, where equation 6.1.23 is its incremental form. The bulk modulus K is therefore given by equation 6.1.24. The stiffness matrix is then given by equation 6.1.25. The yield locus in the p'q space is an ellipse for which the size is specified by the preconsolidation pressure p_c which constitutes the hardening parameter χ and where the critical state parameter M specifies the curvature. The yield criterion is given in equation 6.1.26 and can be rewritten as equation 6.1.27. The hardening rule is given in equation 6.1.28 where η is the stress ratio. The Modified Cam Clay model has an associative flow rule (equation 6.1.29) and is therefore of the same form as the yield criterion of equation 6.1.26. The plastic strain increments are then given in equation 6.1.30, which can be rewritten as the ratio of the plastic strains as given in equation 6.1.31. The hardening rule given in equation 6.1.32 is only a function of the volumetric plastic strains.

$$v = v_\kappa - \kappa \ln p' \tag{6.1.22}$$

$$d\epsilon_p^e = -\frac{dv}{v} = \frac{\kappa}{v} \frac{dp'}{p'} \tag{6.1.23}$$

$$K = \frac{dp'}{d\epsilon_p^e} = \frac{vp'}{\kappa} \tag{6.1.24}$$

$$\begin{bmatrix} dp \\ dq \end{bmatrix} = \begin{bmatrix} \frac{vp'}{\kappa} & 0 \\ 0 & 3G \end{bmatrix} \begin{bmatrix} d\epsilon_p \\ d\epsilon_q \end{bmatrix} \tag{6.1.25}$$

$$f(\boldsymbol{\sigma}, p_c^{'}) = \frac{q^2}{M^2} - p'(p_c^{'} - p') \tag{6.1.26}$$

$$q^2 = M^2 p'(p_c^{'} - p') \tag{6.1.27}$$

$$\frac{dp_0^{'}}{p_0^{'}} = \frac{dp'}{p'} + \frac{2\eta}{M^2 + \eta^2} d\eta \tag{6.1.28}$$

$$g(\boldsymbol{\sigma}) = f(\boldsymbol{\sigma}, p_0') \tag{6.1.29}$$

$$\begin{pmatrix} d\epsilon_p^p \\ d\epsilon_q^p \end{pmatrix} = \lambda \begin{pmatrix} \frac{\partial g}{\partial p'} \\ \frac{\partial g}{\partial q} \end{pmatrix} = \lambda \begin{pmatrix} 2p' - p_0' \\ \frac{2q}{M^2} \end{pmatrix} \tag{6.1.30}$$

$$\frac{d\epsilon_p^p}{d\epsilon_q^p} = \frac{M^2 - \eta^2}{2\eta} \tag{6.1.31}$$

$$\frac{dp'}{p} = \frac{v}{\lambda - \kappa} d\epsilon_p^p \tag{6.1.32}$$

6.1.5 Advanced Modified Cam-Clay based constitutive models with strain softening prediction capabilities

As was described in section 5.3, the Classical Critical State soil mechanics, and therefore the previously introduced Modified Cam-Clay model (MCC), feature limitations in predicting the behaviour of materials such as the Gorinchem Clay. Most of the limitations of the MCC model are due to the fact that this model was originally formulated for remoulded clays under isotropic consolidation (Atkinson et al., 1993). The MCC model was therefore not intended to be used for anisotropic behaviour and effects of destructuration. Both features are to be expected in naturally deposited clays (Huang, Liu, & Sheng, 2011) resulting from depositional history, consolidation and straining (Wheeler et al., 2003). In this thesis, anisotropic behaviour and destructuration, although intimately linked, are considered as two separate characteristics of the soil behaviour since fully remoulded (i.e. destructured) clays may still feature anisotropic behaviour (Gajo & Muir Wood, 2001). This characteristic is linked with the observation that a soil features anisotropic behaviour due to its initial particle assembly (inherent anisotropy) and by the soil's ability to adapt to a particular direction of plastic straining (Abelev & Lade, 2004). In order to reproduce the strain softening, several strategies have been adopted: M. Liu and Carter (2002) proposed an extension to the MCC called the Structured Cam Clay model for associative flow conditions where the destructuration of the material is reproduced using a shrinking yield surface once the material starts yielding as shown in figure 6.1.2. Structure is known to occur in most natural soft clays (Tavenas, 1990) due to cementation by deposition of carbonates, iron and aluminium oxides at the particle contacts (Leroueil & Vaughan, 1990). Ultimately, the yield surface reaches reference yield surface corresponding to the fully remoulded material. The model therefore features an isotropic hardening law. Undrained softening can be predicted by such constitutive model and additionally predict softening under drained normally consolidated conditions (Dafalias, Manzari, & Papadimitriou, 2006). In section 5.2, it was shown the drained test for normally consolidated conditions featuring softening was a faulty test and the remaining test did not show strain softening. Additionally, the results from the CRS tests do not show evidence of structure, although the presence of structure is best determined by comparison of a fully remoulded sample and an intact clay sample (Leroueil & Vaughan, 1990).

The anisotropic behaviour under undrained conditions can also be predicted by implementing a rotational hardening law such as was developed by Wheeler et al. (2003): the yield surface is

able to rotate and the evolution of the inclination of the yield surface varies as plastic shearing further develops thus modelling the development or erasure of the fabric anisotropy (Wheeler et al., 2003). In order to implement softening, a destructuration law is again required as shown in figure 6.1.3. Many of such models rely solely on plastic volumetric strains in expressing the change in rotation of the yield surface, which can seem unrealistic to exclude plastic deviatoric strains from the anisotropic formulation (Wheeler et al., 2003) as plastic deviatoric strains also affect the fabric of the soil. This specific shortcoming was remedied by Wheeler et al. (2003) and Huang et al. (2011) who additionally implemented a destructuration law dependent also on volumetric and deviatoric plastic strains (Huang et al., 2011).
Another method which can be adopted in predicting undrained strain softening is the use of a non-associative flow rule (Dafalias et al., 2006), where the use a separate plastic potential and yield surface enables the Crititical State conditions to occur at other states than the peak of the yield locus as shown in figures 6.1.4 and 6.1.5. This method has shown to be adequate by Yamada, Akaishi, and Dafalias (2001) if the degree of strain softening is small.
The MCC model and the mentioned advance constitutive models are well suited in predicting the behaviour of clays. However, as shown in section 3.1, the material question is not a 'clean' clay but contains significant amounts of organics, silt and minute amounts of sand. Although distortional hardening laws are traditionally used for sands (Wood & Belkheir, 1994), the devatoric hardening mechanisms can be adequate for peats and silts Muraro (2019) and may therefore also be suited to predict the behaviour of a heterogeneous and mixed soil such as Gorinchem Clay. More specifically, the use of deviatoric hardening enables the reproduction of instability states most commonly observed for loose sands and are therefore able to reproduce strain softening.
Most of the previous techniques requires numerous additional parameters to be determined in addition to the five parameters required in the MCC model and often results in tedious work to determine them. In addition, several of these additional parameters require specific tests to be performed on identical material which cannot be performed within the scope of this thesis. The ambition is therefore to use a more simplified constitutive model for which the parameters can be determined with more ease.

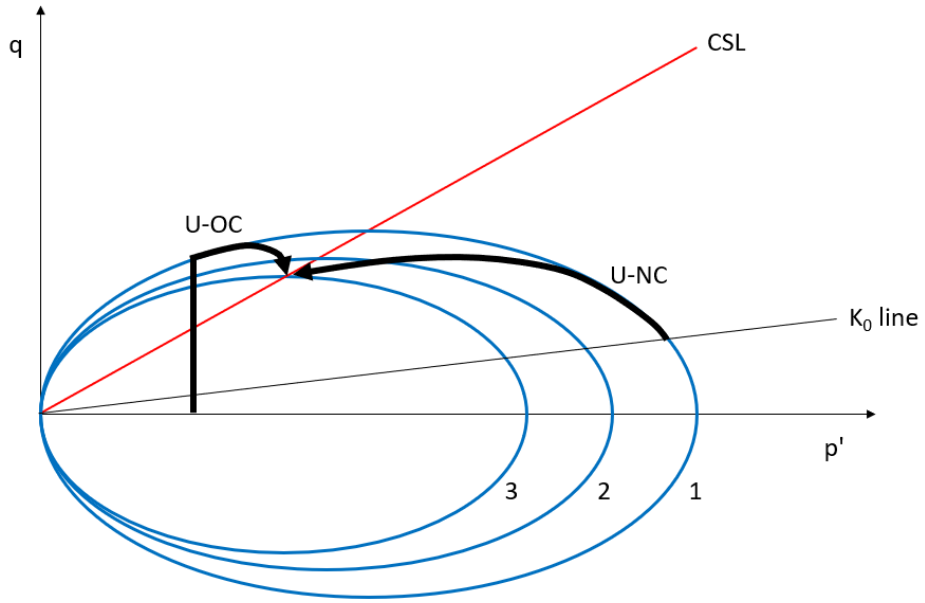

Figure 6.1.2: Visualisation of strain softening mechanism for undrained conditions using a shrinking yield surface according to the Structured Cam-clay model. 1,2,3: successive yield surfaces where 1 is the yield surface of the intact structured clay, 3 the yield surface for a fully remoulded clay and 2 an intermediate state

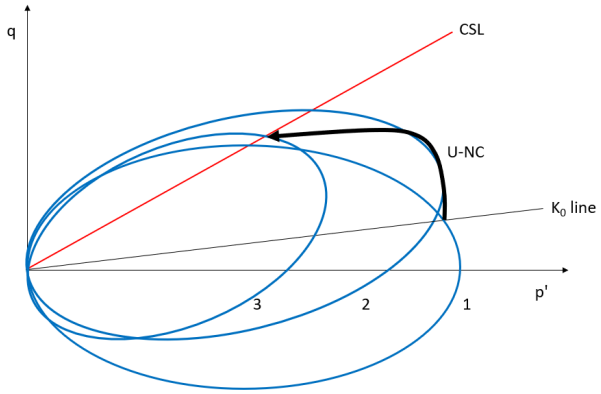

Figure 6.1.3: Visualisation of strain softening mechanism for undrained normally consolidated conditions using a rotational hardening rule and destructuration. 1: yield surface of the intact material, 2: rotated yield surface, 3: rotated and destructed yield surface.

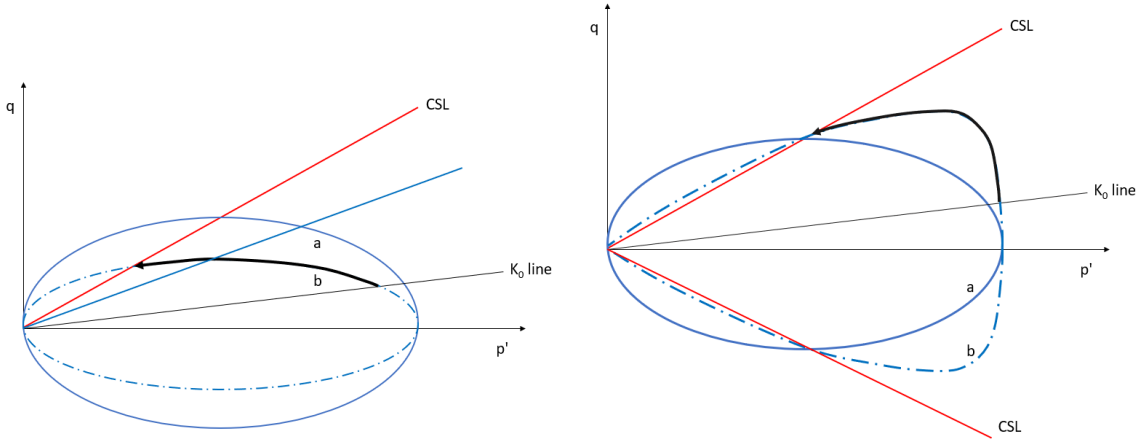

Figure 6.1.4: Stress path for non-associative flow induced strain softening for undrained normally consolidated conditions. (a): elliptical shaped yield locus smaller than the plastic potential locus, (b): tear-drop shaped yield locus

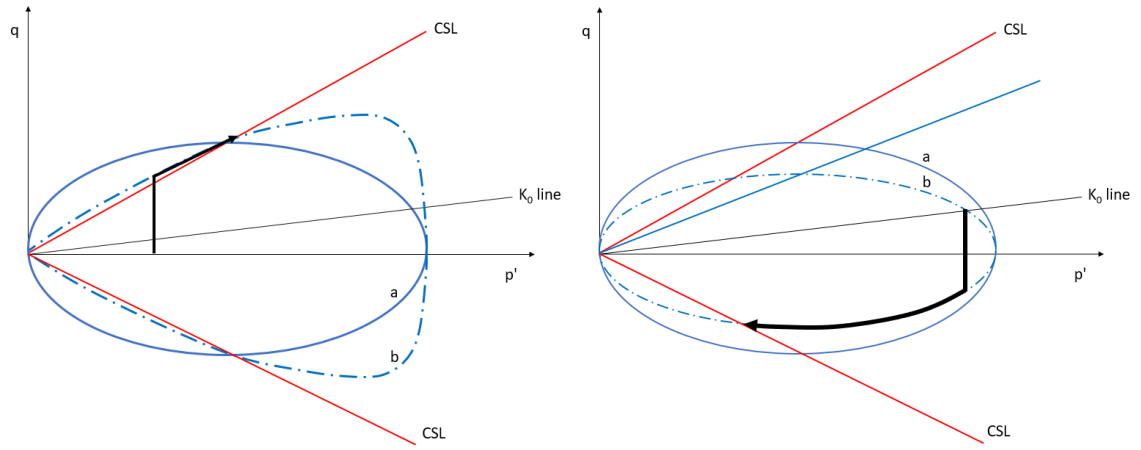

Figure 6.1.5: Stress path for non-associative flow and tear-drop shaped yield locus inducing strain softening. (a): undrained over-consolidated conditions (TC), (b): undrained normally consolidated conditions (TE)

6.2 Use of an non-associative elasto-plastic Constitutive model with volumetric and deviatoric hardening or softening contributions in understanding the experimental results

As mentioned previously in section 5.3, the behaviour of the soil from the laboratory tests is not fully captured by the Classical Critical State theory and Modified Cam Clay model. In this section, an advanced Modified Cam-Clay based constitutive model is presented.

6.2.1 Constitutive model background

The constitutive model which is used for this project is a simple elasto-plastic model which contains both volumetric and deviatoric contributions. This model was initially proposed and used by Chatzis (2018) and Muraro (2019) in modelling the behaviour of peat under Triaxial Compression conditions for both single element tests and Boundary value problems. The model relies on the basic principles of the Modified Cam Clay model (MCC) with the addtition of a non-associated flow rule and deviatoric hardening. As seen previously from the soil composition, the clay samples contain large amounts of organic contents and silt in which case a deviatoric contribution may be considered (Muraro, 2019). In addition, the pre-Critical State softening requires the use of a non-associative flow rule. The model is also able to replicate different yield locus shapes which proved to be necessary in replicating the behaviour of the soil in section 5.3.
The considered flow rule in the used constitutive model is given in equation 6.2.1. The expression for the yield locus (equation 6.2.2) is the same as proposed by McDowell and Hau (2003) and the same expression is used for the plastic potential surface as given in equation 6.2.3. The plastic hardening rule for both volumetric and deviatoric contribution is given in equation 6.2.4. At critical state, the incremental preconsolidation pressure p_c is zero, in which case equation 6.2.5 holds. Rewriting in terms of dilatancy at failure d_f in equation 6.2.6, the expression can be equated to the flow rule and solved for the failure stress ratio η_f as shown in equation 6.2.7. The following shows the failure stress ratio does not equate to the defined Critical State parameter M_g unless the deviatoric contribution to the hardening law D equates zero at failure. The deviatoric contribution is therefore considered to be a function of the deviatoric plastic strains in order to reduce the dilatancy at failure according to the formulation in equation 6.2.8 (Wilde, 1977).
The model consists of a limited set of parameters (10) which can be determined with relative ease: the first five parameters are the classical Modified Cam-Clay parameters i.e. Poisson's ratio ν, isotropic compression index λ , isotropic unloading-reloading index κ, initial void ratio e_0 and Critical State parameter M_g. Parameters e_0, λ and κ can be determined with laboratory tests and the two latter ones with an oedometer test, a CRS test or a K_o triaxial compression test. In this case the CRS test was used as conform to the Dutch guidelines (Ministerie van Infrastructuur en Milieu, 2016). Parameter M_g is to be determined for a soil sheared to critical state. The Poisson ratio is difficult to predict, it can however be estimated by calibrating the results of the modelled stress paths to the experimental stress paths.
The other five parameters are specific to a non-associated flow rule with deviatoric contribution: parameter M_f specifies the size of the yield surface and parameters χ_f and χ_g specify the apex of the yield and plastic potential surface respectively. In the MCC model, χ_g is equal to 2.0 and M_f is equal to M_g by default. Parameters D_0 and D_1 are the input parameters for the deviatoric contribution formulation in equation 6.2.8, where D_0 specifies the initial value of D i.e. at the initial deviatoric plastic strain, and D_1 the decrease rate of the deviatoric plastic strain. The sign of D dictates the behaviour of the deviatoric response: a positive D simulates dilation whilst a negative D reproduces contraction. For a negative D, the size of the yield locus decreases and replicates softening for increasing plastic deviatoric strains as shown in equation 6.2.4 similarly to the destructuration law in the constitutive model from Huang et al. (2011). This type of behaviour differs from the Structured Cam Clay model as M. Liu and Carter (2002) proposed volumetric and deviatoric dependent destructuration.

$$\frac{\delta\varepsilon_p^p}{\delta\varepsilon_q^p} = \frac{M_g^2 - \eta^2}{\chi_g \eta} \tag{6.2.1}$$

$$q^2 = -\frac{M_f^2}{1-\chi_f}\left(\frac{p'}{p'_c}\right)^{\frac{2}{\chi_f}} p_c'^2 + \frac{M_f^2 p'^2}{1-\chi_f} \tag{6.2.2}$$

$$q^2 = -\frac{M_g^2}{1-\chi_g}\left(\frac{p'}{p'_p}\right)^{\frac{2}{\chi_g}} p_c'^2 + \frac{M_g^2 p'^2}{1-\chi_g} \tag{6.2.3}$$

$$\frac{\delta p'_c}{p'_c} = \frac{\nu}{\lambda-\kappa}(\delta\varepsilon_p^p + D\delta\varepsilon_q^p) \tag{6.2.4}$$

$$\delta\varepsilon_p^p + D\delta\varepsilon_q^p = 0 \tag{6.2.5}$$

$$d_f = \frac{\delta\varepsilon_p^p}{\delta\varepsilon_q^p} = -D \tag{6.2.6}$$

$$\eta_f = \frac{D\chi_g}{2} + \frac{\sqrt{D^2\chi_g^2 + 4M_g^2}}{2} \tag{6.2.7}$$

$$D = D_0 e^{-D_1 \varepsilon_q^p} \tag{6.2.8}$$

6.2.2 Work flow in determining the model parameters

The simulation of the behaviour of the material was performed by starting from unconsolidated conditions and from the initial void ratio measured prior to consolidation. The material was then consolidated and brought to the initial confining stress corresponding to the initial confining stress of the simulated test, after which the deviatoric stress was increased to reach $K0$ consolidated conditions. The drainage conditions were adjusted according to the simulated test and the shearing stage was initiated.

From the set of parameters used in the constitutive model, all expect the isotropic compression index λ , isotropic unloading-reloading index κ and the initial void ratio e_0 needed to be determined according to the stress paths of the tests. This requires a step-wise method from the more simple to determine parameters to the more complex ones. In practice, this method requires some degree of iteration in order to achieve a satisfactory fit. The approach which was used is the following: first the Poisson ratio was determined by matching the deviatoric stress to axial strains of the experimental results. The Poisson ratio, being an elastic parameter, is best determined for over-consolidated conditions on the purely elastic response.

The Critical State parameter M was taken as the mean stress ratio of the set of tests at steady state conditions. An alternative method to determine the Critical State parameter M is, according to the classical Critical State soil mechanics theory, to rely on undrained tests which feature minimal deformations such as samples of low OCR (2 to 3) for which less test anomalies are expected to reach Critical State conditions as shown in figure 6.2.1. Due to the large discrepancy in initial confining pressure between over-consolidated and normally consolidated tested samples, this option was not considered in order not to include effects of stress level dependency as was shown by Casey and Germaine (2013). Lastly, parameter M can be determined using drained tests which showed to be reliable for over-consolidated conditions but highly unreliable for normally consolidated conditions as was discussed in section 5.2.

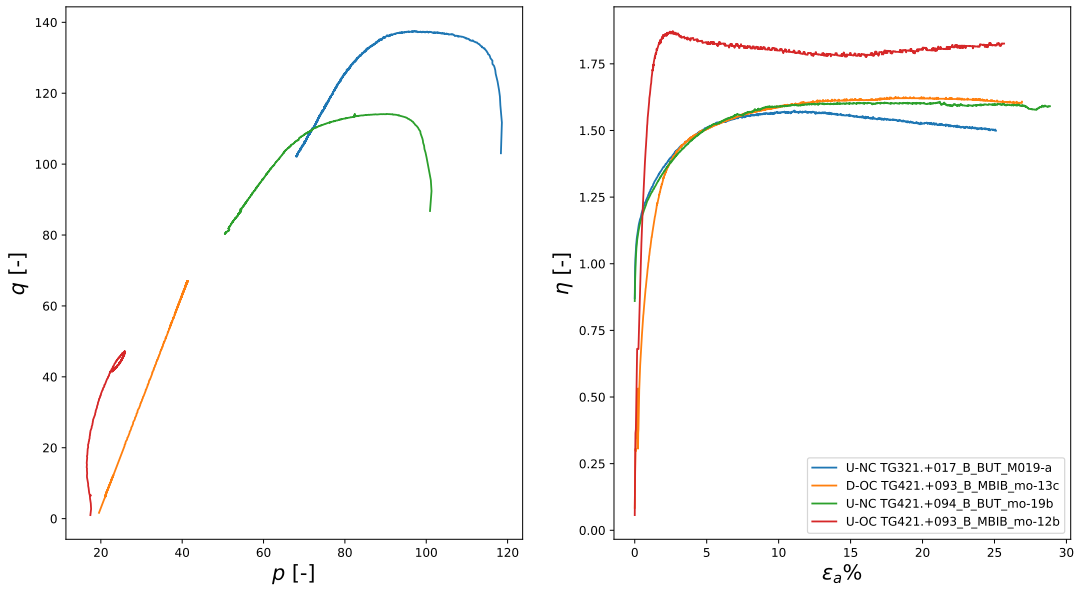

Figure 6.2.1: Comparison of the stress ratio reach for over-consolidated and normally consolidated conditions on similar samples. $TG321.+017\_B\_BUT\_M019-a$: typical undrained normally consolidated test showing excessive softening; $TG421.+093\_B\_MBIB\_mo-13c$: drained over-consolidated test; $TG421.+094\_B\_BUT\_mo-19b$: good quality undrained normally consolidated test; $TG421.+093\_B\_MBIB\_mo-12b$: slightly over-consolidated undrained test

The next step implied determining parameters M_f and χ_f of the non-associative flow rule by matching the shape of the stress path in the $p'q$ space where χ_f determines the shape of the yield locus and M_f its size. The inclusion of a non-associative flow rule enables the simulation of additional softening or hardening on either the wet or dry side. For over-consolidated tests, the strain softening behaviour after reaching the peak stress is further accentuated as M_f is larger than M_g. The opposite is true for M_f smaller than M_g where the stress path will feature strain hardening instead of strain softening.
In order to reproduce softening from both the dry and wet side in undrained test simulations using the same set of parameters, a deviatoric hardening rule may be implemented using a negative hardening law. An important aspect of the flow rule is that the ratio of incremental plastic volumetric stains to the incremental plastic deviatoric strains decreases as the stress ratio approaches the critical state surface i.e. as the axial strains increase. For this case, parameters M_f and χ_f were chosen to fit the stress paths in the early stage of shearing (up to 4% axial strain) and parameters D_0 and D_1 were determined to improve the fit at larger deformations. The last parameter χ_g can either be determined by fine-tuning the stress and strain response and shall in this case be determined as the last step, or as was performed in this case according to equation 6.2.9 (Muraro, 2019) once M_g has been identified.

$$\chi_g = \frac{2}{9}\frac{\lambda}{\lambda-\kappa}\frac{M_g[(6-Mg)^2-9]}{6-M_g} \tag{6.2.9}$$

The Poisson ratio was calibrated for several over-consolidated test for drained conditions: the outcomes were consistent across the different samples which resulted in a Poisson ratio of 0.35. Parameter χ_g was initially fitted by fine-tuning the strain response and resulted in very consistent results as by using equation 6.2.9.

6.3 Modelling Triaxial compression test results for matching Plasticity Index

6.3.1 Results of the Modified Cam-Clay, non-associative and non-associative with deviatoric hardening model in Triaxial Compression

In this section, the advanced Modified Cam-Clay based constitutive model from section 6.2.1 is used to better predict the behaviour of the material and to differentiate (to some extend) between true material behaviour and manifestation of laboratory testing limitations. The matched Triaxial compression test results for plasticity index 47 $\pm$ 5% as shown in figure 6.3.1 were used to evaluate the ability of the constitutive model in predicting the soil behaviour for different test conditions. In figures 6.3.3 to 6.3.5, the experimental results are given for an undrained normally consolidated test, an undrained over-consolidated test and a drained over-consolidated test respectively, together with simulations with the MCC model, a non-associated flow rule model and a non-associated flow rule model with deviatoric hardening. The parameters for each model are given in table 6.3.1, where the Critical State stress ratio (M_g) was taken as the average between the stress ratio reached after large axial strains for normally consolidated and over-consolidated tests. The proposed shape of the plastic potential and yield surface is given in figure 6.3.2 and the combined results of the experimental results and modelling stress paths are reported in figures 6.3.7 to 6.3.9.

Table 6.3.1: Triaxial Compression modelling parameters

name model	λ	κ	μ	Mg	Mf	χ_g	χ_f	D0	D1
MCC	0.14	0.01	0.35	1.65	-	2.0	-	-	-
Non-associative	0.14	0.01	0.35	1.65	1.4	0.9	0.4	-	-
Non-associative, deviatoric hardening	0.14	0.01	0.35	1.65	1.4	0.9	0.4	-1	30

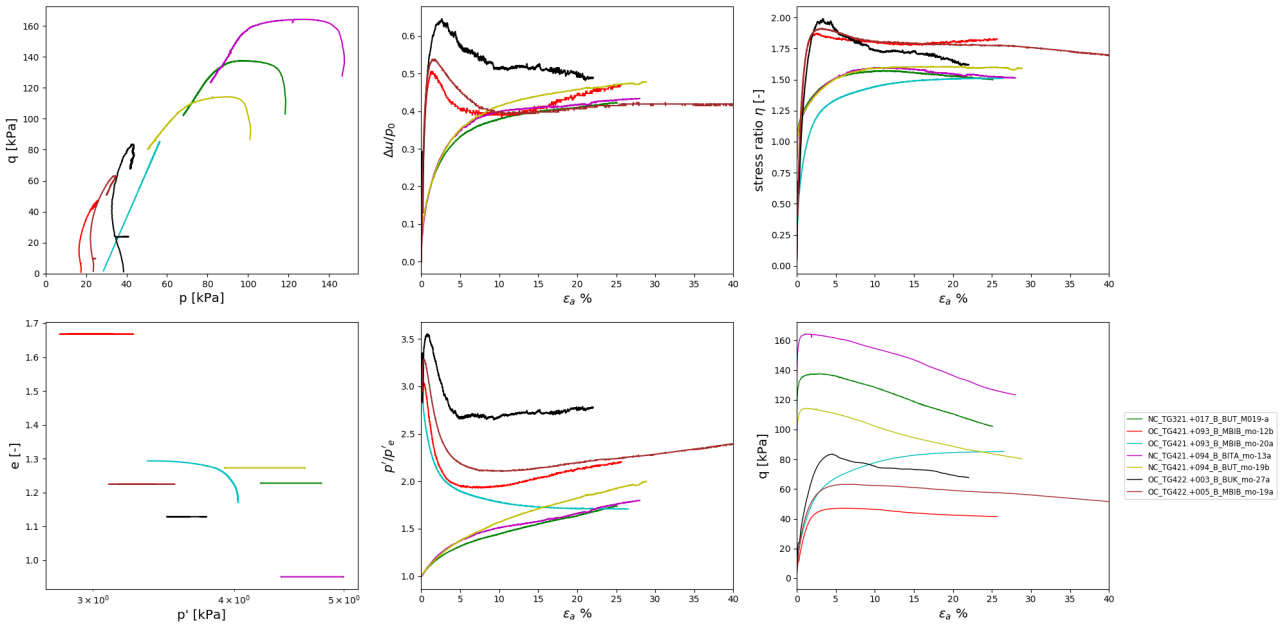

Figure 6.3.1: Considered tests to be modelled

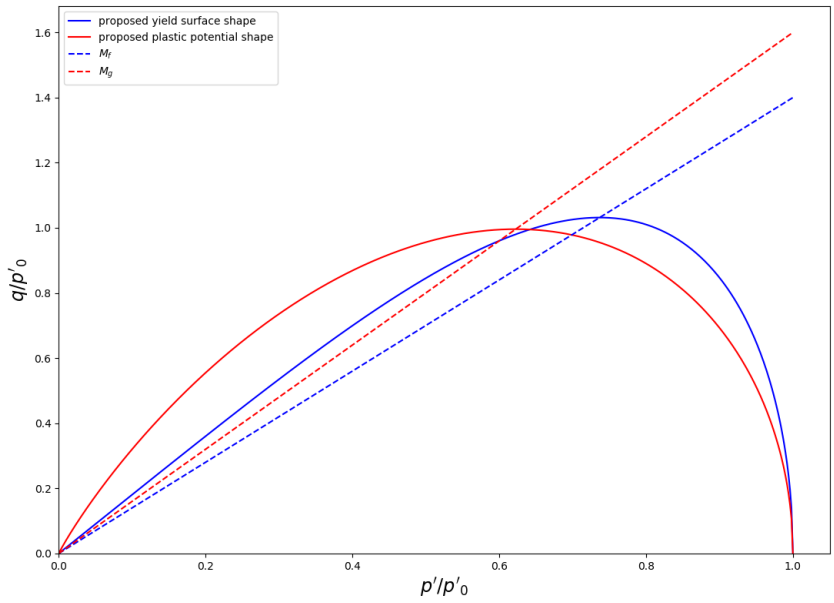

Figure 6.3.2: Shapes of the proposed plastic potential and yield surface

The results show the Modified Cam Clay only predicts strain softening for over-consolidated conditions and cannot reproduce the asymptotic approach of the Critical State line. As its use was intended for isotropic materials, the MCC cannot reproduce the elastic anisotropic response in the elastic region of the undrained over-consolidated test or the elasto-plastic anisotropic response for undrained conditions on normally consolidated conditions and over-consolidated conditions in the post yield region. The MCC model also tends to under-predict the excess pore pressure response and the yield point for over-consolidated conditions is highly over-estimated. For drained over-consolidated conditions, although the Critical State shear strength is over-estimated (mainly due to the use of an average stress ratio larger than the Critical State stress ratio of the given test), the qualitative response of the MCC is excellent. Finally, the MCC model predicts a much stiffer response for undrained conditions than the experimental results.

The use of a non-associative flow rule with solely volumetric hardening shows considerable improvements on the undrained response: for normally-consolidated conditions, the model is able to reproduce the softening and post yield anisotropic response and predicts a more suitable yield point for over-consolidated conditions although the opposite is true for drained conditions. This effect is due to the fact that non-elliptical yield locus will underpass or overpass the modified Cam-Clay shaped yield locus from one side of the apex of the MCC shaped ellipse or another as shown in figure 6.3.6. As a result, the undrained stress path of an over-consolidated test may predict a higher yield point for a MCC model than the yield surface used in the non-associative model for an over-consolidated drained test depending on the over-consolidation ratio. Should the tear drop shaped yield locus have had its apex at the dry side of Critical State, the model would have predicted a higher pre-consolidation pressure with a MCC model for drained conditions and a lower pre-consolidation pressure for undrained conditions. Again, the pre-yield anisotropic response for undrained over-consolidated conditions is not reproduced. From the wet side of Critical State, the yield locus can be shaped such that the stress path for undrained normally consolidated conditions reaches the Critical State line asymptotically, however if the same shape is utilised for undrained over-consolidated conditions, the model would predict an excessively high Critical State shear strength without any strain softening. Both the qualitative as quantitative results would therefore be unsatisfactory. Similarly to the MCC model, the inclusion of a non-associative flow rule produces a much stiffer response than the experimental results for undrained conditions.

The inclusion of deviatoric softening enables improved qualitative results for both the drained and undrained conditions: a negative deviatoric hardening rule enables to reproduce the asymptotic behaviour towards Critical State and reduction of the mobilised shear strength. Especially for over-consolidated conditions, the typical 'curl' observed from strain softening is well reproduced and a significant improvement of the MCC model and non-associative model. The model also predicts a stage of compressive shearing after the initial compressive and dilative stage generally observed for over-consolidated conditions, which is observed in the pore pressure response of figure 6.3.4, although the fact that this feature occurs after 15% strain may involve test specific features rather than material behaviour.
For the same reasons as explained for the non-associative model, the yield point for drained over-consolidated conditions is over-estimated due to shape of the yield locus which cannot be corrected for with a distortional hardening (figure 6.3.5). Another improvement is the better estimation of the axial deformations where the model predicts steady state conditions at 10 to 15% axial strain for undrained conditions and 20% for drained conditions compared to 2 to 5% and 15% axial strain for undrained and drained conditions respectively using the MCC and non-associative flow rule. This model however still features some limitations in reproducing the initial small strain anisotropic response (up to 2% axial strain) for normally consolidated (elasto-plastic strains) and over-consolidated conditions (elastic strains). In addition, some key questions remain on the nature of such deviatoric hardening law: the model formulates better estimations of the undrained stress paths for the Gorinchem clay indeed, however the better estimation of the stress path occurs at larger deformations which involve considerably more uncertainties related to the stress distribution and failure mechanisms as was discussed in section 2.2.1.

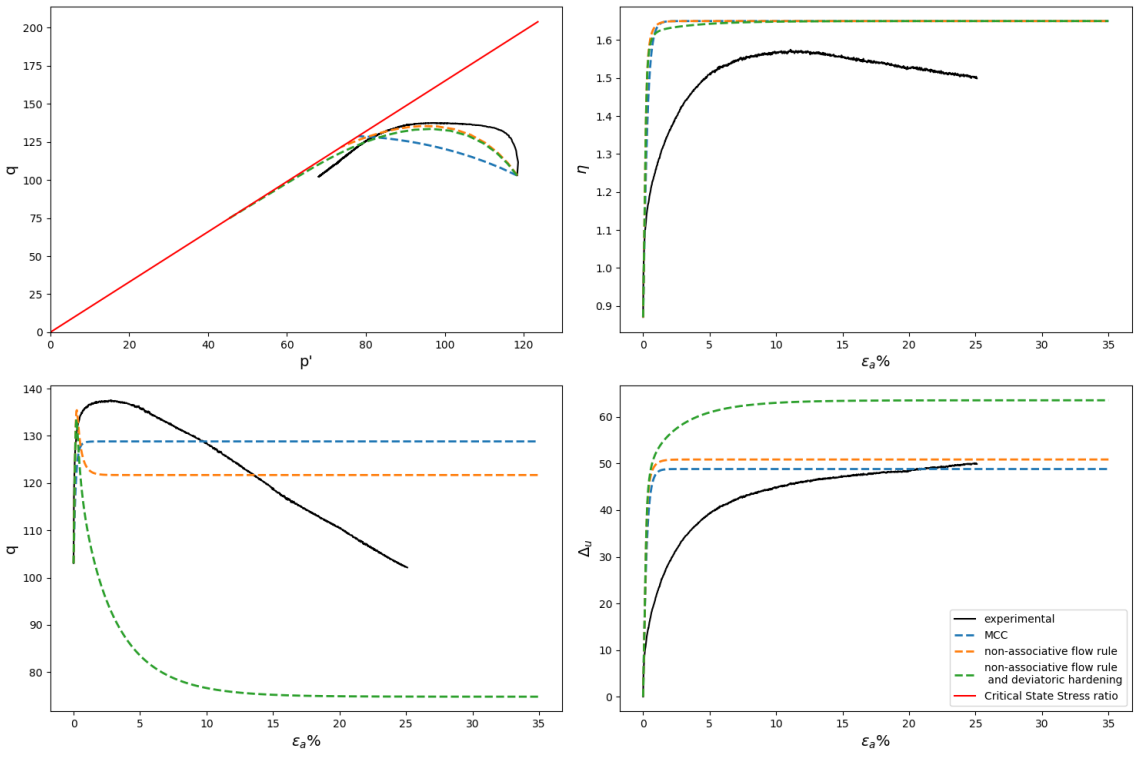

Figure 6.3.3: Experimental results of test TG321.+017_B_BUT_M019-a and simulations using the MCC model, a non-associative flow rule and a non-associative flow rule with distortional hardening.

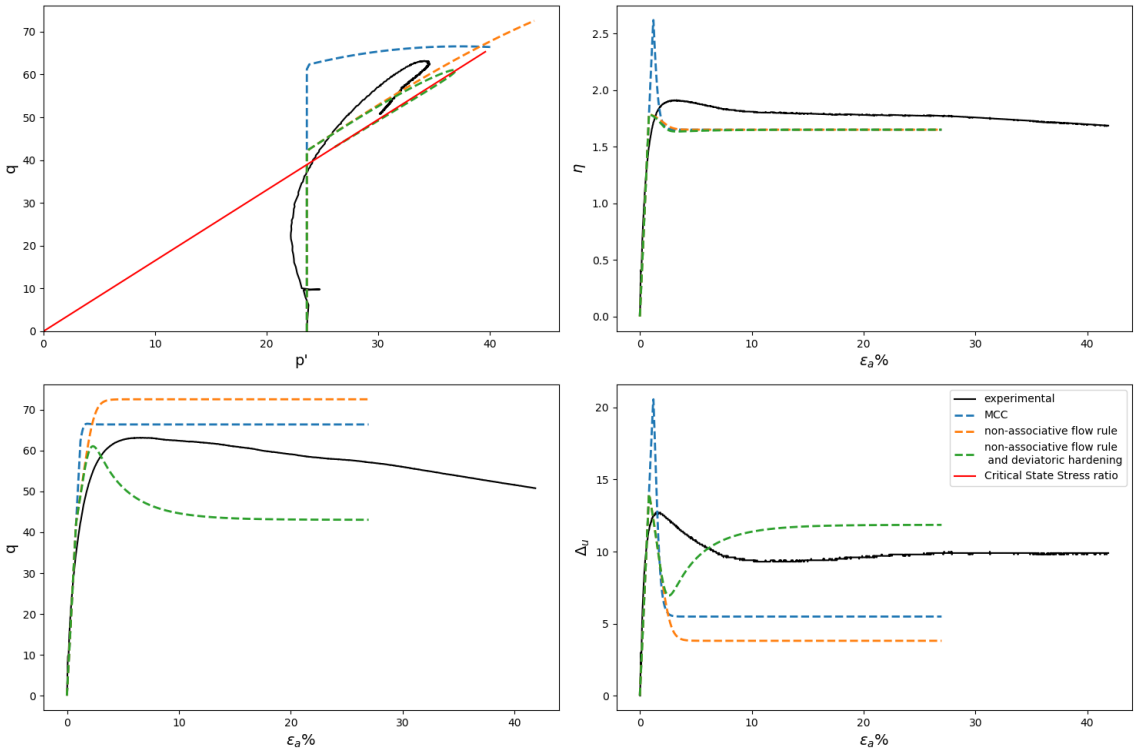

Figure 6.3.4: Experimental results of test TG422.+005_B_MBIB_mo-19a and simulations using the MCC model, a non-associative flow rule and a non-associative flow rule with distortional hardening.

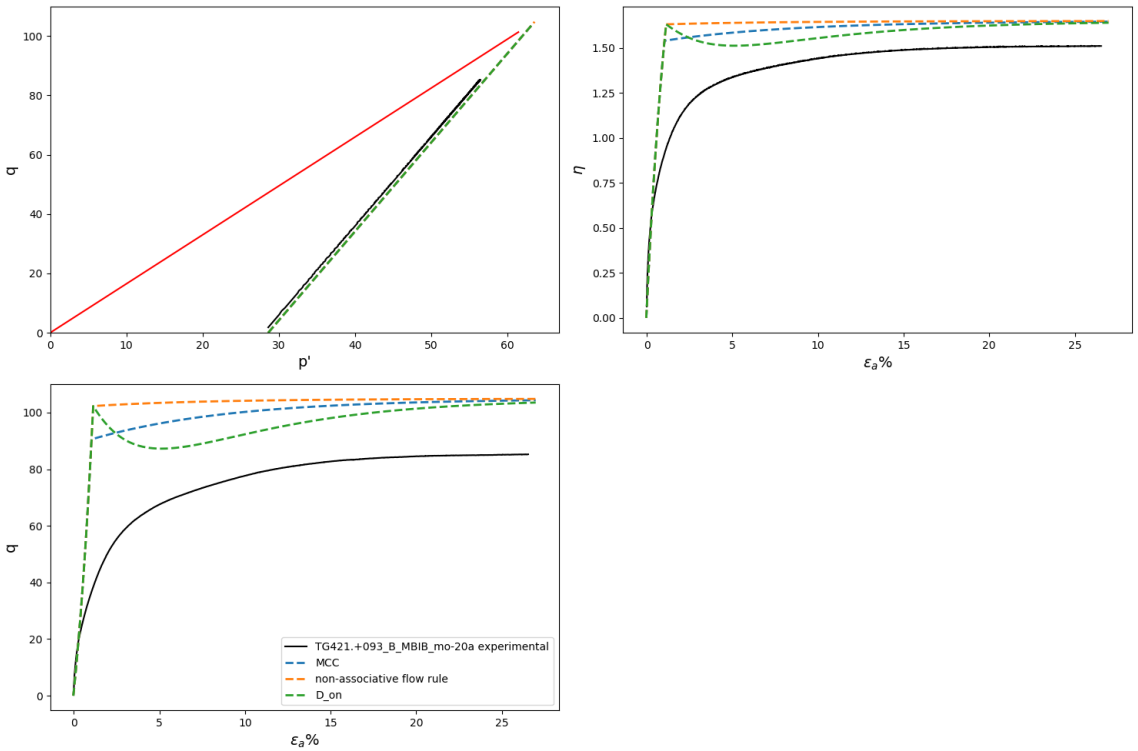

Figure 6.3.5: Experimental results of test TG421.+093_B_MBIB_mo-20a and simulations using the MCC model, a non-associative flow rule and a non-associative flow rule with distortional hardening.

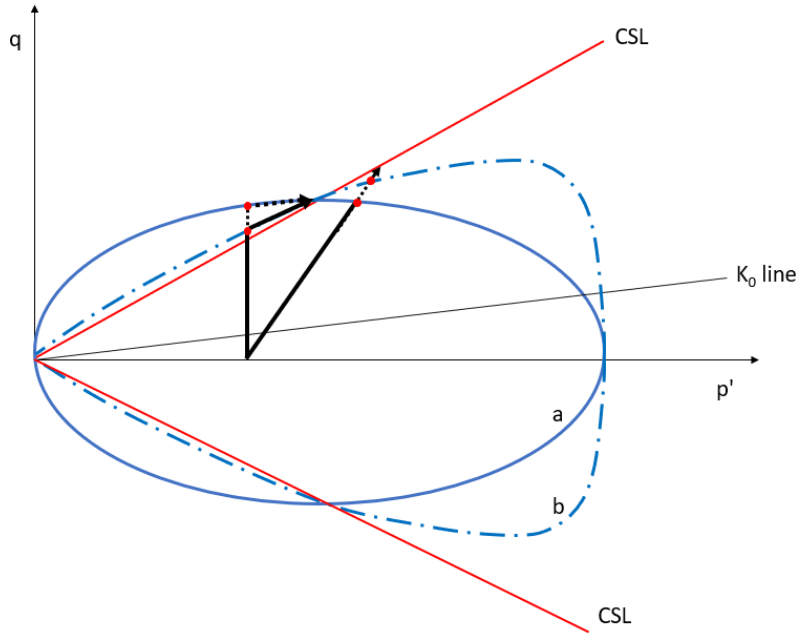

Figure 6.3.6: Drained and undrianed stress path and yield point for MCC model and tear-drop shaped yield locus for non-associative flow rule. a: MCC shaped yield locus, b: tear drop shaped yield locus, a': MCC shaped yield locus at the pre-consolidation pressure, b': tear drop shaped yield locus at the pre-consolidation pressure.

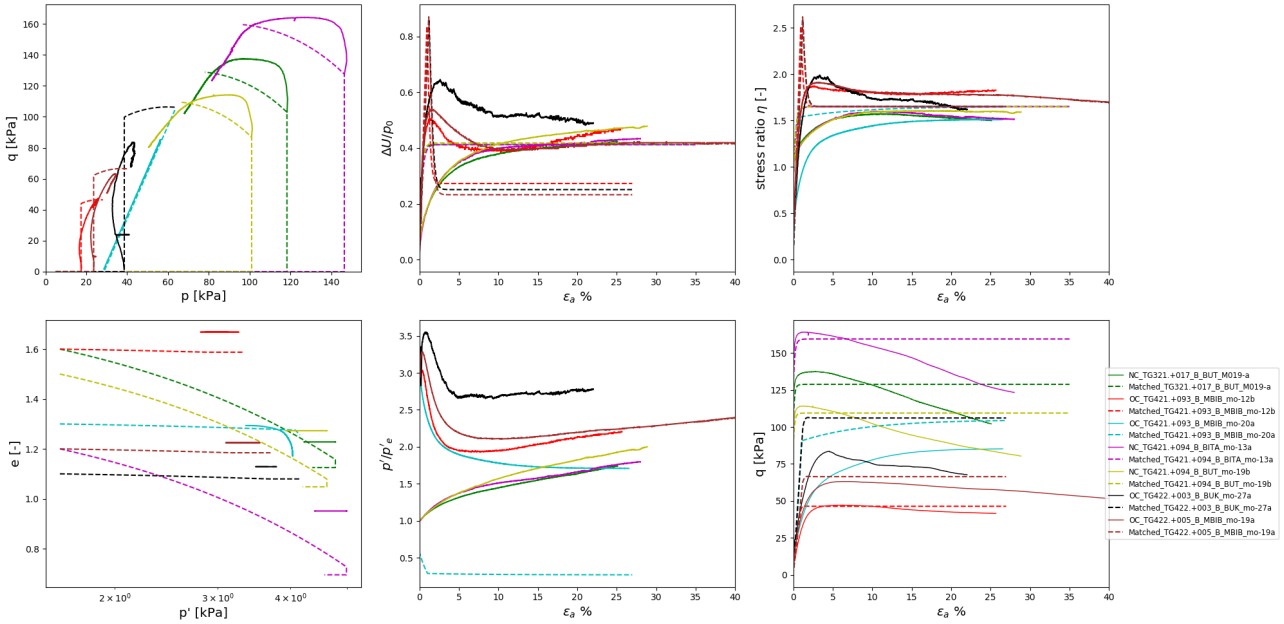

Figure 6.3.7: Triaxial Compression tests of samples with Plasticity Index 47% ± 5% and MCC simulation where λ=0.14, κ=0.01 and M=1.65

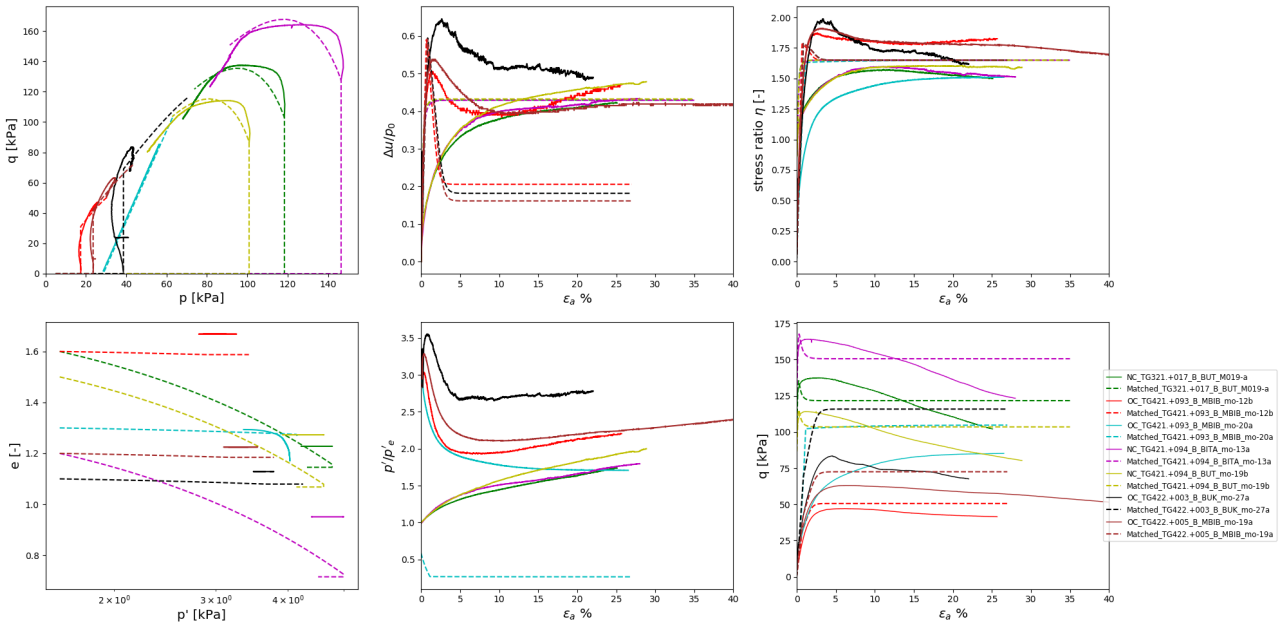

Figure 6.3.8: Triaxial Compression tests of samples with Plasticity Index 47% ± 5% and non-associative flow rule simulation where λ=0.14, κ=0.01, M_g=1.65, M_f=1.4, χ_g=0.9, χ_f=0.4

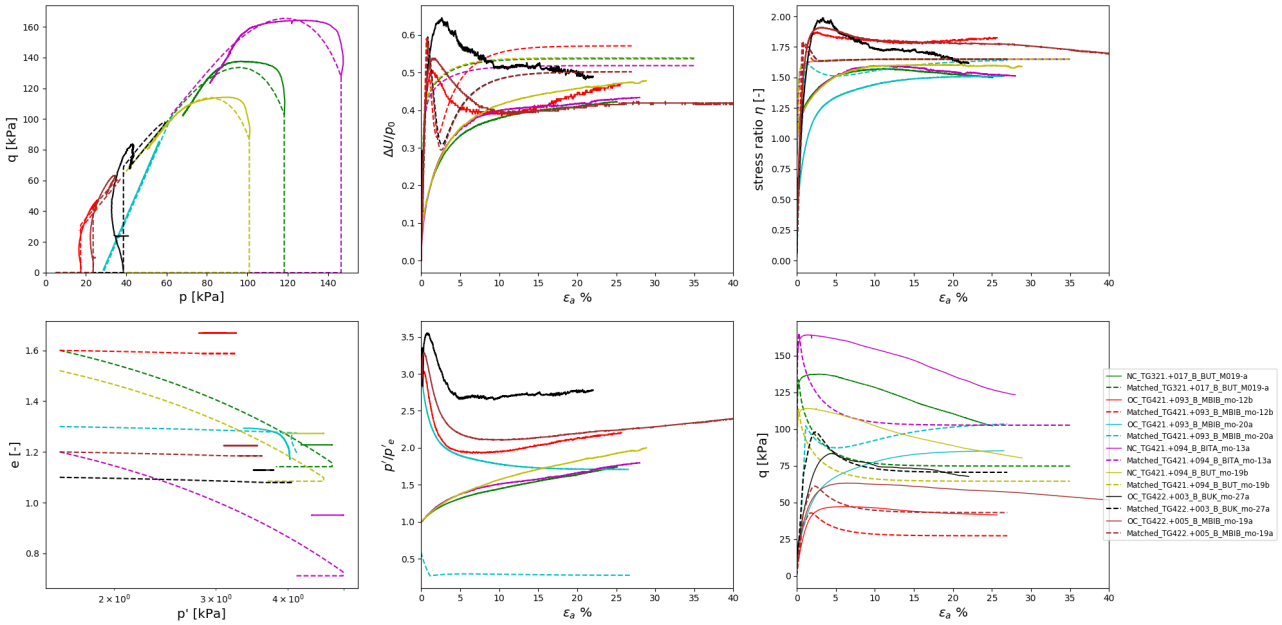

Figure 6.3.9: Triaxial Compression tests of samples with Plasticity Index 47% ± 5% and non-associative flow rule simulation where λ=0.14, κ=0.01, M_g=1.65, M_f=1.4, χ_g=0.9, χ_f=0.4, D_0=-1 and D_1=30

6.3.2 Sensitivity of the shape of the plastic potential

The shapes of the considered plastic potentials are shown in figure 6.3.10 for χ_g of 2.0 (MCC shape), 0.9 (proposed shape) and 0.3 (same shape factor as for the yield surface). The results for undrained normally consolidated and over-consolidated simulations are given in figures 6.3.11 to 6.3.12 respectively. For both normally and over-consolidated conditions, the stiffness of the material is affected by the shape factor such that a lower value of χ_g results in a larger stiffness. For normally consolidated conditions, the steady ultimate strength and corresponding excess pore

pressures of each simulation are respectively higher and lower for larger values of χ_g, which can be explained by the fact that parameter χ_g is a function of the failure stress ratio as was shown previously in equation 6.2.7. Indeed the stress ratio at failure equates parameter M_g and using the same deviatoric hardening rule, a larger value of χ_g causes a larger contribution of the deviatoric hardening (or softening in this case) which causes the simulated test to reach the critical state stress ratio for less deviatoric plastic strains and at larger ultimate strength.
For over-consolidated conditions, this effect on the ultimate strength is not observed. However, the shape factor of the plastic potential mainly affects the peak strength of the material as the shape factor dictates at which stage the behaviour change from a dilative mode of shearing to a compressive mode of shearing. Considering these results, a good estimation of the shape of the plastic potential is required to simulate good qualitative and quantitative estimations of the undrained stress paths, especially for over-consolidated conditions.

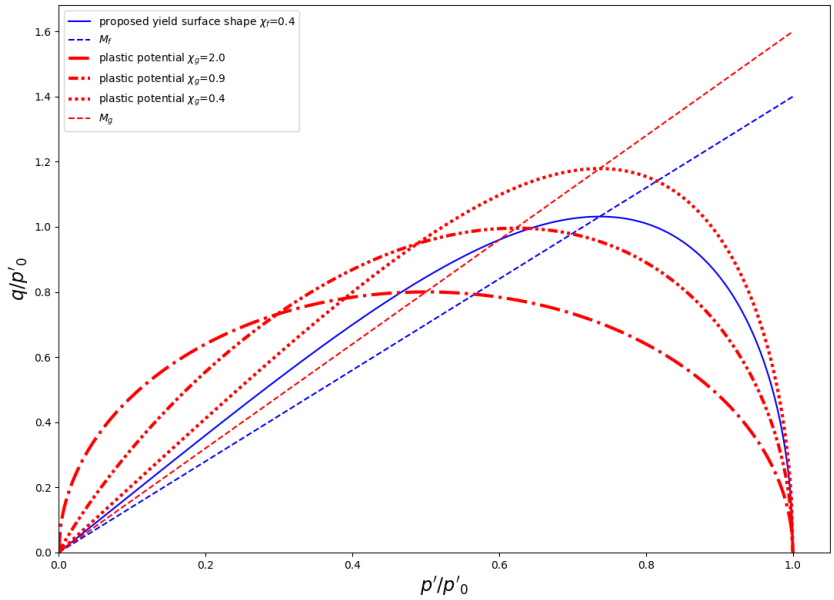

Figure 6.3.10: Shapes of the plastic potential for χ_g=2.0, 0.9 and 0.4

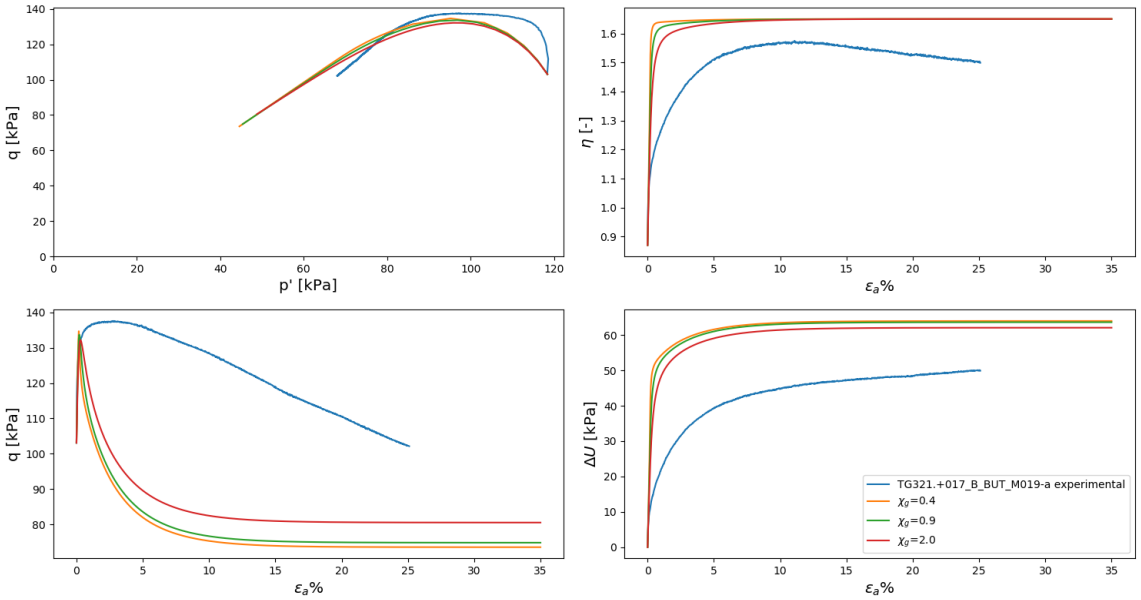

Figure 6.3.11: Sensitivity of parameter χ_g on the stress path simulation for undrained normally consolidated conditions

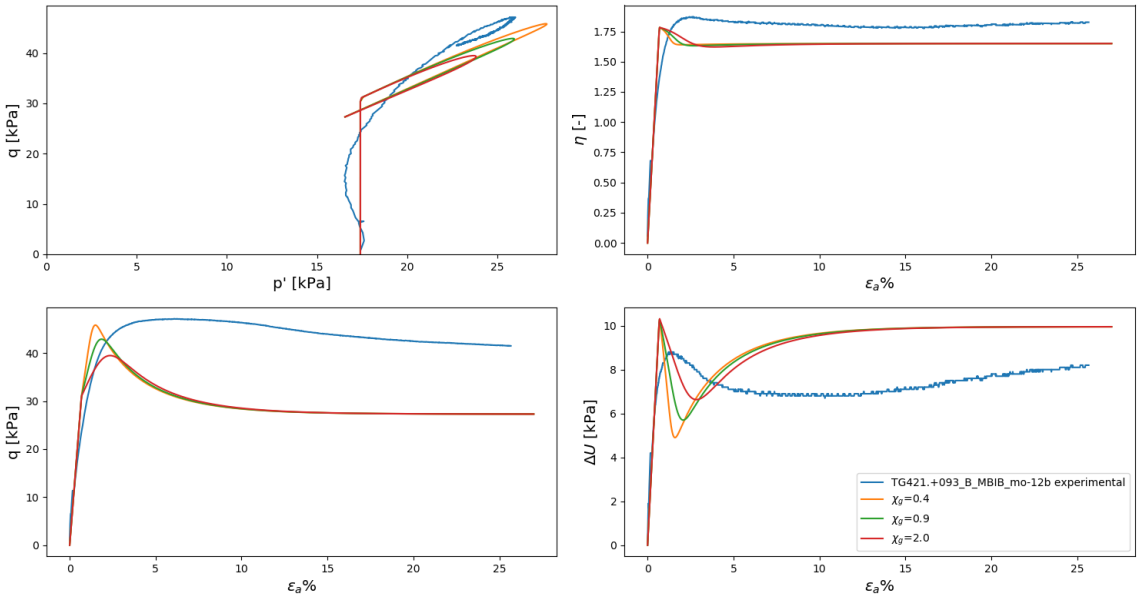

Figure 6.3.12: Sensitivity of parameter χ_g on the stress path simulation for undrained over-consolidated conditions

6.4 Modelling of a Triaxial Extension test

As for the Triaxial Compression tests, the Triaxial Extension tests were filtered based on the conformity of the sample's height to diameter ratio's after anisotropic consolidation. Only test *15-102_31* conformed to the current Dutch guidelines. The Critical State parameter M_g was taken at peak stress ratio.

The results of the simulations using the MCC, non-associative flow rule and non-associative flow rule with deviatoric hardening shown in figure 6.4.1 using the model parameters of table 6.4.1, reveals the main shortcoming of all three constitutive models: the model predicts an elastic response during the unloading of the sample up to the absolute deviatoric stress reached after anisotropic

consolidation, whereas the experimental results shows yielding at zero deviatoric stress. The discrepancy in yield conditions between the experimental results and the constitutive model in addition to the similar difficulty in determining the model parameters as for over-consolidated conditions in Triaxial Compression, results in unreliable model parameters. Again the models predict a much stiffer response and are not able to reproduce the elastic anisotropy. The non-associative flow rule with deviatoric hardening shows the best results in reproducing the experimental results as it is again able to reproduce strain softening along the Critical State line and predicts a less stiff response.

Table 6.4.1: Triaxial Extension modelling parameters

model	λ	κ	μ	Mg	Mf	χ_g	χ_f	D0	D1
MCC	0.18	0.013	0.35	1.14	-	2.0	-	-	-
Non-associative flow rule	0.18	0.013	0.35	1.14	1.2	0.9	0.3	0	0
Non-associative flow rule and deviatoric hardening	0.18	0.013	0.35	1.14	1.2	0.9	0.3	-0.5	30

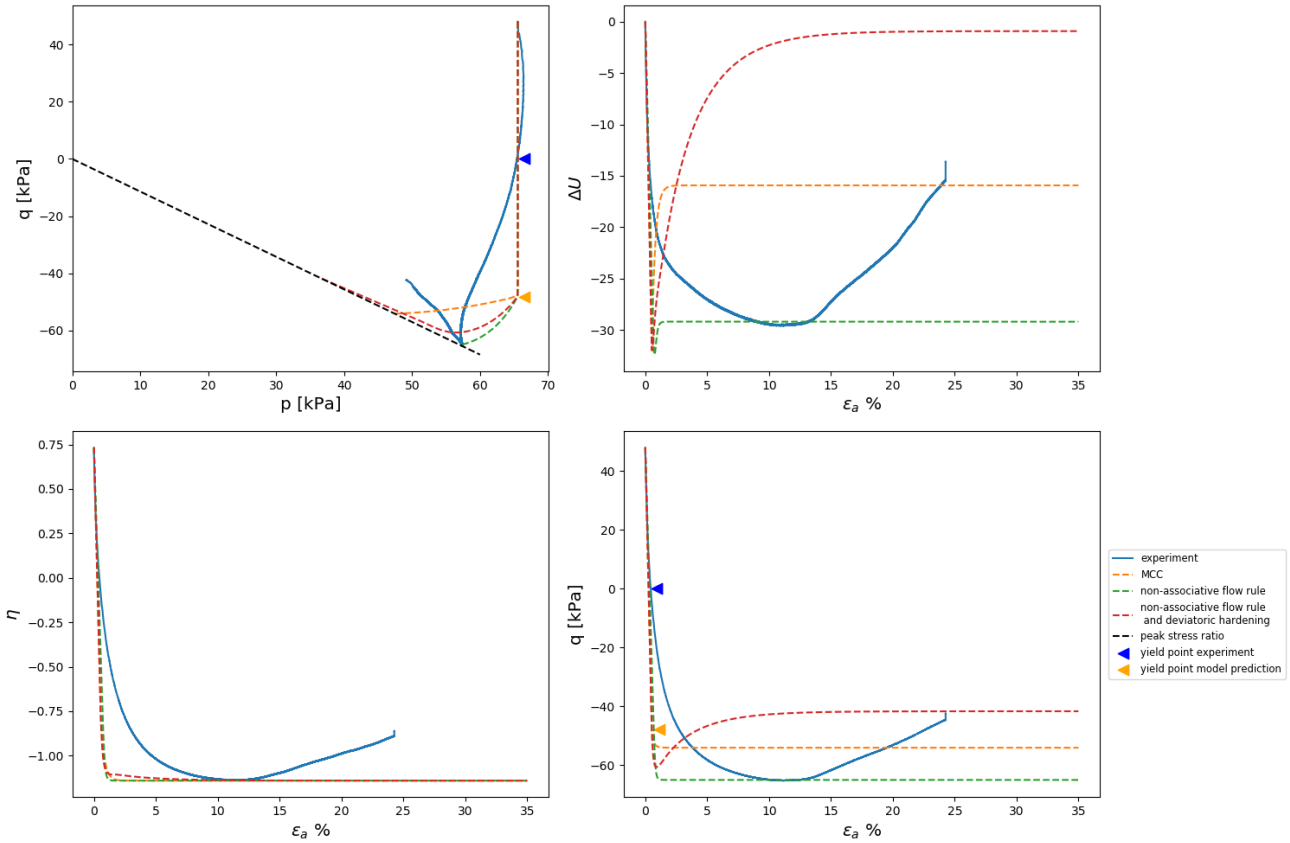

Figure 6.4.1: Triaxial Extension experimental stress path for undrained conditions and simulated results

Chapter 7

Conclusions and Discussions

The main objective of this Master thesis was to better assess the soil behaviour from different laboratory tests in the evaluation of the macro-stability of flood embankments according to the recently introduced Dutch norms. The outcomes of this thesis show the Classical Critical State Soil Mechanics and therefore the current Dutch guidelines do not offer a suitable framework for the Gorinchem Clay in assessing the macro-stability of flood embankments. The laboratory testing programme on the Gorinchem clay additionally showed showed limitations in providing reliable results at large deformations and shows the necessity of an alternative strength parameter assessment methodology than Critical State strengths. The answers to the research questions are given as follows:

- *Is the strain softening experienced in the laboratory tests a result of the limitations of the tests at large displacements or is the softening true material behaviour?*

The analysis showed the excessive strain softening in the post stress-ratio peak for normally-consolidated conditions in undrained Triaxial Compression to be indeed test behaviour caused by the limitations of the testing equipment and practice. The material however does feature strain softening as a result of anisotropic behaviour and possible destructuration. Destructuration could not be proven based on the provided laboratory tests. The Triaxial Extension and Direct Simple Shear tests also suffered from excessive strain softening.

- *What are the limitations of the Classical Critical State Soil Mechanics and hence the SHANSEP model if applied to field scenario's?*

The main limitation of the Classical Critical State Soil Mechanics which was highlighted in this thesis is the assumption of isotropic behaviour : intact samples of Gorinchem Clay showed anisotropic behaviour inducing strain softening in Triaxial Compression and Extension. The Critical State Soil Mechanics framework was derived from fully remoulded clay samples and hence shows its limitations on intact soils. Much of this anisotropic behaviour can be assimilated to the presence of different components of soil (clay, peat, silt and sand) with different orientation, fibres and the formation of structure in the material as a result of previous stress and strain history. Additionally, the Classical Critical State Soil Mechanics states the same Critical State stress ratio is reached regardless of the stress history, drainage conditions or stress levels, in addition to the fact that no strain softening is predicted once the post Critical State stress ratio has been reached. These conditions were not found, it is however still unclear whether all these conditions did not meet the Classical Critical State Soil Mechanics theory due to the limitations of performing conventional laboratory tests on such deformable material, or whether this is due to an outdated statement within the Critical State theory. The implications on the SHANSEP model mean the normalised undrained shear strength for normally consolidated conditions results in different estimates should this parameter be determined from the dry side of Critical State. The effects of structure should be included in the evaluation of the pre-consolidation pressure within the SHANSEP formulation.

- *Is the determination of Critical State strength parameters according to the 2017 Dutch norms applicable on Gorinchem Clay?*

The analysis in Triaxial Compression, Direct Simple Shear and Triaxial Extension showed the Critical State conditions could not be reached reliably according to the traditional understanding of Critical State Soil mechanics and prescribed 2017 Dutch norms in the evaluation of the macro-stability of flood embankments. The results additionally showed the Critical State conditions do not comply with a strain definition since both the nature of soil and the pre-consolidation pressure of the soil sample influence the axial strain required to reach steady state conditions.
The uncertainties in determining steady state conditions and ultimate strengths for Gorinchem Clay in Triaxial Compression, Direct Simple Shear and Triaxial Extension for undrained conditions shows the limitations of the current norms as the strength parameters can result in over-conservative estimations in the case of Gorinchem Clay, or on the contrary to potentially over estimated and unsafe parameters if applied to similar materials as studied by Muraro (2019). Indeed, the experimental data showed to be unreliable beyond 10% axial strain in Triaxial Compression and Extension, and beyond 15% shear strain in Direct Simple Shear where the current guidelines state the Critical State conditions are met at 25% axial strain in Triaxial Compression and 40% shear strain in Direct Simple Shear.

- *Can the use of an isotropic non-associative elasto-plastic constitutive model with volumetric and deviatoric hardening be used to model the behaviour of the material in question?*

The use of an isotropic non-associative elasto-plastic constitutive model with volumetric and deviatoric hardening was found to be adequate to reproduce and understand the qualitative behaviour of the material and showed to be a significant improvement to the Modified Cam-Clay and non-associative model with volumetric hardening only. The non-associative flow rule enables the prediction of softening and anisotropic behaviour whilst the deviatoric hardening law may be used to replicate the asymptotic reach of the Critical State stress ratio in the triaxial test. The model however showed to be sensitive to the shape of the plastic potential in predicting ultimate and peak strengths and therefore requires accurate calibration of this parameter. The constitutive model showed some limitations in its ability to reproduce the behaviour of the soil: the model predicts a much stiffer response than the laboratory tests and isn't therefore able in most cases to accurately reproduce the volume changes of the sample during shearing and consolidation. Additionally, the elastic anisotropic behaviour for over-consolidated conditions cannot be reproduced since the use of a non-associative flow rule to replicate anisotropic behaviour applies to the elasto-plastic strains. In order to reproduce the elastic anisotropic behaviour it would therefore be required to use an anisotropic formulation of the yield surface. Lastly, the yield point for K0-consolidated undrained Triaxial Extension tests was highly over-estimated due to isotropic nature of the model causing yielding to occur at the absolute deviatoric stress reached after anisotropic consolidation.

- *How can the difficulties encountered in determining the parameters of the SHANSEP model from laboratory tests be remedied?*

The difficulties in determining the Critical State undrained shear strength for highly deformable soils in Triaxial Compression can be remedied by performing additional drained or undrained tests on slightly over-consolidated samples (OCR $\sim$ 1.5-2.5). Such test minimises the slow asymptotic reach of the Critical State stress ratio by minimising the deformations and uncertainties involved in reaching the Critical State stress ratio. These results can then be compared to tests performed on normally consolidated conditions in order to identify the Critical State conditions should the test results be difficult to interpret. Triaxial Compression tests on very deformable soils or highly over-consolidated samples showed to considerably suffer from erroneous measurements: for undrained conditions, the large deformations tend to cause exaggerated softening due to due to

excess pore pressure build-up, stress inhomogeneity and cross-sectional area changes of the sample at the location of failure. Drained over-consolidated Triaxial Compression tests appeared to behave particularly well, although the amount of such tests was limited for this particular project. Determining Critical State conditions under undrained conditions for highly over-consolidated samples (OCR >4) also showed to be problematic. The Critical State conditions were likewise found to be problematic to determine on Gorinchem clay using the DSS test.

Chapter 8

Recommendations

The recommendations from this thesis involve both on practices to be adopted in the macro-stability of flood embankments in the Netherlands and recommendations for further research on this topic:
Although the use of a simplified constitutive model as was used in this thesis, the understanding of the behaviour of the material and quantification of properties of the soil can be improved by using a more advanced constitutive model than the classical Modified Cam-Clay model. It is therefore recommended to perform a similar analysis on a model containing a rotational hardening mechanism to reproduce the small strain elasto-plastic anisotropic behaviour of Gorinchem Clay and the elastic anisotropic behaviour for over-consolidated conditions. A destructuration law defined for not only deviatoric plastic strains but also volumetric plastic strains is also recommended. Such analysis should preferably be accompanied by advanced laboratory tests enabling the identification of the material characteristics such as the general shape of the yield surface, the failure shape in the deviatoric plane, the presence of structure (CRS test on remoulded material), and elastic and plastic anisotropy. Particular attention should be given on the determination of the pre-consolidation pressure in CRS tests and presence of structure for improving both the modelling of the material and the determination of the undrained shear strength for over-consolidated conditions from the SHANSEP model. It is also recommended to perform such analysis in a Finite Element code able which is able to reproduce the boundary conditions in a Triaxial test.
The quality of the results from laboratory tests and the ability of a constitutive model to reproduce the behaviour of the soil was hindered by the limitations of the conventional Triaxial test set-up. The creation of better national guidelines with regards to the correction for the severe level of deformations and formation of discontinuities of the tested sample is highly recommended. Higher quality set-ups of the Triaxial test are also recommended such as but not limited to: true K0 Triaxial test and local measurement of excess pore pressure development. More specifically, the Critical State conditions could not be reached reliably for the Gorinchem Clay using conventional laboratory equipment. The author recommends adopting a strain-based strength assessment to strain levels where the laboratory tests are still reliable in order to prevent over-conservative or non-conservative designs. Additionally, it is recommended to perform a similar analysis as was performed in this thesis on reconstituted soil samples and using identical strain rates.
The Dutch norms on the macro-stability of embankments would benefit from the confirmation of the modified SHANSEP formulation from Casey and Germaine (2013) and particularly from the quantification of the effects of stress levels on the SHANSEP parameters for the stress levels encountered in the field. The implementation of the effects of confinement in the strength assessment requires the validation of the correlation of the contribution of stress level on the normalised normally consolidated undrained shear strength with the liquid limit which was found to be particularly high for the Gorinchem Clay. The author additionally recommends the systematic determination of Atterberg limits and its use for correlations as a way to clearly see the effects of stress level on material parameters.

Bibliography

Abdulhadi, N. O., Germaine, J. T., & Whittle, A. J. (2012). Stress-dependent behavior of saturated clay. *Canadian Geotechnical Journal*, *49*(8), 907–916.

Abelev, A. V., & Lade, P. V. (2004). Characterization of failure in cross-anisotropic soils. *Journal of Engineering Mechanics*, *130*(5), 599–606.

Atkinson, J., et al. (1993). *An introduction to the mechanics of soils and foundations: through critical state soil mechanics.* McGraw-Hill Book Company (UK) Ltd.

Bakkenist, S. (2012). *dl. 2]: Inspectiewijzers waterkeringen: technische informatie uitvoering inspecties (inspection guidelines: technical information implementation inspection)* (Tech. Rep.). Tech. Report (in Dutch), STOWA, Amersfoort, The Netherlands.

Boylan, N., & Long, M. (2008). Development of a direct simple shear apparatus for peat soils. *Geotechnical Testing Journal*, *32*(2), 126–138.

Budhu, M. (1984). Nonuniformities imposed by simple shear apparatus. *Canadian Geotechnical Journal*, *21*(1), 125–137.

Casey, B., & Germaine, J. T. (2013). Stress dependence of shear strength in fine-grained soils and correlations with liquid limit. *Journal of Geotechnical and Geoenvironmental Engineering*, *139*(10), 1709–1717.

Chatzis, K. (2018). Advances in modelling the deviatoric response of peat.

D6528-17, A. (2017). *Standard test method for consolidated undrained direct simple shear testing of fine grain soils.* ASTM International West Conshohocken, PA.

Dafalias, Y. F., Manzari, M. T., & Papadimitriou, A. G. (2006). Saniclay: simple anisotropic clay plasticity model. *International Journal for Numerical and Analytical Methods in Geomechanics*, *30*(12), 1231–1257.

Den Haan, E., & Kruse, G. (2007). Characterisation and engineering properties of dutch peats. *Characterisation and Engineering Properties of Natural Soils*, *3*, 2101–2133.

Dounias, G. T., & Potts, D. M. (1993). Numerical analysis of drained direct and simple shear tests. *Journal of Geotechnical Engineering*, *119*(12), 1870–1891.

Ehrgott, J. Q. (1971). *Calculation of stress and strain from triaxial test data on undrained soil specimens* (Tech. Rep.). Army Engineer Waterways Experiment Station Vicksburg MS.

Gajo, A., & Muir Wood, D. (2001). A new approach to anisotropic, bounding surface plasticity: general formulation and simulations of natural and reconstituted clay behaviour. *International journal for numerical and analytical methods in geomechanics*, *25*(3), 207–241.

Gens, A. (1982). Stress-strain and strength characteristics of a low plasticity clay.

Georgiadis, K., Potts, D., & Zdravkovic, L. (2004). Modelling the shear strength of soils in the general stress space. *Computers and Geotechnics*, *31*(5), 357–364.

Głuchowski, A., Soból, E., Szymański, A., & Sas, W. (2019). Undrained pore pressure development on cohesive soil in triaxial cyclic loading. *Applied Sciences*, *9*(18), 3821.

Graham, J., & Li, E. (1985). Comparison of natural and remolded plastic clay. *Journal of Geotechnical Engineering*, *111*(7), 865–881.

Greeuw, G., Adel, H. d., Schapers, A. L., & Haan, E. J. d. (2001). Reduction of axial resistance due to membrane and side drains in the triaxial test. In *Soft ground technology* (pp. 30–42).

Grognet, M. (2011). The boundary conditions in direct simple shear tests: developments for peat testing at low normal stress.

Hanzawa, H., Nutt, N., Lunne, T., Tang, Y., & Long, M. (2007). A comparative study between the ngi direct simple shear apparatus and the mikasa direct shear apparatus. *Soils and foundations*, *47*(1), 47–58.

Hobbs, N. (1987). A note on the classification of peat. *Géotechnique*, *37*(3), 405–407.

Huang, M., Liu, Y., & Sheng, D. (2011). Simulation of yielding and stress–stain behavior of shanghai soft clay. *Computers and Geotechnics*, *38*(3), 341–353.

Hvorslev, M. J. (1937). *Über die festigkeitseigenschaften gestörter bindiger böden (about the strength properties of disturbed cohesive soil)* (No. 45). Danmarks naturvidenskabelige samfund, i kommission has GEC Gad.

Imai, G., Tanaka, Y., & Saegusa, H. (2003). One-dimensional consolidation modeling based on the isotach law for normally consolidated clays. *Soils and Foundations*, *43*(4), 173–188.

Knabe, T. (2010). Constitutive models for subsoil in the context of structural analysis in construction engineering.

Koutsoftas, D. C., & Ladd, C. C. (1985). Design strengths for an offshore clay. *Journal of Geotechnical Engineering*, *111*(3), 337–355.

Kremer, R., Van der Meer, M., Niemeijer, J., Koehorst, B., & Calle, E. (2001). Technisch rapport waterkerende grondconstructies; geotechnische aspecten van dijken, dammen en boezemkaden. *TR19-prepared by GeoDelft*.

Ladd, C. C. (1991). Stability evaluation during staged construction. *Journal of Geotechnical Engineering*, *117*(4), 540–615.

Ladd, C. C., & DeGroot, D. J. (2003). Recommended practice for soft ground site characterization: Arthur casagrande lecture. In *12th panamerican conference on soil mechanics and geotechnical engineering* (Vol. 1, pp. 1–57).

Ladd, C. C., & Foott, R. (1974). New design procedure for stability of soft clays. *Journal of Geotechnical and Geoenvironmental Engineering*, *100*(Proc Paper 10064).

Lade, P., Yamamuro, J. A., & Skyers, B. D. (1996). Effects of shear band formation in triaxial extension tests. *Geotechnical Testing Journal*, *19*(4), 398–410.

Lade, P. V., & Wang, Q. (2012). Effects of stiff and flexible boundary conditions in triaxial extension tests on cross-anisotropic sand behavior. *Geotechnical Testing Journal*, *35*(5), 715–727.

Leroueil, S., & Vaughan, P. (1990). The general and congruent effects of structure in natural soils and weak rocks. *Géotechnique*, *40*(3), 467–488.

Liu, J., Wang, L., Zhang, X., Yang, J., & Zhang, S. (2019). Asymptotic state model of saturated low liquid-limit clay under partial drainage condition. *Bulletin of Engineering Geology and the Environment*, 1–8.

Liu, M., & Carter, J. (2002). A structured cam clay model. *Canadian Geotechnical Journal*, *39*(6), 1313–1332.

Lupini, J., Skinner, A., & Vaughan, P. (1982). Discussion: The drained residual strength of cohesive soils. *Géotechnique*, *32*(1), 76–76.

Mayne, P. W. (1985). A review of undrained strength in direct simple shear. *Soils and foundations*, *25*(3), 64–72.

McDowell, G., & Hau, K. (2003). A simple non-associated three surface kinematic hardening model. *Géotechnique*, *53*(4), 433–437.

Ministerie van Infrastructuur en Milieu. (2016). *Schematiseringshandleiding macrostabiliteit-wbi 2017 (design manual macro-stability)* (Tech. Rep.). Rijkswaterstaat, Water Verkeer en Leefomgeving.

Muraro, S. (2019). *The deviatoric behaviour of peat: a route between past empiricism and future perspectives* (Unpublished doctoral dissertation). Delft University of Technology.

Nakase, A., & Kamei, T. (1983). Undrained shear strength anisotropy of normally consolidated cohesive soils. *Soils and foundations*, *23*(1), 91–101.

Nakase, A., Kamei, T., & Kusakabe, O. (1988). Constitutive parameters estimated by plasticity index. *Journal of Geotechnical Engineering*, *114*(7), 844–858.

Prevost, J. H. (1979). Undrained shear tests on clays. *ASCE J Geotech Eng Div*, *105*(1), 49–64.
Schofield, A., & Wroth, P. (1968). *Critical state soil mechanics* (Vol. 310). McGraw-Hill London.
Sheahan, T. C., Ladd, C. C., & Germaine, J. T. (1996). Rate-dependent undrained shear behavior of saturated clay. *Journal of Geotechnical Engineering*, *122*(2), 99–108.
Stoop, J. (2010). Schuifsterkteparameters in de stabiliteitsanalyse van dijken, vanuit de praktijk van de waterkeringbeheerder (shear strength parameters in the stability analysis of dikes, from the water authority practice. *Geotechniek*, *14*(1), 38.
Tavenas, F. (1990). " laboratory and in situ stress-strain-time behaviour of soft clays,"-state-of-the-art paper. In *Int. symp. geotech. engrg. soft soils.*
Tejchman, J., & Bauer, E. (2005). Fe-simulations of a direct and a true simple shear test within a polar hypoplasticity. *Computers and Geotechnics*, *32*(1), 1–16.
Van Baars, S., & Van Kempen, I. (2009). The causes and mechanisms of historical dike failures in the netherlands. *E-WAter journal, 2009*.
van Duinen, T. (2014). *Handreiking voor het bepalen van schuifsterkte parameters, wti2017 toetsregels stabiliteit (shear strength parameter guidelines, according to the wti (2017) norm)* (Tech. Rep.). Technical Report 1209434-003, Deltares.
Westerberg, B. (1995). Lerors mekaniska egenskaper (mechanical properties of clays). *Licentiate thesis*.
Wheeler, S. J., Näätänen, A., Karstunen, M., & Lojander, M. (2003). An anisotropic elastoplastic model for soft clays. *Canadian Geotechnical Journal*, *40*(2), 403–418.
Wilde, P. (1977). Two invariants-dependent models of granular media. *Archives of Mechanics*, *26*(6), 799–809.
Wood, D. M. (2014). *Geotechnical modelling*. CRC press.
Wood, D. M., & Belkheir, K. (1994). Strain softening and state parameter for sand modelling. *Geotechnique*, *44*(2), 335–339.
Wroth, C. (1984). The interpretation of in situ soil tests. *Geotechnique*, *34*(4), 449–489.
Wu, W., & Kolymbas, D. (1991). On some issues in triaxial extension tests. *Geotechnical Testing Journal*, *14*(3), 276–287.
Yamada, M., Akaishi, M., & Dafalias, Y. F. (2001). Undrained strain softening behavior of normally consolidated clays and mud rocks. *Doboku Gakkai Ronbunshu*, *2001*(687), 1–8.
Yamamuro, J. A., & Lade, P. V. (1995). Strain localization in extension tests on granular materials. *Journal of engineering mechanics*, *121*(7), 828–836.
Zdravković, L., & Jardine, R. (2001). The effect on anisotropy of rotating the principal stress axes during consolidation. *Geotechnique*, *51*(1), 69–83.
Zentar, R., Abriak, N.-E., & Dubois, V. (2009). Effects of salts and organic matter on atterberg limits of dredged marine sediments. *Applied Clay Science*, *42*(3-4), 391–397.
Zhu, J.-G., & Yin, J.-H. (2000). Strain-rate-dependent stress-strain behavior of overconsolidated hong kong marine clay. *Canadian Geotechnical Journal*, *37*(6), 1272–1282.
Zwanenburg, C. (2016). *Blauwdruk EEM (Blueprint FEM)* (Tech. Rep.). POV-Macrostabiliteit.

Appendix A

Soil Classification

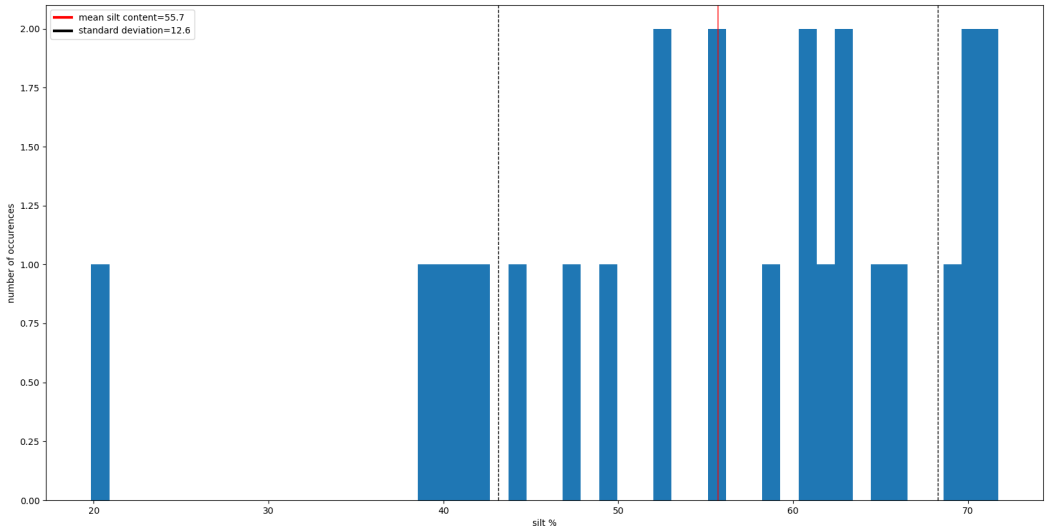

Figure A.0.1: Silt content of samples tested in Triaxial Compression

.

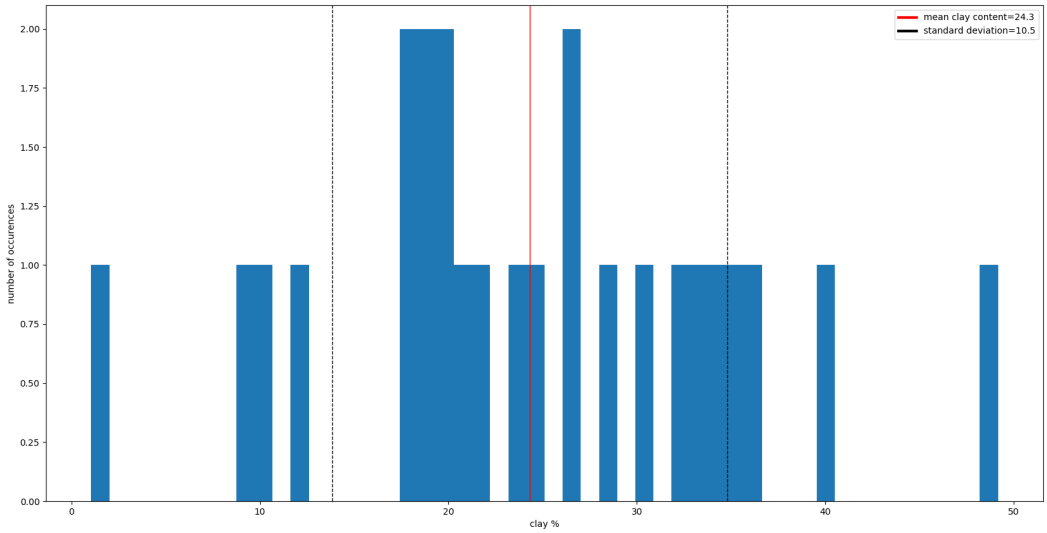

Figure A.0.2: Clay content of samples tested in Triaxial Compression

.

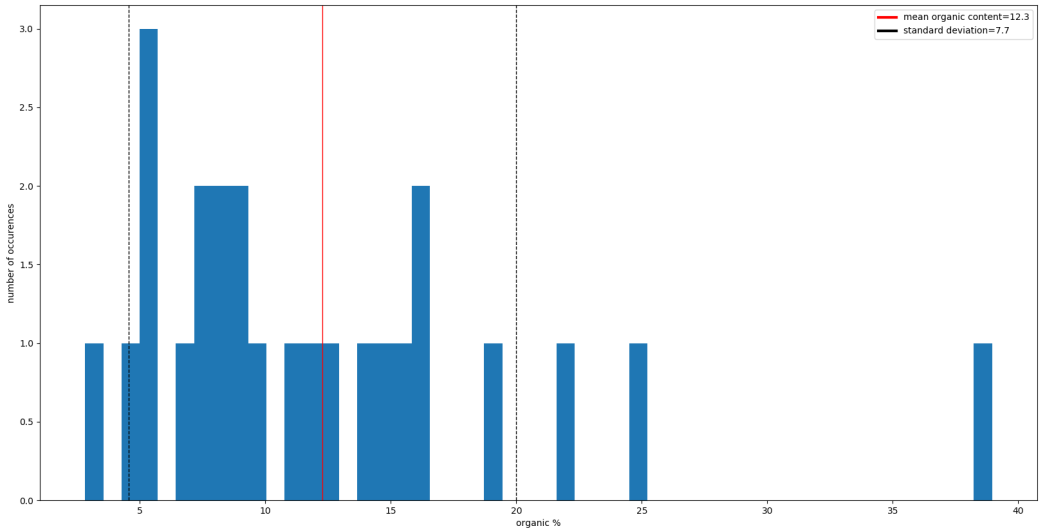

Figure A.0.3: Organic content of samples tested in Triaxial Compression

.

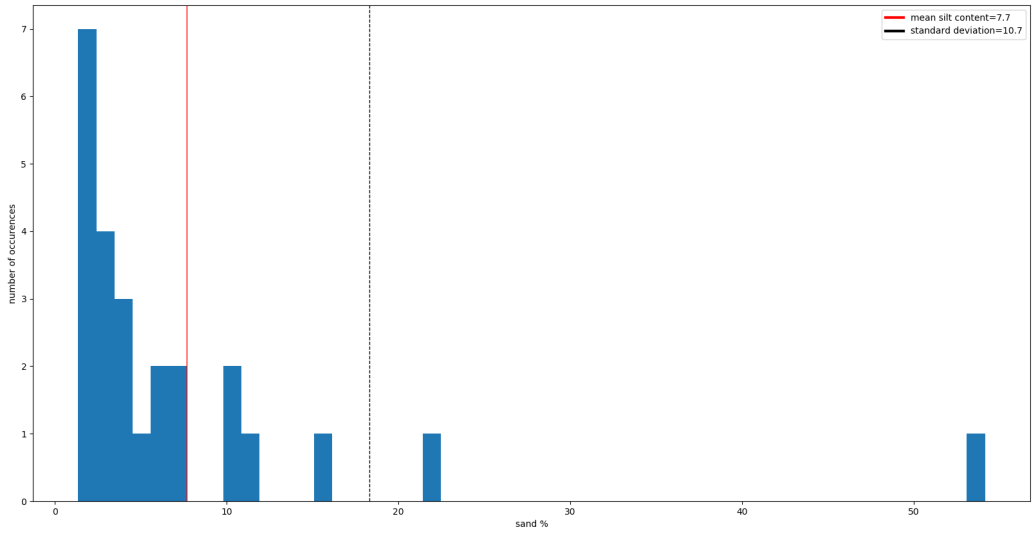

Figure A.0.4: Sand content of samples tested in Triaxial Compression

.

Appendix B

Results Triaxial Compression tests and Direct Simple Shear tests

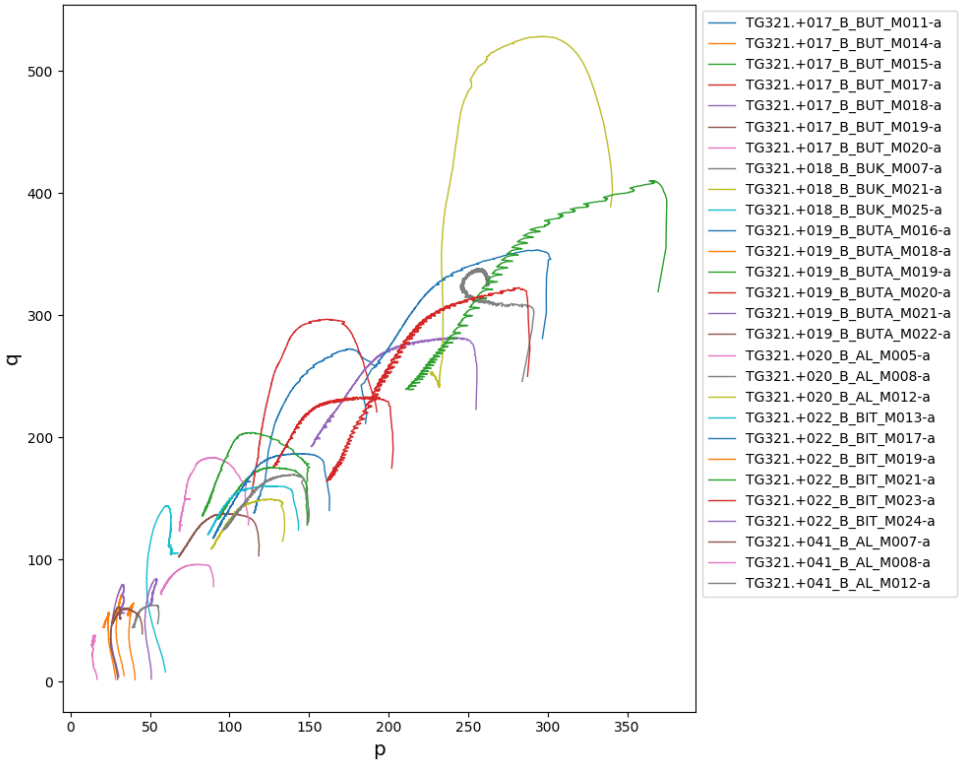

Figure B.0.1: Triaxial test stress Paths for dike section 7h

.

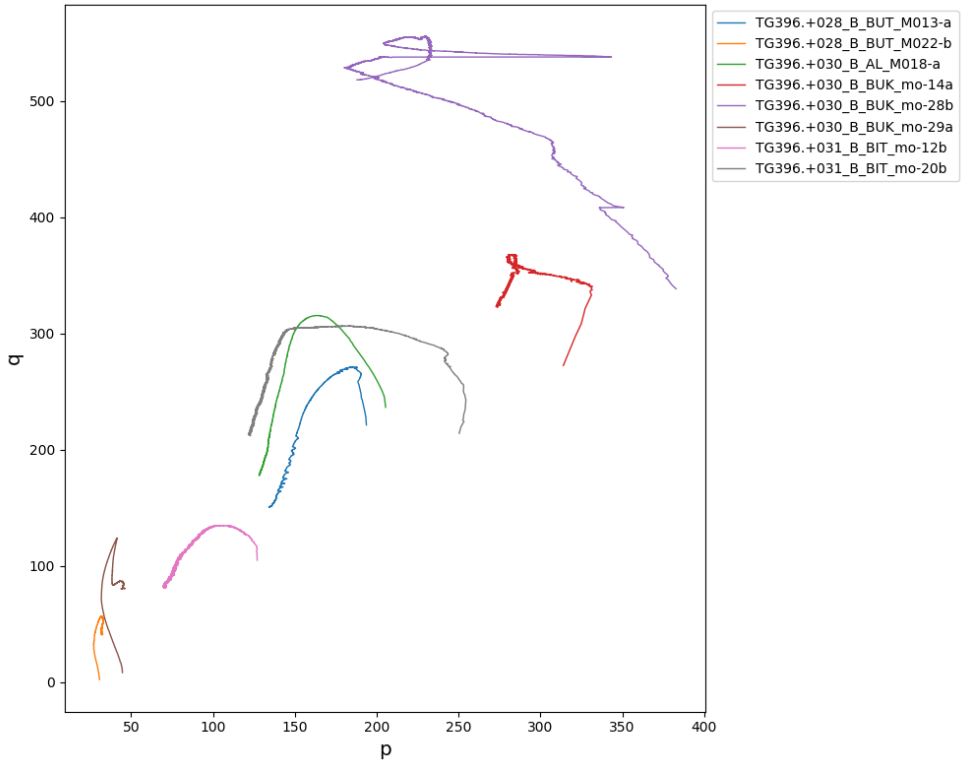

Figure B.0.2: Triaxial test stress Paths for dike section 10b

.

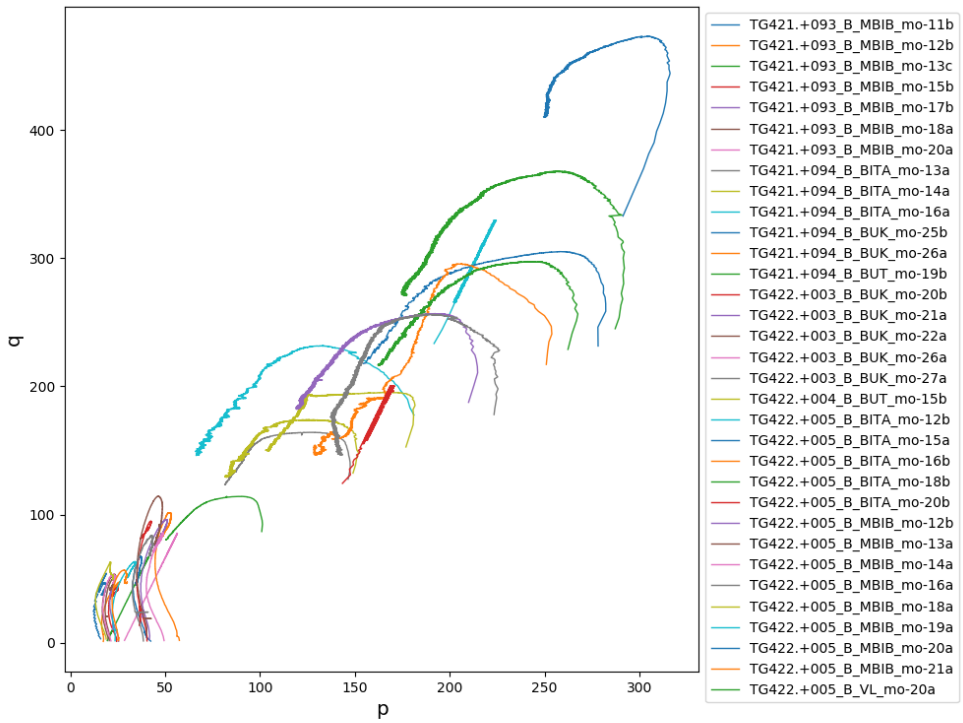

Figure B.0.3: Triaxial test stress Paths for dike section 12g

.

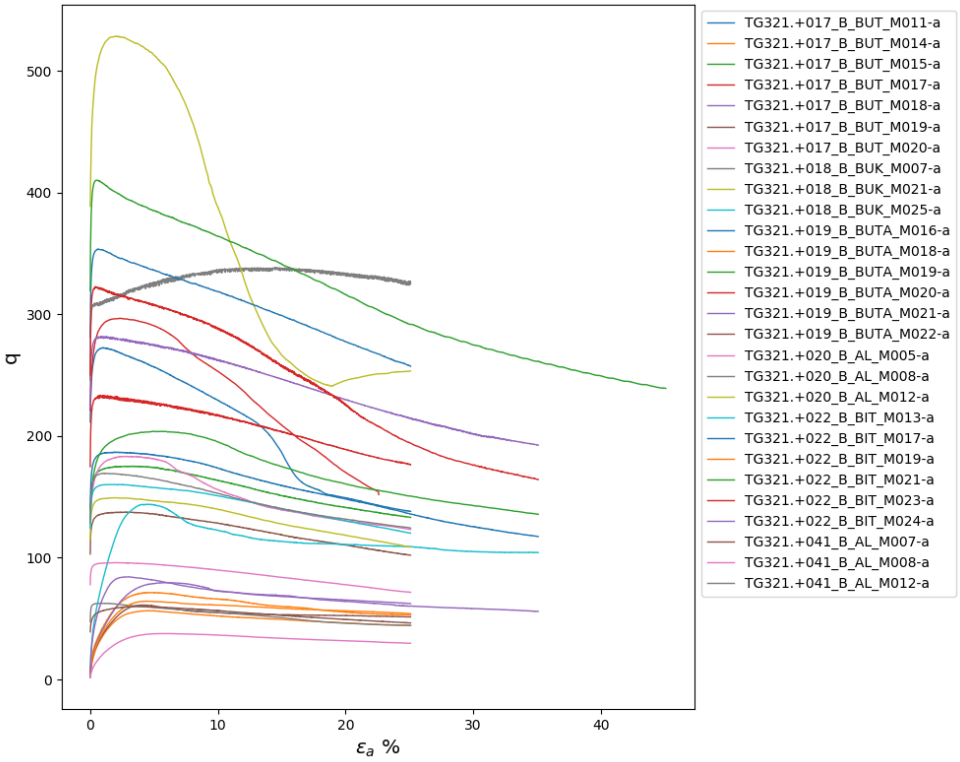

Figure B.0.4: Triaxial test stress Paths for dike section 7h

.

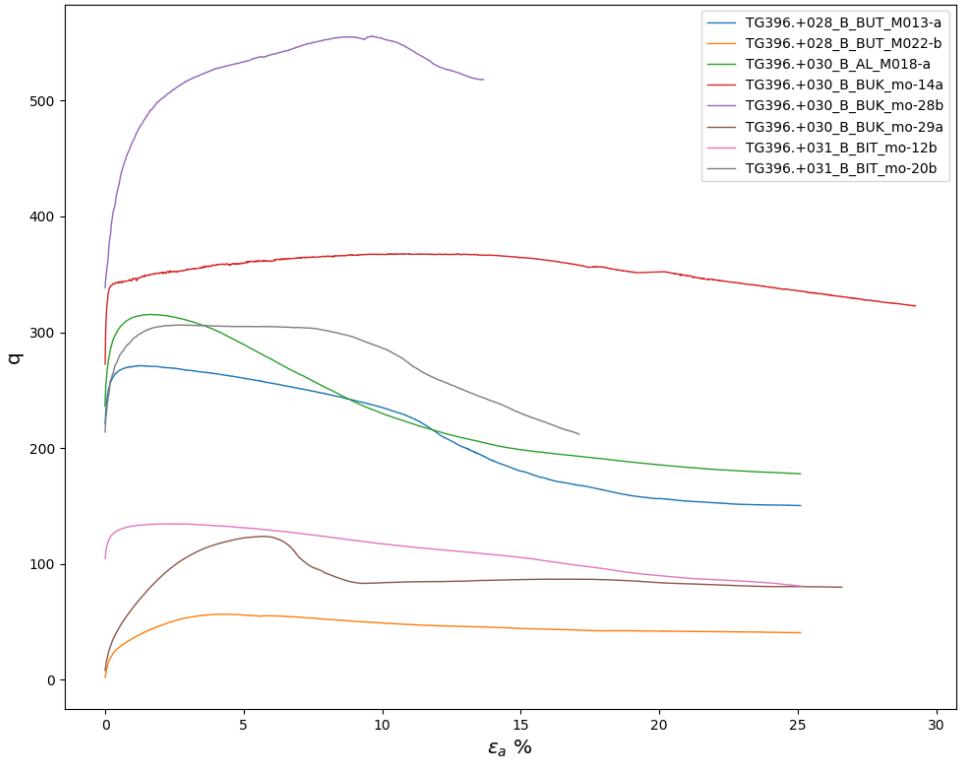

Figure B.0.5: Triaxial test stress Paths for dike section 10b

.

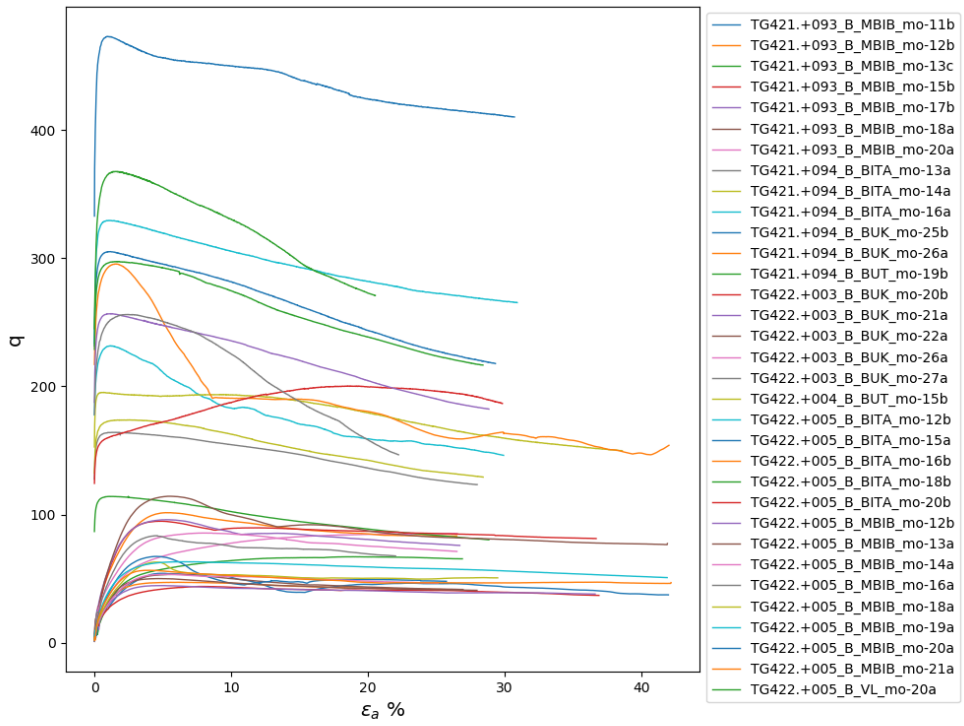

Figure B.0.6: Triaxial test stress Paths for dike section 12g

.

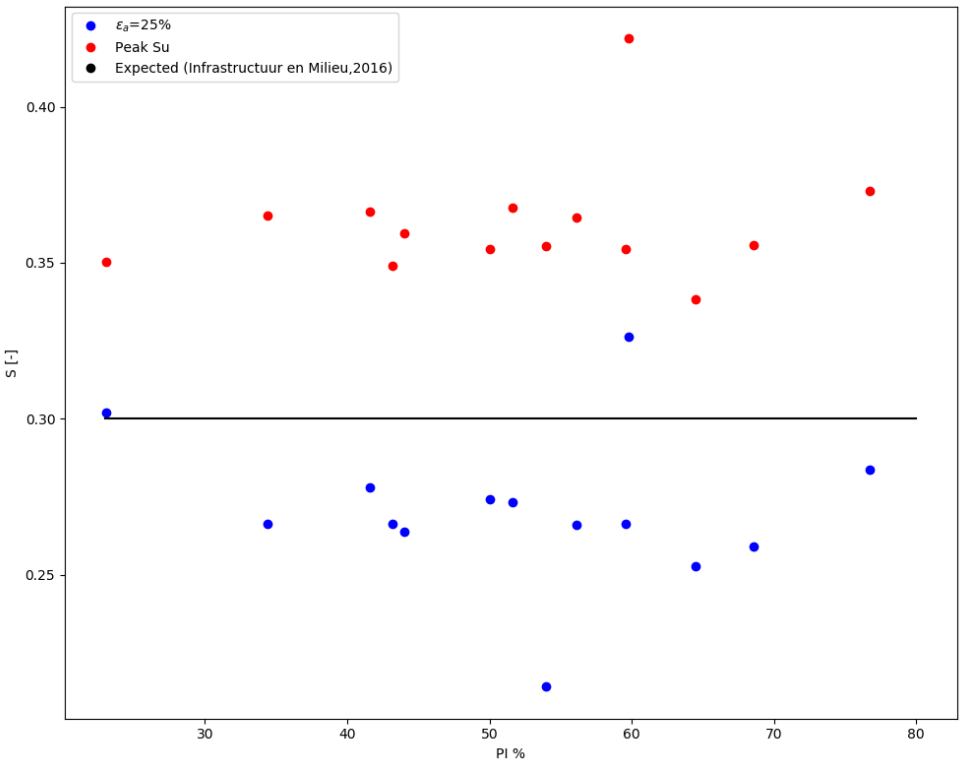

Figure B.0.7: Normalised undrained shear Strength S in Triaxial Compression

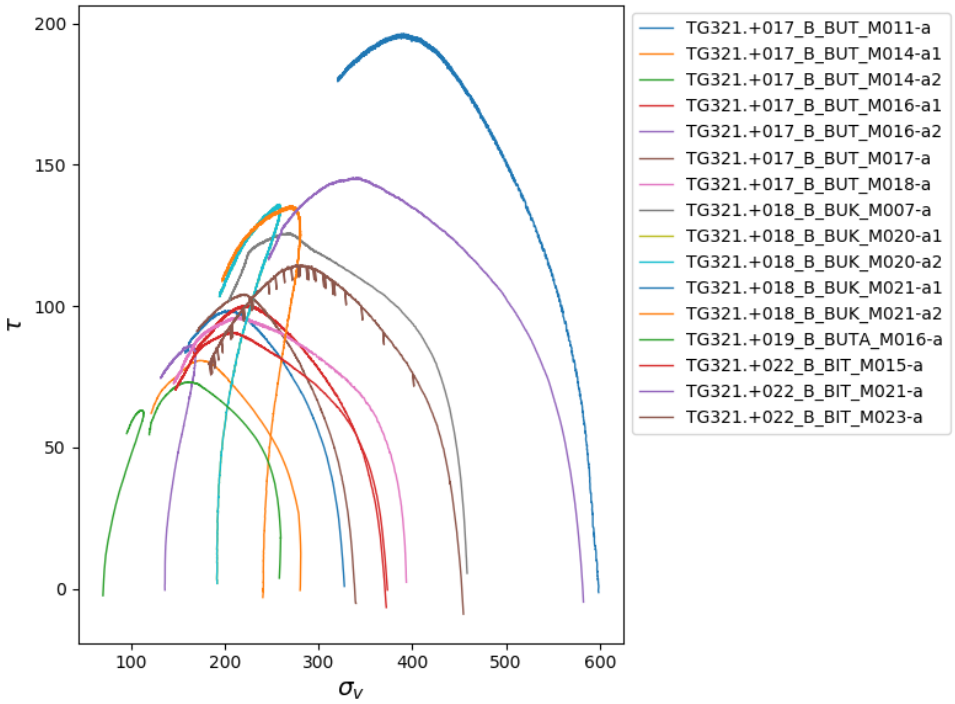

Figure B.0.8: DSS test stress Paths for dike section 7h

.

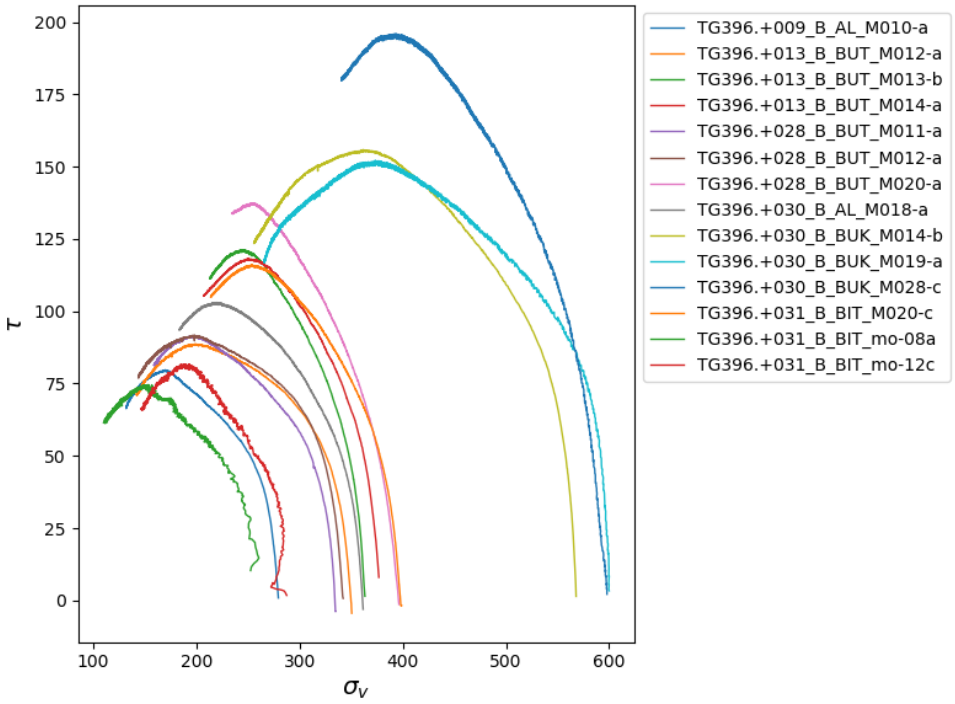

Figure B.0.9: DSS test stress Paths for dike section 10b

.

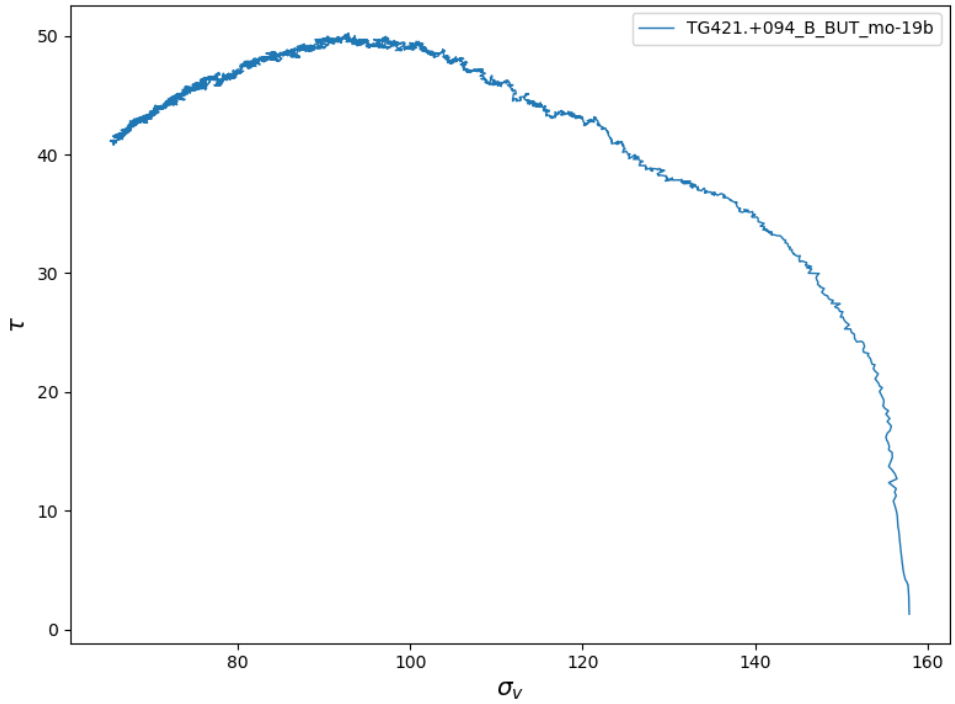

Figure B.0.10: DSS test stress Paths for dike section 12g

.

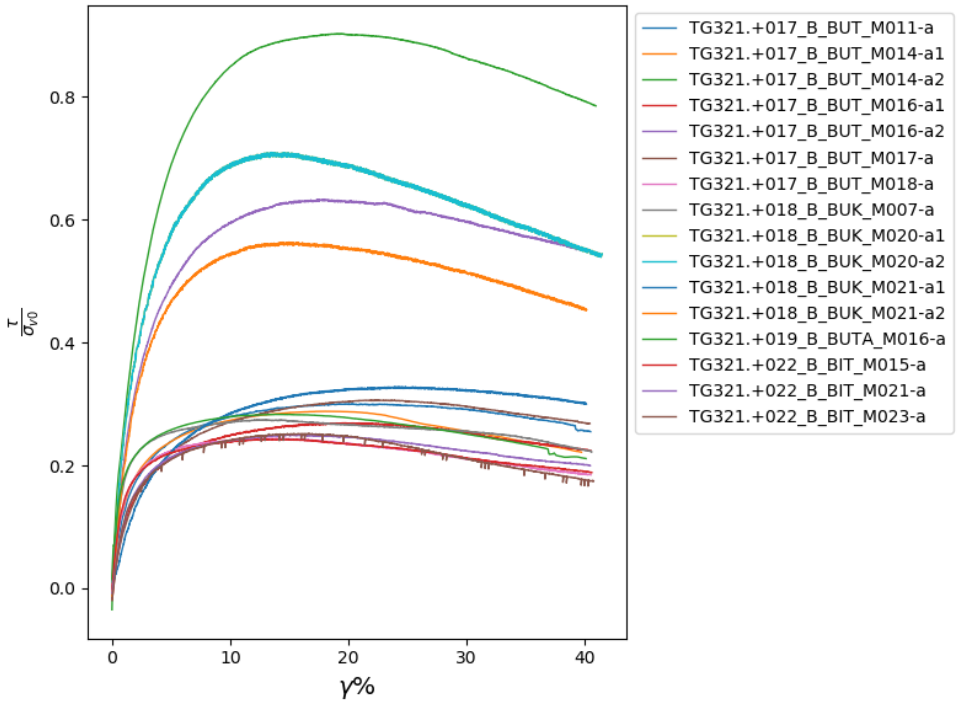

Figure B.0.11: DSS test stress Paths for dike section 7h

.

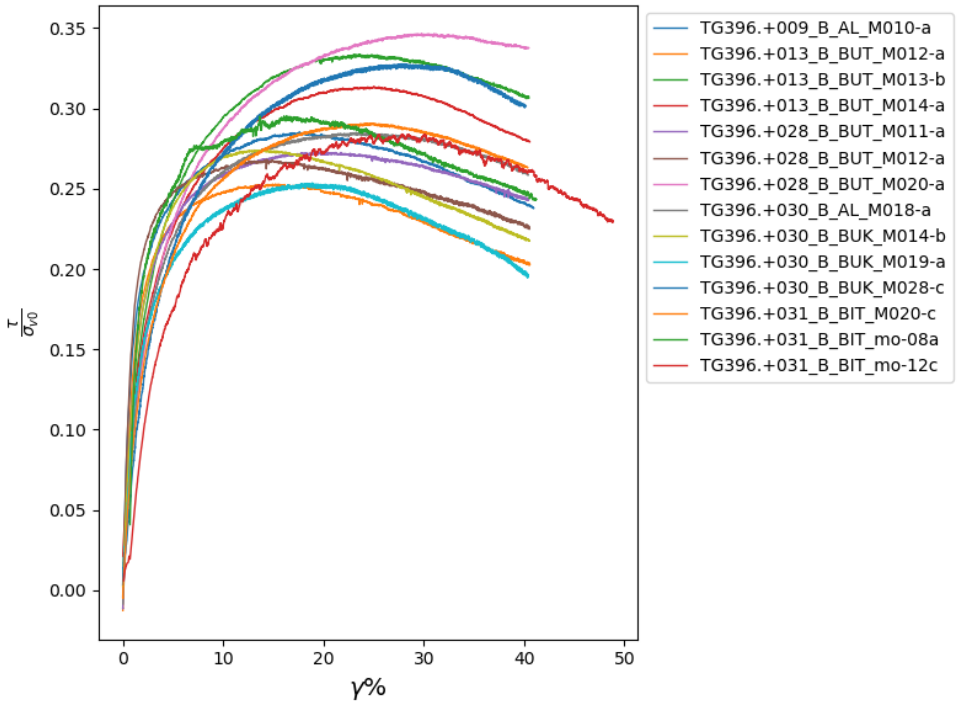

Figure B.0.12: DSS test stress Paths for dike section 10b

.

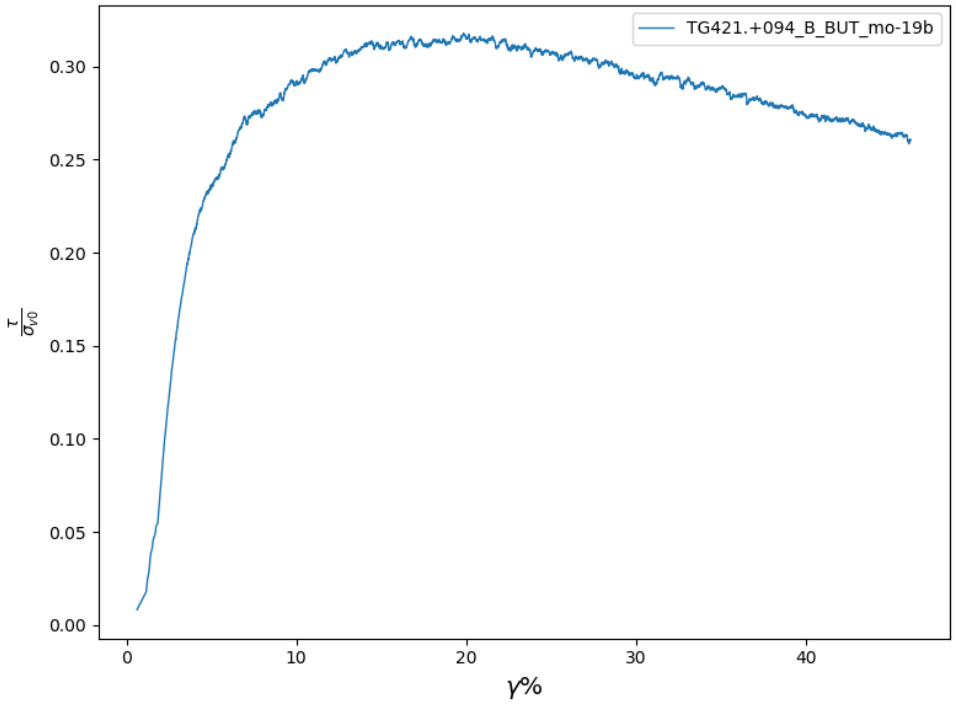

Figure B.0.13: DSS test stress Paths for dike section 12g

.

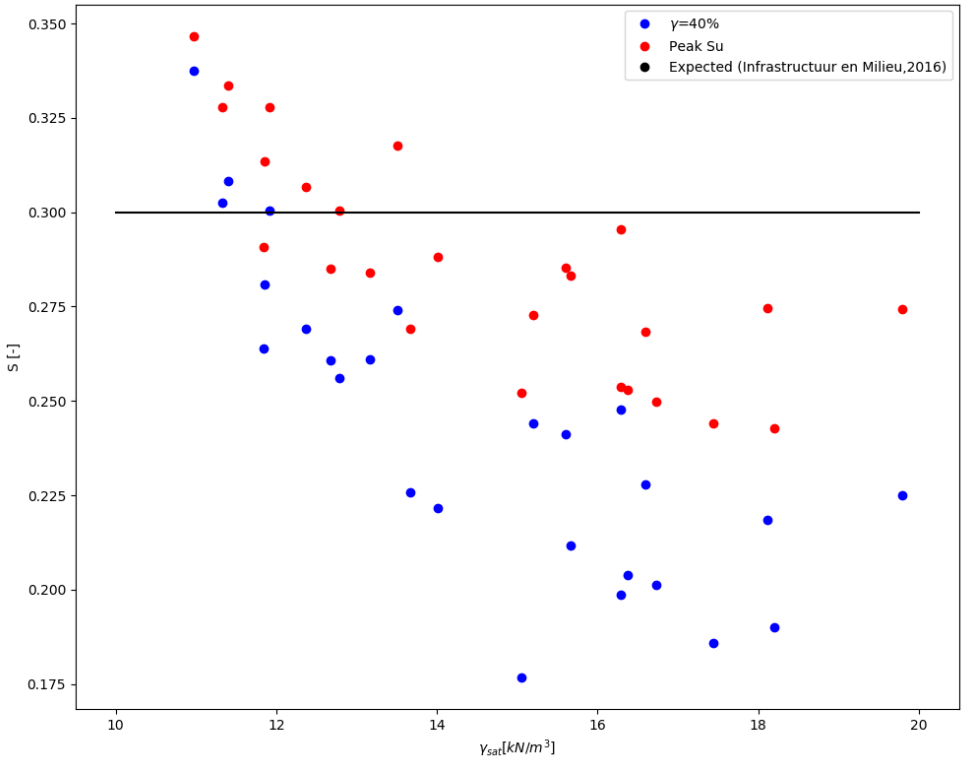

Figure B.0.14: Normalised undrained shear Strength S in DSS

Appendix C

Results CRS tests

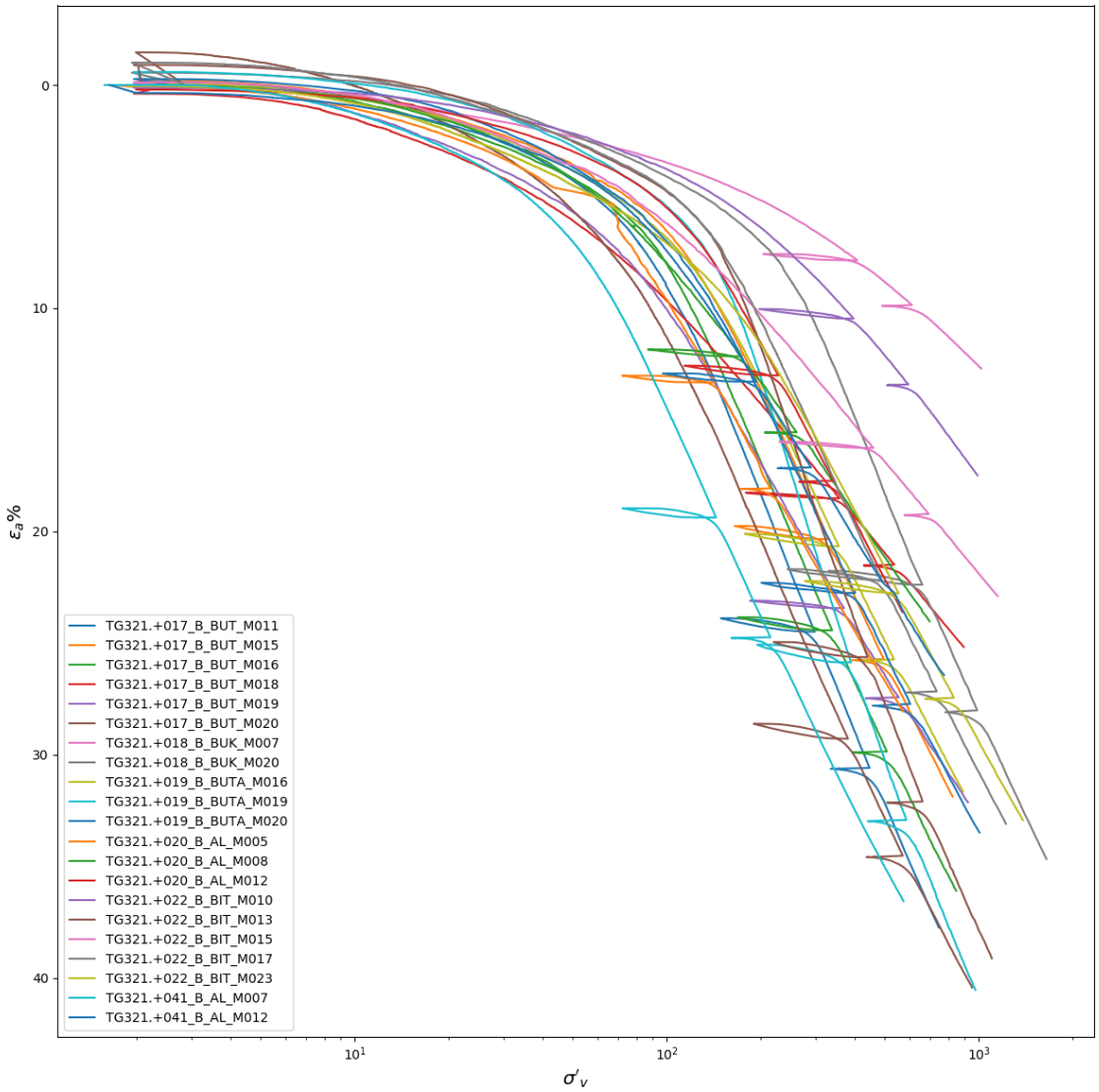

Figure C.0.1: CRS test results for dike section 7h

.

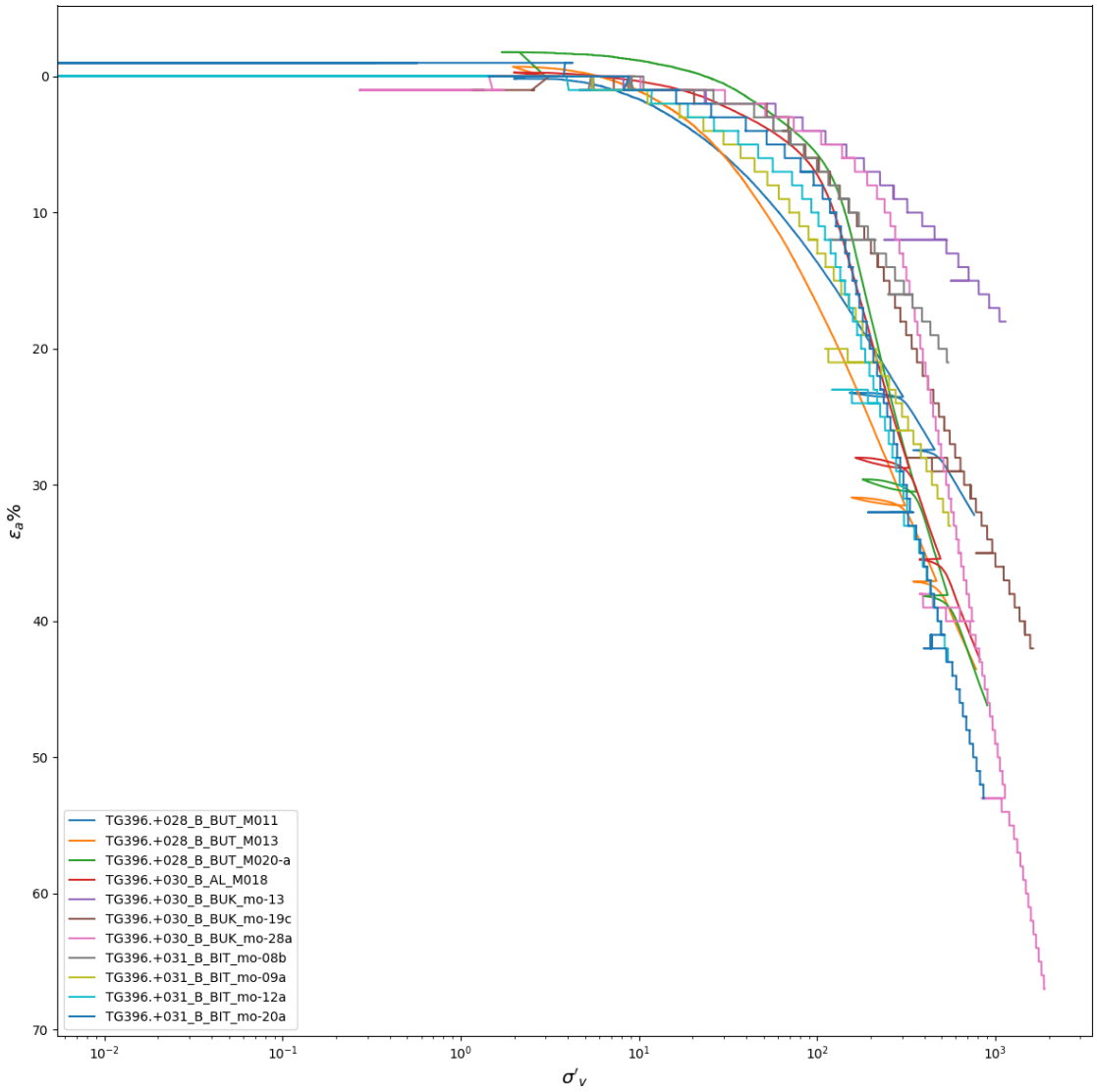

Figure C.0.2: CRS test results for dike section 7h

.

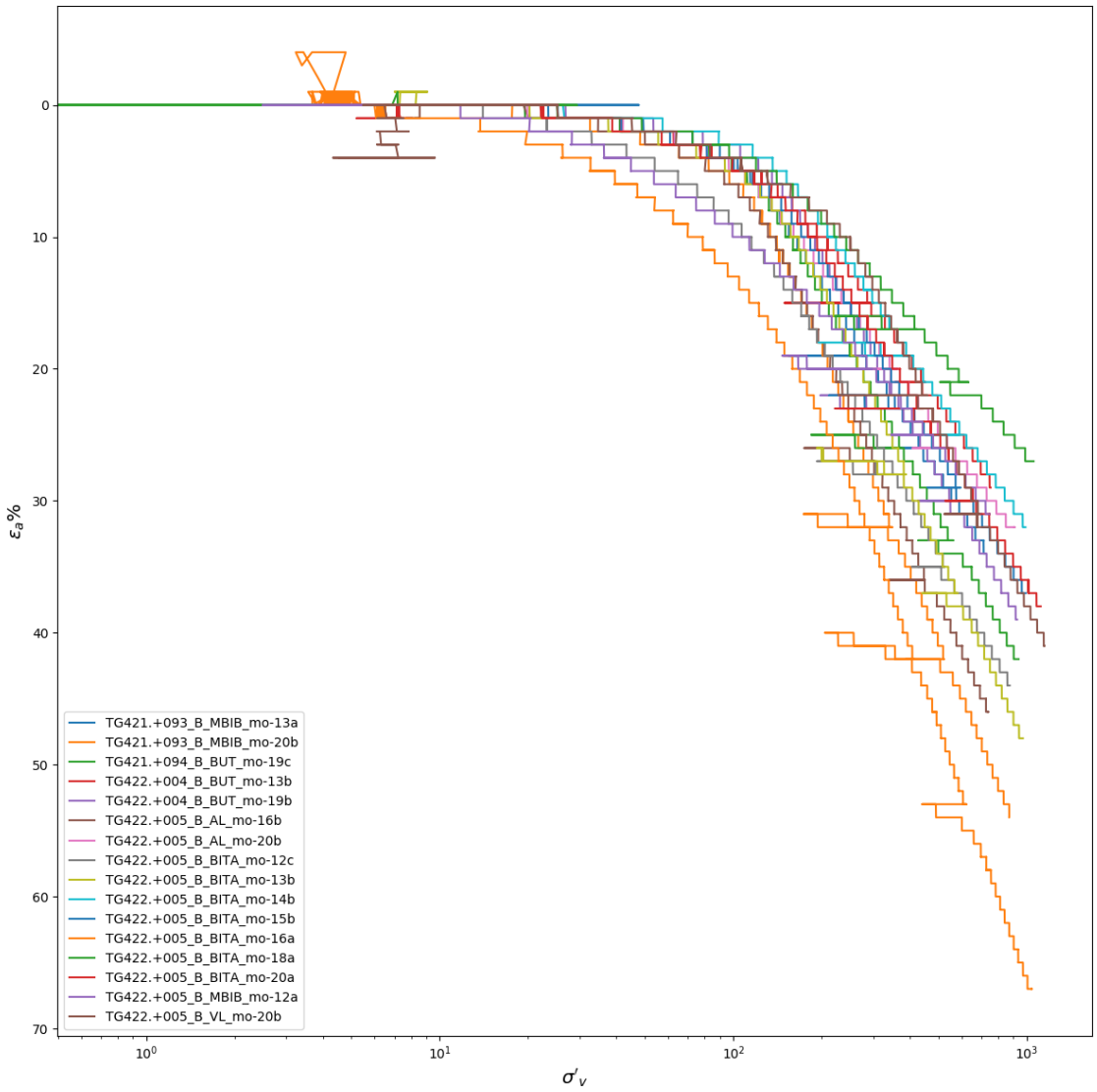

Figure C.0.3: CRS test results for dike section 7h

.

Appendix D

Correlations parameters a and b from CRS tests

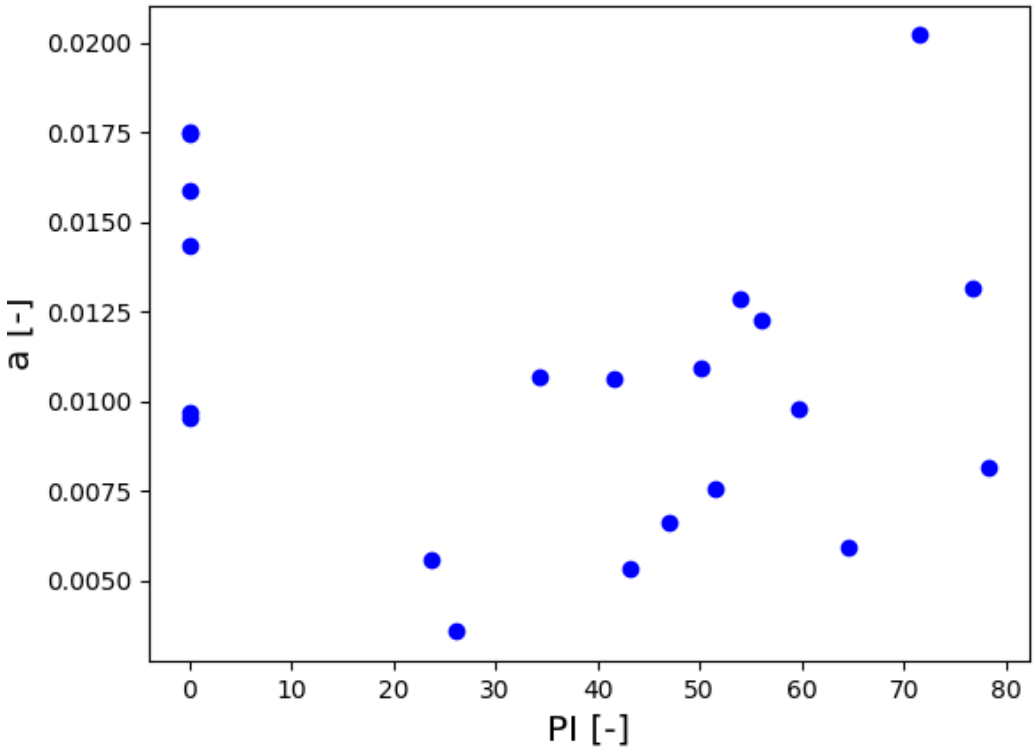

Figure D.0.1: Parameter a versus Plasticity Index

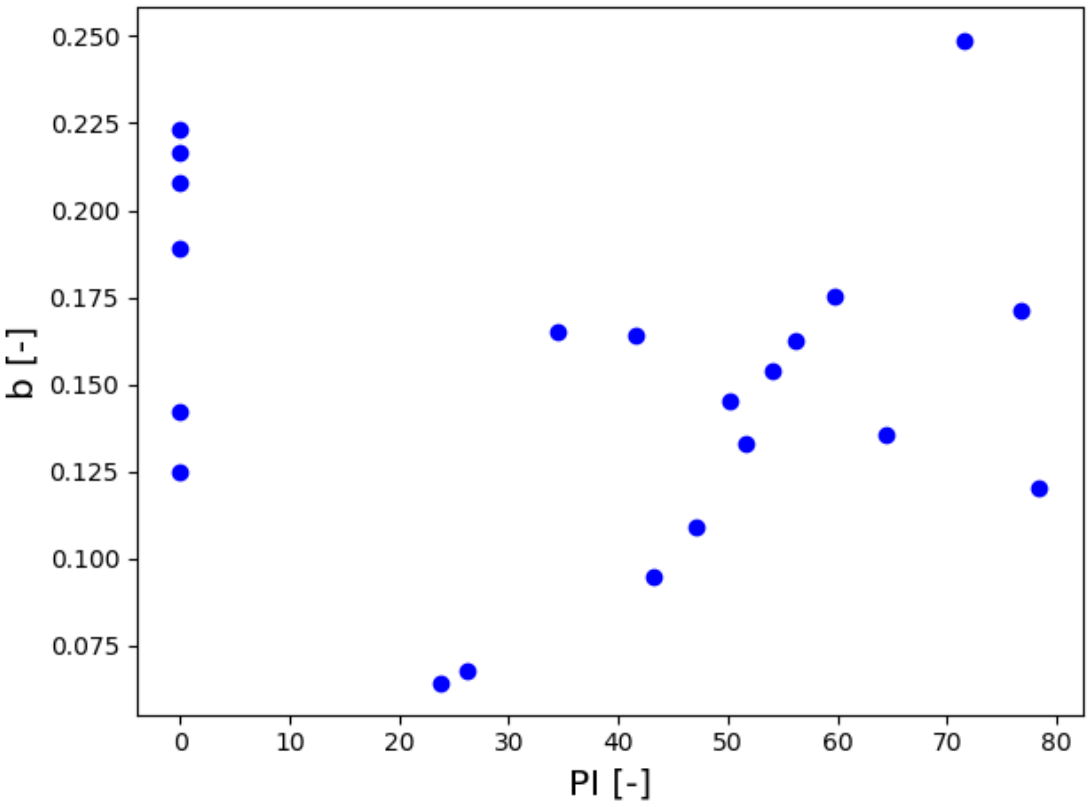

Figure D.0.2: Parameter b versus Plasticity Index

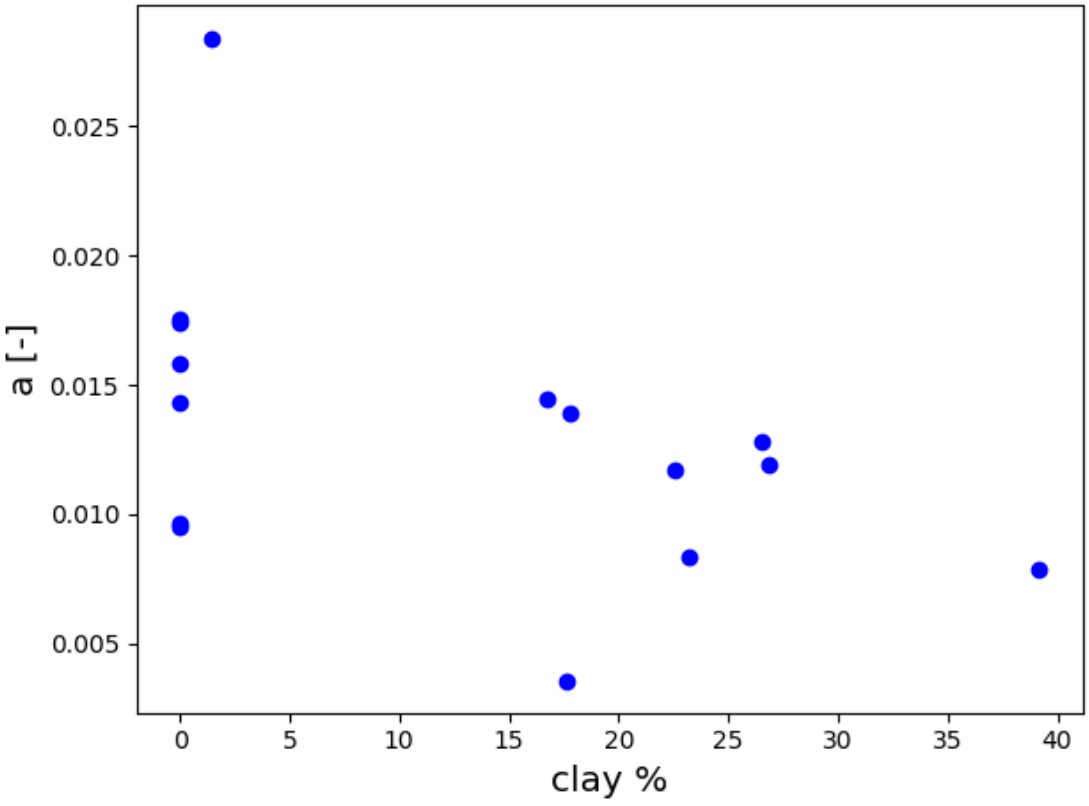

Figure D.0.3: Parameter a versus clay content

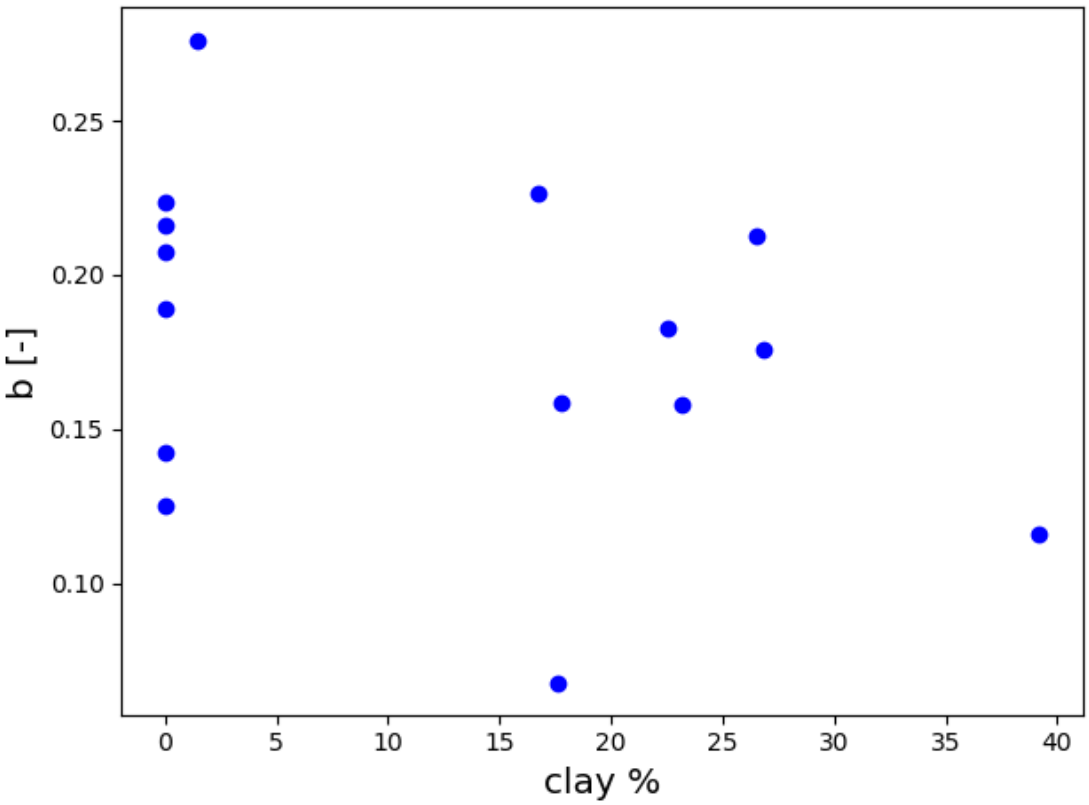

Figure D.0.4: Parameter b versus clay content

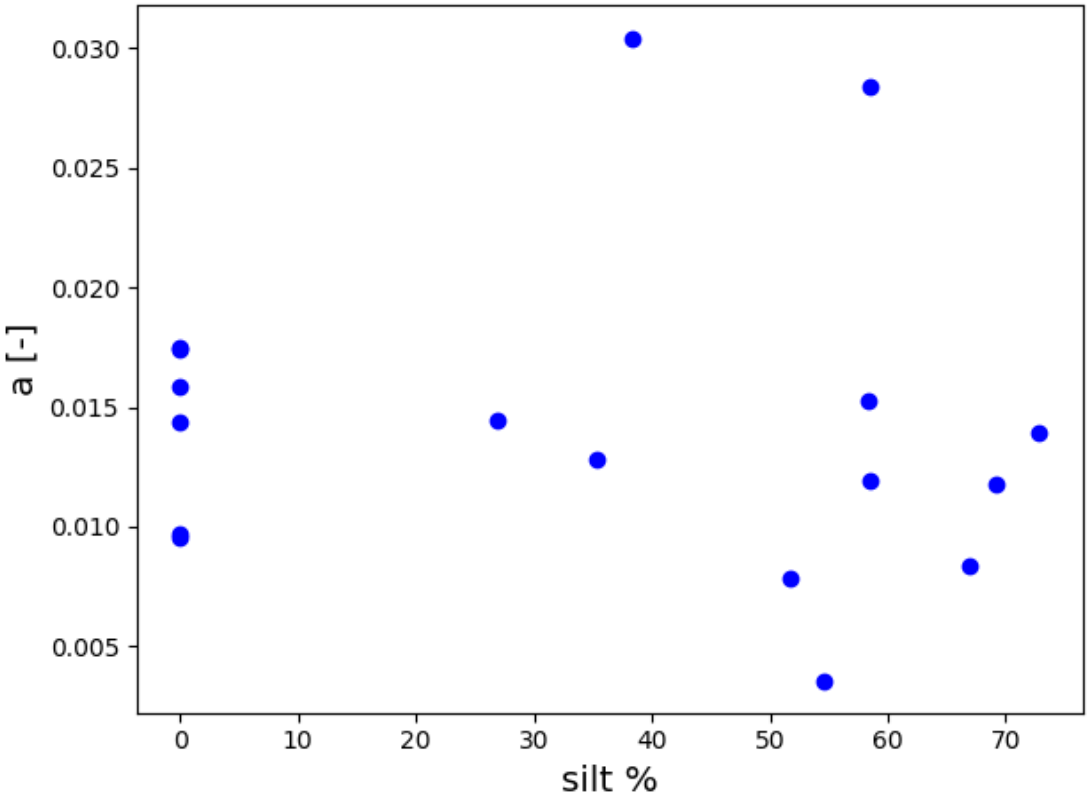

Figure D.0.5: Parameter a versus silt content

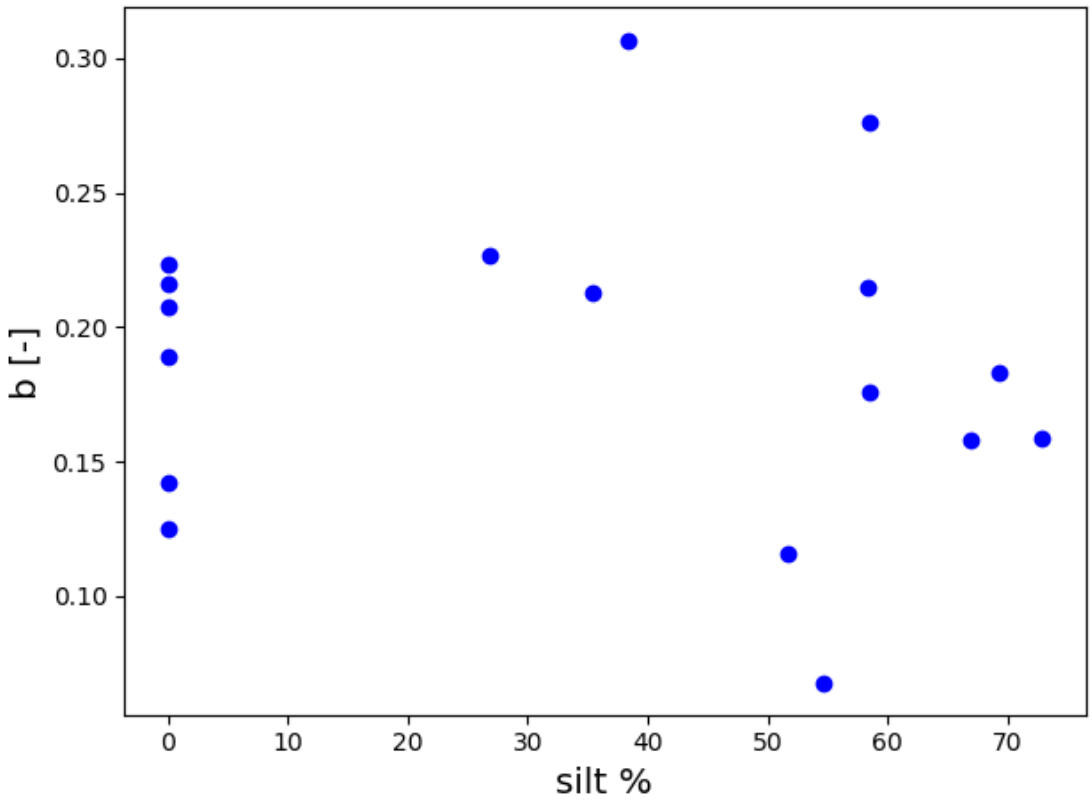

Figure D.0.6: Parameter b versus silt content

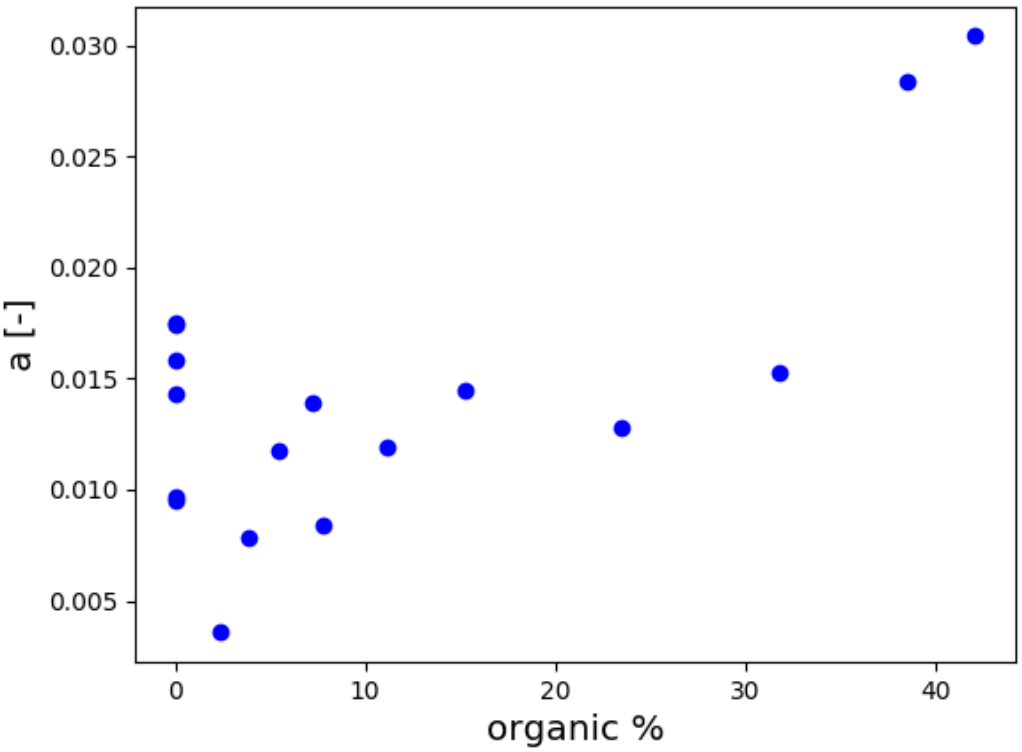

Figure D.0.7: Parameter a versus organic content

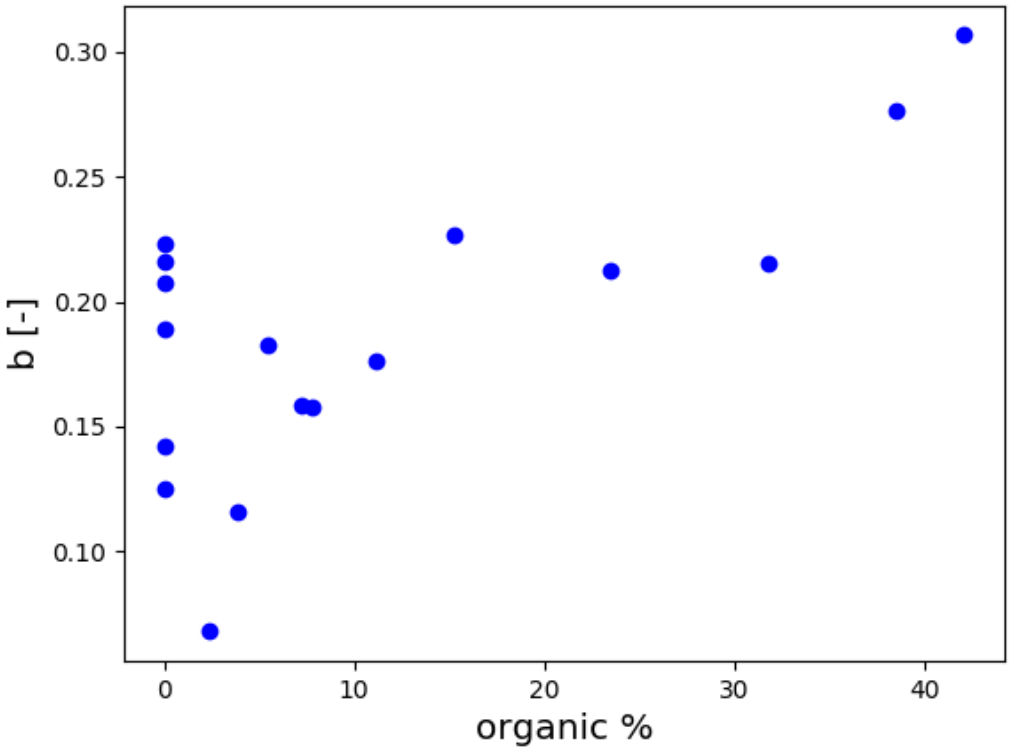

Figure D.0.8: Parameter b versus organic content

Appendix E

Constitutive model basic parametric analysis

E.1 Modified Cam-Clay

Table E.1.1: MCC parameters for a Norwegian Clay (Westerberg, 1995)

M_g	λ	κ	ν	e_0
1.2	0.2	0.02	0.36	2.5

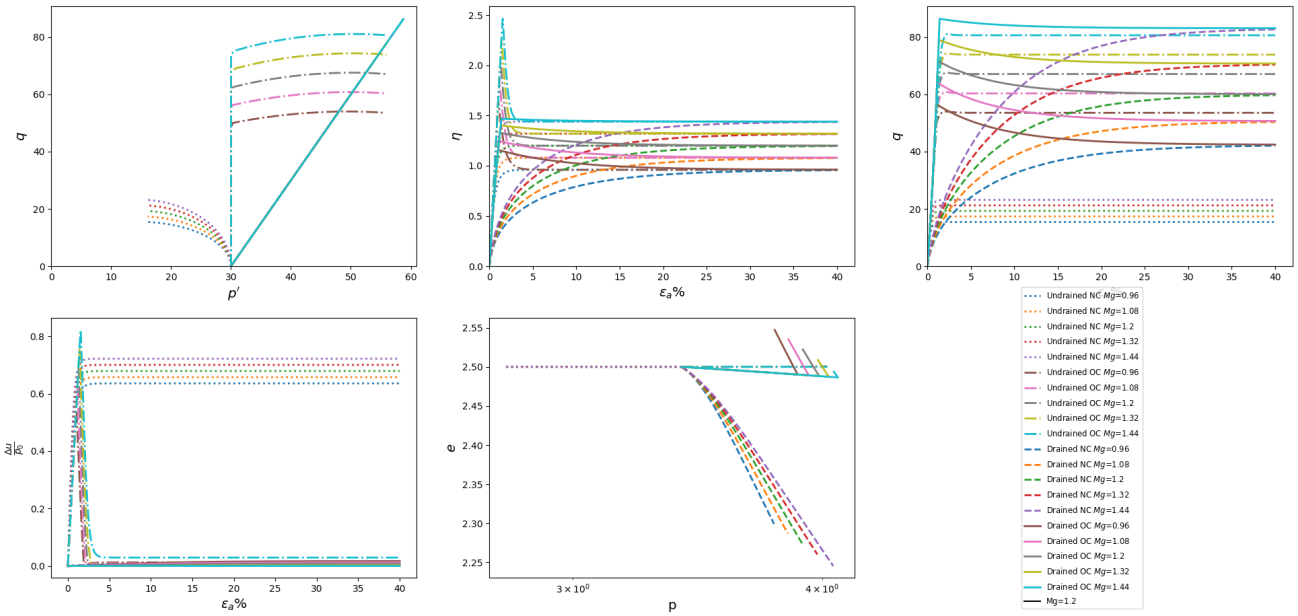

Figure E.1.1: MCC analysis parameter Mg.

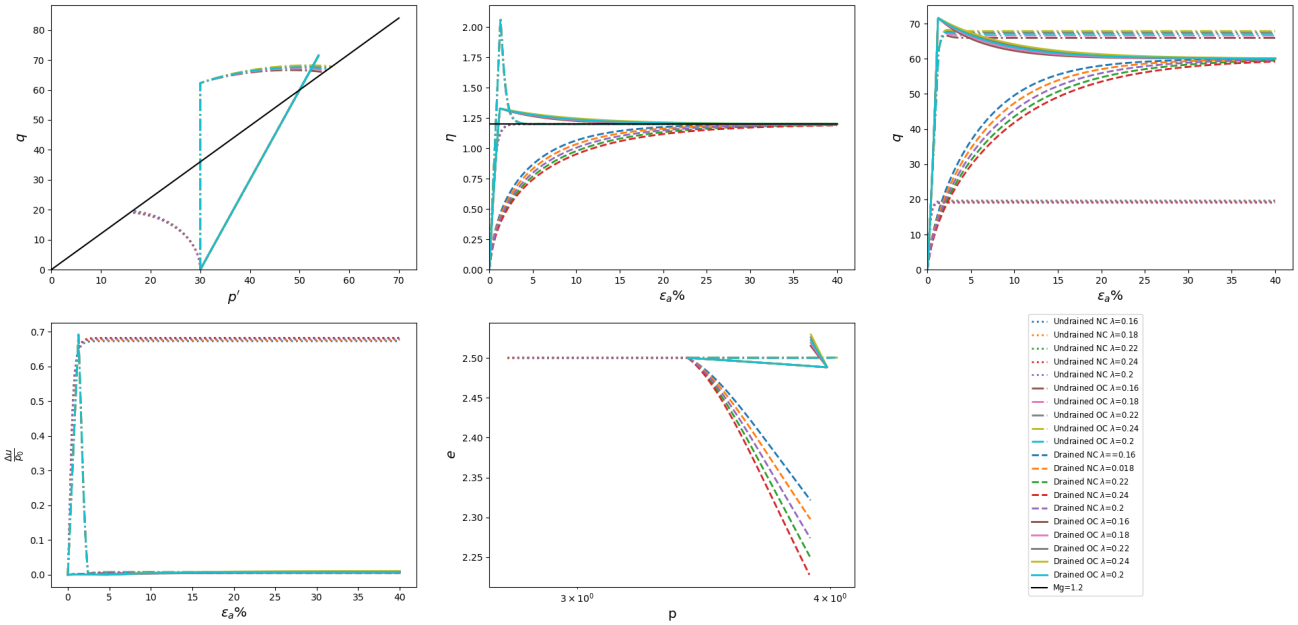

Figure E.1.2: MCC analysis parameter λ.

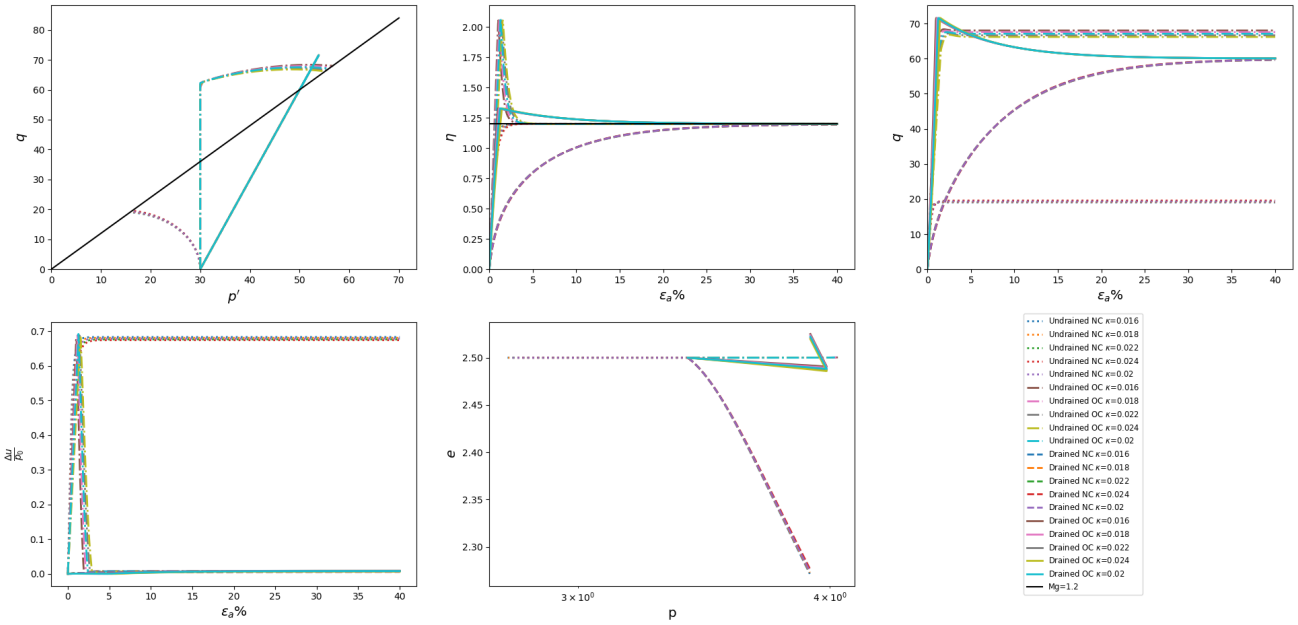

Figure E.1.3: MCC analysis parameter κ.

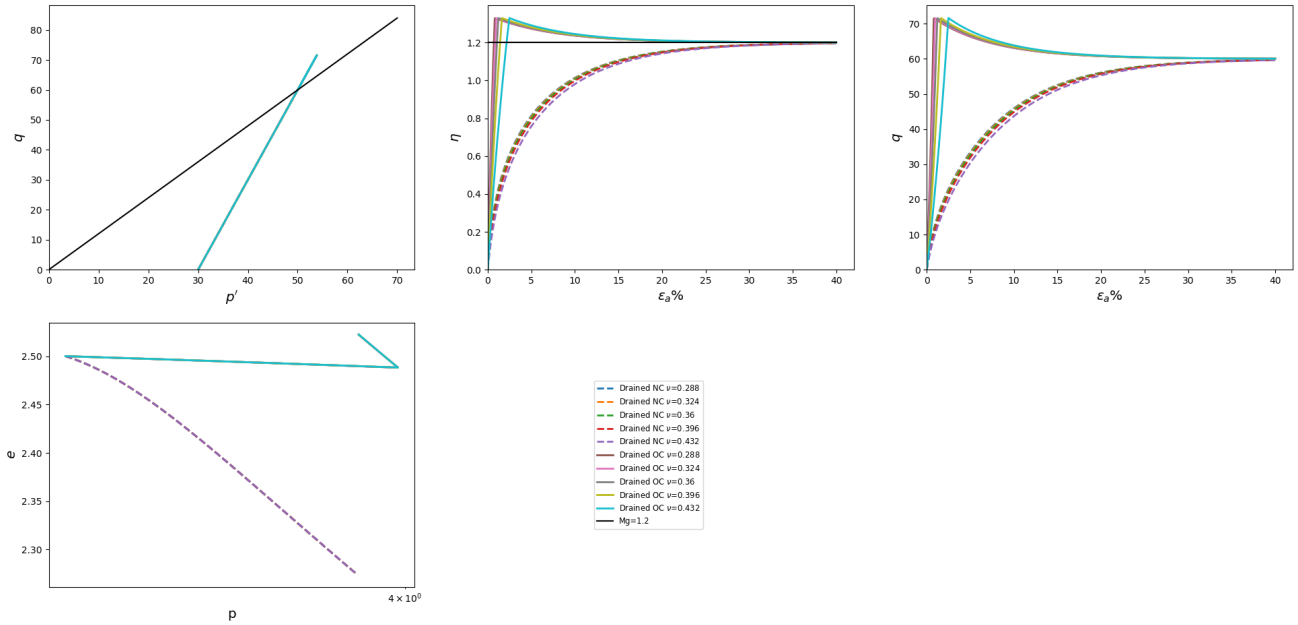

Figure E.1.4: MCC analysis parameter ν.

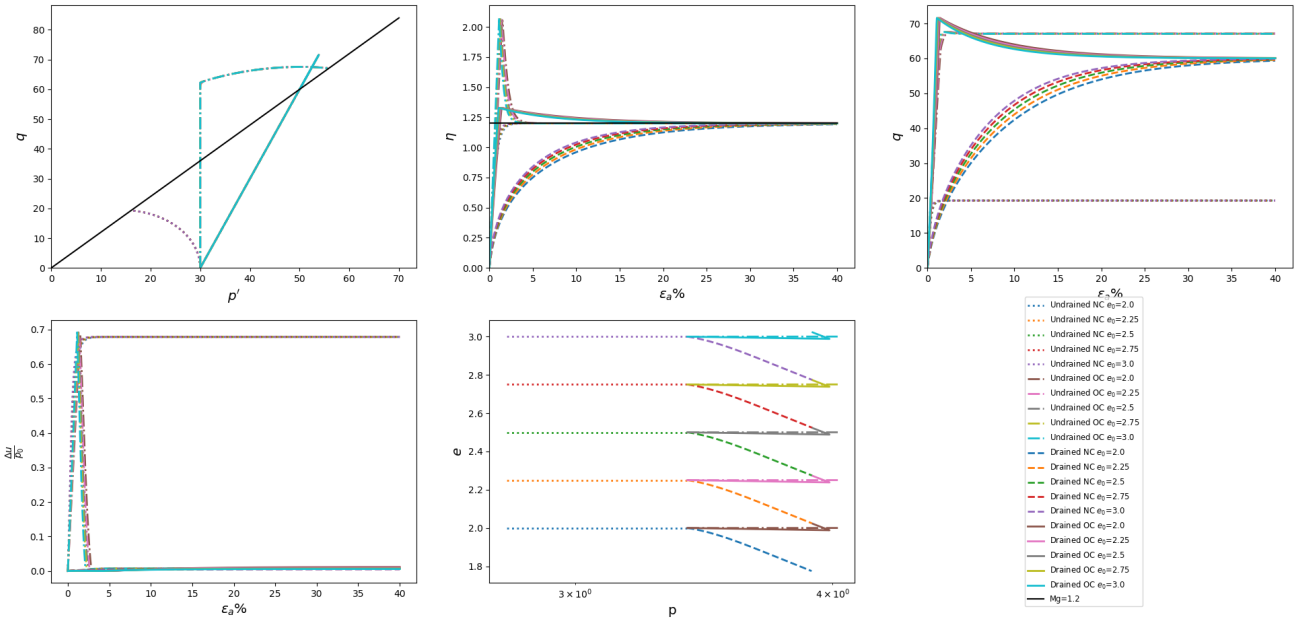

Figure E.1.5: MCC analysis parameter e_0.

E.2 Non-associative flow rule

Table E.2.1: Non-associated flow rule parameters

M_f	χ_g	χ_f
1.2	2.0	2.0

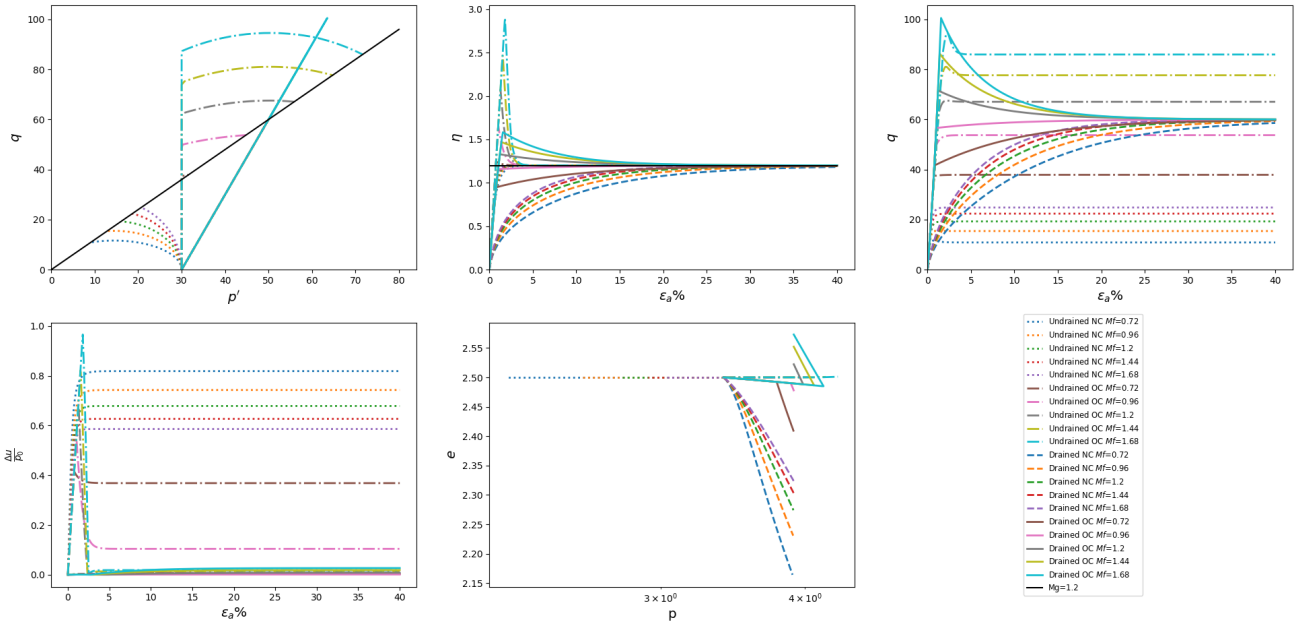

Figure E.2.1: Non-associative flow rule analysis parameter M_f.

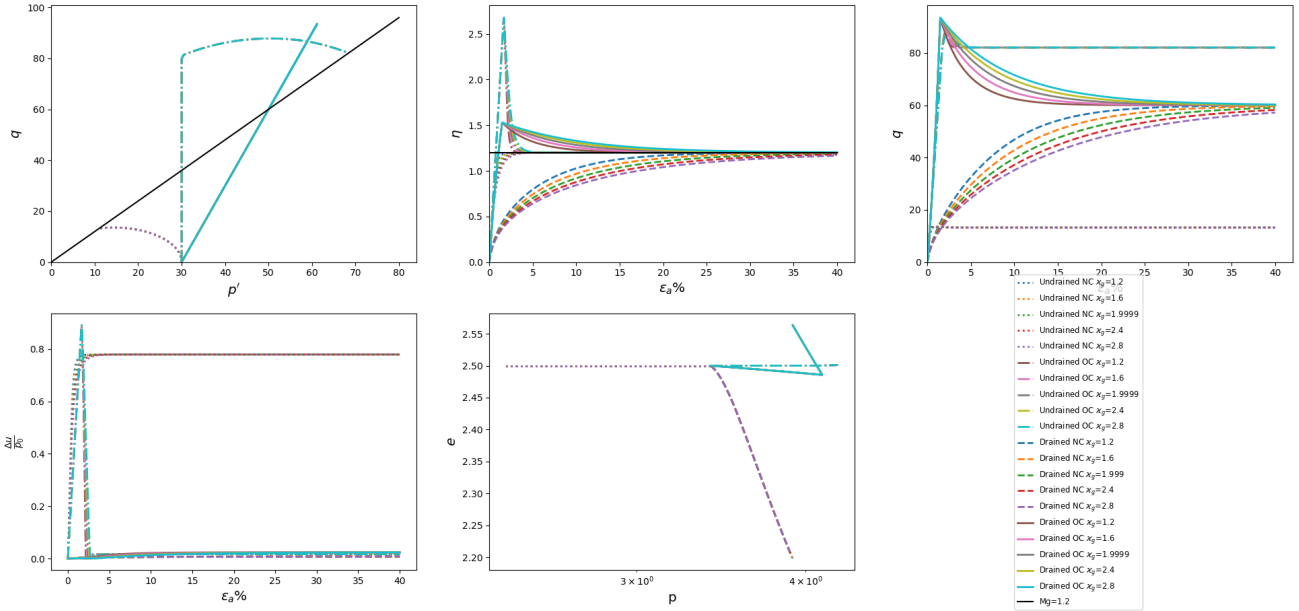

Figure E.2.2: Non-associative flow rule analysis parameter $\varkappa_g$ for $M_f > M_g$.

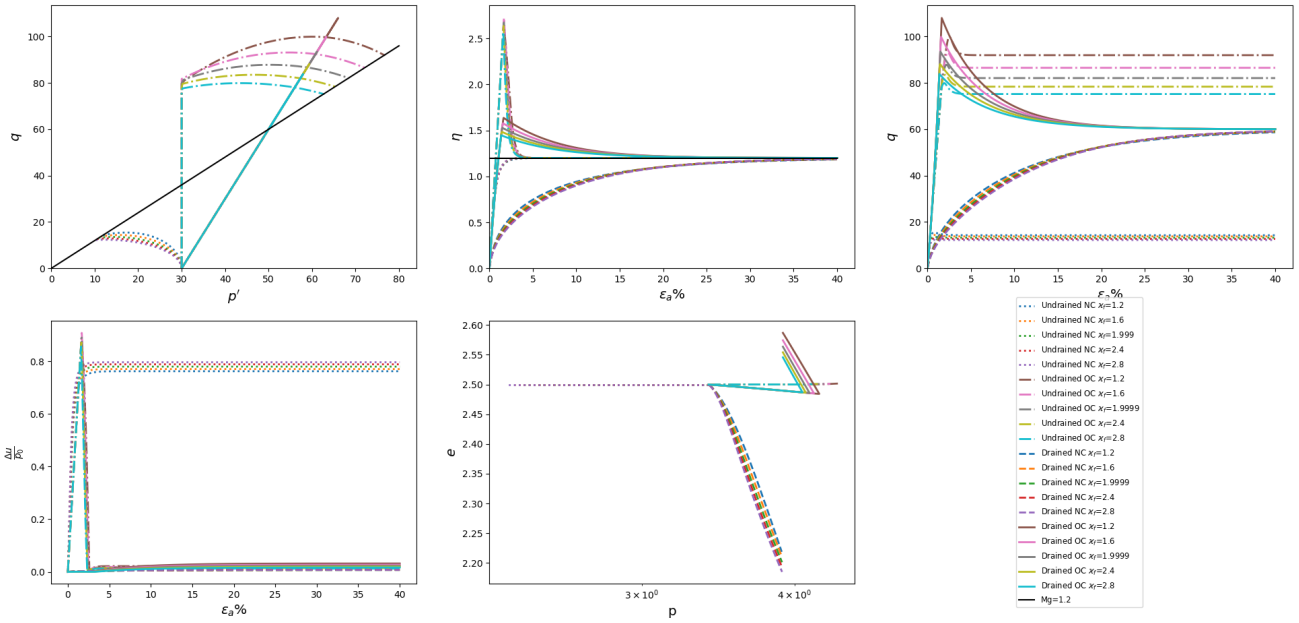

Figure E.2.3: Non-associative flow rule analysis parameter $\varkappa_f$ for $M_f > M_g$.

E.3 Deviatoric hardening or softening

Table E.3.1: Non-associated flow rule parameters for deviatoric softening parametric analysis.

M_g	λ	κ	ν	e_0	M_f	χ_g	χ_f
1.2	0.2	0.02	0.36	2.5	1.68	3.0	3.0

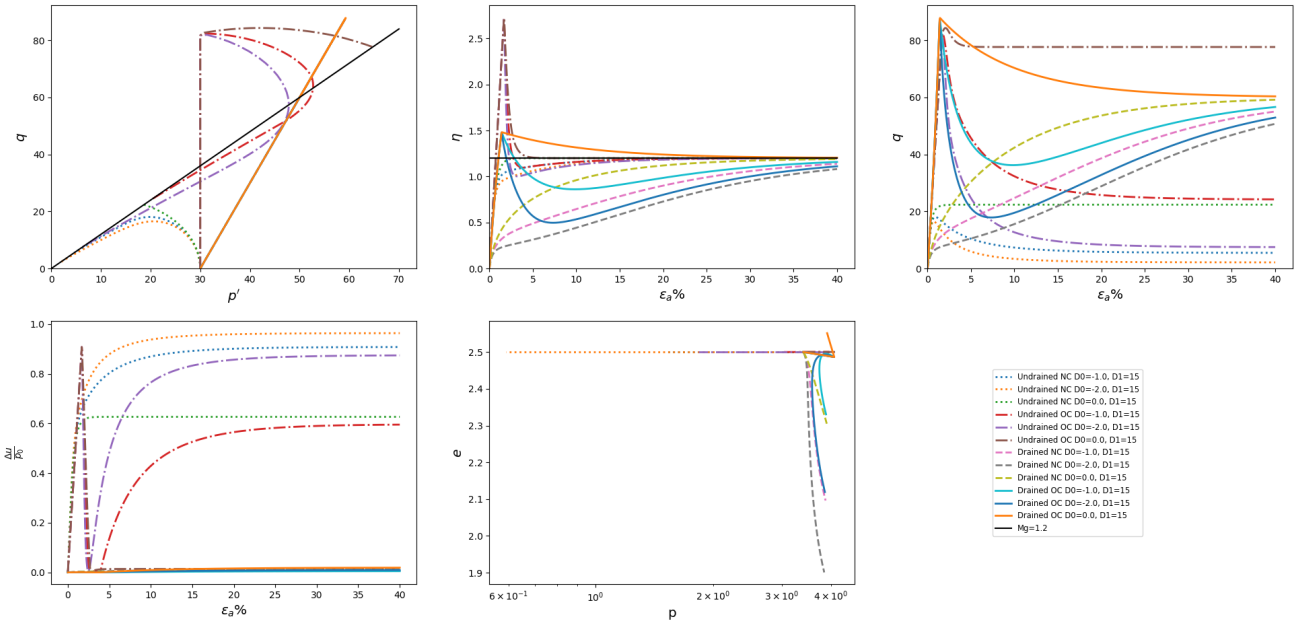

Figure E.3.1: Softening parameter analysis D_0.

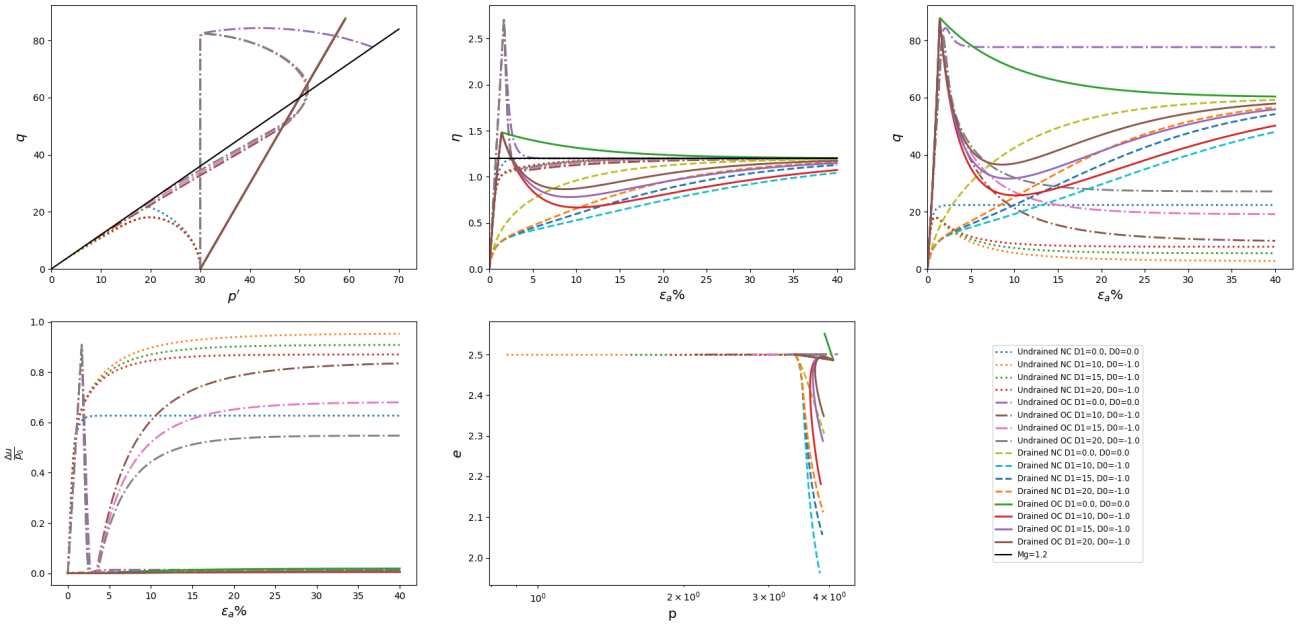

Figure E.3.2: Softening parameter analysis D_1.

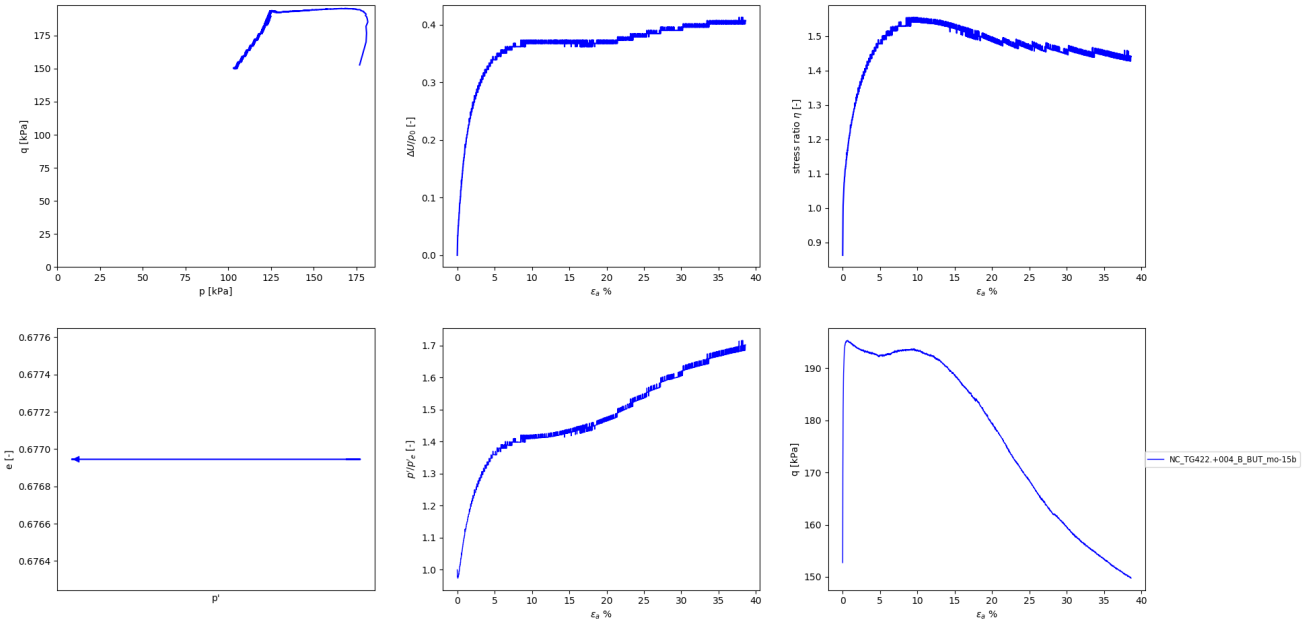

Figure E.3.3: Results Triaxial compression tests for matched Plasticity Index 23%

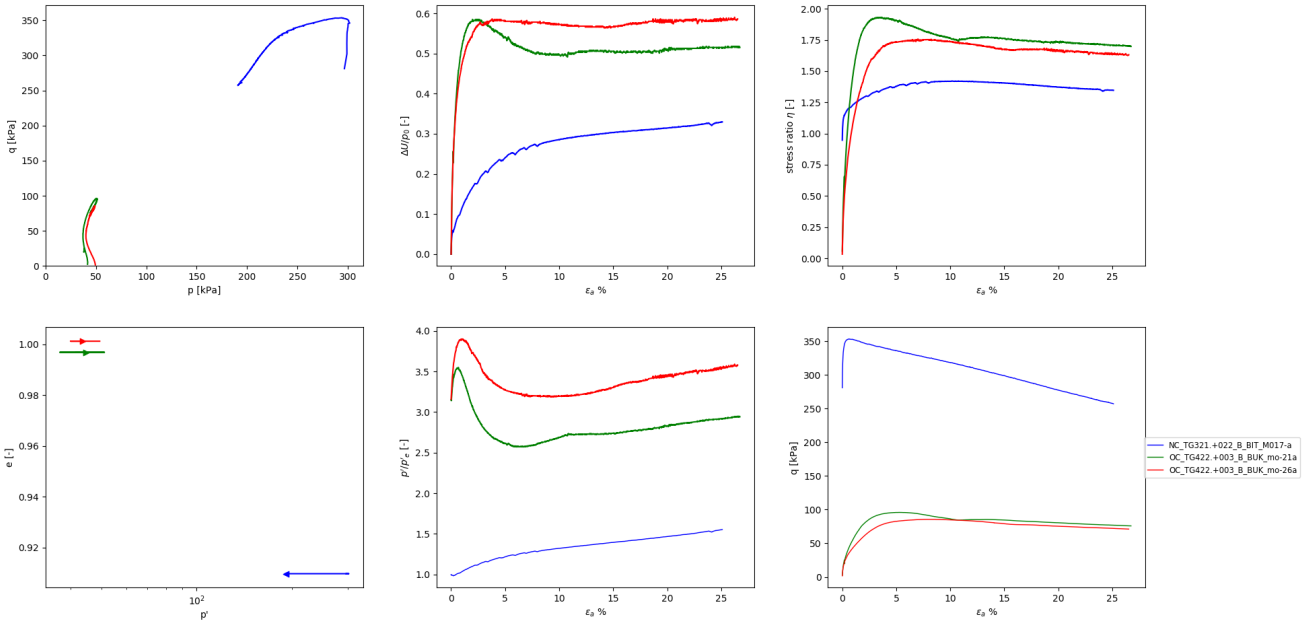

Figure E.3.4: Results Triaxial compression tests for matched Plasticity Index 34%

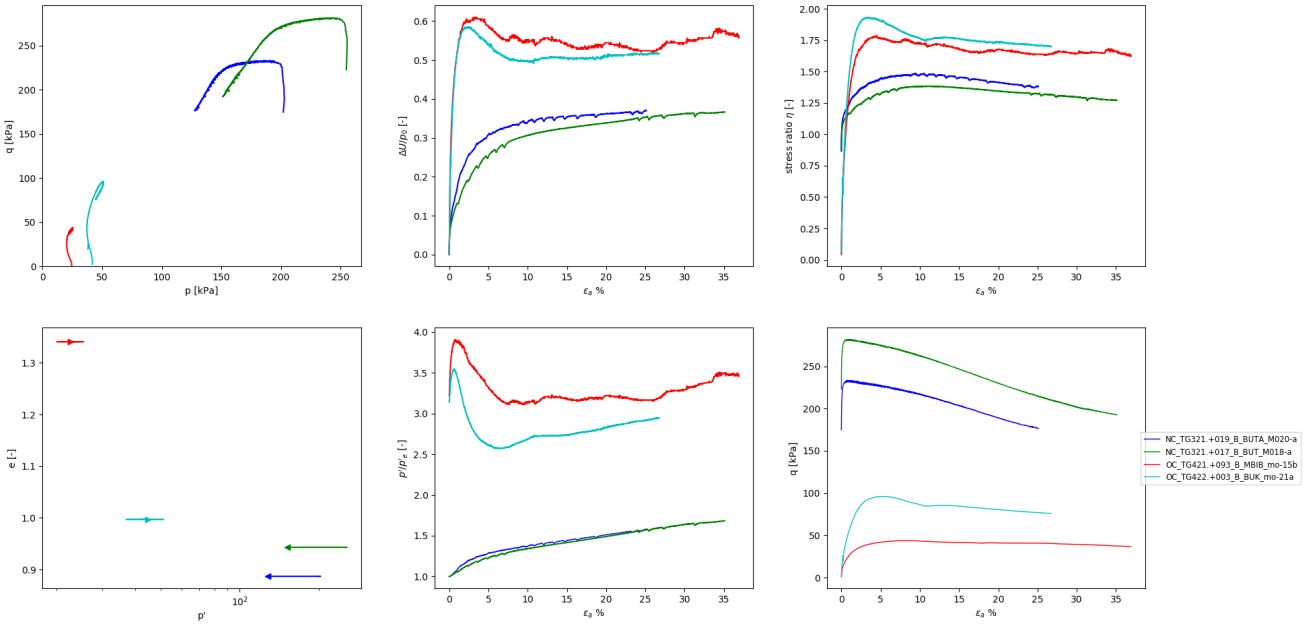

Figure E.3.5: Results Triaxial compression tests for matched Plasticity Index 42%

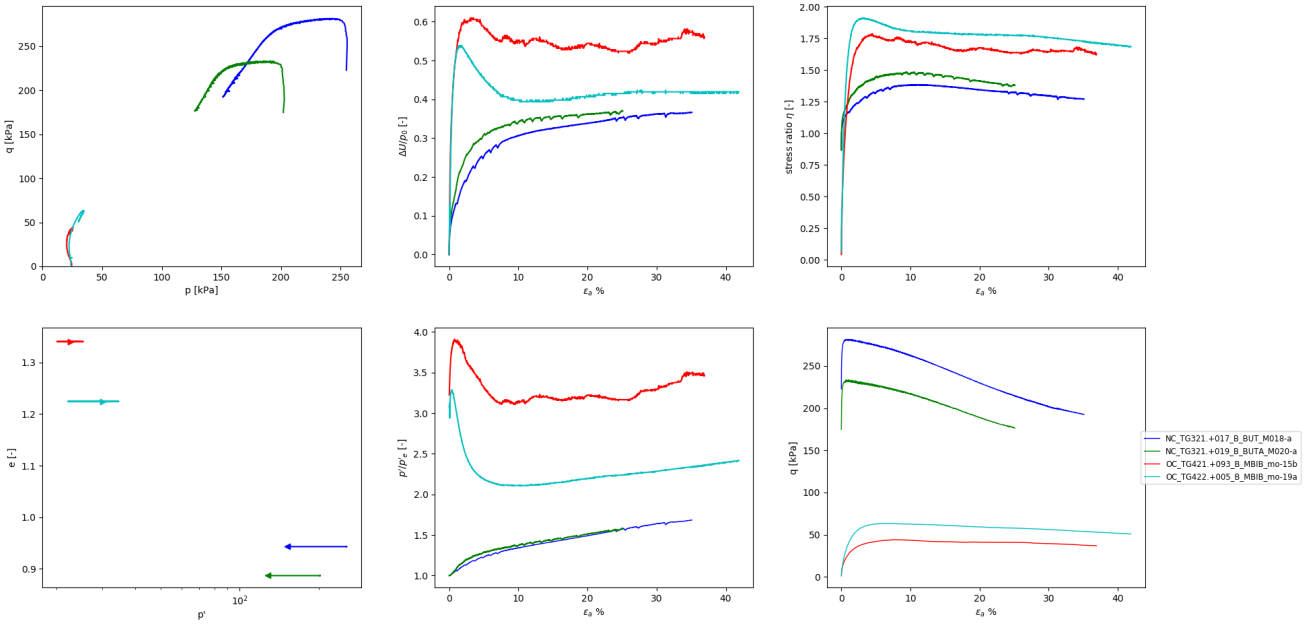

Figure E.3.6: Results Triaxial compression tests for matched Plasticity Index 43%

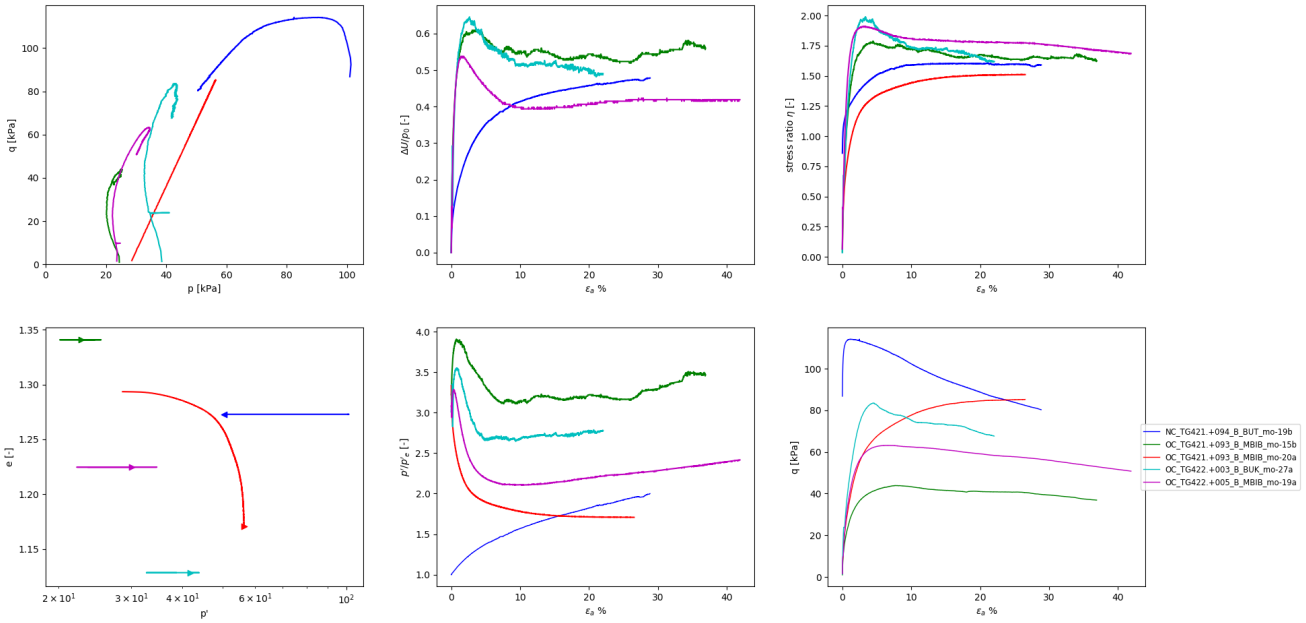

Figure E.3.7: Results Triaxial compression tests for matched Plasticity Index 44%

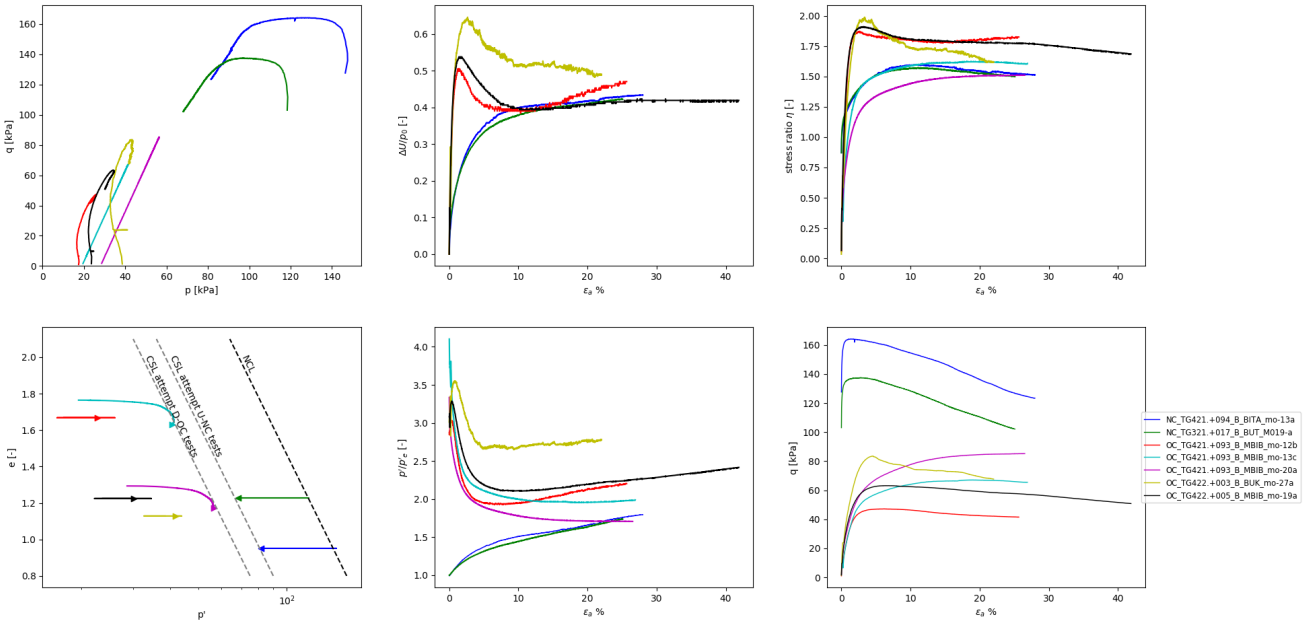

Figure E.3.8: Results Triaxial compression tests for matched Plasticity Index 50%

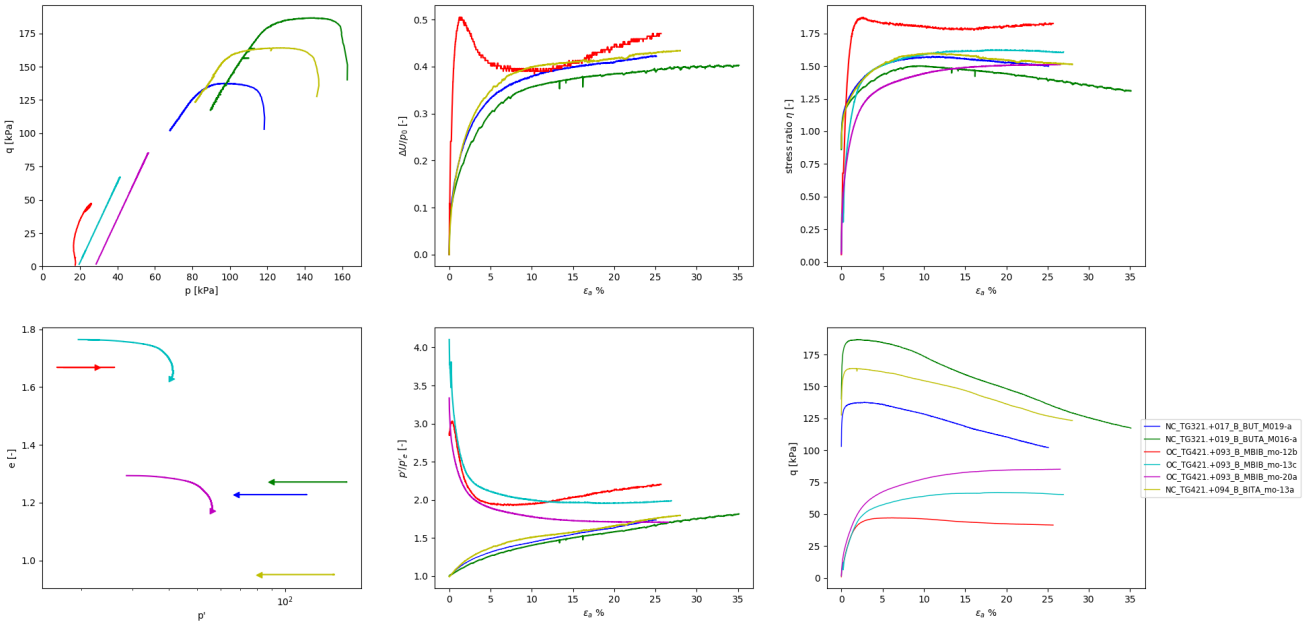

Figure E.3.9: Results Triaxial compression tests for matched Plasticity Index 52%

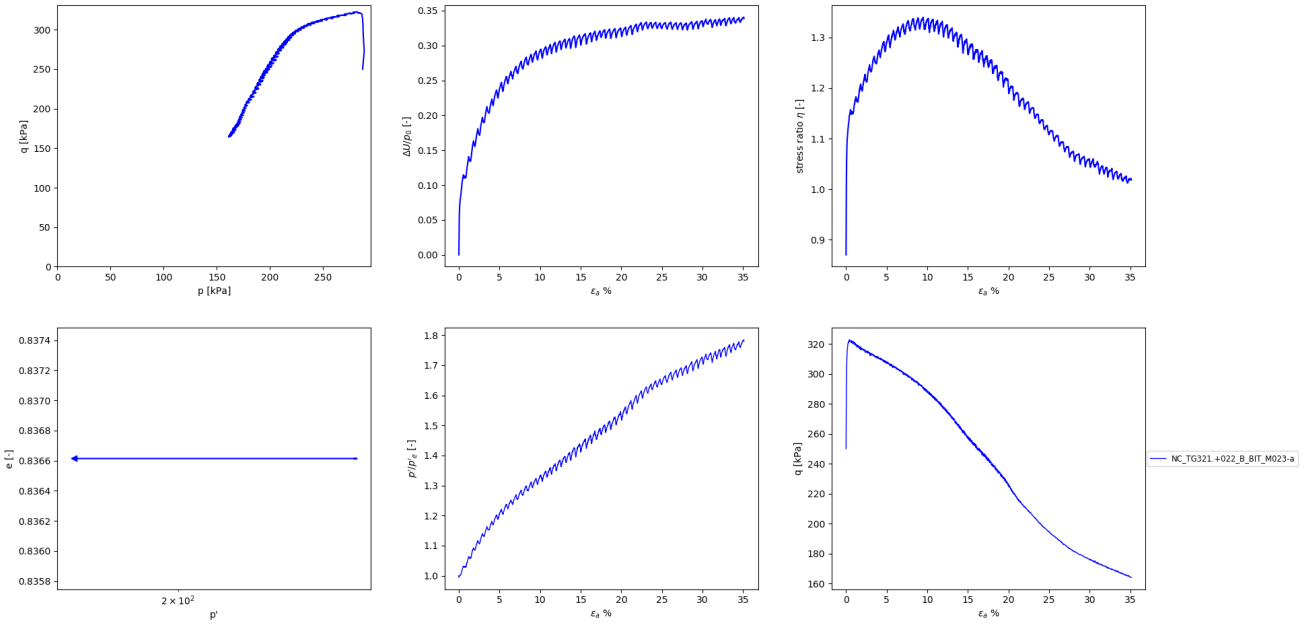

Figure E.3.10: Results Triaxial compression tests for matched Plasticity Index 54%

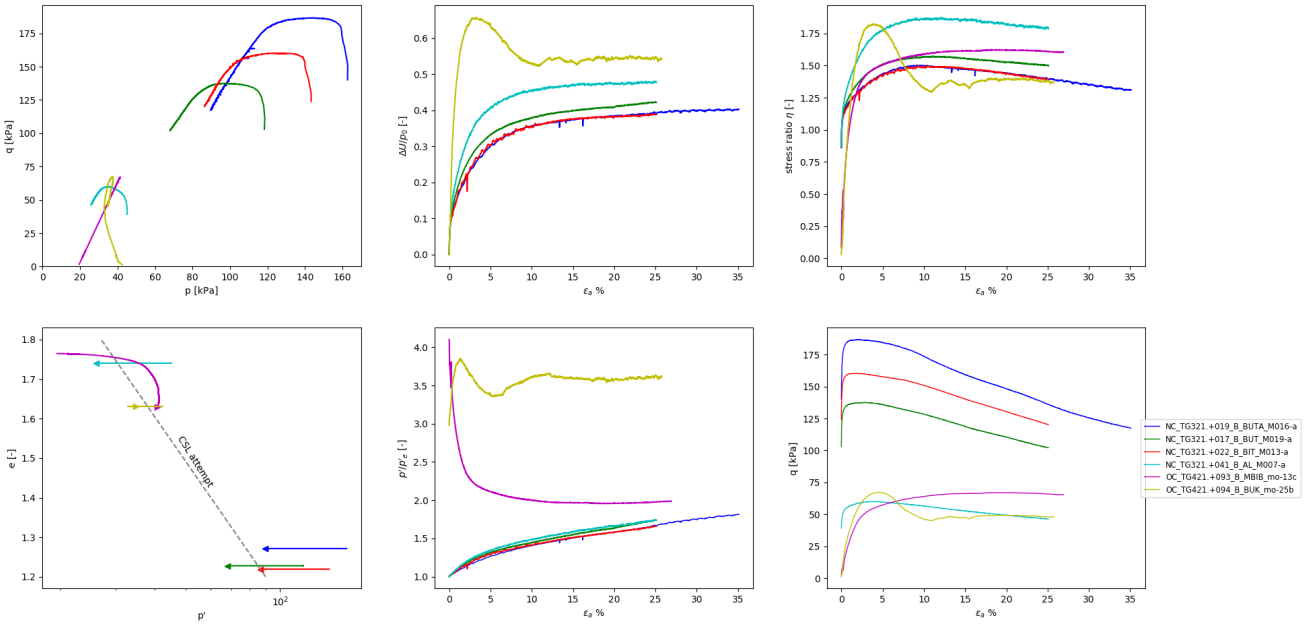

Figure E.3.11: Results Triaxial compression tests for matched Plasticity Index 56%

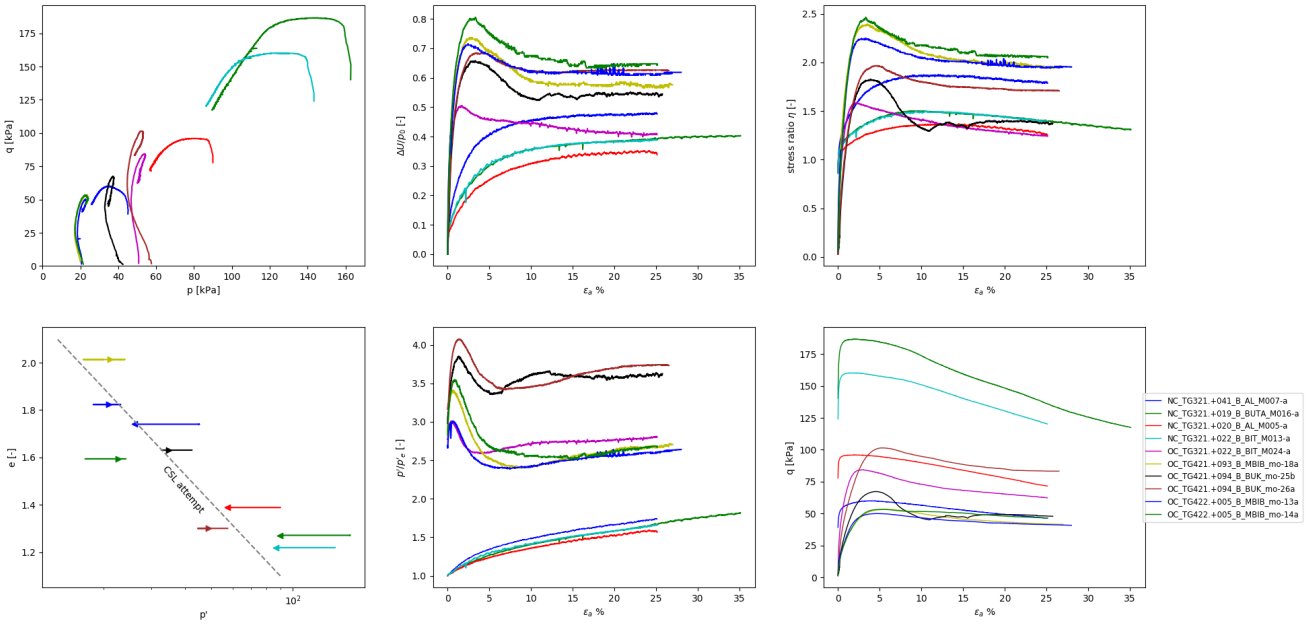

Figure E.3.12: Results Triaxial compression tests for matched Plasticity Index 60%

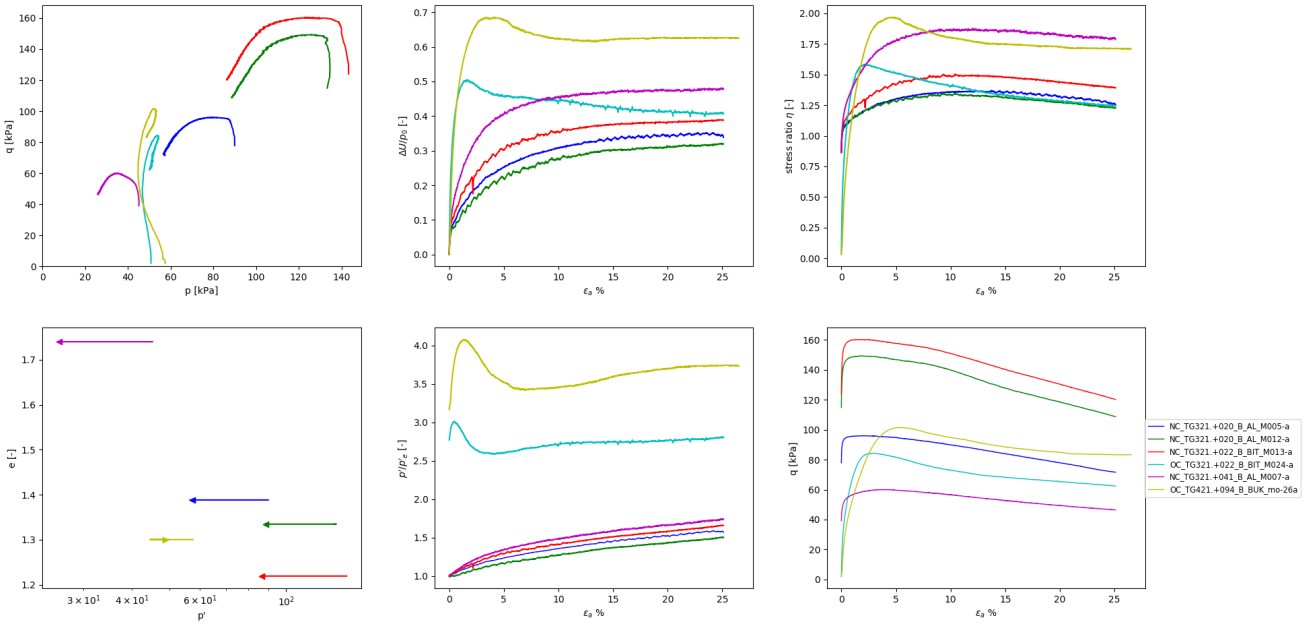

Figure E.3.13: Results Triaxial compression tests for matched Plasticity Index 64%

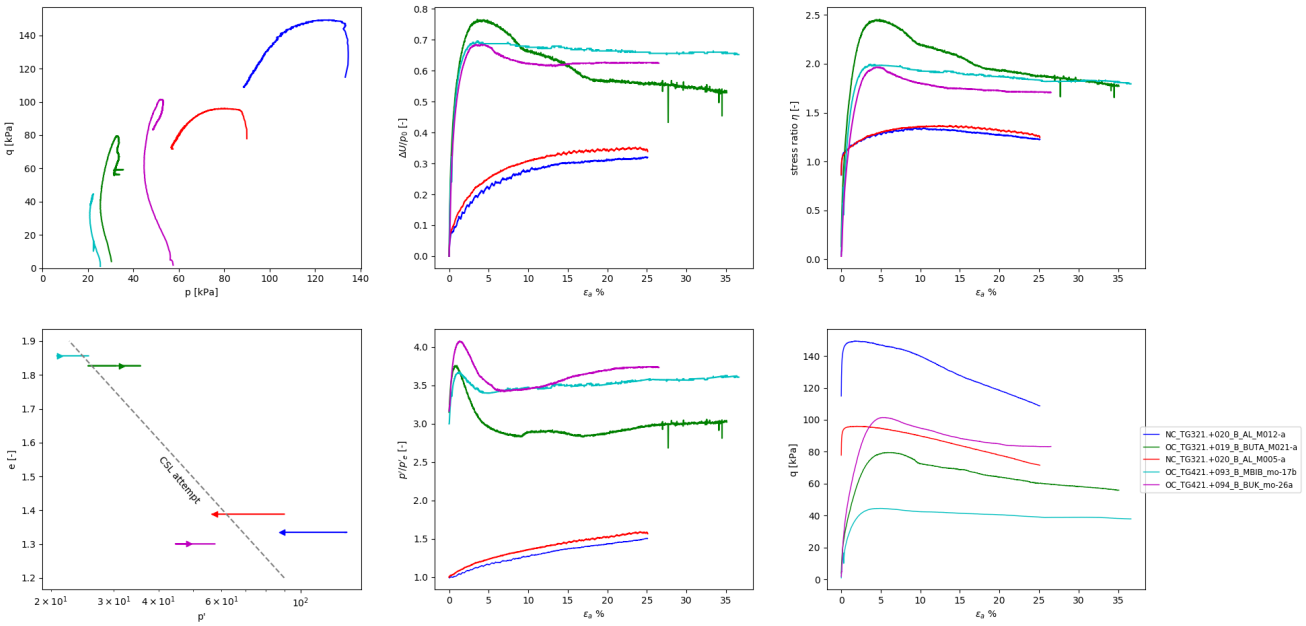

Figure E.3.14: Results Triaxial compression tests for matched Plasticity Index 69%

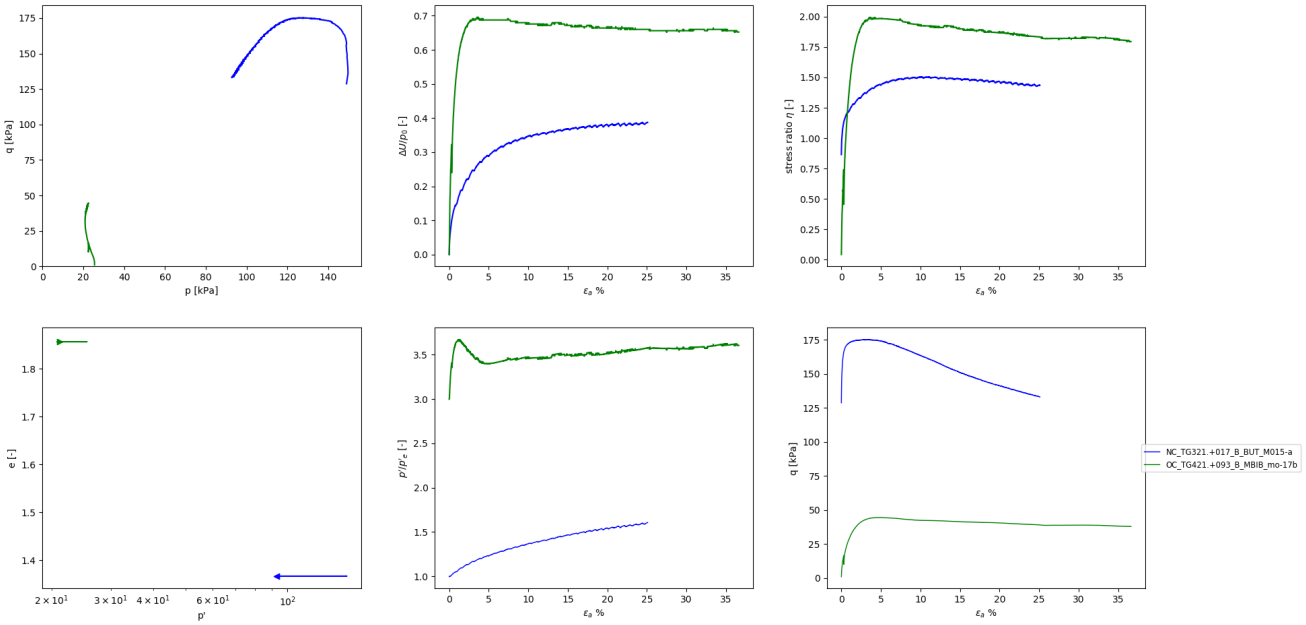

Figure E.3.15: Results Triaxial compression tests for matched Plasticity Index 77%